8-29-2012

Computational Evaluation of Wind Loads on Low- and High- Rise Buildings

Agerneh Dagnew
Florida International University, adagn001@fiu.edu

FLORIDA INTERNATIONAL UNIVERSITY

Miami, Florida

COMPUTATIONAL EVALUATION OF WIND LOADS ON LOW- AND HIGH-RISE BUILDINGS

A dissertation submitted in partial fulfillment of

the requirements for the degree of

DOCTOR OF PHILOSOPHY

in

CIVIL ENGINEERING

by

Agerneh Kenubih Dagnew

2012

To: Dean Amir Mirmiran
College of Engineering and Computing

This dissertation, written by Agerneh Kenubih Dagnew, and entitled Computational Evaluation of Wind Loads on Low-and High-rise Buildings, having been approved in respect to style and intellectual content, is referred to you for judgment.

We have read this dissertation and recommend that it be approved.

_____
Arindam Gan Chowdhury

_____
Emil Simiu

_____
George S. Dulikravich

_____
Fernando Miralles-Wilhelm

_____
Girma T. Bitsuamlak, Major Professor

Date of Defense: August 29, 2012

The dissertation of Agerneh Kenubih Dagnew is approved.

_____
Dean Amir Mirmiran
College of Engineering and Computing

_____
Dean Lakshmi N. Reddi
University Graduate School

Florida International University, 2012

DEDICATION

This dissertation research is dedicated to my grandmother Tena Mebiratu, my parents Kenubih Dagnew and Alemitu Zewidu, and to my brothers Abay and Amare Kenubih. Without them this dream would have not been possible.

ACKNOWLEDGMENTS

It gives me an immense pleasure to thank my major advisor Dr. Girma T. Bitsuamlak for introducing me to the world of Computational Wind Engineering and his guidance throughout my stay at Florida International University. Only with his active support did this document make its way into your hands. I also would like to extend my sincere gratitude to Dr. Emil Simiu, Dr. George Dulikravich, Dr. Fernando Miralles, and Dr. Arindam G. Chowdhury for their constructive input in the completion of this research.

I would like to acknowledge the Civil and Environmental Engineering department, the National Science Foundation (NSF), and the Florida Department of Emergency Management (FDEM) for their financial support during my doctoral program.

I would also like to thank the Multidisciplinary Analysis, Inverse Design, Robust Optimization and Control (MAIDROC) laboratory and the National Center for Super-computing Applications (NCSA) high performance computational facility centers that were instrumental for the completion of the present study.

The help and the moral supports I have received from Edward Ledesma, Adane Abegaz, Workamaw Warsido, Daniel Shawul, and the rest of all my friends are greatly appreciated.

Finally, I would like to thank my brothers and sisters for their unconditional love, encouragement and solid support in my academic career.

ABSTRACT OF THE DISSERTATION

COMPUTATIONAL EVALUATION OF WIND LOADS ON LOW- AND HIGH-RISE BUILDINGS

by

Agerneh Kenubih Dagnew

Florida International University, 2012

Miami, Florida

Professor Girma Bitsuamlak, Major Professor

Buildings and other infrastructures located in the coastal regions of the US have a higher level of wind vulnerability. Reducing the increasing property losses and causalities associated with severe windstorms has been the central research focus of the wind engineering community. The present wind engineering toolbox consists of building codes and standards, laboratory experiments, and field measurements. The American Society of Civil Engineers (ASCE) 7 standard provides wind loads only for buildings with common shapes. For complex cases it refers to physical modeling. Although this option can be economically viable for large projects, it is not cost-effective for low-rise residential houses.

To circumvent these limitations, a numerical approach based on the techniques of Computational Fluid Dynamics (CFD) has been developed. The recent advance in computing technology and significant developments in turbulence modeling is making numerical evaluation of wind effects a more appealing method. The present study targeted those cases that are not addressed by the standards. These include wind loads on complex roofs for low-rise buildings, aerodynamics of tall buildings, and effects of

complex surrounding buildings. Among all the turbulence models investigated, the large eddy simulation (LES) model performed the best in predicting wind loads. Systematic grid sensitivity analysis was conducted and computational grids that resolve the inner boundary layer adequately were used to estimate wind flow parameters. The application of a spatially evolving time-dependent wind velocity field with the relevant turbulence structures at the inlet boundaries was found to be essential. All the results were compared and validated with experimental data. The study also revealed CFD's unique flow visualization and aerodynamic data generation capabilities along with understanding of the complex three-dimensional aerodynamics of wind-structure interactions.

With the proper modeling that realistically represents the actual turbulent atmospheric boundary layer flow, CFD can offer an economical alternative to the existing wind engineering tools. CFD's easy accessibility is expected to transform the practice of structural design for wind, resulting in more wind-resilient and sustainable systems by encouraging optimal aerodynamic and sustainable structural/building design. Thus, this method will help ensure public safety and reduce economic losses due to wind damage.

TABLE OF CONTENTS

CHAPTER PAGE

LIST OF TABLES

TABLE PAGE

LIST OF FIGURES

FIGURE PAGE

1 INTRODUCTION

1.1 Problem statement

The elevated ocean surface temperatures resulting from the complex interactions between the ocean, the atmosphere, and the land surface have led to the intensification and frequent incidence of meteorological phenomena such as severe thunderstorms (tornados) and cyclones (hurricanes) on regions where this kind of occurrence was rarely verified before (Dailey et al., 2009). Buildings and other infrastructures located in the coastal regions of the United States of America have a higher level of wind vulnerability. The increase in population density and built properties in hurricane prone regions worsen the societal vulnerability to such catastrophic events (Pielke et al., 2008). As a result the reported property losses associated with hurricane winds have grown from $1.3B/yr pre-1990 to $36B/yr post-2000 (Lott and Ross, 2006). For example, the 2004/05 post damage assessments alone have reported that hurricane induced losses surpassed $100billion and caused over 1,400 fatalities (Government Accountability Report, 2006).

Limiting future damages for new constructions and retrofitting the existing structures require a better understanding and accurate estimation of the intensity, magnitude, and probability of occurrence of these events and their complex interaction with the built environment. In principle, components of the built environment such as buildings, bridges, large span roofs, and other civil engineering structures must be able to withstand the loads imposed by winds, at least to the extent that the disastrous damage of natural force is reduced to the acceptable limit (Irwin, 2008). The effect of wind on a structure is three-fold. The structure must have sufficient strength to resist the mean wind-induced forces, the structure must have adequate stiffness to satisfy occupant

comfort and serviceability requirements, and the wind may produce a dynamic response of the structure (typical of flexible structures) and may amplify the first two effects. The wind engineering community has long sought building reliable and hurricane-resilient structures, developing aerodynamic mitigation devices for retrofitting existing structures, and economical design of structures.

Structures subjected to high winds require realistic estimates of wind effects on components and wind-load resisting systems. Low- and high-rise buildings show different responses for wind. For low-rise buildings, the roof systems are exposed to higher loading than any other building structural element and are subjected to wind forces from many directions (Smith et. al, 1991). Worst suction pressures are known to occur in the corner on the roof, caused by the development of conical vortices during oblique winds (Bank et al., 2000). The alternating vortices triggered at the leading corner of the building have resulted in worst suction pressure coefficients of over 20 (Kopp et al., 2005). This amplified pressure load could result roof lift, both in roof cladding and sheathing, leading to water intrusion and cause further content damages.

High-rise buildings, in addition to the mean and the background loads, are subjected to resonant wind loads. The primary source of the along-wind motion is the pressure fluctuations in the windward and leeward faces, which are affected by the turbulent nature of the approach flow and its interaction with the building itself. The cross-wind motion is mainly caused by fluctuations in the separating shear layers. Torsional motion can be caused by imbalance of instantaneous pressure distribution on faces of the building. This could be either due to oblique wind directions, unsteadiness in the approaching flow, partial sheltering and interference effect from neighboring

buildings or due to its own shape and dynamic structural properties, including eccentricity of the center of mass with respect to the elastic center. Studies have shown that for many high-rise buildings, the across-wind and torsional response may exceed the along wind response in terms of both limit state and serviceability requirements (Kareem, 1985).

1.2 Commonplace wind engineering tools

In current practice, buildings and other wind-sensitive structures are designed following building standard and code procedures. The American Society of Civil Engineers Standard (ASCE7-05/-10) specifies provisions for the design of Main Wind Force Resisting Systems (MWFRS) and Cladding and Components (C&C) of buildings with common regular shapes in open and suburban exposure. However, many real world structures such as low rise buildings with complex roofs and tall buildings, in particular, fall outside this category. For example, the Standards do not provide provisions for the across-wind load evaluation of tall building which could governs the design load. Exceptionally, the Australian/New Zealand Standard (AS-NZ, 2002) code attempted to provide provisions for the across-wind direction but for very limited cases of tall buildings. For complex cases, the Standards refer to physical model testing in boundary layer wind tunnel (BLWT) facilities.

Model scale testing in a boundary layer wind tunnel is the most commonly used and industry wide accepted wind engineering tool. A BLWT is mainly employed for evaluating wind loads on structures ranging from low-rise to high-rise buildings with complex configurations, and from bridge aerodynamics to topographic study. Figure 1.1 shows a typical BLWT setup for wind load evaluation of a high-rise building. Wind

tunnel tests can predict wind-induced effects on structures, addressing some of the difficulty encountered by codes, by accounting for project-specific factors such as the aerodynamic effect of the actual shape of the structure, the influence of adjacent buildings and upstream topography, detailed wind directionality effects, and aero-elastic interaction between the structural motion and wind flow. Although aerodynamic studies using the wind tunnel technique is economically feasible for large and complex cases, it is not cost-effective for low-rise buildings. In addition, there are some concerns regarding scale modeling of low-rise buildings.

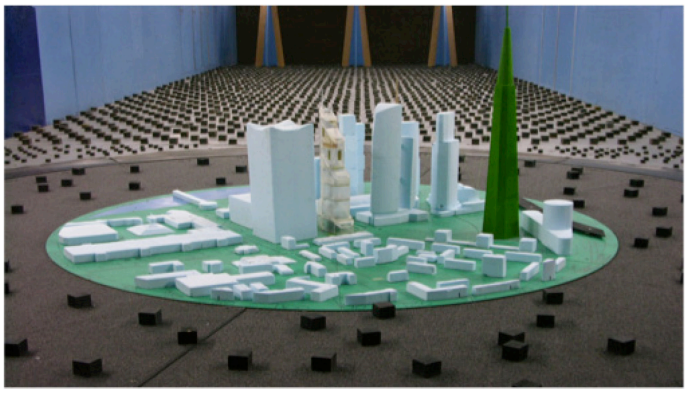

Figure 1.1 Photograph of a typical wind tunnel setup of high-rise building (courtesy of RWDI Inc., Canada).

Low-rise residential buildings, that constitute a large proportion of the building stocks in the world, are suffering from the most damages. The high vulnerability is the result of inadequacy of the load estimation method, the enforcement of the codes and quality of construction practice, and the region where the building is located. To deal with this, novel large-scale and full-scale research facilities are being built around the world. The Wall of Wind (WoW) facility at Florida International University is one of the first major initiatives to operate a large-scale facility dedicated to hurricane damage

mitigation (Leatherman et al., 2007). The insights from WoW full-scale experiment results are very significant for the wind engineering community in terms of understanding the performance of buildings under hurricane winds or wind-driven rain and devising mitigation plans to increase the resilience of low-rise buildings under such loads (Chowdhury et al., 2009; Bitsuamlak et al. 2009). The multi-peril applied research facility build by the Institute for Business and Home Safety (IBHS) and the WindEEE dome by the UWO are another notable move towards understanding wind hazards in its entirety (Figure 1.2). One noticeable advantage of this type of facility is that their ability for testing a full-sized residential building, single story dwelling. Residential construction is typically built using prescriptive building codes, and is characterized by the use of materials with large variability and structures with significant static indeterminacy making load paths and over-all performance difficult to ascertain. These new facilities are able to deal with these issues by bringing realistic wind loads to full-scale structures, enabling the development of improved building code requirements, product safety standards and loss models.

WoW IBHS WindEEE

Figure 1.2 Full-scale facilities

Nevertheless, the concerns pertaining to the limited coverage/ or provisions given by the standards and codes, the cost of experimental testing and their scarce availability in one hand, and the encouraging progress in hardware and software technology on the

other hand have been the motivation to investigate the potential of numerical modeling, such as CFD applications, as an alternative to the exiting commonplace wind evaluation tools. CFD's easy accessibility is expected to transform the practice of structural design for wind, resulting in a more wind-resilient and sustainable systems by encouraging optimal aerodynamic and sustainable structural/building design.

1.3 Objectives of research

The main objective of this research is to develop strategies for computational evaluation and assessment of wind loads on buildings under turbulent wind flow. Building on achievements to date, the current study evaluates wind loads on low-rise buildings with complex roof shapes, investigates numerical the aerodynamics of a standard tall building, and assesses the effects of surrounding conditions on the study building for multiple wind directions. The sub-objectives include:

- Comparative study on various turbulence modeling
- Numerical generation of spatially evolving transient wind velocity field
- Pressure time-history measurements from high resolution CFD simulations
- Examining responses of buildings from multiple wind directions
- Wind-structure interactions studies of low- and high-rise buildings
- Validation and comparison using experimental and field data

1.4 Current state of CWE

Following the successful application of computational fluid dynamics (CFD) in aeronautical engineering, several attempts have been made to incorporate computational wind engineering (CWE) technique in the evaluation of wind-induced effects. This is particularly so considering the recent advances in hardware and software technology, the

development of reliable sub-grid turbulence models and numerical reproduction of inflow turbulences (Tamura et al., 2008). Significant progress has been made in the application of CWE to evaluate wind loads on buildings (e.g. Murakami et al., 1998; Tamura, 2008). Some countries have already established working groups to investigate the practical applicability of CWE and develop recommendations for their proper use. Guidelines for wind resistant design of buildings and the practical application of CFD to pedestrian level wind within the framework of the Architectural Institute of Japan (AIJ) (Tamura et al., 2008; Tominaga et al., 2008a) and CFD simulation of flows in the urban environment by the European cooperation in the field of scientific and technical research (COST, 2007; Franke et al., 2006) are some of the most recent accomplishments. Thus far, the majority of the numerical studies of wind loads on buildings have been devoted to basic cubes immersed in turbulent boundary layer flow. These have been done only for few wind directions using simple turbulence modeling techniques. Surface mounted cubes are chosen for their geometrical simplicity yet represent the basic complex features of building aerodynamics, often the advantage of availability full-scale data for validation purpose, and acceptable costs (Stathopoulos & Wu, 2004).

1.5 Research methodology

The following procedures have been adopted in for implementation of Reynolds averaged Navier-Stokes (RANS) and large-eddy simulation (LES) CFD techniques in the numerical investigation of wind effects on low and high-rise buildings.

1.5.1 Explanatory investigation on turbulence modeling

After a thorough review of the literature, the investigation of various turbulence models for their relative suitability was necessary. To achieve this, preliminary

exploratory studies have been done on buildings employing both RANS and LES for the following cases: (1) External aerodynamic simulation on surface mounted cube (Wright and Easom, 2003), representative of low-rise residential houses, and (2) simplified model of CAARC standard tall building model with and without a neighboring building (Dagnew et al 2009, 2010). The LES, a multi-scale computational modeling approach capable of capturing fluctuating turbulent flow, reproduced the flow features that have pivotal importance for turbulent wind flow.

1.5.2 Wind tunnel ABL simulation

One of the critical parts for the success of numerical based simulations is the proper prescription of upwind flow parameters. CFD being at its validation phase, comparing CFD simulation with wind tunnel data is a practical way of assessing its prediction accuracy. For this purpose, flow statistics from wind tunnel data are indispensable for defining inlet boundaries of LES simulations. ABL simulations on an empty BLWT were carried out for open and suburban terrain at RWDI Inc. Miramar, Miami, FL facility. Time histories of turbulent velocity fluctuation components were measured. The mean velocity and turbulence intensity profiles and the integral length scales that were obtained from the BLWT were used for the numerical inflow turbulence data generation.

1.5.3 Numerical generation of inflow turbulence

Spatially evolving transient inflow turbulence fluctuations were numerically generated by incorporating the in-house C/C++ developed codes with the finite volume CFD software known Ansys Fluent. The random fluctuations that possess the inherent characteristics of natural wind were generated using various methods such as, for

example, velocity recycling and synthetic methods. Homogenous and inhomogeneous anisotropy turbulent flow fields were applied at the inlet boundaries and their effects on the wind pressure loads prediction accuracy of LES were investigated.

1.5.4 Geometrical modeling

CAD models that realistically represent the actual building configurations and the surface roughness of the complex upwind terrain of an urban setup were produced. Proper modeling of these factors will significantly improve the outcome of the computational simulation. This was done by using commercial CAD software like Google SketchUp, SolidWorks and Design modeler. The created models include structures within 1km radius of the target building. Once the water tight topologies were ready, the models were used by the grid generator tool.

1.5.5 Grid sensitivity analysis

High quality computational grids with efficient strategies for solution-dependent grid adaptation and optimization dedicated for building aerodynamics were implemented. For corner wind, high fractions of hexahedral grid cells were generated using Gambit, ICEM CFD and the CutCell methods of Ansys Meshing softwares. Economical meshes were produced by dividing the flow domain into multi-body parts. Very fine grids cell were clustered in the near wall to resolve the inner boundary layer and the high gradient flow regions.

1.5.6 Computational evaluation of wind loads and validation with experimental data

The envelope of the target buildings were systematically instrumented with pressure taps, created in the flow domain. Pressure time histories were measure from the

high frequency pressure integration (HFPI) type LES simulation. The wind pressure coefficients (mean, root-mean-square), the load coefficients (drag and along-wind force coefficients), the moment coefficients (bending and over turning), and the peak values were calculated and validated with wind tunnel, full-scale, and field measurements.

1.6 Scope of research

This dissertation document provides the background of the multi-scale computational and experimental wind engineering research effort carried out at FIU and other commercial and academic institute organizations generously provided the wind tunnel data used for validation purposes (see acknowledgment). Each section, excluding the introduction, represents a published paper, in press, or under review. Chapter 2 presents the state-of-the-art of CFD applications for real world industrial problems, special efforts has been made to understand the underlying modeling principles and practices of numerical wind load evaluation. Recent advancements in the field of CWE, various aspects of turbulence modeling, boundary conditions, spatial and temporal discretization techniques, computational cost of preforming of high Reynolds number flow simulation, illustration on numerical wind pressure loads estimation for low-and high-rise buildings, and the need for validation are discussed in Chapter 2. Chapter 3 documents the application of Reynolds-Averaged Navier-Stokes (RANS) simulations for assessing the proximity effects of test specimen for the development of the Wall-of-Wind testing facility. Blockage issues related to the relative model and WoW wind field sizes are investigated. Chapter 4 focuses on the computational evaluation of wind pressure loads on actual Florida residential houses with complex roof shapes. A boundary layer wind tunnel data for isolated and with surrounding building cases used to validate the

LES models are also described. The test cases are similar to the buildings studied as part of the Florida Coastal Monitoring Program (FCMP) project. The mean and peak values obtained from LES simulations for oblique wind angle are computed and elaborated. Chapter 5 covers aspects of atmospheric turbulence that are of interest to structural and wind engineers and explains the principles and methods of HFPI-type LES simulations for a standard tall building with and without adjacent buildings. In addition, simulation algorithms of various random turbulence for generation techniques are examined. Chapter 6 presents LES simulation of tall buildings under complex urban settings. The sheltering and interference effects of neighboring buildings were investigated. The wind loads obtained for the various configurations are discussed in great depth. Finally, Chapter 7 summarizes conclusions about CFD applications for wind engineering and recommend for future research avenues.

References

American Society of Civil Engineers, American National Standard: Minimum design loads for buildings and other structures, *ASCE 7-05/10*.

Australian/New Zealand Standard: Structural Design Actions Part 2: Wind Actions Standards. *AS/NZS 1170.2:2002*.

Banks, D., Meroney R.N., Sarkar, P.P, Zhao, Z., Wu, F. (2000). "Flow visualization of conical vortices on flat roofs with simultaneous surface pressure measurement." *J.Wind Eng. Ind. Aerodyn. (84) 65–85.*

Bitsuamlak, G.T., Gan Chowdhury, A., Sambare, D. (2009). "Development of full-scale testing facility for water intrusion." *Building and Environment, 44(12), 2430-2441*

Chowdhury, A., Simiu, E., and Leatherman, S. (2009). "Destructive Testing under Simulated Hurricane Effects to Promote Hazard Mitigation." *Nat. Hazards Rev., 10(1), 1–10.*

COST. (2007). "Best practice guideline for the CFD simulation of flows in the urban environment." *COST Action 732.*

Dagnew, A.K., Bitsuamalk, G.T. (2010). "LES evaluation of wind pressures on a standard tall building with and without a neighboring building." *The Fifth International Symposium on CWE, Chapel Hill, North Carolina, USA May 23-27*.

Dailey, P.S. Ljung, G., Zuba, G., Guin, J. Elsner, J. B. Jagger, T.H. (2009). "Probability of Hurricane Intensification and United States *Hurricane Landfall under Conditions of Elevated Atlantic Sea Surface Temperatures Book Title." Hurricanes and Climate Change. Page 121-138.*

Franke. J. (2006). "Recommendations of the COST action C14 on the use of CFD in predicting pedestrian wind environment." *The Fourth Intenational Symposium on Computational Wind Engineering (CEW2006), Yokohama, Japan*.

United State Government Accountability Office (GAO). 2006. "Hurricane Katrina and Rita, Contrasting for Response and Recovery Efforts." GAO-06-235T.

Irwin, P.A. (2008). "Bluff body aerodynamics in wind engineering." *J. Wind Eng. Ind. Aerodyn. 96, 701-712.*

Kareem ,A. (1985). "Lateral-torsional motion of tall buildings to wind loads." *J. Struct. Eng., ASCE111 (11), 2479–2496.*

Kopp, G.A, Mans, C., Surry, D., (200). "Wind effects of parapet on low buildings: Part . Mitigation of corner loads with alternative geometries." *J. Wind Eng. Ind. Aerodyn. 93, 873-888.*

Leatherman, S. P., Gan Chowdhury, A., and Robertson, C. (2007). "Wall of wind full-scale destructive testing of coastal houses and hurricane damage mitigation." *J. Costal Res., 23, 1121-1217.*

Lott, N., Ross, T. (2006). "Tracking and evaluating U.S. billion dollar weather disasters, 1980-2005." *NOAA's National Climatic Data Center, North Carolina.*

Lund,T. S., Wu, X., Squires, K. D. (1998). "Generation of turbulent inflow data for spatially developing boundary layer simulations." *J. Comp. Phys. 140, 233–258.*

Murakami, S. (1997). "Overview of turbulence models applied in CWE–1997". *J. Wind Eng. Ind. Aerodyn.* 74-76, 1-24.

Pielke, R.A., Gratz, J., Landsea., C.W., Collins, D., Ssaunders.M.A., Musulin.R. (2008). "Normalized hurricane damage in the United States: 1900-2005." *ASCE* 9:1(29), 1527-6988.

Tamura, T. (2008). "Towards practical use of LES in wind engineering." *J. Wind Eng. Ind. Aerodyn.* 96, 1451-1471.

Tamura, T., Nozawa, K., Kondo, K. (2008). "AIJ guide for numerical prediction of wind loads on buildings." *J. Wind Eng. Ind. Aerodyn. 96, 1974-1984.*

Tominaga, Y., Mochida, A., Murakami, S., Sawaki, S. (2008). "Comparison of various revised k–ε models and LES applied to flow around a high-rise building model with 1:1:2 shape placed within the surface boundary layer." *J. Wind Eng. Ind. Aerodyn. 96, 389-411.*

Wright, N.G., Easom, G.J. (2003) "Non-linear k–e turbulence model results for flow over a building at full-scale." *Applied Mathematical Modelling. 27(12), 1013-1033.*

2 COMPUTATIONAL EVALUATION OF WIND LOADS ON BUILDINGS: A REVIEW

Agerneh K. Dagnew[a] and Girma T. Bitsuamlak[*, b]

Accepted for Publication in the Journal of Wind and Structures

Abstract

This paper reviews the current state-of-the-art in the numerical evaluation of wind loads on buildings. Important aspects of numerical modeling including (i) turbulence modeling, (ii) inflow boundary conditions, (iii) ground surface roughness, (iv) near wall treatments, and (vi) quantification of wind loads using the techniques of computational fluid dynamics (CFD) are summarized. Relative advantages of Large Eddy Simulation (LES) over Reynolds Averaged Navier-Stokes (RANS) and hybrid RANS-LES over LES are discussed based on physical realism and ease of application for wind load evaluation. Overall LES based simulations seem suitable for wind load evaluation. A need for computational wind load validations in comparison with experimental or field data is emphasized. A comparative study among numerical and experimental wind load evaluation on buildings demonstrated generally good agreements on the mean values, but more work is imperative for accurate peak design wind load evaluations. Particularly more research is needed on transient inlet boundaries and near wall modeling related issues.

[a] Ph.D. Candidate, [*] Adjunct Prof., Laboratory for Wind Engineering Research (LWER), International Hurricane Research Center (IHRC) /Department of Civil and Environmental Engineering (CEE), Florida International University (FIU), Miami, FL 33174, USA

[b] Associate Prof., Department of Civil and Environmental Engineering, University of Western Ontario in London, ON, Canada.

Keywords: Wind loads, building, computational fluid dynamics, turbulence, ABL, RANS, LES, hybrid LES-RANS, and validation.

2.1 Introduction

Buildings, bridges, and all other civil engineering structures must be able to withstand external loads imposed by nature, such as wind, at least to the extent that the disastrous damage of natural force is reduced to the designed acceptable limit (Irwin, 2008, 2009). Traditionally wind loads on buildings are obtained from building standards and codes. The majority of building codes and standards usually provide loads for along-wind direction of regular shape buildings under open and suburban exposure. Most often, building standards and codes utilize the quasi-steady and strip theories approach where the gustiness of wind is customarily factored in by a random-vibration using the "gust factor approach" to predict the along-wind response (Davenport, 1967; Simiu, 1976). For example, the American Society of Civil Engineers (ASCE) 7-05 Standard contains provisions on wind loads for the design of Main Wind Force Resisting Systems (MWFRS), as well as Cladding and Components (C&C) of buildings with common shapes in open and suburban terrain. Additionally, the National Building Code of Canada 2005 (NBCC 2005) provides acceleration calculations for the along-wind and across-wind directions. The Australian/New Zealand Standards (AS-NZ) (2002) code and the Architectural Institute of Japan (AIJ) recommendations (2400a) have made an exceptional attempt to provide the across-wind response using a cross-wind spectrum and expressions for both the across-wind and torsional root-mean-square acceleration. For

cases not addressed by the building codes and standards, a physical testing in a boundary layer wind tunnel (BLWT) is referred. Although this option is economically viable for large projects such as the aerodynamics of tall buildings and long span bridges, performing building specific BLWT testing might not be cost-effective for most buildings such as low-rise residential buildings. Moreover, the variations in the wind flow and surrounding conditions that result from one project may not be extendable to a new project making generalizations more difficult.

To address this gap at least for a preliminary wind load evaluation case, a computational model that can simulate the atmospheric boundary layer (ABL) flow and predict the parameters of interest can be an alternative approach. It is to be noted, however, computational approaches also have their own share of challenges and shortcomings yet to be resolved before their use for a final wind resistant design of buildings immersed in a turbulent ABL flows. At present, the cost of performing CFD is not lower than BLWT testing either. However, the computational cost is in a decreasing trend due to encouraging advances both in the hardware and software technology. This paper attempts to present a comprehensive review of the state-of-the-art of Computational Wind Engineering (CWE) as it relates to wind load evaluation on buildings. Recognizing significant progress made in the last decades, the paper will also pinpoint the area where the current practice of CFD needs further improvement, and attempts to discuss the direction of future CWE avenues based on the literature and authors' perspective, and draw some observatory conclusions relevant for practical applications of CWE.

Significant progress in CWE has been reported in literature. Ranging from: 2D to 3D flow field analysis; building to human scale; isolated buildings situated in open terrain to high-rise buildings located in urban city centers to complex environmental problems (Murakami 1998; Tamura et al., 2008; and Jiang et al., 2006). Several published CWE findings dedicated to wind load evaluations supported with experimental validation have demonstrated encouraging results. Murakami (1997, 1998) have presented a historical review of turbulence modeling up to the late 1990s and pointed out the challenges that limited the practical applicability of CWE during that period. Some of the difficulties were: (a) high Reynolds number (*Re*); under this type of flow condition the accuracy of CWE is dependent on the grid resolution near the solid wall of the bluff body, (b) wind is complex, unsteady, and the 3D turbulent flow field is mainly characterized by impinging, separation, and vortex shedding. This requires 3D computation with an advanced turbulence model such as LES. However, the limitation in computing resources has hindered LES adoption in various CWE applications. Hence, it was common to carry out 2D RANS simulations during this period, (c) the presence of sharp edges at building corners make it very difficult to analyze the wind flow field by CFD, and (d) bluff body wake causes problems to inflow and outflow boundaries of LES and direct numerical simulation (DNS).

To overcome the aforementioned problems, several revisions have been made on RANS turbulence model closures mostly in an ad hoc manner. The revisions on RANS models, especially the modifications made on standard $k-\varepsilon$ models, succeeded in correcting the overestimation of kinetic energy production in the impinging region and reproduction of flow separation and reattachment around building roofs (Murakami,

1997, Murakami and Mochida, 1999). The LK model by Launder and Kato (1993) reduced the production of the kinetic energy at the windward corner but had some mathematical inconsistency (Tsuchiya et al., 1997). Later Murakami et al. (1998) proposed the MMK model which provided significant improvements by removing the inconsistency of the LK model. A discussion on progress of CWE until the late 1990 was also provided by Stathopoulos (1999).

Some notable studies in the early 2000 include: non-linear RANS modeling for a full-scale low-rise building such as the Silsoe Cube (Wright and Easom, 2003) where comparison of several $\kappa - \varepsilon$ family of turbulence models were provided in comparison with the field measurement data; computational prediction of flow-induced pressure fluctuations on Texas Tech University building (TTU) (Selvam, 1999; Senthooran et al., 2004). Gomes et al. (2005) simulated flow around L- and U- shape buildings by using the RNG $\kappa - \varepsilon$ turbulence model. Although good agreement between Gomez et al. (2005) and experimental results for upwind C_P values were observed, large discrepancies were found for C_P values of the wake regions mostly attributed to the use of isotropic turbulence model. More recently several CFD works have been reported on a bench mark tall building called the Commonwealth Advisory Aeronautical Research Council (CAARC) model building, which also commonly used as a benchmark for calibration/validation new BLWT facilities (Huang et al., 2007; Braun and Awruch, 2009; Dagnew et al., 2009, 2010). Other works on tall buildings include: LES of a full-scale supper-tall building with *Re* greater than 10^8 (Huang and Li, 2010); LES of flow and building wall pressure in a city center (Nuzu et al., 2008; Tamura, 2010a); flow

around a high-rise building using various turbulence models (Tominaga et al., 2008a); aerodynamic characteristics of a tall building inside a dense city district using LES (Tamura, 2010b). The use of advanced turbulence modeling such as LES, and development of reliable and robust subgrid models and numerical algorithms which perform well in a wide range of flow parameters (Tamura et al., 2008) and prescriptions of transient inflow boundary (Sagaut et al., 2004; Tutar and Celik, 2007; Xie and Castro, 2008) reportedly have increased computational prediction accuracy.

Some countries have already established working groups to investigate the practical applicability of CWE (and for its potential inclusion in building codes and standards) and have developed recommendations and guidelines for efficient implementation and use for wind resistant design of actual buildings and for assessing pedestrian level winds. Within the framework of the Architectural Institute of Japan (AIJ) (Tominaga et al., 2008b) and the European cooperation in the field of scientific and technical research (COST, 2007; Franke, 2006). The AIJ provides methods for predicting wind loading on buildings by RANS and LES while COST Action 732 (COST, 2007) outlined best practice guidelines for successful CFD simulations of wind flows in an urban environment using steady RANS equations. To this effect ASCE has also a task force which examines the potential use of CWE.

Wind loads and wind induced responses are affected in a complex way by several factors, such as oncoming wind characteristics (wind speed, turbulence intensity, integral length scales, etc.), topography and ground roughness, immediate surroundings, building shape, orientation, and dynamic structural properties (for flexible buildings). Hence, before getting to the wind load evaluation phase any CWE modeling should make an

effort to incorporate these factors in the modeling process as realistically as possible to produce a usable outcome, just as is typically done in wind tunnel experiments. It is important to adopt/develop numerical models that realistically represent the complexity of the flow encountered while evaluating wind loads on buildings characterized as "bluff bodies" and submerged in a turbulent ABL flow. Because of this, challenges remain in numerically analyzing transient flow fields around bluff bodies. With this in mind, major aspects of numerical wind evaluation focusing on turbulence modeling, computational domain (CD) and boundary conditions (BCs) will be discussed in the following sections. Existing numerical work on low- and high-rise buildings from literature and authors' own work will be compared among each other and with the experimental data. It is to be noted that the scope of this paper does not include non-conventional winds such as tornado and downburst.

2.2 Turbulence models

Choosing the right type of turbulence model is essential for accurate wind load evaluation. The selection of turbulence models is carried out by considering computational cost, level of modeling and resolution, and flow unsteadiness. The RANS and Reynolds Stress Model (RSM) have been widely used to simulate wind flow around bluff-bodies in the early stage of CWE. Encouraged by the increased computing power, the present trend in the modeling of complex wind/structure interactions are characterized by the desire to capture the unsteady turbulent motion, primarily to resolve the large-scale motions in time and space. Thus, Direct Numerical Simulation (DNS) and LES are better suited for such type of simulations. The multi-scale aspect and the concept of the kinetic energy cascade often describe the nature and complexity of turbulent flow. All the

relevant active turbulence scales can be accurately represented by the DNS method without involving any modeling assumptions. In this method the total number of computational nodes may be scaled as (Re_L^3), where Re_L denotes the *Re* number based on the spatial integral length. The presence of solid walls in the flow and the high magnitude of the relevant *Re* number ($10^5 - 10^8$, typical of tall buildings) substantially increase the computational cost and making DNS unpractical for wind load evaluations. Hereafter only LES and RANS or a combination of them will be discussed. Recently, the Hybrid method which includes a combination of RANS with LES (RANS-LES), very large-eddy simulation (VLES), and Partially Averaged Navier Stokes (PANS) equations is emerging as an alternative. Figure 2.1 shows the classification of unsteady turbulence modeling approaches according to the level of modeling and readiness. The hybrid RANS-LES falls in the middle of the modeling and readiness level.

2.2.1 The RANS models

Averaging of N-S equations in time and space can reduce the physical complexity of turbulent flow. Time averaging (steady RANS) or ensemble averaging (URANS) of N-S equations eliminate or partially eliminate the time dimension and produce mean flow characteristics. RANS based on linear eddy-viscosity models have been widely used in CWE applications. Various modifications and new modeling concepts have been developed, ranging from ad hoc remedies (empirical tuning of a set of constants), complex non-linear-eddy-viscosity approaches (NLEVM) to multi-equation and multi-scale second-moment closures, particularly for flows characterized by strong three-dimensional turbulence in which mean flow information is not sufficient enough to

accurately predict unsteady flow behaviors (Hanjalić and Kenjereš, 2008). However, oversimplified assumptions and the failure of the RANS modeling to capture some of the key phenomena (for example flow separations and reattachment for flow past a building) have limited its application for wind load evaluations. For wind–resistant design of an actual building, the use of RANS is limited to estimating time-averaged forces on the building, i.e. along-wind load (Tamura et al., 2008; AIJ, 2004a; AIJ, 2005). In the work of Hanjalić and Kenjereš (2008) some of the new advancements of RANS models aimed at robust application of realistic flows, in line with treatment of wall functions, have been discussed. Some of these new developments are identified as unsteady RANS, Multi-scale RANS, transient RANS, VLES and hybrid RANS/LES (Hanjalić, 2005). Even though, RANS is assumed to be the main strategy to drastically reduce computational cost, researchers are migrating from the traditional RANS modeling approach to advance turbulence modeling such as LES and Hybrid methods (Spalart, 2009).

2.2.2 Large eddy simulation

As pointed out in the introduction, wind flows around buildings are complex, three dimensional, highly unsteady, and primarily characterized by high *Re* numbers and flow separations and reattachments "bluff bodies". This result is significant in scale separation between the large-scale energy carrying structures and the small-scale dissipative eddies. Experience based knowledge showed that the calibration techniques in RANS, time and ensemble averaging, are very questionable for such flows. Decomposition of the resolved velocity field, prior to scale separation into "large-scale" and "small-scale" partitions, and the construction of a sub-grid stress tensor based on this decomposition is the foundation of the multi-scale approach of LES. LES offers a more

comprehensive way of capturing unsteady flows. The dynamics of the large-scale structures are resolved, while the effect of small-scale turbulence is modeled using a sub-grid-scale (SGS) model. These basic strategies resolve most of the turbulent kinetic energy (κ) of the flow and model the dissipation (ε) which are assumed to have a weak effect (see Fig. 2.2) (Walters and Bushan, 2005; Tucker and Lardeau, 2009; Frölich et al., 2008).

LES modeling works well for high-*Re* number flow away from wall boundaries. However for an attached wall boundary where detailed near-wall treatment is required to capture the scale of motion responsible for turbulence production, a very large number of grid points and very small time steps are needed (Spalart, 2009). For example, in the classical LES approach the wall units $\Delta x^+ \approx 50$, $\Delta y^+ \approx 1$, $\Delta z^+ \approx 15$ are used to capture the excited length and time-scales of turbulence near-wall regions (Sagaut and Deck, 2009). However, for an attached wall boundary where detailed near-wall treatment is required to capture the scale of motions responsible for turbulence production, high resolution both in space and time is needed (Spalart, 2009) suggested that the level of resolution is attainable approximately in the year 2045. To alleviate the high computational cost of LES simulations, researchers suggested the hybridization of LES and RANS methods. While the free shear flow region with massive separation is treated by LES, the boundary layer is treated with RANS (Terracol et al., 2001). Recent studies by Grinstein and Drikakis (2007) showed that there is a growing interest in the implicit LES (ILES) method, particularly for external flows around buildings (Patnaik et al., 2007). In this method no subgrid scale (SGS) model is required for unresolved scales. In

the standard SGS model this is done by setting the Smagorinsky constant (C_s) to zero. The influence of the unresolved scales on the resolved scales is accounted for by the numerical dissipation of the discretization scheme of the convective terms in the momentum equations. The essential feature is that the numerical dissipation mimics sufficiently well the physical process of dissipation of the turbulent eddies.

2.2.2.1 SGS model in LES

In LES simulation, subgrid-scale stresses resulting from filtering operation of the N-S equations are unknown and requires modeling. Murakami (1997) reported the new trends in LES subgrid-scale modeling commonly applied for CWE applications. Since the introduction of the standard Smagorinsky SGS model (Deardorff, 1970), the dynamic Smagornisky-Lilly SGS model based on Germano et al. (1996) and Lily (1992) have become the standard of LES computation. The Smagornisky constant (C_s) is computed dynamically based on the resolved scales of motion. Later Kim and Menon (1997) proposed the dynamic SGS kinetic energy model arguing that the subgrid-scale turbulence can be better modeled by accounting for the transport of the SGS turbulence kinetic energy. This approach was reported to perform better than an algebraic expression based on the local equilibrium assumption given by the standard and dynamic Smagorinsky models (Huang et al., 2007).

2.2.3 Hybrid RANS/LES

Maintaining the balance between computational accuracy and computational cost is essential for turbulence modeling. The objection, i.e., because of high computational cost, of applying LES for the entire flow domain and the inadequacy of RANS modeling

to capture the fluctuating components of lead to an alternative method, the Hybrid LES-RANS. This hybridization is assumed to efficiently blend the best features of RANS and LES and has recently become an attractive proposition for boundary layer flow simulations (Fröhlich and Dominic, 2008). For pure LES simulation, the grid density increases with $Re^{1.8}$ in near-wall regions while in RANS grid clustering in the wall-normal direction is proportional to ln*(Re)* (Hanjalić et al., 2008). Hence, for flows where the attached boundary layer plays a dominant role in the flows, coupling of the models (LES and RANS) is arguably a better strategy to drastically reduce the computational cost of a stand-alone LES (Leschiziner, 2009; Tucker and Lardeau, 2009; Sagaut and Deck, 2009; Hanjalić et al., 2008). Hybrid LES-RANS has been applied in various field of applications ranging from aeronautical (Forsythe et al., 2006), ground vehicles (Spalart & Squires 2004), scalar transport in urban environment (Lien et al., 2008) (Sreenivas et al., 2006) to buildings (Camarri et al., 2005; Wilson et al., 2006; Song and Park, 2009).

The most common approaches in hybrid method are classified into two major classes, namely zonal (two-layer) and global (seamless) models. The zonal approaches are based on explicit splitting of computational domain into two distinct sub-domains and discontinuous treatment of RANS-LES interface. Coarse–grid LES is applied in the outer turbulent region, away from a solid wall, while a one-point RANS model is applied in the near-wall region. This is then coupled via appropriate boundary conditions at the RANS-LES interface (Sagaut et al., 2005; Hanjalić and Kenjereš, 2008). In the seamless approach instead of switching models at the RANS-LES interface, a continuous treatment of flow variables are applied throughout the solution domain. The respective turbulence models will be activated by changing length scales. RANS, in the near wall flow regime,

will be initiated using wall distance and LES in the outer turbulent region will be turned on using a representative grid size.

Despite the appealing feature of hybrid LES-RANS in reducing computational cost, there still remains some work to be done in both the "zonal" and "seamless" methods. For the zonal method, ensuring the proper matching of the conditions at the interface, location and definition of interface, and nature of matching condition are keys to it success. One way of attaining proper matching is by equaling the total stress or total viscosity. Since the RANS model contributes large portions of modeled quantities than LES, by either damping the eddy viscosity of RANS (using damping coefficient C_μ), decreasing RANS kinetic energy (increasing dissipation) the proper matching at the interface can be achieved (Hanjalić et al., 2004; Temmerman et al., 2005). Figure 2.3(a) illustrates the zonal method with a different interface location. In addition, the stochastic backscatter approach by Piomelli et al (2003); the addition of turbulent fluctuation by Davidson and Dahlstom (2004), and the use of instantaneous C_μ by Hanjalić et al. (2004) are some of the proposed approaches for the reduction of non-physical features at the RANS-LES interface. In seamless method the continuity of the model (i.e., gradient continuity of eddy viscosity) throughout the whole flow domain eliminates the need of a predefined interface. The "grid detecting" function controls the switching of the characteristic turbulence length scale L_{RANS} to L_{LES} (Fig. 2.3b). One of the most known hybrid approach under the seamless category is detached eddy simulation (DES) originally proposed by Spalart and Allmaras (1994), also called SA method. It applies a one-equation RANS modeling in the entire boundary layer while employing LES to

separated regions. Later, Spalart et al. (1997) applied a modification to the original model by using a local equilibrium assumption, in which the production term is balanced by the destruction term. This approach turns the one equation SA model into an LES subgrid-scale model in regions where the grid resolution is high, and as RANS in the coarse mesh region. The gray area between the boundary layer and massive separation usually causes problems. This is usually handled using DES limiter by synthesizing to the grid spacing, i.e., replacing the wall distance ($\tilde{d} = min(d, C_{DES}.\Delta)$, where $\Delta = max(\Delta x, \Delta y, \Delta z)$) by the filter width Δ will turn on LES (Travin et al., 2000; Breuer et al., 2003; Fröhlich and Terzi, 2008). It is to be note that numerous studies have exhibited that the DES fails to serve its intended purpose when applied to flows with thick boundary layers and shallow separation regions (Breuer et al., 2003; Sagaut and Deck, 2009).

Another challenge in the DES method is the mismatch of the mean velocity between the RANS and the LES region caused by the steep velocity gradient at the interface. In order to address this and other issues, recently a modified method called shielded and delayed detached eddy simulation (DDES) is proposed (Menter & Kuntz, 2002; Spalart et al., 2006). In the new approach the DES limiter depends on the solution, i.e., the length scale, and preserve RANS mode by delaying the activation of LES, irrespective of the grid spacing. As an alternative approach, Girimaji et al. (2003) suggested the Partially Averaged Navier-Stokes (PANS) method based on the ratio of unresolved to total kinetic energy (k) and dissipation rate (ε). The ease of its implementation into an existing RANS solver makes PANS a more attractive proposition for CWE application (Frohlich and Terzi, 2008). Although hybrid RANS/LES is showing promising progress in terms of balancing computational cost and prediction accuracy

more work needs to be done to address some of the challenges in merging RANS and LES. Based on the literature review and author's experience, LES is now a mature technique and is recommended for wind load evaluation application. In addition, the following numerical techniques contribute to the success of numerical wind evaluations: numerical generation of transient inflow turbulence (Kraichan, 1970; Lund et al., 1998; Nozawa et al., 2002, 2003; Smirnov et al., 2001; Batten et al., 2004; Huang et al., 2010); development of advanced sub-grid scale turbulence modeling techniques capable of solving unsteady three-dimensional boundary separated flows; and numerical discretization with conservation of physical quantities for modeling complicated geometry. Because of these LES holds promise to becoming the future CWE modeling option of where turbulent flow is of pivotal importance (Tucker and Lardeau, 2009; Sagaut and Deck, 2009).

2.3 Computational domain and boundary conditions

The computational domain (CD) defines the region where the flow field is computed. The size of the CD should be large enough to accommodate all relevant flow features that will have potential impact on the characteristics of the flow field within the region of interest. In most cases, the stretch of the CD in the vertical, lateral and flow direction depends on the type of boundary conditions used. Franke (2006) and COST (2007) suggested that for a single building of height H, vertically the domain should extend 3H to 4H above the roof level if smaller blockage and up to 10H if larger blockage is anticipated. Based on these recommendations and from author's previous experience, the CD that extends 5H upwind will ensure the ABL to develop fully. If the inlet boundary is too far from the study building, the turbulence fluctuation will dissipate,

this is true especially for wind load evaluation using LES, before it reaches to the study building. For RANS, the distance between the inlet and the incident plane should be long enough to preserve the mean velocity (U), the turbulent kinetic energy (k), and the turbulence dissipation rate (ε). The outflow/or outlet boundary should be at far enough distance to allow the wake development. Hence 15H downstream of the target building is recommended. Laterally it can extend 5H from the sidewall surfaces. For LES additional requirements should be also taken into consideration when sizing the CD for example whether it is large enough to accommodate the formation of the largest energy containing flow structures (COST, 2007).

Boundary conditions (BC) represent the effect of the surroundings that have been cut off by the CD and idealize the influence of the actual flow environment under consideration. BCs could dictate the solution inside the CD and have significant effects on the accuracy of the solution. At the inlet boundary, the mean wind velocity profile can be prescribed using either the power law or log-law profile. As a good practice a preliminary CFD simulation of an empty computational domain that accurately represents the ABL flow field should be performed by incorporating the measured flow data at the inlet boundary through numerical modeling (Blocken et al, 2007) (Fig.2.4) . For velocities, no-slip boundary is commonly used at solid walls (COST, 2007). Although researchers have commented on the inadequacy of a smooth wall assumption, because of its relative ease of implementation, it is common to see simulations using this assumption (Tominaga et al., 2008a; Yoshie et al., 2007). For LES simulations, Murakami (1998) discussed the ineffectiveness of the no-slip boundary when applied to a bluff body with high *Re* and advised the use of the Werner and Wengle (1991) wall function. One

approach to address surface roughness issues is to evaluate the shear stress from the logarithmic relationship incorporated in the momentum equation between the wall and the first grid point (Mochida et al., 2002; Bitsuamlak et al., 2005). Blocken et al. (2007) who reviewed works of various researchers also emphasized on the effect of surface roughness in generating a homogeneous mean velocity profile and turbulent kinetic energy for RANS simulation. Symmetry boundary condition is usually employed at the top and lateral surfaces. Since details of the flow variables are not known prior to the simulation, an outflow boundary is usually applied at the outlet plane.

2.4 Sources of wind inflow data for inlet boundary conditions

2.4.1 Target mean wind speed and turbulence intensity

Mean wind speed and turbulence intensity information at the study building location is obtained from meteorological data sources. Other common sources are building codes and standards. For example, ASCE 7-05 provides a 3sec gust basic design wind speed map for open terrain conditions at 33ft height, derived largely from meteorological stations at local airports. Field measurements and weather research forecasting (WRF) models (Skamarock et al., 2005) are also alternative sources. The ground surface roughness length is usually estimated by visually examining aerial photographs such as Google Earth photographs for each wind direction in comparisons with representative pictures given in building standards and codes. For inhomogeneous upwind terrain conditions and city centers this task is even more complicated. Some BLWT consulting firms, for example, use the Engineering Science Data Unit (ESDU) approach (ESDU 1993a and 1993b). The mean wind speed values could be expressed in the form of logarithmic (Eq. (1)) or power law (Eq. (2)) equations. Target turbulence

statistics such as length-scale and turbulence intensity should be used as input as well. The turbulence intensity is defined as the ratio of the root mean square (σ_u) to the mean wind speed $(U(z)), I(z)=\sigma_u / U(z)$. Figure 2.5(b) shows a typical streamwise velocity and turbulence intensity profiles for an open exposure. Figure 2.5(c) and (d) show the typical streamwise velocity time history and power spectrum at the building height.

$$U(z)=\frac{1}{\kappa}u_* ln\left(\frac{z}{z_0}\right) \tag{2.1}$$

$$U(z)=u(z_g)(z/z_g)^{\alpha} \tag{2.2}$$

where κ is the von Karman constant ($\kappa \approx 0.4$), u_* is the frictional velocity, z is the height above the ground surface, z_0 is the roughness length, α is an exponent dependent upon roughness of terrain, z_g is the gradient height, and $U(z)$ is the mean velocity at z distance from ground.

2.4.2 Numerical generation of transient inlet boundary for LES

For transient numerical modeling, in addition to the mean wind speed and turbulent intensity profiles, the transient wind characteristics are required in order to produce the peak or *rms* wind load. The success of LES and RANS/LES-based wind engineering applications, which require the transient time-history of fluctuating wind fields, heavily depends on the generation of accurate inflow turbulence at the inlet boundary. Inlet boundary conditions of LES simulation, of high *Re* turbulent flow, should possess an accurate representation of oncoming inflow turbulence, satisfying prescribed spatial and temporal correlations (Kondo et al., 1997, 2002; Tamura, 2008).

In high Re flows, the grid spacing is usually too coarse to resolve any large component of the turbulent spectrum due to computational power limitations. This especially occurs very near the inlet boundary, where few cells are allocated in order to reduce computational cost; the majority of the cells are allocated to resolve boundary layers, flow separation and attachment wakes and recirculating regions. The objective of the inlet boundary conditions is to supply turbulence integral length and time scales relevant to the grid Δx, Δy, Δz, and the computational time step Δt. Thus for transient simulation (such as URANS, LES, hybrid RAN-LES, and DNS), the inflow turbulence should be generated in accordance with the spatial and temporal resolution of the inlet boundary.

Most often the inflow turbulence due to the fluctuating velocity components are generated artificially using various numerical methods (Smirnov et al., 2001; Tutar and Celik, 2007; Davidson, 2007). The inflow turbulent generator could use flow statistics from existing BLWT database as well. There are several techniques to generate turbulence fluctuations. Huang et al. (2010) and Tabor and Baba-Ahmadi (2009) discussed various methods commonly used for generation of inflow turbulence at the inlet boundary of LES and hybrid RANS/LES simulation. These include recycling methods; precursor databases; and synthetic turbulence methods also briefly discussed here for completeness.

For unsteady numerical modeling, in addition to the mean wind speed and turbulent intensity profiles, the transient wind characteristics are required in order to produce the peak or *rms* wind load. The success of LES-based wind engineering applications, which require the transient time-history of fluctuating wind fields, heavily

depends on the generation of accurate inflow turbulence at the inlet boundary. Inlet boundary conditions of LES simulations, of high Re turbulent flow, should possess an accurate representation of oncoming flow turbulence, satisfying prescribed spatial and temporal correlations (Kondo et al., 1997, 2002; Tamura, 2008). In high Re flow simulations, computational grids are usually distributed systematically to manage the computational cost. As a result, in most cases, the grid spacing becomes too coarse to resolve any large component of the turbulent spectrum. This especially occurs very near the inlet boundary, where few cells are allocated in the upstream domain; whereas the majority of the cells are allocated in near-wall regions to resolve boundary layers, flow separation and attachment wakes and recirculating regions. However, the objective of the inlet boundary condition is to supply turbulence integral length and time scales relevant to the grid ($\Delta x, \Delta y, \Delta z$) and the computational time step (Δt). Thus, for transient simulation (such as URANS, LES, hybrid RAN-LES, and DNS) in addition to using high quality grid cells, the inflow turbulence should be generated in accordance with the spatial and temporal resolution of the inlet boundary. For example the spectrum depends on integral length scale $L(z)$, which is a function of height. One of the following approaches can be adopted to generate transient inflow boundaries.

2.4.2.1 Precursor simulation

Here, the simulation generates a library of turbulence databases that possess required flow characteristics such as temporal and spatial correlations. Once the desired turbulence flow characteristics are reached to a statistically stationary state, a time sequence of a 2D velocity field data will be extracted and stored. The inlet boundary of the main calculation uses these stored fluctuations by reading a plane of inflow data per

time step (see Fig. 2.6(a)). This method is convenient when simulating inlet boundaries of small-scale high-resolution simulations from multi-scale CFD simulation that accounts the surface roughness of the upstream exposure directly (Bitsuamlak and Simiu, 2010). Geographic Information System (GIS) applications such as LIDAR data, height of each structure and location-specific geographical information, that reflects realistically, the complexity of upwind roughness in urban areas and complex upwind terrain are very instrumental (Fig.2.7). Although computationally expensive, the use of numerical simulations on roughness geometry defined by LIDAR representing different exposure conditions on the upstream flow domain produced realistic inflow conditions at the inlet boundary (Abdi and Bitsuamlak, 2010).

2.4.2.2 Recycling method

The recycling method is based on the Lund et al. (1998) proposal where the CD is divided into two domains. The domain upstream of the calculation domain, also called the "driver domain", is used to generate spatially developing boundary layer flow. This is usually done by re-scaling the instantaneous velocity at the recycling plane and remapping the flow back to the inlet boundary. Once the simulation is performed for enough through-times and flow statistics are stable, a plane of data will be stored for later use by the main simulation. For the case where a combined simulation is carried out, the "calculation domain" will use the plane of data generated on the fly by the "driver domain" (see Fig. 2.6(b)). Nozawa and Tamura (2002) subsequently extend Lund's method and employed it to a rough-wall boundary-layer flow. They applied this technique to simulate LES of flow around low-rise buildings immersed in a turbulent boundary layer flow and demonstrated that the mean and *rms* pressure coefficients were

in good agreement with the BLWT data. Kataoka and Mizuno (2002) further simplified Lund's method by assuming the growth of the inner boundary layer thickness is insignificant and assuming it is constant. Hence, instead of recycling the whole value of instantaneous velocity components only the fluctuating components are recycled. The velocity components at the inlet boundary are given as follow

$$u_{inlet}(y,z,t)=\langle u\rangle_{inlet}(z)+\phi(\theta)\times\{u(y,z,t)-\langle u\rangle(y,z)\}_{recy} \tag{2.3}$$

$$v_{inlet}(y,z,t)=\phi(\theta)\times\{v(y,z,t)-\langle v\rangle(y,z)\}_{recy} \tag{2.4}$$

$$w_{inlet}(y,z,t)=\phi(\theta)\times\{w(y,z,t)-\langle w\rangle(y,z)\}_{recy} \tag{2.5}$$

where the parenthesis $\langle . \rangle$ denotes a time-averaged value in the span-wise direction and $\langle u\rangle_{inlet}$ is the prescribed mean velocity profile. The damping function $\phi(\theta)$ which prevents development of the turbulence in the free stream is given by

$$\phi(\theta)=\frac{1}{2}\left\{1-\frac{tanh\left[8.0(1-\theta)/(-0.4(\theta-0.3)+0.7)\right]}{tanh(8.0)}\right\} \tag{2.6}$$

where $\theta = z/z_G$, z is the height, and z_G is the gradient height.

Inhomogeneous anisotropic inflow fluctuation fields can be generated by superimposing Lund's recycling method with an artificially generated random perturbation for example by using the weighted amplitude wave superposition method (WAWS) (Swaddiwudhipong et al., 2007). The WAWS method is based on Shinozuka, (1985) where a fluctuation velocity field is generated from samples of a single random Gaussian process with zero mean and prescribed model energy spectral. For CWE

application the wind energy spectrum in each direction is assumed to be described by the von Karman model spectrum (Simiu and Scanlan, 1996).

$$u'(t)=\sqrt{2}\sum_{k=1}^{N}\sqrt{S_u(f_k)}\Delta f\cos(2\pi f_k t+\varphi_k) \tag{2.7}$$

where $S_u(f_k)$ is the one-sided von Karman spectral model of $u'(t)$, $f_k, k=1,...,N$ are the central frequencies of the interval Δf, and φ_k is the random phase angle uniformly distributed from 0 to 2π.

2.4.2.3 Synthesized turbulence

The synthesized turbulence fluctuation generation method proposed by Kraichnan (1970) uses an arbitrary energy spectrum as a function of a wave number to produce an isotropic perturbation. Inhomogeneous and anisotropic fluctuations have been investigated by various researchers (Smirnov et al., 2001; Batten et al., 2004; Billson et al., 2004), where the fluctuations were scaled in such a way that the time-averaged synthesized fluctuations match a prescribed Reynolds stress tensor. Smirnov et al. (2001) modified Kraichan's method by incorporating turbulence length- and time -scales and succeeded in generating divergence-free fluctuations by synthesizing the velocity vector field from summation of the Fourier harmonic. A brief presentation of the random flow generation technique is given as follows

$$u_i(\tilde{x},t)=\sqrt{\frac{2}{N}}\sum_{n=1}^{N}[p_i^n\cos(\tilde{k}_j^n\tilde{x}_j+\omega_n\tilde{t})+q_i^n\sin(\tilde{k}_j^n\tilde{x}_j+\omega_n\tilde{t})] \tag{2.8}$$

where $\tilde{x}_j$, $\tilde{t}$ are scaling parameters for the length- and time-scale of turbulence, k_i^n and ω_n are sample of wave number vectors and frequencies of the modeled turbulence

spectrum, respectively. The Gaussian model spectrum employed in this method is expressed as

$$E(k) = 16(2/\pi)^{1/2} k^4 \exp(-2k^2) \tag{2.9}$$

The spectrum model is mainly designed to represent the large energy carrying structures and thus undermine the eddies within the inertial subrange (as shown in the shaded region of Fig. 2.8). However, turbulent ABL flows have demonstrated a cascade of energy between turbulent eddies. In such flow the inertial sub-range plays a vital role in transferring energy from large-energy containing range to small-scale eddies of dissipation range. The small-scale eddies in the dissipation range are in the same order of Kolmogorov scale (η) and the energy will eventually be converted to internal energy and dissipate. Considering the modeling principles of LES, i.e. resolving the flow up to the filtering (grid size) and modeling small-scales, the length-scale of inertial sub-range lies between the integral length scale and Kolmogorov scale and their contribution is very significant. For example the ANSYS Fluent 13 package has implemented this technique as a Spectral Synthesizer for generation of inflow turbulence at the inlet boundary of unsteady simulations. Hence, for computational wind engineering applications such as the wind effect on structures submerged in the ABL region, the inflow fluctuations should be representative of a realistic turbulence spectrum such as the von Karman spectrum model (Lumley and Panofsky, 1964; Li et al., 2007).

Later Huang et al. (2010) extended Kraichnan's (1970) synthesizing technique to generate inhomogeneous inflow turbulence. The method, which is called the discretizing and synthesizing random flow generation (DSRFG) has the flexibility to prescribing any

arbitrary 3D spectrum for the amplitude of the fluctuation, for example the von Karman spectral. The synthesized velocity field is presented below for discussion purposes and the detailed formulation and derivation can be found in the original paper

$$u(x,t)=\sum_{m=k_0}^{K_{ma}}\sum_{n=1}^{N}[\,p^{m,n}\cos(\tilde{k}^{m,n}\tilde{x}+\omega_{m,n}t)+q^{m,n}\sin(\tilde{k}^{m,n}\tilde{x}+\omega_{m,n}t)] \tag{2.10}$$

where $p^{m,n}$ and $q^{m,n}$ are the vector form of the fluctuation amplitude. For inhomogeneous and anisotropic turbulence the distribution of $k^{m,n}$ is done by remapping the surface of the sphere after the components of $P^{m,n}$ and $q^{m,n}$ are aligned with the energy spectrum.

In addition to the flexibility of prescribing any arbitrary 3D spectrum, the DSRFG method uses the length scale ($L_s=\sqrt{L_u^2+L_v^2+L_w^2}$) as a scaling factor and this resulted in the generation of spatially correlated flow fields with the relevant length scales. However, the method is M times expensive compared to the method proposed by Simirnov et al. (2001), where M is the number of discretization points.

Castro et al. (2011) pointed out some of the limitations on the DSRFG technique and suggested some modifications for the inhomogeneous and anisotropic field of the DSRFG method. In the DSRFG method the representation of the kinetic energy using diverging series and the quality of the generated flow field is heavily dependent on the number of discretization point M . The other is regarding the temporal correlation of the flow field generated by the DSRFG method. To address these issues the study proposed

some modifications to the equations based on the shape of the energy spectrum. The formulation for the modified DSRFG also called MDSRFG method is presented as follow

$$u(x,t)=\sum_{m=1_0}^{M}\sum_{n=1}^{N}[\,p^{m,n}\cos(\tilde{k}^{m,n}\tilde{x}+\omega_{m,n}\frac{t}{\tau_0})+q^{m,n}\sin(\tilde{k}^{m,n}\tilde{x}+\omega_{m,n}\frac{t}{\tau_0})] \tag{2.11}$$

$$p_i^{m,n}=sign\left(r_i^{m,n}\right)\sqrt{\frac{4c_i}{N}E_i(k_m)\Delta k_m\frac{\left(r_i^{m,n}\right)^2}{1+\left(r_i^{m,n}\right)^2}} \tag{2.12}$$

$$q_i^{m,n}=sign\left(r_i^{m,n}\right)\sqrt{\frac{4c_i}{N}E_i(k_m)\Delta k_m\frac{1}{1+\left(r_i^{m,n}\right)^2}} \tag{2.13}$$

where τ_0 is time scaling parameter and $\boldsymbol{c}_i$ is a function that depends on the shape of the energy spectrum. The comparative studies on the inhomogeneous velocity fluctuation generated by the two methods are shown in Table 2.1. As it can be seen, in Table 2.1, although both the proposed methods, resulted *rms* value comparable to the target value, calculated as $TI*U_{avg}$, the MDSRFG method showed considerable improvement. Both methods with aligning and remapping techniques produced anisotropic flow field with strong spatial correlations, while MDSRFG showed better temporal correlation of the turbulence field.

2.5 The need for CWE validation with experimental data

CWE applications are at a fairly young stage, it would be prudent to evaluate their prediction accuracy through comparison with experimental laboratory as well as field measurements data. As described in Fig. 2.9, both full-scale and model-scale experiments could be used for validating CFD results of low- and high-rise buildings. In general, it is worthwhile to stress that comparing numerical simulations with experimental data should

be carried out with full knowledge of basic facts such as wind flow field, the surrounding conditions, and exposure type. Steady and fluctuating wind forces (along- and across-wind) computed from a time history of pressures is very sensitive to data averaging length (Obsaju, 1992). This is also true when applying LES for such evaluations, hence averaging time comparable with experimental data should be taken. Hence, the level of validation of these simulations should involve well sampled statistical analysis (Sagaut and Deck, 2009). Table 2.2 summarized grades of various levels of validation.

2.6 Computational evaluation of wind load on buildings

2.6.1 Illustration of wind pressure loads on surface mounted cube

For testing and validating the accuracy of computational evaluations of wind pressures, the majority of numerical studies refer to the basic cube shape exposed to wind perpendicular to its face (Stathopoulos, 2002 and 2003). This is because the cube has a simple geometry with important complex features of a real building flow and abundant full-scale and experimental results available in literature. Figure 2.10 shows numerical and experimental studies of the surface mounted cube, Silsoe 6m cube, by several researchers. Wright and Easom (2003) compared the mean pressure coefficient on the surface of the Silsoe cube using standard $k-\varepsilon$, RNG $k-\varepsilon$ models (Yakhot et al., 1992) derived from the renormalization group of analysis of Navier-Stokes equations and MMK $k-\varepsilon$ (Tsuchiya et al, 1997), which intends to improve the prediction of turbulent kinetic energy and eddy viscosity for a bluff body field, and DSM (Differential Stress Model) of Launder et al. (1975), which is a more complex anisotropic turbulence model. The prediction by RNG $k-\varepsilon$, especially in the windward face where the standard $k-\varepsilon$ model over-estimates the suction pressure, is in better agreement with the BLWT data.

The revised $k-\varepsilon$ models have improved the prediction accuracy on the separation region. However such adjustments are of an ad hoc nature and added improvements are only for some particular cases. Lim et al. (2009) C_P values obtained through LES simulation showed better agreement with the experimental data.

Köse and Dick (2010) investigated the performance of RANS, hybrid RANS/LES, and implicit LES (ILES) turbulence models on coarse meshes. For the cases with coarse meshes, the study showed no significant differences between the results of the RANS and hybrid (DED SST) simulations, as shown in Fig. 2.11. In the case of the hybrid model, the poor prediction of the mean C_P at the front and side faces is attributed to the fact that the LES model in the outer region failed to behave as a pure LES. This is attributed to the coarseness of the grid used in the simulation. Considering the coarseness of the meshes used in the simulations, both the LES and ILES were reported to give better results. Figure 2.12 shows CFD and experimentally obtained pressure coefficients at 45^0 wind angle of attack (Wright and Easom, 2003). As expected the standard $k-\varepsilon$ appears to over predict the mean C_P, although the error seems to be reduced as compared to the prediction for the cube with the normal wind angle of attack, because of the reduced flow impingement.

2.6.2 Illustration of wind pressure loads on low-rise buildings

Several numerical studies have been reported for wind load evaluation of low-rise buildings. Tsuchiya et al. (1997) and Nozawa and Tamura (2002) predicted the mean pressure coefficients of short buildings with a size of H: H: 0.5H. Figure 2.13 shows the distribution of time-averaged pressure coefficients on the mid vertical plane of a low-rise

building. Because of the impinging flow, the approaching flow did not separate from the leading edge of the roof, the standard $k-\varepsilon$ overestimates the C_p value on the frontal face. On the other hand, the approaching flows simulated with the modified $k-\varepsilon$ models, $\kappa-\varepsilon-\varphi$ (Kawamoto et al., 1998), and the *MMK* model (Tsuchiya et al., 1997) were separated from the leading edge of the roof and they resulted an improved prediction of the mean C_p at the windward face that were in closer agreement with the experiment data carried by Kondo (1997). Another noticeable observation is that, in all the $k-\varepsilon$ models the absence of velocity fluctuation due to vortex shedding effect, produced in smaller production of kinetic energy behind the building. While the LES simulation by Nozawa and Tamura (2002) well predicted the pressure coefficients on the surfaces of the building. However, the same study reported that the discrepancy in the inlet velocity profile caused the LES to overestimate *rms* coefficients on the roof.

The TTU building is considered to be one of the extensively studied standard short buildings for wind loads. Senthooran et al. (2004) evaluates the wind-induced pressure fluctuation of TTU using Kato and Launder's (1993) modified $k-\varepsilon$ turbulence model. The stochastic technique is used to generate the inflow turbulence fluctuation. The revised *MMK* model (Launder and Kato, 1993), which eliminates the excessive production of kinetic energy around the impinging region performed better and the results are in a good agreement with the experimental data and field results (Fig. 2.14). Recently, Köse and Dick (2011) performed an implicit LES (ILES) and LES simulations to investigate the influence of inflow conditions on the quality of the mean pressure distribution on the same building. Figure 2.15 compares the LES and ILES prediction

along the centerline of a vertical plane of the TTU. Improvements on the mean C_P value have been observed after adjusting the inflow turbulence by reducing the kinetic energy. In both studies (Selvam, 1997; Köse and Dick, 2011) there was a considerable discrepancy between the numerical and the BLWT prediction, particularly the overproduction of the mean C_P at the windward face and roof surfaces. The overproduction is mainly caused by strong deformation of the oncoming flow velocity profile in the incident region. This shows how the wind pressure load distribution is sensitive to the incoming turbulence.

There is also an effort towards using the Partially Averaged Navier-Stokes (PANS) turbulence modeling for wind effect evaluation which is regarded as an alternative to the hybrid RANS/LES. The PANS modeling aims to capture/or resolve the energy containing structures at a reasonable computational cost, by using coarse computational meshes. The method uses the Boussinesq approximation technique for modeling the unresolved-scales (Abdol-Hamid and Girimaji, 2005). Song and Park (2009) carried out a two-stage PANS simulation to evaluate the wind- pressure load on a square cylinder. Figure 2.16 shows their PANS simulation, for various grid resolution cases, fairly predicted the mean C_P of the windward face, while it slightly over-predicted the pressure distributions on the sidewalls. The case with fine grids reproduced the velocity in the wake and recirculation region very well and resulted in an accurate prediction of the mean C_P on the leeward face and the mean drag coefficient by the high resolution simulation. The PANS method seems heading in the right direction in addressing some of the grid dependence issues related to hybrid RANS/LES turbulence

modeling. Although C_P comparison with the hybrid RANS/LES and LES would have provide more insight on the cost effectiveness and prediction accuracy of PANS.

Overall the CFD results showed reasonable agreement with the measured BLWT and field data for time-averaged wind loads on low-rise buildings. However, more work is needed regarding the peak- wind load estimation using the some of the models such as LES. Numerical research should also look into how well the peak-loads compare with the experimental data in addition to the mean and *rms* values. As this will give strong ground for CWE application for design wind load evaluation.

2.6.3 Wind load estimation on high-rise buildings

The Commonwealth Advisory Aeronautical Research Council (CAARC) building model (Melbourne, 1980) is used by several wind engineering experimental laboratories for calibration and validation purposes to study external aerodynamic loads of tall buildings. The CWE community is also using the same model to assess the performance of numerical wind load evaluation techniques for tall buildings. As part of this review study, the authors carried out a limited investigation for various inflow turbulence generation techniques for LES. Figure 2.17 presents the LES and wind tunnel data for the mean pressure coefficient acting on the wind- and lee-ward faces of the CAARC building model, produced by using the various numerical methods in Sec. 2.1.3.1). The BLWT test was carried out at RWDI Inc. The pressure coefficient distributions agree well with each other even from a quantitative point of view. On the wind-ward face, the LES mean C_p contours estimated by the three inlet boundaries (Inflow 1: Smironv et al. (2001); Inflow 2: Lund et al. (1998); Inflow 3: following synthesizing method) showed a good

agreement with the BLWT data. The LES predictions of the mean C_p for the lee-ward face showed marginal discrepancy with the BLWT, compared to the better agreement observed for wind-ward face. Among, the three inflow conditions, Inflow-3 was marginally performing better than the Inflows-1 and -2 predictions. The distributions of fluctuating pressure coefficients presented in Fig. 2.18. The *rms* produced by the Inflow-3 on the wind-ward face, a place where the inflow fluctuation effect could be seen more apparently (compared to other faces which potentially experience more fluctuation due to flow separation) was in better agreement with the BLWT's *rms*. On the lee-ward face, the numerical result slightly deviated from the BLWT data. Although superimposing random fluctuations on a mean velocity profile (for example Inflow-1) is a simple way of generating inflow turbulence, the turbulence has weak spatial correlation and tends to decay rapidly (Kempf et al., 2005). The authors further investigated the effect of inflow turbulences on the dynamic wind load evaluation of a standard tall building using LES. It has been found that the fluctuating wind loads are very sensitive to perturbation imposed at the inlet boundary. Random inflow turbulence generated using the synthetic inflow generation technique showed a good spatial correlation of the fluctuating velocity component and the resulted predications were reasonably comparable with the BLWT data, especially the across-wind force spectra (Fig. 2.19). The along-wind force spectra also showed promising results, however better results could have been obtained if a longer averaging time was taken for the pressure time-history analysis of the LES simulation. For this study only two seconds (flow time) of data was recorded, because of computational resource limitation, and this greatly contributed to the discrepancy of the drag force compared to the BLWT data. Moreover, inhomogeneous turbulence with the

von Karman spectrum better represents a realistic wind flow field and will significantly improve the prediction accuracy of LES. The authors are working at the moment on LES of a tall building under urban settings using the synthesized techniques of a random flow generator (such as DSRFG) as inlet boundary.

The comparison between the mean pressure coefficients of several computational (LES and RANS) and experimental studies of the CAARC building model extracted at $2/3$ of H (H is the height of CAARC building model) is shown in Fig. 2.20. On the wind-ward face the RANS based on the RNG $\mathrm{K}-\varepsilon$ model over-predicted, as expected, the mean C_p while the LES showed a better agreement with the BLWT data. Considerable discrepancy has been observed at the side face, where the flow separated because of the sharp corner. Similar studies (Huang et al., 2007, Braun and Awruch, 2009) showed a good C_P prediction at the wind-ward face but a slight deviation in the side and lee-ward faces from the BLWT measurements have been observed. This discrepancy is due to the random inflow turbulence generated using the Gaussian spectrum model which under-estimated the eddies in the inertial subrange (as discussed in Sec. 4.4.3) and the assumption of the no-slip wall boundary condition used in the simulation. Dagnew et al. (2009) investigated the effect of the grid resolution for LES under turbulent flow. The case (LES1) with a high resolution mesh ($1 < y^+ < 5$) in the near-wall region resulted in a better prediction, especially in the windward face, with the BLWT data than the case (LES2) with Werner and Wengle (1991) wall function applied in the near-wall region. Hence it is a good practice to resolve the flow in the region of interest, such as the wall boundary and upwind domain.

Nozawa and Tamura (2003) predicted the time-averaged pressure coefficients on a high-rise building (1:1:4) using an LES simulation (see Fig. 2.21(a)). Inflow turbulence was generated at the inlet boundary using a modified recycling method. This improved the numerical prediction of the mean pressure coefficient on the frontal surface of the high-rise building and the results are in good agreement with the BLWT data done by Ohtake (2002) and Kawai (1982). Figure 2.21(b) shows the *rms* of pressure coefficients of the same study. There is a discrepancy in the *rms* coefficients on the roof of the high-rise building, this deviation was caused by a variation in the mean velocity profile. Tamura et al. (2008) presented the AIJ guidelines to the numerical prediction of wind loads on a building. The wind load on low-rise (1:1:0.5) buildings predicted by CFD was compared with those obtained from experiments and AIJ recommendations.

Figure 2.22(a) and (b) show the comparison between numerical and experimental design loading on the structural frame and cladding of a typical short building. The LES overestimated both the structural frame and cladding loading compared to the experimental result. The over-estimation of the wind loads is associated mainly to the insufficient reproduction of the inflow turbulence at the inlet boundary (Tamura, 2008). For the high-rise building (1:1:4) the LES well predicted the design wind loads and coincides well with the experimental results, as shown in Figure 2.23 and 2.24. The transient wind pressure analyses coupled with the realistic inflow turbulence modeling imposed at the inlet boundary were reasons behind the success of the LES results.

2.7 High performance computing for wind engineering applications

One of the main challenges with CFD applications is the amount of computational resources needed to perform the simulation. The computational cost increases

exponentially when attempting to perform large-scale simulations, for example a turbulent wind simulation in a city center requires a staggering amount of computational resources. This is traditionally handled by using parallel computations on a cluster of central processing units (CPUs) (more recently in combination with graphics processing units (GPUs)). The majority of the available CFD platforms follow this commonly used practice of parallelism. However, the cost of building such a facility could be very high. Hence, the application of CWE for realistic simulations of bluff-body aerodynamics with high Reynolds number (*Re)* numbers flow using advanced turbulence modeling LES has been limited and it still remain more costly than carrying a wind tunnel test. Recently, coupling the general purpose graphics processing units (GPGPUs) that are traditionally designed for graphic rendering purposes with the CPU have been considered as a potential cost-effective alternative of parallel computing for CFD simulations. Implementation of the mixed CPU-GPU techniques have resulted in a substantial speedup of computations (Thibault and Senocak, 2009; Tolke & Krafczyk, 2008). Selvam and Landrus (2010) reported that a decent size parallel computing facility with 40 processors configured with the traditional parallel platforms could cost up to $50,000 while using GPU computing technology which costs $300 could achieve same efficiency (10 to 20%). And a speed up factor of 10 to 100 could be acquired with a GPU that costs $100 to $10,000.

Hence, CFD toolboxes that can effectively exploit the hardware of personal computers have economical appeal for the CWE community. This is very encouraging progress towards addressing the computational cost issues involving bluff-body aerodynamics and industrial applications of CWE techniques. Currently there are large

number of high performance computing facilities (for example TeraGrid in the US and Sharcnet in Canada) where one can get access for research. Some private firms such as Amazon are also offering the sale of computing time to perform large-scale simulation

2.8 Conclusions and future avenues

The work of several researchers on computational evaluation of wind load both on low- and high-rise buildings have been revisited and key findings on selecting turbulence modeling techniques, boundary conditions, sizing of the computational flow domain, and the dynamics of high Reynolds numbers turbulent flows have been discussed. The significant progresses made in turbulence modeling, high performance computing and developments in novel parallel algorithms is allowing a high-resolution simulation of complex flows useful for wind load evaluation. Comparisons made between computationally obtained data with full-scale and model scale wind tunnel experiments showed good agreement, especially on the windward face. However, some discrepancies have been observed in the sidewalls and leeward face. These are mainly attributed to the resolution of the computational meshes and boundary conditions, such as oncoming flow. Numerical inflow turbulence generator that take into account the basic ABL flow statistics (such as TI, wind speed, integral length scale, and the time scale) performed well in reproducing a realistic wind flow field. The along-wind and cross-wind loads on the standard tall building model predicted by the LES simulation showed a good estimation with the experimental data. However, the torsional wind loads obtained by the LES simulation showed some discrepancy with the experiment. Among all the numerical methods considered, LES and hybrid RANS/LES showed a good agreement with the experimental data in most cases. It has also been observed that for wind load estimation

an accurate time-dependent analysis using LES is essential to produce a time-history of pressure fluctuation data, similar to what is being done in wind tunnel experiments. The pressure time-history data obtained from HFPI type LES simulation are very valuable for the estimation of peak-type quantities for the preliminary design of buildings.

The peak pressure values are essential wind load parameters in the design of roofs of residential and C&C of tall buildings. Hence enough length of data should be recorded to obtain a good quality of peaks from the LES simulation. However, performing such computationally demanding analyses are limited by current computational resource capabilities and as a result studies on peak pressures are missing from existing literature. It is also to be noted that the cost of performing LES at the moment still appears higher than conducting the BLWT test. Nevertheless, recent developments in the hybrid RANS/LES turbulence modeling show a promising future for CWE practical applications that involve very large projects. The majority of the studies on low- and high- rise buildings have mainly been limited to a single regular shape building for one wind direction. Further research by simulating buildings with more complex shapes, with interference of neighboring buildings, and for multiple winds including oblique wind directions will accelerate its use as a design tool.

References

Abdi, D., Bitsuamlak, G.T (2010), "Estimation of surface roughness using CFD simulation", The fifth International Symposium on Computational Wind Engineering Conference (CWE2010), Chapel hill, NC, May 23-27.

AIJ Recommendation for loads on buildings. (1996), *Architectural Institute of Japan, Japan.*

American Society of Civil Engineers, American National Standard: Minimum design loads for buildings and other structures, *ASCE 7-05*.

Ansys Inc. (2010), "Ansys Fluent 13 User's Guide", *Ansys Inc., Lebanon. 13.0.*

Architectural Institute of Japan, (2004a), "Recommendation for loads on buildings".

Architectural Institute of Japan (AIJ), (2005), "Guide for numerical prediction of wind loads on buildings".

AS/NZS 1170.2:2002, Australian/New Zealand Standard: Structural Design Actions Part 2: Wind Actions Standards.

Baker, C.J. (2007), "Wind engineering-Past, present and future", *J. Wind Eng. And Ind. Aerodyn. 95, 843-870.*

Batten, P., Goldberg, U., Chakravarthy, S. (2004), "Interfacing statistical turbulence closures with large-eddy simulation", *AIAA Journal 42(3), 485–492.*

Barone, M.F., Roy, C.J. (2006), "Evaluation of detached eddy simulation for turbulent wake applications" *AIAA Journal* 44 (12), 3062–3071.

Bitsuamlak, G.T., Stathopoulos, T., Bedard, C. (2000), "Progress on numerical simulation of wind load on buildings", *8th Annual Conference of the CFD Society of Canada (CFD2K).*

Bitsuamlak, G.T., Bedard, C., Stathopoulos (2005), "Numerical evaluation of wind flow over complex terrain using an object-oriented approach", *33rd Annual General Conference of the Canadian Society for Civil Engineering.*

Bitsuamlak, G.T., Dagnew, A.K., and Chowdhury, A.G. (2010), "Computational assessment of blockage and wind simulator proximity effects for a new full-scale testing facility", *Wind and Structures, An Int'l Journal* Vol. 13 No. 1, 21-36.

Bitsuamlak, G.T., Simiu, E. (2010), " CFD's potential applications: a wind engineering perspective", *The fifth International Symposium on Computational Wind Engineering Conference*, Chapel hill, NC, May 23-27.

Billson, M., Eriksson, L.E. and Davidson L. (2004), "Modeling of synthetic anisotropic turbulence and its sound emission", The *10th AIAA/CEAS Aeroacoustics Conference, AIAA 2004- 2857*, Manchester, United Kindom.

Blocken, B., Stathopoulos, T., Carmeliet, J. (2007), "CFD simulation of the atmospheric boundary layer: wall function problems", *Atmospheric Environment* 41, 238-252.

Braun, A.L., Awruch, A.M. (2009), "Aerodynamic and aeroelastic analyses on the CAARC standard tall building model using numerical simulation", *Computers and Structures* 87, 567-581.

Breuer, M, Jovici´c. N, Mazaev K. (2003), "Comparison of DES, RANS and LES for the separated flow around a flat plate at high incidence", *Int. J. Numer. Methods Fluids* 41:357–88.

Camarri, S., Salvetti. M.V., Koobus B., Dervieux A. (2005), "Hybrid RANS/LES simulations of a bluff-body flow", *Wind and Structures, An Int'l Journal Vol. 8 No. 6.*

Cermak, J.E. (2003) "Wind-tunnel development and trends in applications to civil engineering", *J. Wind Eng. and Ind. Aerodyn.91, 355–370.*

Chi-Su Song, SeungO Park. (2009), "Numerical simulation of flow past a square cylinder using Partially-Averaged Navier–Stokes model", *J. Wind Eng. and Ind. Aerodyn. 97–47.*

Castro, G.H., Paz, R.R., Sonzogni, V.E. (2011), "Generation of turbulent inlet velocity vonditions for large eddy simulations", *Mecánica Computacional* Vol XXX, pags, 2275-2288.

COST, (2007), "Best practice guideline for the CFD simulation of flows in the urban environment COST Action 732".

Davidson, L., Dahlstöm S., (2004), "Hybrid LES–RANS: an approach to make LES applicable at high Reynolds number *(CD) CHT-04, Proceedings of the International Symposium on Advances in Computational Heat Transfer, ICHMT, April 19–25,* Norway, Begell House Inc., USA (2004).

Davidson, L, (2007), "Using Isotropic Synthetic Fluctuations as Inlet Boundary Conditions for Unsteady Simulations", *Advances and Applications in Fluid Mechanics*, Vol. 1(1), pp. 1-35.

Dagnew, A.K., Bitsuamalk, G.T., Ryan, M. (2009), "Computational evaluation of wind pressures on tall buildings", *The11th American conference on Wind Engineering,* San Juan, Puerto Rico, June 20-26.

Dagnew, A.K., Bitsuamalk, G.T. (2010), "LES evaluation of wind pressures on a standard tall building with and without a neighboring building", *The Fifth International Symposium on Computational Wind Engineering(CWE2010),* Chapel Hill, North Carolina, USA May 23-27.

Davenport, A. G. (1967), ''Gust loading factors'', *J. Struct. Div*., ASCE, 93(3), 11–34.

Davenport, A.G. (2002), "Past, present and future of wind engineering", *J.Wind Eng. And Ind. Aerodyn.*90, 1371–1380.

Deardorff, J.W. (1970), "A three-dimensional numerical study of turbulent channel flow at large Reynolds numbers", *J. Fluid Mech.* 41, 453-480.

ESDU (1993a), "Strong winds in the atmospheric boundary layer, Part 1: mean hourly wind speeds", *ESDU Report 82026*, ESDU International.

ESDU (1993b), "Strong winds in the atmospheric boundary layer, Part 2: discrete gust speeds", *ESDU Report 83045*, ESDU International.

Forsythe JR, Strang WZ, Squires KD. (2006), "Six degree of freedom computation of the F-15E entering a spin", Presented *at AIAA Aerosp*. *Sci. Meet. Exhib. 44th, Reno,* Pap. No. AIAA-2006-0858.

Franke, J. (2006), "Recommendations of the COST action C14 on the use of CFD in predicting pedestrian wind environment", *In: proceeding of the forth international Symposium on Computational Wind engineering (CWE2006)*, Yokohama, Japan, July 16-19, pp. 529-523.

Frölich, J. & von Terzi, D. 2008 Hybrid RANS/LES methods for the simulation of turbulent flows. Prog. Aerosp. Sci. 44, 349–377.

Germano, M. U. Piomelli, P. Moin, and W. H. Cabot. 1996. Dynamic Subgrid-Scale Eddy Viscosity Model". In Summer Workshop. Center for Turbulence Research, Stanford, CA.

Gomes, M.G., Rodrigues, A.M., and Mendes, P. (2005) "Experimental and numerical study of wind pressures on irregular-plan shapes", *Jnl. of Wind Eng. Ind. Aerodyn*, 93, 741-756.

Grinstein, F.F., Drikakis, D. (2007), "Computing turbulent flow dynamics with implicit large eddy simulation", *J. Fluids Eng*. 129, 1481–1482.

Girimaji, S., Sreenivasan, R., Jeong, E., (2003), "PANS turbulence model for seamless transition between RANS, LES: fixed-point analysis and preliminary results", *In: Proceedings of ASME FEDSM'03 2003 fourth ASME-JSME Joint Fluids Engineering Conferences*, Honolulu, Hawai.

Girimaji, S., Abdol-Hamid, K.S., (2005), "Partially averaged Navier Stokes model for turbulence: Implementation and Validation", AIAA paper 2005-502.

Hanjalic´, K., Hadzˇiabdic´, M., Temmerman, L., Leschziner, M.A. (2004b), "Merging LES and RANS strategies: zonal or seamless coupling", *In: Friedrich, R., Geurts, B., Me´tais, O. (Eds.), Direct and Large-Eddy Simulations V. Kluwer Academic Publishers, Dordrecht,* pp. 451–464.

Hanjalic´, K. (2005), "Will RANS survive LES? A view of perspectives", *ASME J. Fluid Eng*. 27, 831–839.

Hanjalić, K., Kenjereš, S. (2008), "Some developments in turbulence modeling for wind and environmental engineering", *J. Wind Eng. and Ind. Aerodyn.*96, 1537–1570.

Huang, S., Li, Q.S., Xu, S. (2007), "Numerical evaluation of wind effects on a tall steel building by CFD", *Journal of Constructional Steel Research* 63, 612-627.

Huang, S.H., Li, Q.S., Wu, J.R. (2010), "A general inflow turbulence generator for large eddy simulation", *J. Wind Eng. and Ind. Aerodyn* 98, 600-617.

Huang, S.H., Li, Q.S. (2010), "Large eddy simulation of wind effects on a super-tall building", *Wind and Structures, An Int'l Journal* Vol. 13 No. 6.

Holscher, N., Niemann, H.J. (1998), "Towards quality assurance for wind tunnel tests: A comparative testing program of the Windtechnologische Gesellschaft", *Jnl. of Wind Eng. Ind. Aerod.*, 74, 599-608.

Irwin, P.A. (2008), "Bluff body aerodynamics in wind engineering", *J. Wind Eng. and Ind.Aerodyn.*96, 701–712.

Irwin, P.A. (2009), "Wind engineering challenges of the new generation of super-tall buildings*", J. Wind Eng. and Ind. Aerodyn* 97, 328-334.

Itoh, Y., Tamura, T. (2008), "Large eddy simulation of turbulent flows around bluff bodies in overlaid grid systems", *J. Wind Eng. And Ind. Aerodyn.* 96, 1938–1946.

Kawai, H., (1982), "Pressure on three dimensional prisms in a turbulent boundary layer", in*: Proceeding of the Seventh National Symposium on Wind Engineering*, pp. 67–74.

Kawamoto, S., Miyamoto, K., Tsuchiya, N., Ohtake, K., (1998), " Estimation of wind loading by computational fluid dynamics -Part2: High-rise building case", *In: Proceeding of AIJ Annual Meeting,* pp. 297–298.

Kataoka, H., Mizuno, M. (2002), "Numerical flow computation around aeroelastic 3D square cylinder using inflow turbulence", *Wind and Structure*, *An Int'l Journal* Vol 5 2–4, pp. 379–392.

Kato, M., Launder.B.E. (1993), "The modeling of turbulent flow around stationary and vibrating square cylinders"*, Ninth Symposium on Turbulent Shear Flows,* 1993, pp. 10.4.1–10.4.6.

Kempf, A., Klein, M., Janicka, J. (2005), "Efficient generation of initial- and inflow-conditions for transient turbulent flows in arbitrary geometries", Flow Turbulence Combust. 74, 67–84.

Kim, W.W., Menon, S., (1997), "Applicatio of the localized dynamic subgrid-scale model to turbulent wall-bounded flows", *Technical Report AIAA, 97-0210, Aerospace Science Meeting, Reno, NV American Institute of Aeronautics and Astronautics.*

Kuai, L., Haan F.L, Jr., William A. Gallus, Jr., Partha Sarkar P. (2008), "CFD simulations of the flow field of a laboratory-simulated tornado for parameter sensitivity studies and comparison with field measurements", *Wind & Structures, An Int'l Journal* Vol. 11 No. 2.

Kondo, K., Murakami, S., Mochida, A. (1997),"Generation of velocity fluctuations for inflow boundary condition of LES", *J. Wind Eng. and Ind.l Aerodyn.s* 67-68, 51-64.

Kondo, K., Tsuchiya M., Mochida A., Murakami S. (2002), "Generation of inflow turbulent boundary layer for LES computation", *Wind & Structures, An Int'l Journal* Vol. 5 No. 2.

Köse, D.A., Dick, E. (2010), "Prediction of the pressure distribution on a cubical building with implicit LES", *J .Wind Eng. and Ind. Aerodyn* 98, 628-649.

Kraichnan R.H. (1970), "Diffusion by a random velocity field", *Physics of Fluids*, **13(**1), pp. 22–31.

Launder, B.E., Reece, G.J., Rodi, W. (1975), "Progress in the development of Reynolds stress turbulence closure", *J. Fluid Mech*, 68, 537-566.

Launder, B.E., Kato M. (1993), "Modeling flow-induced oscillations in turbulent flow around a square cylinder", *ASME Fluid Eng. Conf*, **157,** pp. 189–199.

Levitan, M.L., Holmes J.D., Mehta K.C., Vann W.P. (1989), "Field measured pressures on the Texas Tech building", *Proceedings of the eighth Colloquium on Industrial Aerodynamics,* pp. 13–24.

Leschziner, M., Li, N. & Tessicini, F. (2009), "Simulating flow separation from continuous surfaces: routes to overcoming the Reynolds number barrier", *Phil. Trans. R. Soc. A* 367, 2885–2903.

Lien, F.S., Yee, E., Ji, H., and Hsieh, K.J. (2008) "Partially Resolved Numerical Simulation and RANS Modeling of Flow and Passive Scalar Transport in an Urban Environment", Special Issue of *J. Wind Eng. and Ind. Aerodyn.*, Vol. 96, pp. 1832-1842.

Li, C., Li Q.S., Huang S.H., Fu J.Y., Xiao Y.Q. (2010), "Large eddy simulation of wind loads on a long-span spatial lattice roof", *Wind and Structures, An Int'l Journal* Vol. 13 No. 1.

Lin, N. (2005), "Characteristics of wind forces acting on tall buildings", *J.Wind Eng. and Ind.Aerodyn.*93, 217-242.

Li, Q.S., Xiao, Y.Q., Fu, J.Y., Li, Z.N. (2007), "Full scale measurements of wind effects on the Jin Mao Building", *J. Wind Eng. and Ind. Aerodyn.* 95, 445–466.

Lim, C.H., Thomas, T.G., Castro, I.P. (2009), "Flow around a cube in a turbulent boundary layer: LES and experiment", *J. Wind Eng. and Ind. Aerody, 97, 96-106.*

Lilly, D.K., 1992, "A Proposed Modification of the Germano Subgrid-Scale Closure Model",. *Physics of Fluids*. 4. 633–635.

Lumley, J.L., Panofsky, H.A. (1964), "The Structure of Atmospheric Turbulence", *Wiley-Interscience*, New York, pp. 239.

Martinuzzi, R., Tropea, C., 1993. The flow around surface-mounted, prismatic obstacles placed in a fully developed channel flow. J. Fluids Eng. 115, 85–92.

Melbourne, W. H. (1980), "Comparison of measurements of the CAARC standard tall building model in simulated model wind flows", *Jnl. of Wind Eng. Ind. Aerodyn.* 6:78–88.

Menter, FR, Kuntz M. (2002), "Adaptation of eddy-viscosity turbulence models to unsteady separated flow behind vehicles", See McCallen et al. 2004, pp. 339–52.

Mochida, A., Murakami, S., Kato, S., Ishida,Y.(1993), "Numerical Simulation of flow field around Texas Tech Building by Large Eddy Simulation", *J. Wind Eng. and Ind. Aerodyn.* 46 & 47, 455-460.

Mochida, A., Murakami, S. (1999), "Past, present, and future of CWE: The view from 1999", *NST Report No. 14, 1999, pp. 104–117.*

Mochida, A., Tominaga,Y., Murakami,S., Yoshie,R., Ishihara ,T., R. Ooka,R., (2002), " Comparison of various k–ε models and DSM applied to flow around a high-rise building", -*Report on AIJ cooperative project for CFD prediction of wind environment*, *Wind and Structures, An Int'l Journal* Vol. 5, No. 2~4 , 227-244

Murakami, S. (1997), "Current status and future trends in computational wind engineering*", J. Wind Eng. and Ind. Aerodyn.* 67-68, 3-34.

Murakami, S. (1998), "Overview of turbulence models applied in CWE–1997", *J. Wind Eng. and Ind. Aerodyn.* 74-76, 1-24.

Murakami, S., Mochida, A., Kondo, K., Ishida, Y., Tsuchiya, M. (1998), "Development of new *k–ε* model for flow and pressure fields around bluff body", *CWE96, Colorado, USA, J. Wind Eng. Ind. Aerodyn.* 67&68, 169–182.

Murakami, S., Mochida, A., (1999), "Past, present, and future of CWE: the viewpoint from 1999", *In: Proceedings of the Tenth International Conference on Wind Engineering*, pp. 91–104.

"National Building Code of Canada 2005" issued by the Associate Committee on the National Building Code, National Research Council of Canada, Ottawa 2005.

Nozu, T., Tamura, T., Okuda, Y., Sanada, S. (2008), "LES of the flow around building wall pressures in the center of Tokyo", *J. Wind Eng. and Ind. Aerodyn.* 96, 1762-1773.

Nozawa, K., Tamura, T. (2002), "Large eddy simulation of the flow around a low-rise building immersed in a rough-wall turbulent boundary layer", *J. Wind Eng. And Ind. Aerodyn.* 90, 1151–1162.

Nozawa, K., Tamura, T. (2003), "Numerical prediction of pressure on a high-rise building immersed in a turbulent boundary layer using LES", *In: Proceeding of annual meeting of JACWE 95*, pp. 169–170.

Ning, Lin.N., Letchford.C.,Tamura,Y.,Bo Liang,B., Nakamura,O. (2005), "Characteristics of wind forces acting on tall buildings", *J. Wind Eng. and Ind. Aerodyn.93, 217-242.*

Okada, H., Ha Y.C. (1992), "Comparison of wind tunnel and full-scale pressure measurement tests on the Texas Tech building", *J. Wind Eng. and Ind. Aerodyn.* 43 1601–1612.

Patnaik, G., Boris, J.P., Young, T. R., Grinstein, F.F, 2007. Large scale urban contaminant transport simulations with MILES. *J. Fluids Eng.* 129, 1524–1532.

Rehm, R.G., McGrattan K.B., Baum H. R. (2002), "Large eddy simulation of low over a wooded building complex", *Wind and Structures, An Int'l Journal* Vol. 5 No. 2.

Richards, P.J., Hoxey, R. P., Connell, B.D., Lander, D. P. (2007), "Wind-tunnel modelling of the Silsoe Cube", *J. Wind Eng. and Ind. Aerodyn.* 95, 1384–1399.

Rodi, W. (1997), "Comparison of LES and RANS calculation of the flow around bluff bodies", *J. Wind Eng. and Ind. Aerodyn.* 69–71, 55–75.

Rodi, W. (2002), "Large-eddy simulation of the flow past bluff bodies", *In: Launder, B.E., Sandham, N.D. (Eds.), Closure Strategies for Turbulent and Transitional Flows*. Cambridge University Press, Cambridge, pp. 361–391.

Patnaik, G., Boris, J.P., Young, T.R., Grinstein, F.F (2007), "Large scale urban contaminant transport simulations with MILES". *J. Fluids Eng.* 129, 1524–1532.

Piomelli, U., Balaras, E., Pasinato, H., Squires, H., Spalart, P., (2003), "The inner–outer layer interface in large-eddy simulations with wall-layer models", *Int. J. Heat Fluid Flow* 24, 538–550.

Sagaut, P., Garnier, E., Tromeur, E., Larchevêque, L., Labourasse, E. (2004), "Turbulent inflow conditions for LES of subsonic and supersonic wall-bounded flows", *AIAA J.* 42, 469–478.

Sagaut, P. (2006), "Large eddy simulation for incompressible flows, and introduction", *3rd edn.* Berlin, Germany; New York, NY: Springer.

Sagaut, P., Deck, S. & Terracol, M. (2006), "Multiscale and multiresolution approaches in turbulence", London, UK: Imperial College Press.

Sagaut, P., Deck, S. (2009), "Large eddy simulation for aerodynamics: status and prespectives" *Phil Trans R. S. A* 367, 2849-2860.

Senthooran, S., Lee, D.D., Parameswaran, S. (2004), "A computational model to calculate the flow-induced pressure fluctuations on buildings", *J. Wind Eng. and Ind. Aerodyn.* 92, 1131–1145.

Selvama, R.P, Landrus, K. (2010) "GPU computing for wind engineering", *The Fifth International Symposium on Computational Wind Engineering(CWE2010),* Chapel Hill, North Carolina, USA May 23-27.

Selvam, P.R. (1996), "Computation of flow around Texas Tech building using $\kappa - \varepsilon$ and Kato-Launder $\kappa - \varepsilon$ turbulence model", *Eng. Structures*, Volume 18, Issue 11, 856-860.

Shinozuka M. (1985), "Lecture at CISM course on stochastic methods in structural engineering"*, International Centre for Mechanical Science*, Udine.

Simiu, E. (1976),"Equivalent static wind loads for tall building design", *J. of Struct. Div., ASCE*, 102(4) 719-737.

Simiu, E., Scanlan, R.H. (1996), "Wind Effects on Structures - Fundamentals and Applications to Design", *John Wiley & Sons, Inc*., NewYork.

Smirnov, R., Shi, S., Celik, I., (2001), "Random flow generation technique for large eddy simulations and particle-dynamics modeling", *J. of F. Eng.* 123, 359–371.

Skamarock, W. C., Klemp, J. B. Dudhia, J. Gill, D. O. Barker, D. M. Wang, W. Powers, J. G. (2005), "A description of the Advanced Research WRF Version 2", *NCAR Tech. Note/TN-468+STR*, 88 pp.

Stathopoulos, T. (1997), "Computational wind engineering: Past achievements and future Challenges", *J. Wind Eng. and Ind. Aerodyn.* 67&68,509-532.

Stathopoulos, T. (2002), "The numerical wind tunnel for industrial aerodynamics: Real or virtual in the new millennium?", *Wind and Structures, An Int'l Journal* Vol. 5, No. 2~4, 193-208.

Stathopoulos, T. (2003), "Wind loads on low buildings: in the wake of Alan Davenport's contributions" *J. Wind Eng. and Ind. Aerodyn.* Vol. 91, 12-15, pp 1565-1585.

Spalart, P.R., Allmaras, S.R. (1994), "A one-equation turbulence model for aerodynamic flows", *La Recherche Aerospatiale*, No.1, pp. 5-21.

Spalart, P. R., Jou, W.-H., Stretlets, M., and Allmaras, S. R. (1997), "Comments on the Feasibility of LES for Wings and on the Hybrid RANS/LES Approach", Advances in DNS/LES, *Proceedings of the First AFOSR International Conference on DNS/LES*.

Spalart, P. R. (2000), "Strategies for turbulence modelling and simulations*", Int. J. Heat Fluid Flows,* 21, 252–263.

Spalart, P. R, Squires KD. (2004), "The status of detached-eddy simulation for bluff bodies", *The Aerodynamics of Heavy Vehicles: Trucks, Buses, and Trains*, R. McCallen, F. Browand and J. Ross, eds., Springer, 19.

Spalart, P. R, Squires KD. (2004), "The status of detached-eddy simulation for bluff bodies", *See McCallen et al. 2004*, pp. 29–45.

Spalart, P. R., Deck, S., Shur, M.L., Squires, K.D., Strelets, M.K. and Travin, A. (2006), "A new version of detached-eddy simulation, resistant to ambiguous grid densities", *Theor. Comput. Fluid Dyn.*, pp. 181-195.

Spalart, P. R. (2009), "Detached-eddy simulation", *Annu. Rev. Fluid Mech.* 41, 181–202.

Sreenivas, K, Pankajakshan R, Nichols DS, Mitchell BCJ, Taylor LK, Whitfield DL. (2006), "Aerodynamic simulation of heavy trucks with rotating wheels. *Presented at AIAA Aerospace", Sci. Meet. Exhib. 44th, Reno, Pap. No.* AIAA-2006-1394.

Song, C., Park, S. (2009), "Numerical simulation of flow past a square cylinder using Partially-Averaged Navier–Stokes model", *J. Wind Eng. and Ind. Aerodyn.* 97, 37-47.

Sohankar, A., Davidson, L., Norberg, C. (2000), "Large eddy simulation of flow past a square cylinder: comparison of different subgrid scale models", *J. Fluids Eng.* 122, 39–47.

Swaddiwudhipong, S., Anh, T.T.T, Liu, Z.S., Hua. J. (2007), "Modeling of wind load on single and staggered dual buildings", *Engineering with Computers* Vol. 23, No.3, 215-22.

Tabor, G.D, Baba-Ahmadi. M.H. (2009), "Inlet condition for large eddy simulation: A review", *J. of Computers and Fluids*, Vol 39 (4), 553-567.

Tamura. ,T., Kawai, H., Kawamoto, S., Nozawa, K., Sakamoto, S., Ohkuma, T. (1997), "Numerical prediction of wind loading on buildings and structures-Activities of AIJ cooperative project on CFD", *J. Wind Eng. and Ind.Aerodyn.* 67&68,671-685.

Tamura, T. (1999), "Reliability on CFD estimation for wind-structure interaction problems", *J. Wind Eng. and Ind. Aerodyn.* 81, 117-143.

Tamura, T. (2008), "Towards practical use of LES in wind engineering", *J. Wind Eng. And Ind. Aerodyn.* 96, 1451–1471.

Tamura, T., Nozawa,K., Kondo,K. (2008), "AIJ guide for numerical prediction of wind loads on buildings", *J. Wind Eng. and Ind. Aerodyn.* 96, 1974–1984.

Tamura, T. (2010a), "Application of LES-based model to wind engineering-Implmentation of meteorological effects", *The Fifth International Symposium on Computational Wind Engineering Conferenfe (CWE2010),* Chapel Hill, North Carolina, USA May 23-27.

Tamura, T. (2010b), "LES for aerodynamic characteristics of a tall building inside a dense city district", *The Fifth International Symposium on Computational Wind Engineering Conferenfe (CWE2010,* Chapel Hill, North Carolina, USA May 23-27.

Terracol, M., Sagaut, P. & Basdevant, C. (2001), "A multilevel algorithm for large-eddy simulation of turbulent compressible flows", *J. Comput. Phys.* 167, 439–474.

Temmerman, L., Hadžiabdic´, M., Leschziner, M.A., Hanjalic´, K. (2005), "A hybrid two-layer URANS–LES approach for large-eddy simulation at high Reynolds numbers", *Int. J. Heat Fluid Flow* 26, 173–190.

Tieleman. H.W. (1998), "Wind tunnel simulation requirements to assess wind loads on low-rise buildings", *J. Wind Eng. and Ind. Aerodyn.*74-76,675-685.

Thibault, J.C., Senocak, I. (2009) "CUDA Implementation of a Navier-Stokes Solver on Multi-GPU Desktop Platforms for Incompressible Flows",47th AIAA .

Travin, A, Shur M, Strelets M, Spalart PR. (2000), "Detached-eddy simulations past a circular cylinder", *Flow Turbul. Combust.* 63:293–313.

Tominaga, T., Mochida,A.,Murakami, S., Sawaki, S. (2008a), " Comparison of various revised $k-\varepsilon$ models and LES applied to flow around a high-rise building model with 1:1:2 shape placed within the surface boundary layer", *J. Wind Eng. and Ind. Aerodyn.* 96, 389 –411.

Tominaga, Y., Mochida, A., Yoshiec, R., Kataokad, H., Nozu, T., Masaru Yoshikawa, M., Shirasawa, T. (2008b), "AIJ guidelines for practical applications of CFD to pedestrian wind environment around buildings", *J. Wind Eng. and Ind. Aerodyn.* 96, 1749–1761.

Tolke, J., Krafczyk, M. (2008) "TeraFLOP Computing on a Desktop PC with GPUs for 3D CFD," International Journal of Computational Fluid Dynamics, Vol. 22, No. 7, pp. 443-456.

Tsang, C. F., Kenny C. S. Kwok, Hitchcock P.A, Desmond K. K. Hui. (2009), "Large-eddy simulation and wind tunnel study of flow over an up-hill slope in a complex terrain", *Wind and Structures, An Int'l Journal* Vol. 12 No. 3.

Tsuchiya, M., Murakami, S., Mochida, A., Kondo, K., Ishida, Y. (1997), "Development of a new $k-\varepsilon$, model for flow and pressure fields around bluff body", *J. Wind Eng. and Ind. Aerodyn.* 67&68,169 -182.

Tutar, M., Celik, I. (2007), "Large eddy simulation of a square cylinder flow*:* Modelling of inflow turbulence", *Wind and Structures, An Int'l Journal* Vol. 10 No. 6.

Tucker, P. G, & Lardeau, S. (2009), "Applied large eddy simulation", *Phil. Trans. R. Soc. A July 28,* 367 (1899) 2809-2818.

Yakhot, A., .Liu, H., Nikitin, N. (2006), "Turbulent flow around a wall-mounted cube: A direct numerical simulation", *Int. J. Heat Fluid Flow.*27, 994–1009.

Meyers, J., Sagaut, P. & Geurts, B. J. (2006), "Optimal model parameters for a multi-objective large eddy simulation", *Phys. Fluids* 18, 095 103.

Levitan, M.L., Holmes, J.D., Mehta, K.C., Vann, W.P. (189), "Field measured pressures on the Texas Tech building", *Proceedings of the eighth Colloquium on Industrial Aerodynamics*, pp. 13–24.

Lund, T.S., Wu, X., Squires, K.D. (1998), "Generation of turbulent inflow data for spatially-developing boundary layer simulations", *J. of Computational Physics*, vol. 140, 233-258.

Lyn, D.A., Einav, S., Rodi, W., Park, J.H. (1995), "A laser-Doppler velocimetry study of ensemble-averaged characteristics of the turbulent near wake of a square cylinder", *J. Fluid Mechanics* 304, 285–319.

Werner, H., H. Wengle, H. (1991), "Large-eddy simulation of turbulent flow over and around a cube in a plate channel", *Proceeding of the 8th Symposium on Turbulent Shear Flows,* 19(4), 155-165.

Wright, N.G., Easom, G.J. (2003), "Non-linear $k-\varepsilon$ turbulence model results for flow over a building at full-scale", *Applied Mathematical Modeling* 27(12), 1013-1033.

Xie, X.T., Castro. I.P. (2008), "Efficient generation of inflow conditions for large eddy simulation of street-scale flow", Flow, Turbulence and Combustion, Vol 81, No. 3, 449-470.

Yakhot, V. Orszag, S.A. Thangam, S. Gatski, T.B., and Speziale, C.G. (1992), "Development of turbulence models for shear flows by a double expansion technique", *Phys.Fluids A*, 4(7), 1510-1520.

Yoshie, R., Mochida, A., Tominaga, Y., Kataoka, H., Harimoto, K., Nozu, T., Shirasawa, T. (2007), "Cooperative project for CFD prediction of pedestrian wind environment in the Architectural Institute of Japan", *J. Wind Eng. and Ind. Aerodyn.* 95, 1551-1578.

Wilson, RP, Haupt SE, Peltier LJ, Kunz RF. (2006), "Detached Eddy Simulation of a surface mounted cube at high Reynolds number", *Proc. ASME Joint U.S. Eur. Fluids Eng. Summer Meet. New York: ASME Int.*

Zhang, N., Jiang W., Miao S. (2006), "A large eddy simulation on the effect of buildings on urban flows", *Wind and Structures, An Int'l Journal* Vol. 9 No. 1.

Table 2.1 Comparison of the *rms* values of simulated velocity fluctuations (After Huang et al., 2010 and Castro et al., 2011)

Inflow turbulence generation method	**Distribution method** of $p_i^{m,n}$, $q_i^{m,n}$, and $k^{m,n}$	σ_u	σ_v	σ_w
DSRFG	Scaling & transformation	0.9968	2.4400	2.9956
DSRFG	Aligning & remapping	0.9500	1.9987	3.0800
MDSRFG	Aligning & remapping	1.0527	2.1850	3.1123
Target		1.1200	2.2400	3.3600

Table 2.2 Levels of validation of simulation techniques (Sagant & Deck, 2009)

Grade	**Level of validation**
1	Forces (Lift, drag and moment)
2	Mean aerodynamic field (velocity profiles)
3	Second order statistics (*rms* quantities)
4	One-point spectral analysis (power spectral densities)
5	Two-point spectral analysis (correlation, coherence and phase spectra)
6	High-order and time-frequency analysis (time-frequency)

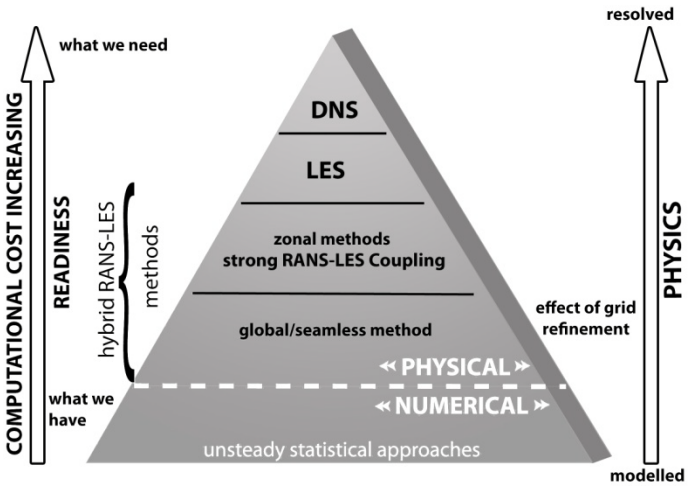

Figure 2.1 Classification of unsteady approaches according to level of modeling and readiness (after Sagaut et al., 2009).

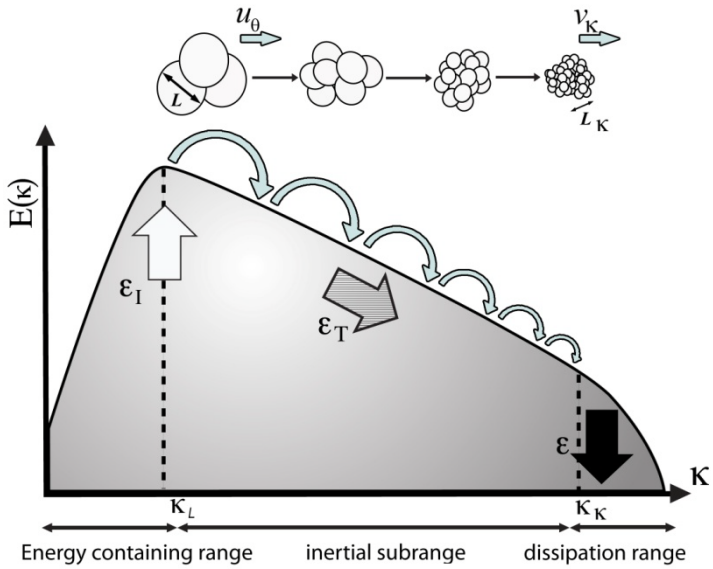

Figure 2.2 Sketch of the energy cascade. In physical space, the large eddies are broken into smaller and smaller eddies (after Sagaut et al., 2006).

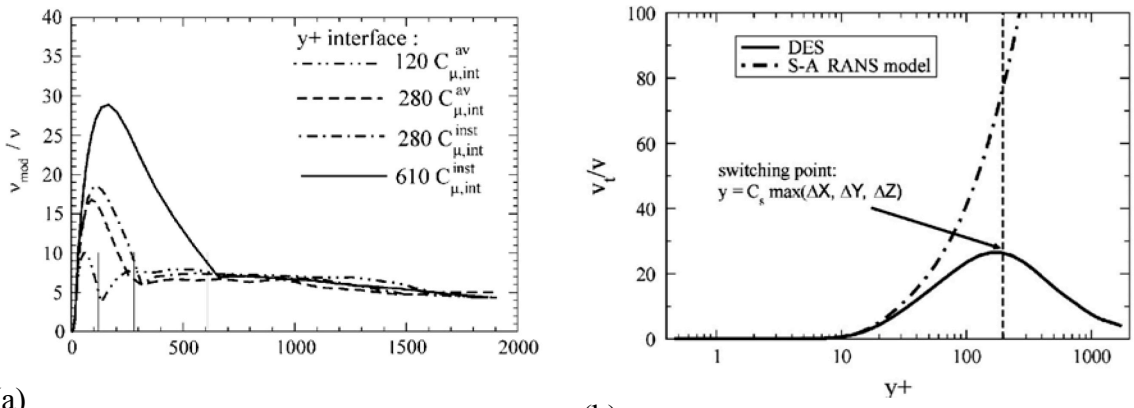

(a) (b)

Figure 2.3 Modeled eddy viscosity in hybrid RANS/LES method. (a): zonal method, (b): seamless approach (after Hanjalić & Kenjereš, 2008).

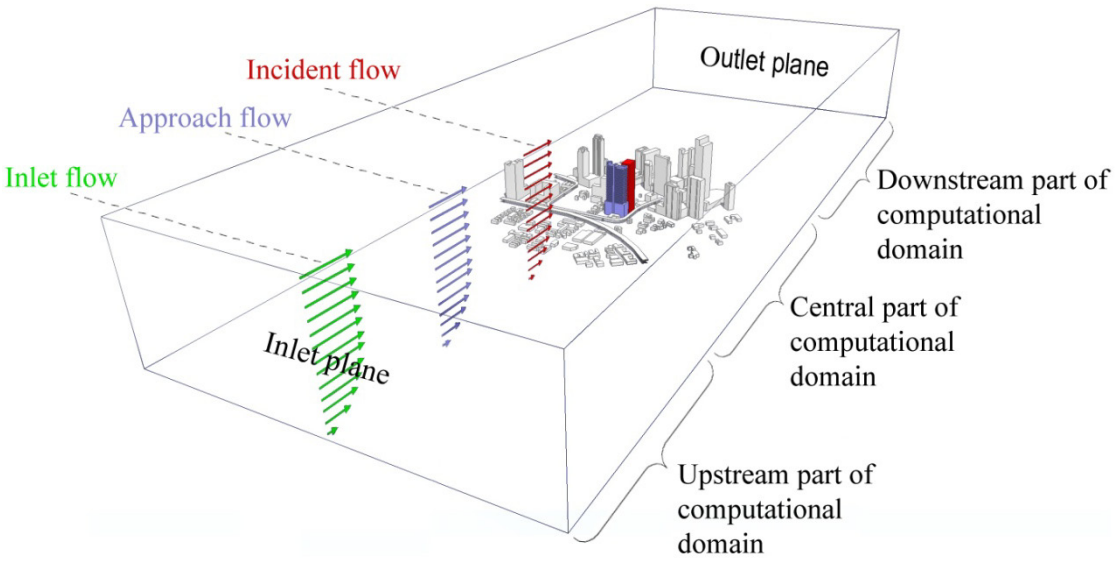

Figure 2.4 Computational domain with building models for CFD simulation of ABL flow modeling (adopted and modified from Blocken et al., 2007).

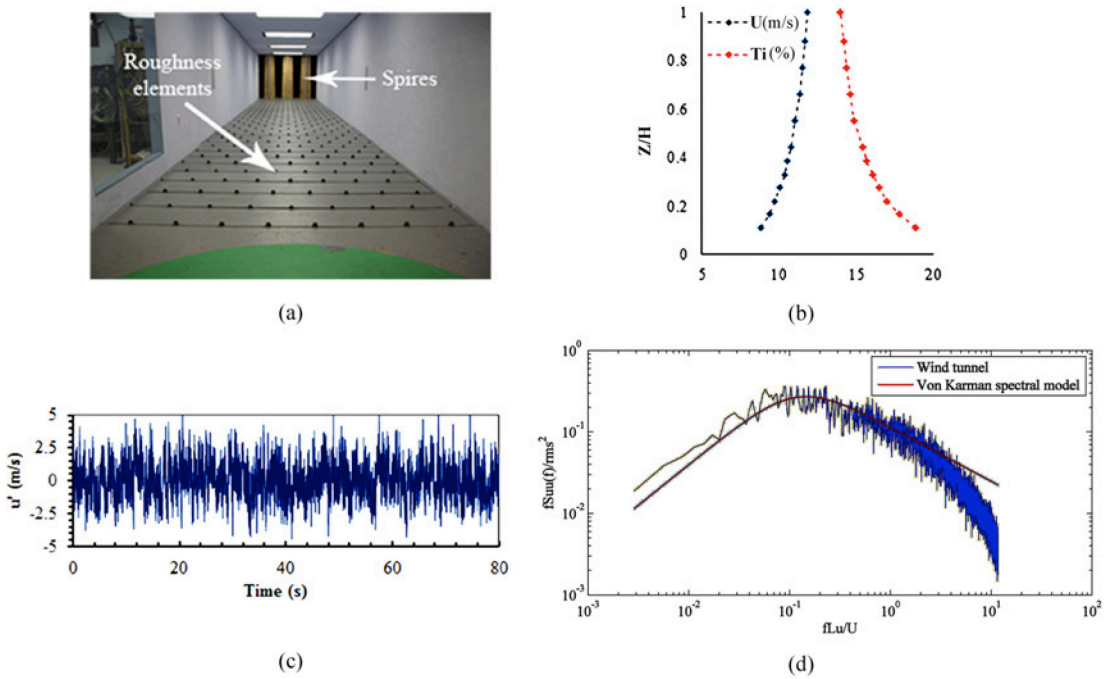

Figure 2.5 (a) Trapezoidal planks & triangular floor roughness elements used for open exposure ABL simulation; (b) velocity profile (power law with $\alpha = 0.14$) & turbulence intensity; (c) time history of streamwise velocity fluctuation; (d) Comparison of BLWT generated turbulence spectrum with von Karman spectrum model ($U_H = 12m/s$).

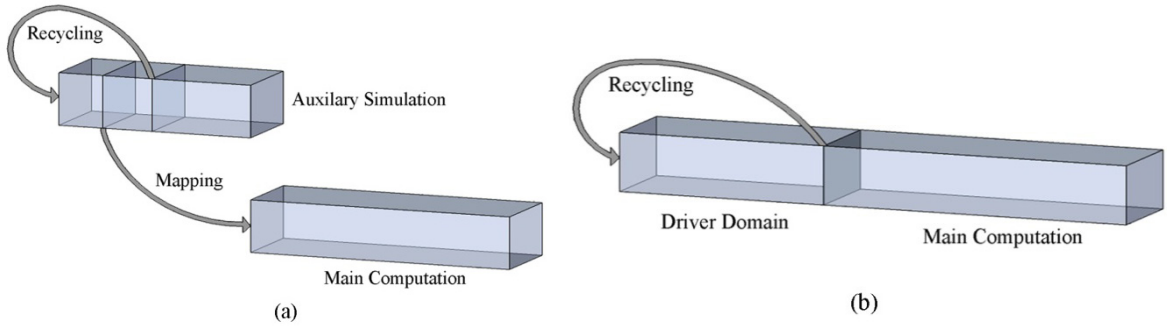

Figure 2.6 Implementation of recycling method (Lund et al., 1998): (a) in which an auxiliary pre-computation is mined to produce the inlet velocity data and (b) Combined computation domain where data is passed on-the-fly to the main computation.

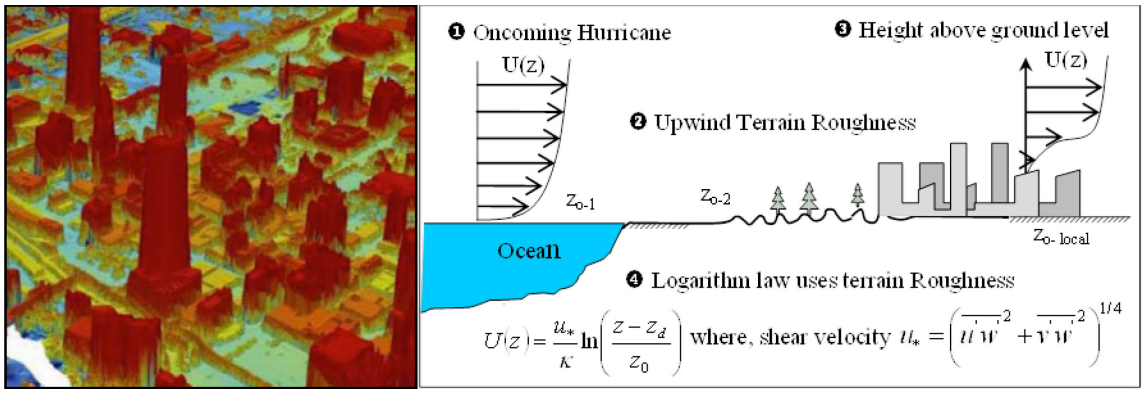

(a) (b)

Figure 2.7 (a) Surface roughness from LIDAR data and (b) the effect of surface roughness on the oncoming wind speed profiles (after Bitsuamlak et al., 2010).

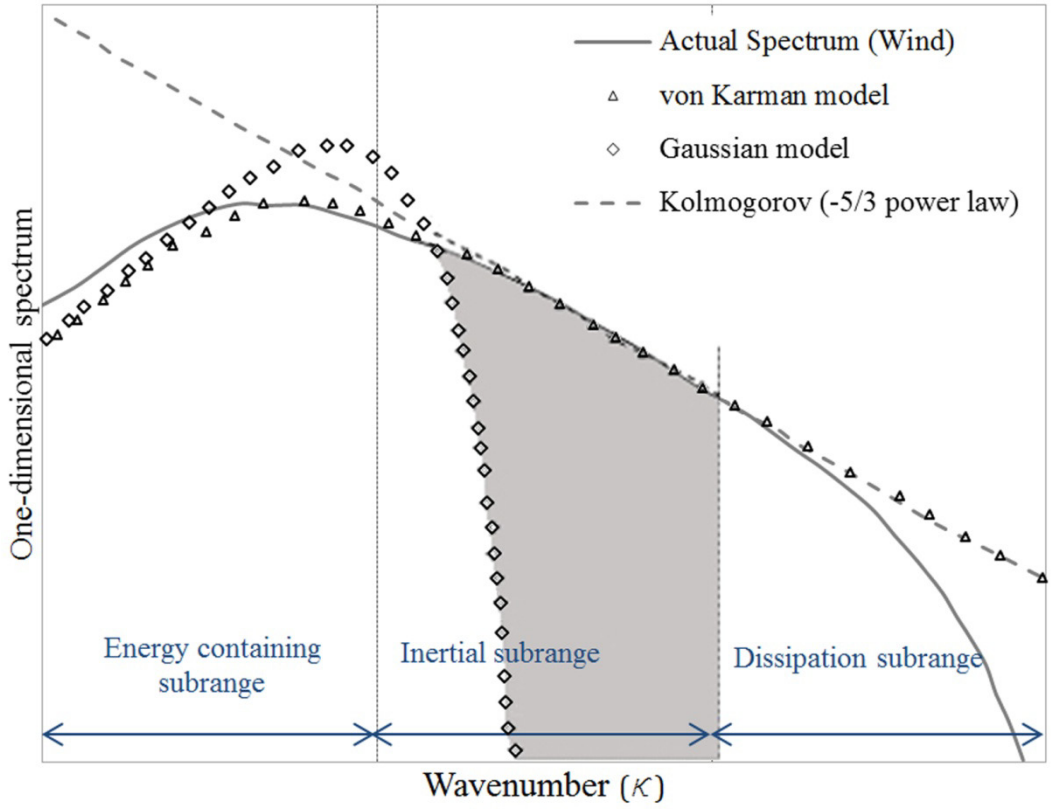

Figure 2.8 Turbulence ranges at high *Re* numbers flow: Comparison of actual wind spectra with the von Karman and the Gaussian spectral model (after Hunag et al., 2010).

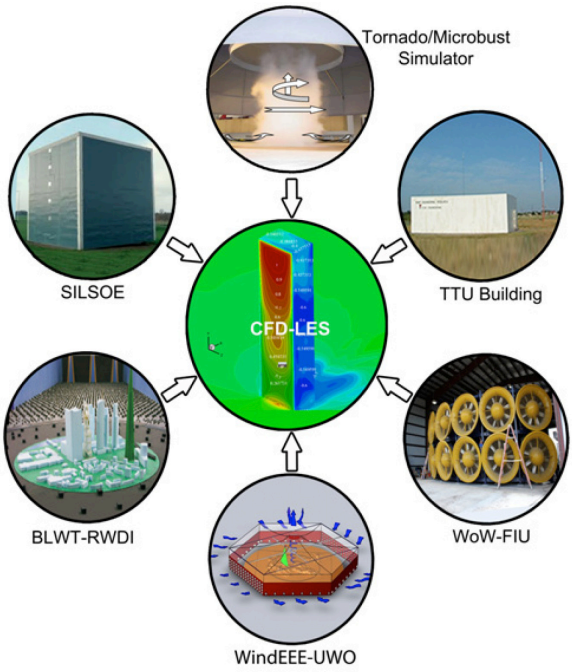

Figure 2.9 Validation of CFD with model-scale, full-scale experiments, and field measurement. Note: Tornado simulator is from Iowa State University; TTU: Texas Tech University; FIU: Florida International University; UWO: University of Western Ontario.

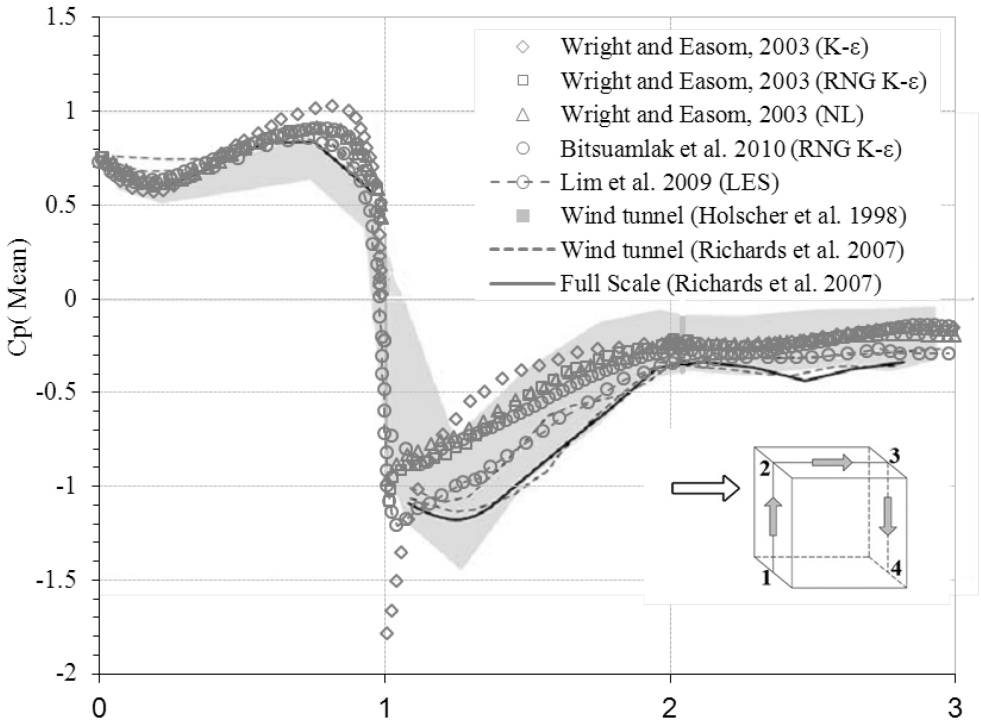

Figure 2.10 Surface mounted cube: Comparison of mean wind pressure coefficients between wind tunnel experiments and numerical simulation by using several turbulence models (Bitusamlak et al., 2010).

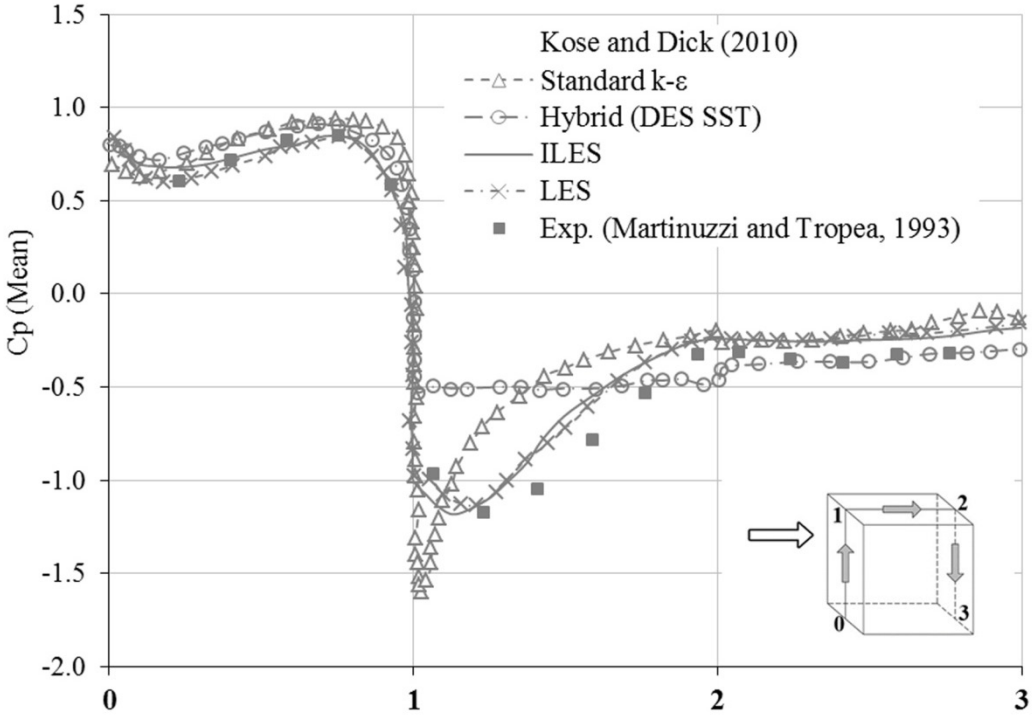

Figure 2.11 Cubical building in ABL flow. Comparison of pressure coefficient profiles on the vertical section using several turbulence models (after Köse & Dick, 2010).

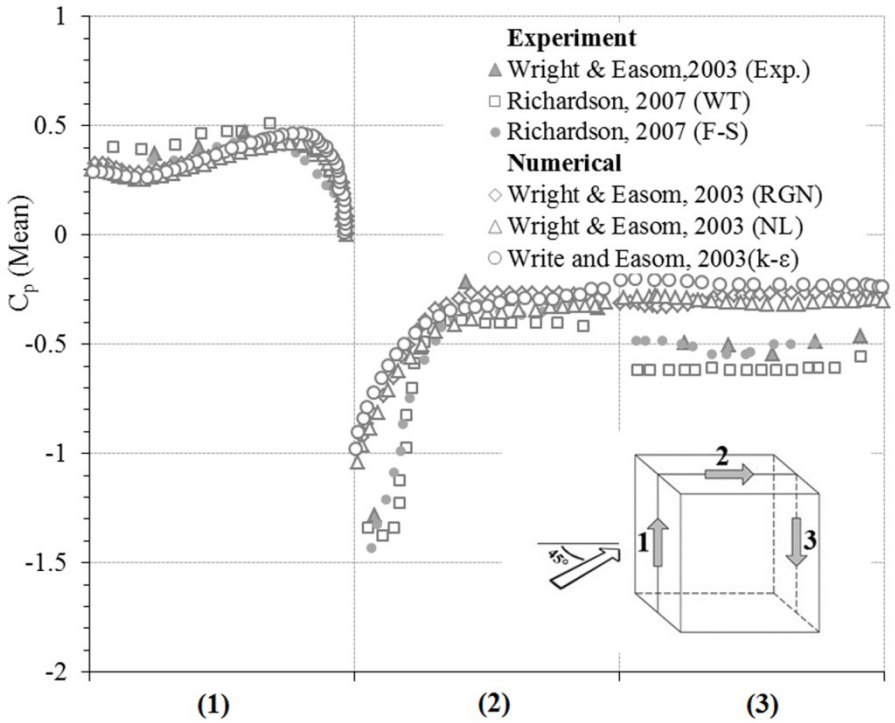

Figure 2.12 Silsoe 6m cube: Comparison of mean pressure coefficient between full scale measurements, wind tunnel and numerical simulations- cube skewed at 45^0.

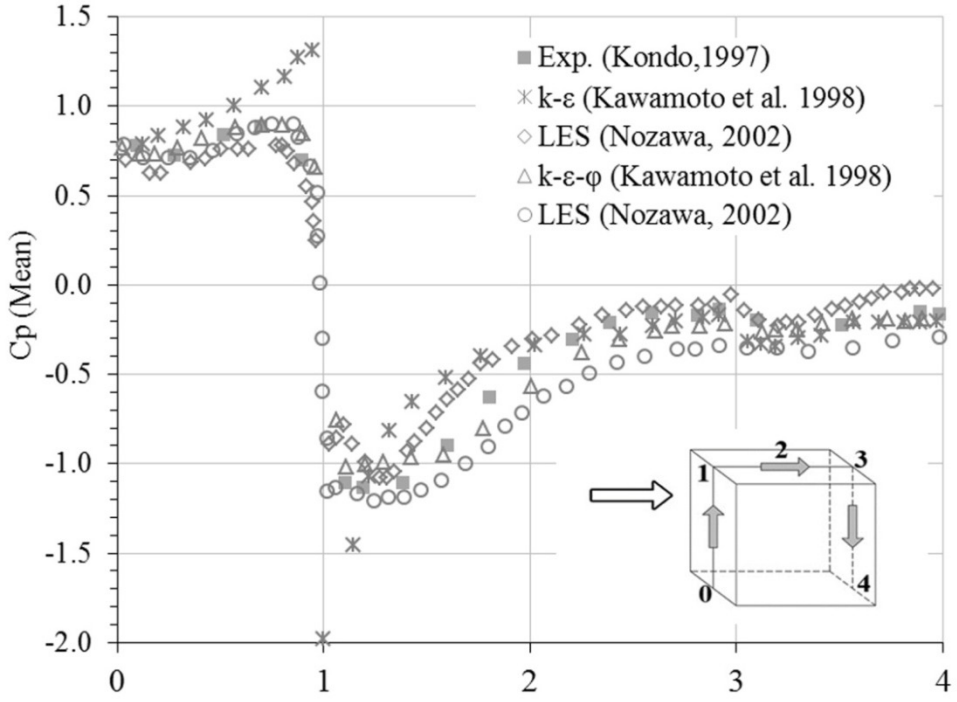

Figure 2.13 Low-rise building: Comparison of mean wind pressure coefficients experiment and numerical (after Nozawa & Tamura, 2002).

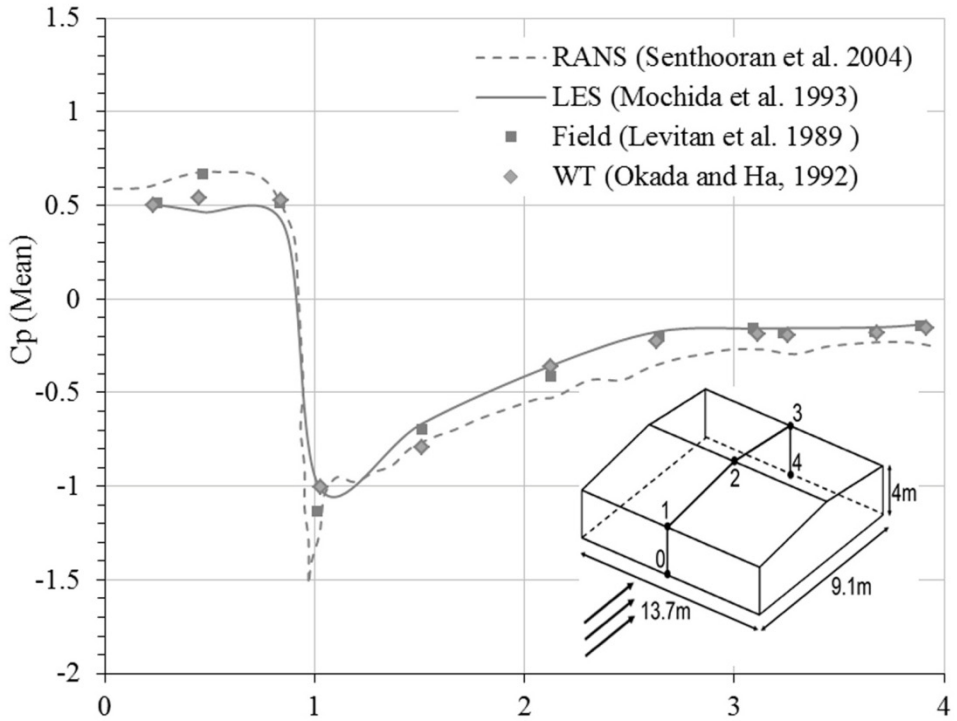

Figure 2.14 The TTU building: Comparison between mean pressure coefficients for straight wind computational and WT and field measurements (after Senthooran et al., 2004).

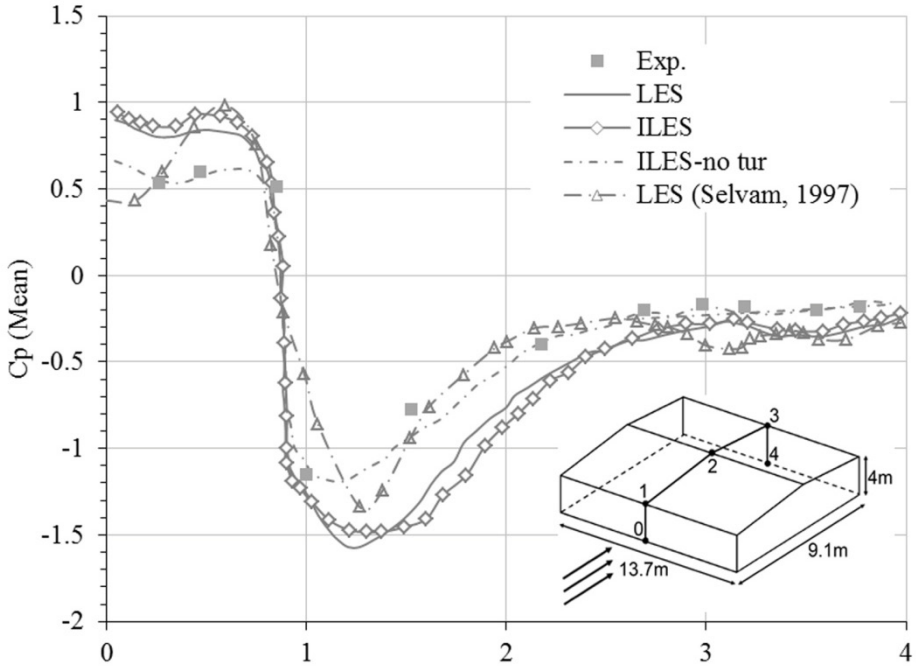

Figure 2.15 The TTU building in ABL flow condition: Comparison of pressure coefficient profiles on the vertical section between wind tunnel experiments and numerical simulations (after Köse & Dick, 2011).

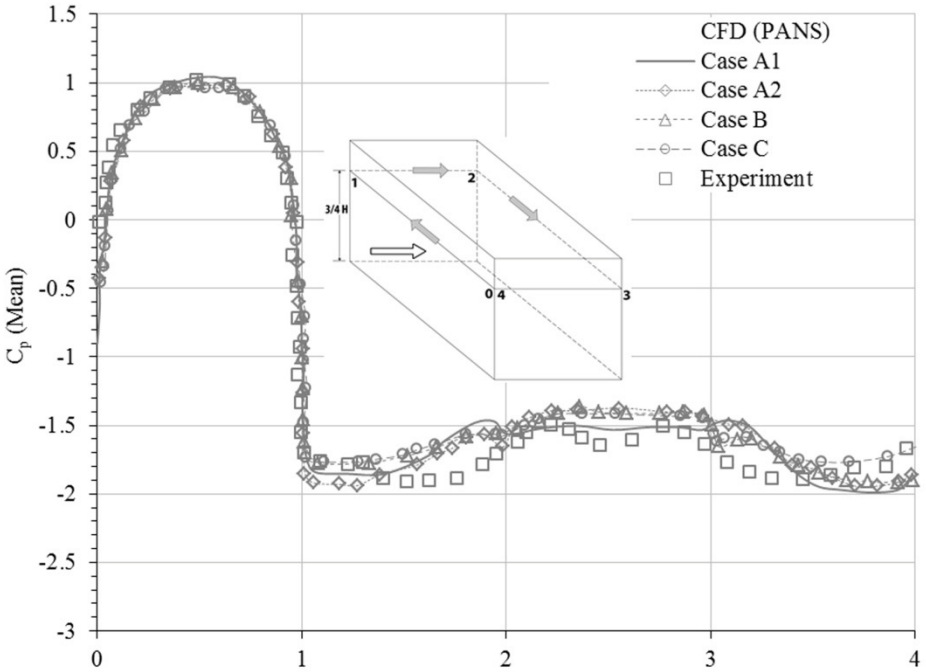

Figure 2.16 Distribution of averaged pressure coefficient along the surface of the square cylinder Where Case A1 and Case A2 have the same number of grids (204×122) in the vertical and stream-wise direction but the same spans-wise grids as C (after Song & Park, 2009).

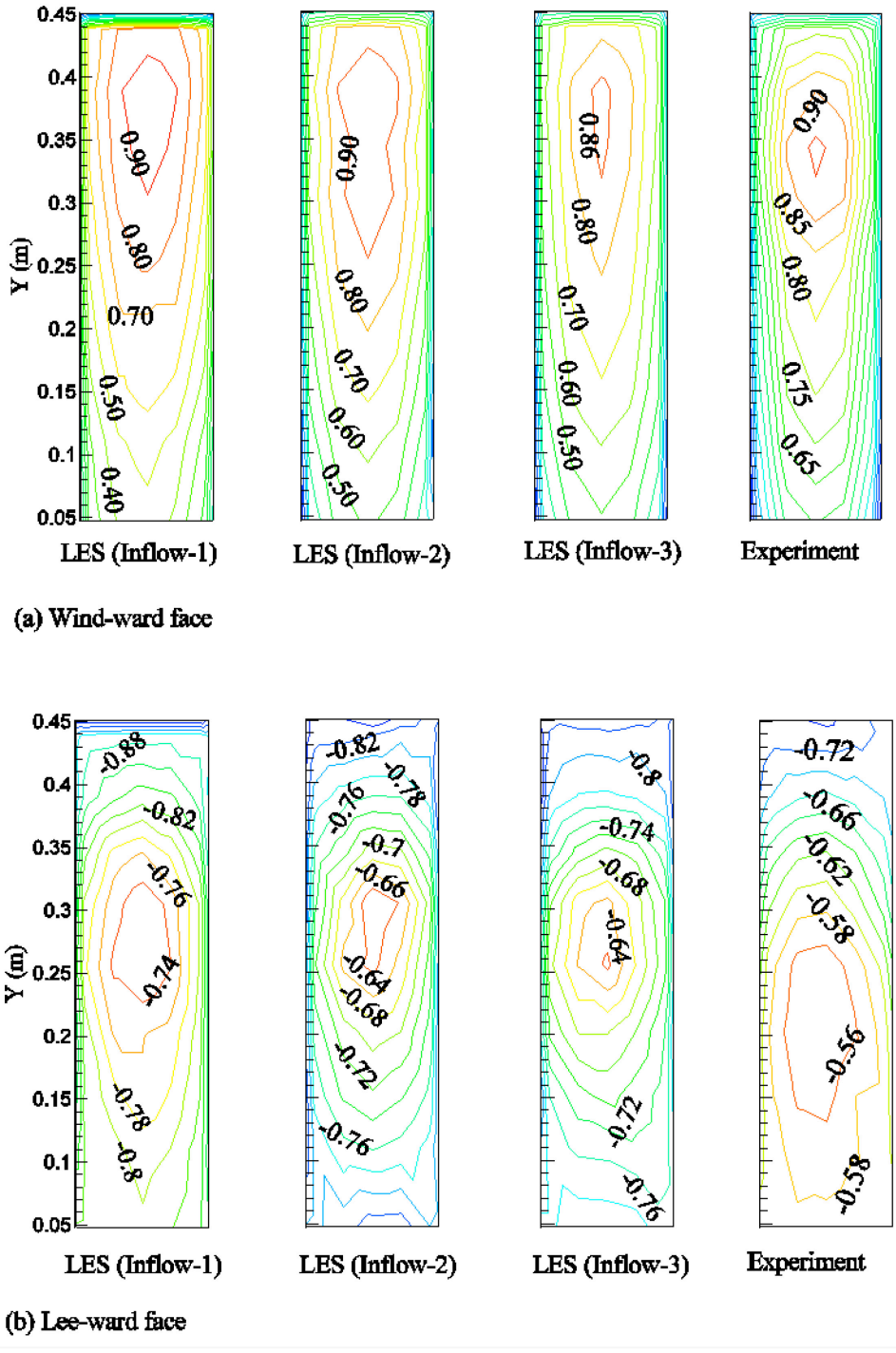

Figure 2.17 Comparison between the mean pressure coefficients of CAARC in a simulated ABL flow using LES with various inflow turbulence models and BLWT experiment.

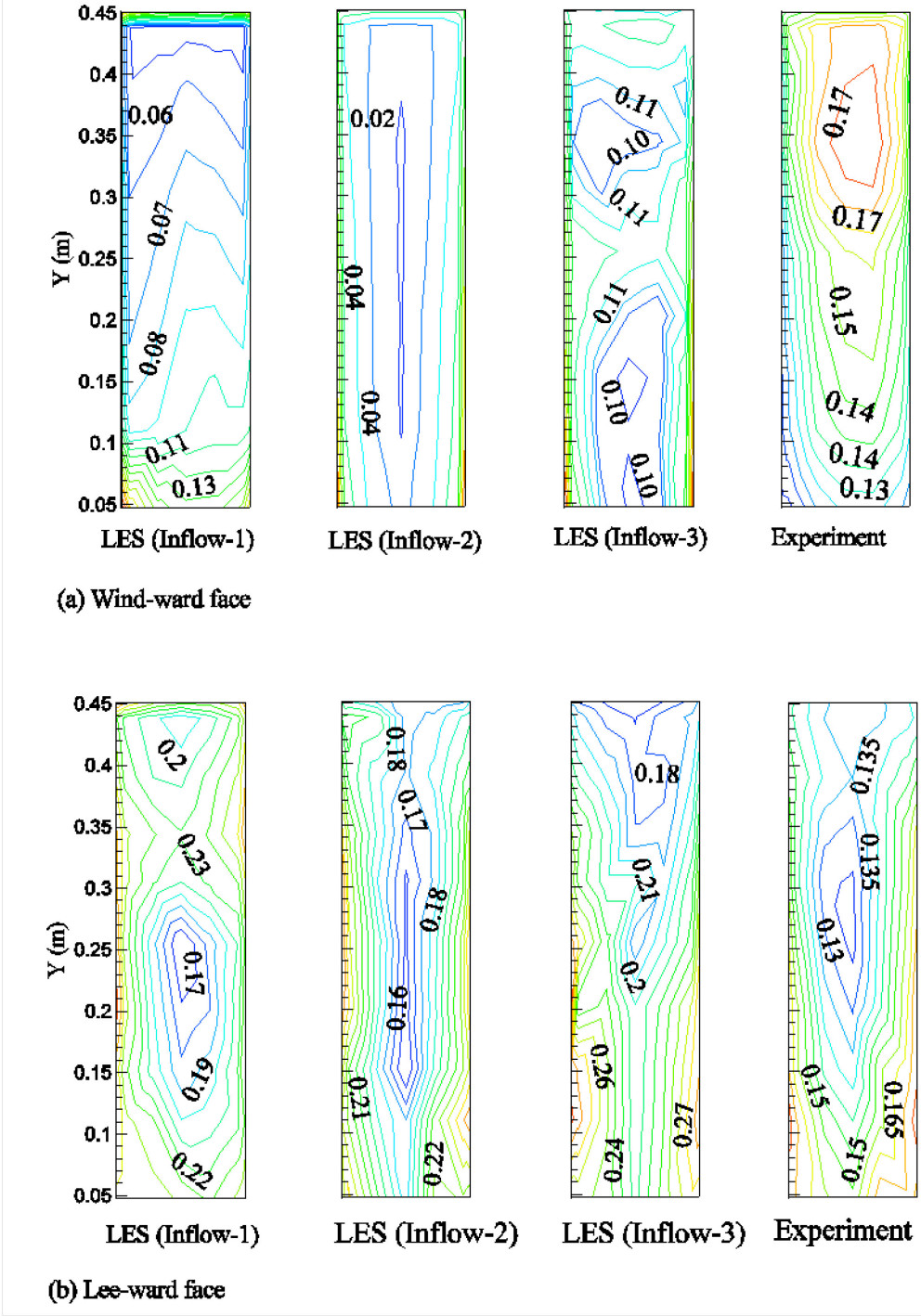

Figure 2.18 Distribution of fluctuating pressure coefficient (rms) over the frontal and lee-ward faces of CAARC in a simulated ABL flow filed: Comparison between LES with various inflow turbulence models and BLWT experiment.

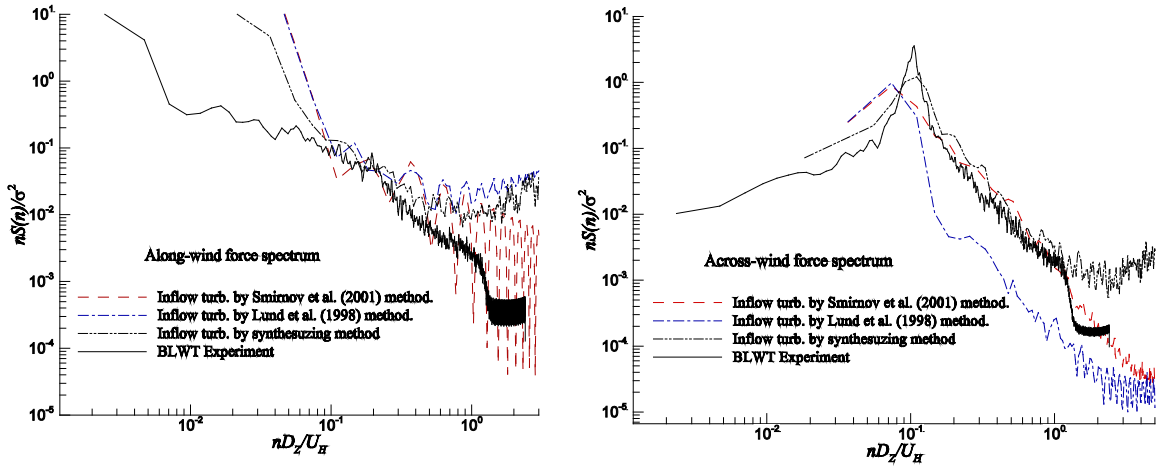

Figure 2.19 Along- and across-wind force spectra of a standard tall building using various inflow turbulences.

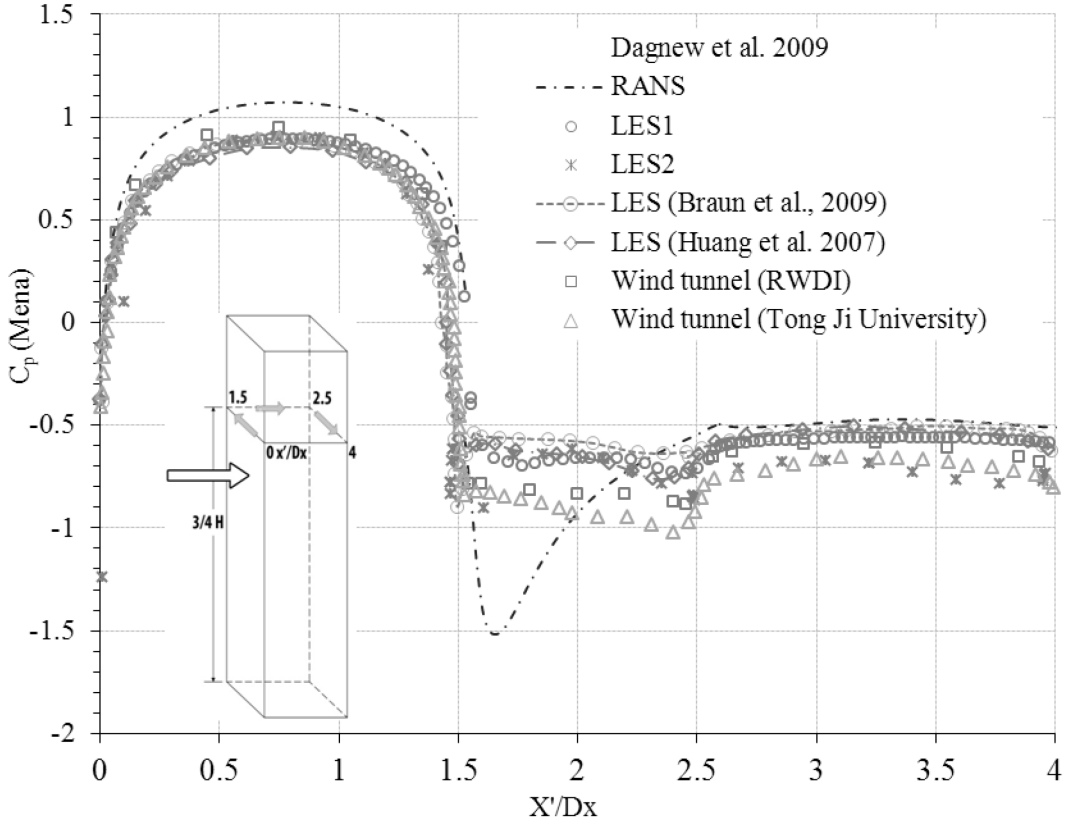

Figure 2.20 Mean wind pressure coefficient on CAARC building model. Where the numbers 0 to 4 represent the length of different faces of the CAARC model: from 0 to 1.5: wind-ward, 1.5 to 2.5: side and 2.5 to 4: lee-ward faces.

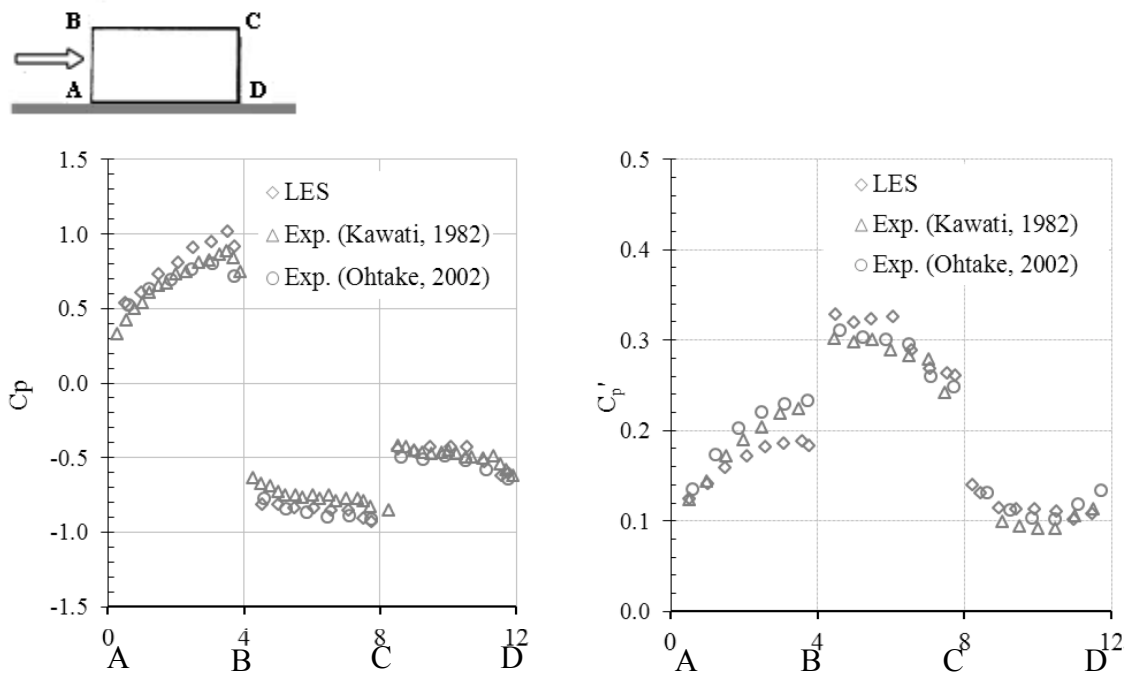

Figure 2.21 LES of high-rise building: (a) mean pressure coefficient at a vertical section, and (b) *rms* of pressure coefficient (after Nozawa & Tamura, 2002).

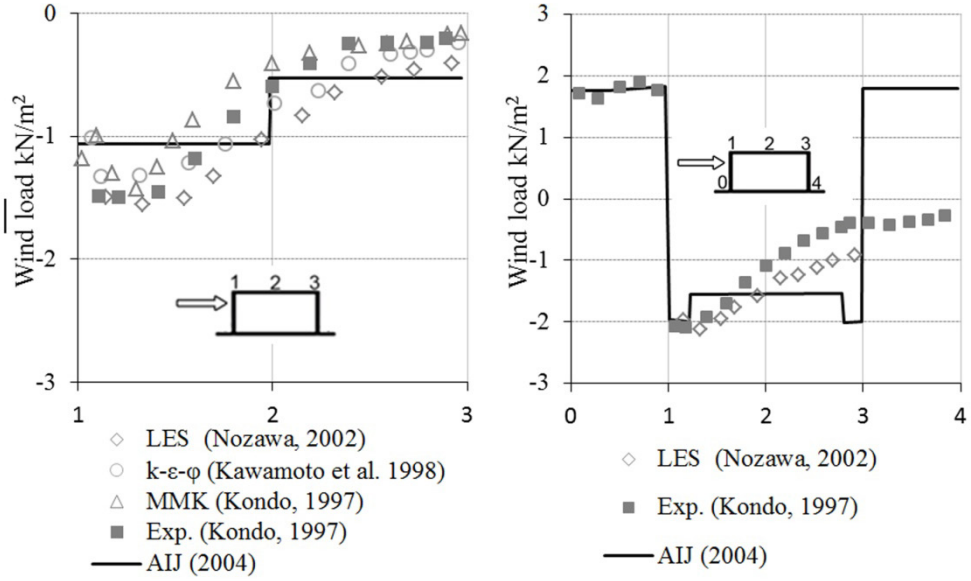

Figure 2.22 Comparison of wind loads on low-rise building: (a) structural frame wind load, (b) wind load on cladding (after Tamura et al., 2008).

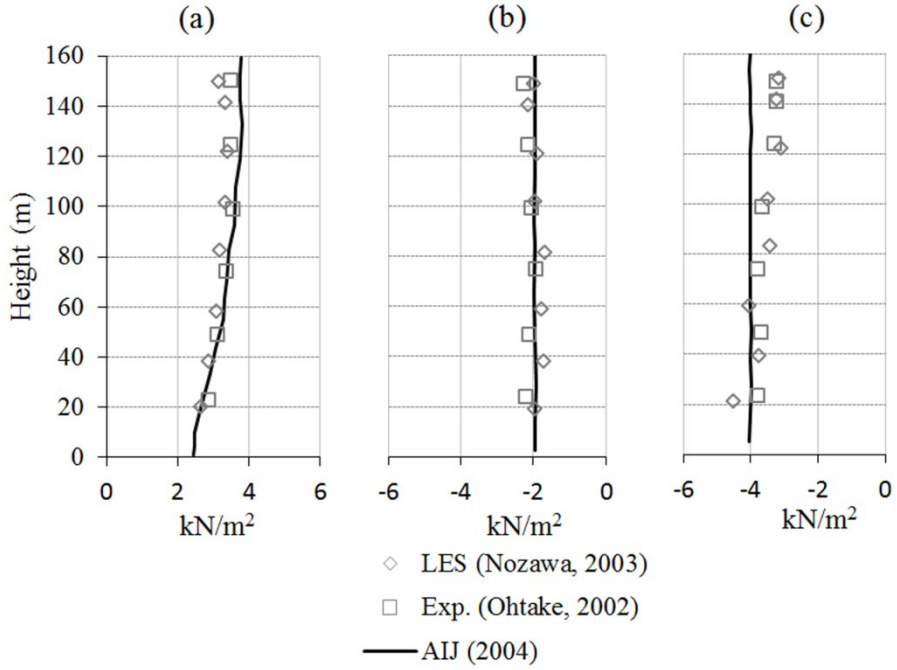

Figure 2.23 Wind loads on cladding of high-rise building (AIJ, 2005). (a) wind-ward wall, (b) lee-ward wall, and (c) side wall (after Tamura et al., 2008).

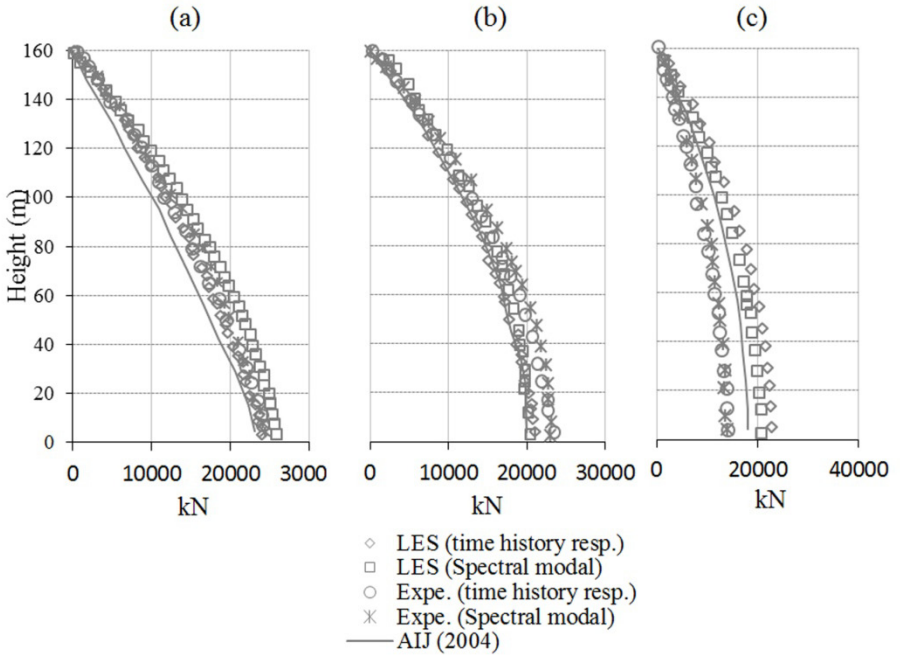

Figure 2.24 Wind loads on structural frame of high-rise building: (a) wind-ward, (b) lee-ward, and (c) side (after Tamura et al., 2008).

3 COMPUTATIONAL ASSESSMENT OF BLOCKAGE AND WIND SIMULATOR PROXIMITY EFFECTS FOR A NEW FULL-SCALE TESTING FACILITY

Girma T. Bitsuamlak[a], Agerneh Dagnew[b], Arindam Gan Chowdhury[c]

Published in the Journal of Wind and Structures

Abstract

A new full scale testing apparatus generically named the Wall of Wind (WoW) has been built by the researchers at the International Hurricane Research Center (IHRC) at Florida International University (FIU). WoW is capable of testing single story building models subjected up to category 3 hurricane wind speeds. Depending on the relative model and WoW wind field sizes, testing may entail blockage issues. In addition, the proximity of the test building to the wind simulator may also affect the aerodynamic data. This study focuses on the Computational Fluid Dynamics (CFD) assessment of the effects on the quality of the aerodynamic data of (i) blockage due to model buildings of various sizes and (ii) wind simulator proximity for various distances between the wind simulator and the test building. The test buildings were assumed to have simple parallelepiped shapes. The computer simulations were performed under both finite WoW wind-field conditions and in an extended Atmospheric Boundary Layer (ABL) wind flow. Mean pressure coefficients for the roof and the windward and leeward walls served as measures of the blockage and wind simulator proximity effects. The study uses the commercial software FLUENT with Reynolds Averaged Navier Stokes equations and a

[a] Assistant professor; [b] Ph.D. Candidate; [c] Assistant prof. Laboratory for Wind Engineering Research, International Hurricane Research Center/ Department of Civil and Environmental Engineering, Florida International University, Miami, FL 33174, USA.

Renormalization Group (RNG) k-ε turbulence model. The results indicated that for larger size test specimens (i.e. for cases where the height of test specimen is larger than one third of the wind field height) blockage correction may become necessary. The test specimen should also be placed at a distance greater than twice the height of the test specimen from the fans to reduce proximity effect.

Keywords: Full scale testing, blockage, wind simulator proximity, CFD, pressure coefficient, turbulence.

3.1 Introduction

Central to FIU's research is the development in stages of full-scale testing facilities of the type generically called Wall of Wind (WoW), capable of producing hurricane level winds, in conjunction with wind-driven rain and wind-borne debris. The WoW, capable as it is of testing to failure entire structures at full scale, is an effective way of acquiring the experimental knowledge needed to mitigate hurricane damage in real buildings, and of powerfully demonstrating the damage wreaked by hurricanes on buildings as well as the dramatic loss reductions inherent in effective mitigation measures. As a first phase of this development effort, the International Hurricane Research Center (IHRC) team at Florida International University (FIU) has built a full-scale 2-fan WoW facility (Figs. 1a and 1b) for testing small structures and assemblies, including roof fascias, barrel tile roofs, hurricane mitigation products, and Florida Power & Light utilities, (Gan Chowdhury et al. 2009a and 2009b). Building on this experience FIU has subsequently built a larger, more powerful Renaissance-Re 6-fan WoW generating up to category 3 hurricane winds and wind-driven rain (Huang et al. 2009, Bitsuamlak 2009) with sufficient wind field size to engulf a small single-story building (Figs. 1c and 1d). To house this and future larger WoW systems, a 30.5 x 24.4 x 10.7 m building is under construction at FIU. The North and South faces of the building consist largely of folding doors that will remain open during operation/testing. The WoW will be located on the South end. A dynamically controllable 4.9 m diameter turntable is located 2.7 m downstream of the WoW. Test buildings will be placed on the turntable to allow simulation of the effect of wind directionality. The WoW system forms a large open circuit system during operation. Further expansion and improvements on the current

design of WoW using more number of fans are underway with financial support from the State of Florida Legislature. A 1:8 scale replica of the current 6 fan WoW has been built (Fig. 2) to help design flow management components (contraction, airfoil layouts, etc) before testing and implementing them at full-scale on the 6-fan WoW (Huang et al. 2008, 2009). This approach has been found to be efficient and economical. In this study, it is not the intention to use the reduced-scale model of the WoW yet.

Testing larger test specimens within the finite WoW wind field, either to achieve Reynolds number similarity or to assess performance of full-scale building components under wind, wind-driven rain, and debris impact resistance, may entail blockage issues. The blockage effect discussed in the present study is concerned with the size of the test specimen compared to the finite size of the wind field generated at the inlet. The need to keep the test specimen as close as possible to the wind simulator in order to subject the test model to strong wind before it diffuses and loses its strength may also affect the quality of the aerodynamic data. The objectives of this study are, therefore, to assess computationally (i) the blockage effect as a function of the size of the test specimens, and develop correction strategies for those cases where those effects are significant, and (ii) the wind simulator proximity effect for various distances between the wind simulator and the test building, and develop proper test guidelines to ensure that this effect is acceptably small. The evolution of computational wind engineering (CWE) based on computational fluid dynamics (CFD) principles is making numerical evaluation of wind effects on built environment a potentially attractive proposition. This is particularly true in light of the positive development trends in hardware and software technology, as well as numerical modeling. Significant progress has been made in the application of CWE to evaluate

wind loads on buildings (e.g. Murakami and Mochida 1988; Selvam 1997; Stathopoulos 1997; Wright et al. 2003; Camarri et al. 2005; Tamura 2006; Tutar and Celik 2007; El-Okda et al. 2008; Tominaga et al. 2008a; Cóstola et al. 2009 and others). Significant progress has also been made on the evaluation of wind load modifications due to topographic elements (Bitsuamlak et al. 2004, 2006). Some countries have already established working groups to investigate the practical applicability of CWE and develop recommendations for their use for wind resistant design of actual buildings and for assessing pedestrian level winds, within the framework of the Architectural Institute of Japan (AIJ) (Tamura et al. 2008, Tominaga et al. 2008b) and the European cooperation in the field of scientific and technical (COST) research, Franke et al. (2007). Further, AIJ provides methods for predicting wind loading on buildings by the Reynolds Averaged Navier Stokes equations (RANS) and LES. Practical applications of CWE are widespread in areas such as pedestrian level wind evaluation Chang (2006), Lam and To (2006), and Blocken and Carmeliet (2008), where only the mean wind speeds are required for evaluating pedestrian comfort Stathopoulos and Hu (2004). CWE applications for wind driven rain are reported by researchers such as Choi (2000), and Blocken and Cameliet (2004). Some CFD wind flow studies for urban neighborhood include Zhang et al. (2006), Huang et al. (2006), and Jiang et al. (2008). While most of studies mentioned above focus on straight winds, studies by Lin and Savory (2006), and Hangan and Kim (2008) focused on simulation of downburst. Other common uses of CWE, to which the present study belong to, include augmentation of experimental wind engineering research: Sengupta and Sarkar (2008) augmented their microburst and tornado wind simulator facility with numerical simulation; Moonen et al. (2006, 2007) used CFD to

assess quality of wind tunnel flow conditions and design of wind tunnels. Merrick and Bitsuamlak (2008) used numerical simulation to facilitate selection of an artificial surface roughness length to be applied on curved surfaced buildings during wind tunnel testing as a means to compensate for High Reynolds number effects that is usually missing from low wind speed tunnels. Okajima (1997) computationally assessed the effects of blockage pertaining to the effect of tunnel walls on various aerodynamic features.

In the present study, numerical wind flow simulations around parallelepipeds of various sizes, and located at various distances from the wind simulator and engulfed inside the numerical WoW and Atmospheric Boundary Layer (ABL) model have been carried out. In parallel, work is in progress to study the blockage and proximity effects experimentally by using the 1:8 scale small WoW replica in conjunction with the full-scale WoW. When they become available, the test results will be used to validate the Computational Fluid Dynamics (CFD) studies, following the approach of Bitsuamlak (2006). In the meantime, wind tunnel data from literature has been used to validate the present numerical models, resulting in a reasonable agreement with the CFD simulations, as will be discussed in section 3. Previous computational blockage assessments for wind tunnels include studies by Okajima (1997) pertaining to the effect of tunnel walls on various aerodynamic features as mentioned earlier. In the present blockage and wind simulator proximity effect study, however, the focus is on the effect of the size of the test buildings with respect to the finite size of WoW wind field and test building's proximity to the wind simulator. The WoW wind field can for practical purpose be considered to be a wind jet generated by an array of fans with controlled wind-profile characteristics.

3.2 Numerical modeling

The commercial software FLUENT 6.2 was utilized for the present numerical simulation, and the governing equations employed were the Reynolds Averaged Navier-Stokes (RANS) equations, together with the Renormalization Group (RNG) k-ε turbulence model. For blockage assessment studies, the upstream (U/S) , top, downstream (D/S), and two sides of the computational domain (CD) were set to 3.5H, 7H, 10.5H, and 5.5H from the center of the base of the parallelepiped, respectively, as shown in Fig. 3, where H is the parallelepiped height under investigation, as shown in Fig. 4. For wind simulator proximity assessments, cubical buildings with windward faces located at H, 2H, 3H, 4H and 5H from the wind source (fans) were considered, as shown in Figure 3.5.For wall bounded flow, Fluent 6.2 provides two different approaches for modeling flows in the inner viscous layer, i.e. use of wall functions or near-wall modeling based on the non-dimensional wall units. The first grid point y_p is placed at 0.01m from the surface of the test specimen and unstructured grids of hexagonal type were used for the CFD simulation. Considering the computational cost in resolving the inner layer, standard wall functions has been used in all present simulations by maintaining the wall unit y+ between 30 and 500. In addition, the inlet power law velocity profile with exponent α=0.25, a turbulence intensity TI = 12%, and a 10 m integral length scale were assumed. The latter is less than the typical accepted value for suburban terrain, owing to the need to limit to a minimum the computational domain (CD) size -- assumed to be three times the length scale -- to reduce computational time. These are reasonable assumptions considering the comparative nature of this study. When simulating the ABL, the velocity inlet profile as described above was applied to the whole upstream face of

the computational domain. However, when simulating the WoW flow, the application of the velocity inlet was limited to the 12 m x 9 m area of the U/S face of the CD representing the WoW type wind-field condition, as shown in Fig. 3; on the remaining inlet area the atmospheric pressure condition was applied.

A segregated pressure-velocity solver has been used to all the discretization schemes. Pressure interpolation is standard and second order upwind and third order MUSCL schemes were used for convection and momentum terms respectively. The convergence criterion for residuals has been limited to 10^{-5}.

For blockage assessment studies, computational models mimicking the WoW and the ABL test model conditions were developed for the three cases shown below. It is to be noted that the blockage effect discussed in the present study is concerned with the size of the test specimen compared to the finite size of the wind field generated at the inlet (see Fig. 4).

Case 1A - Base case for a 3x3x3 m (height x width x depth) cube placed in ABL wind-field condition (for this case $H=H_b=3m$);

Case 1B - Same as Case 1A but placed inside WoW wind-field condition; \z

Case 2A - A 4x4x3 m (height x width x depth) parallelepiped placed in ABL wind-field condition ($H=1.33H_b$);

Case 2B - Same as Case 2A but placed inside WoW wind-field condition;

Case 3A - A 5x5x3 m (height x width x depth) parallelepiped placed in ABL wind-field condition ($H=1.66H_b$);

Case 3B - Same as Case 3A but placed inside WoW wind-field condition.

For wind proximity effect studies, computational models mimicking the WoW and the ABL test model conditions for the 3x3x3 m base cube were developed for the following three cases:

Case 4A – Windward face of base cube located at distance H from the wind simulator and placed in ABL wind-field condition;

Case 4B - Same as Case 4A but placed inside WoW wind-field condition;

Case 5A - Windward face of base cube located at distance 2H from the wind simulator and placed in ABL wind-field condition;

Case 5B - Same as Case 5A but placed inside WoW wind-field condition;

Case 6A - Windward face of base cube located at distance 3H from the wind simulator and placed in ABL wind-field condition (note this case is the same as Case 1A);

Case 6B - Same as Case 6A but placed inside WoW wind-field condition (note this case is the same as Case 1B);

Case 7A - Windward face of base cube located at distance 4H from the wind simulator and placed in ABL wind-field condition;

Case 7B - Same as Case 7A but placed inside WoW wind-field condition;

Case 8A - Windward face of base cube located at distance 5H from the wind simulator and placed in ABL wind-field condition;

Case 8B - Same as Case 8A but placed inside WoW wind-field condition;

Figure 3.4 describes the relative size of the parallelepipeds relative to the WoW wind-field (5Hbx3Hb) and the ABL wind-field (11Hx7H) for Cases 1 to 8, where Hb represents the height of the base cube (Hb= 3m) and H represents the height of the study

building for each case. Note that the depth (along the wind flow direction) of all the parallelepipeds considered in the present study is 3 m. Figure 3.5 describes the distances from the windward face of the study base cube (3x3x3 m) from the wind simulator used for cases 4, 5, 6, 7 and 8. In all simulations the wind direction was perpendicular to the upwind face of the parallelepiped. Although the parallelepiped has simple geometry, it represents the complex bluff-body aerodynamic characteristics of a real building. In addition, several experimental studies and results are available for parallelepipeds, which allow the validation of results from the present study against values available in the literature.

3.3 Results and discussion

To validate the present simulation, results for the base case (i.e. Case 1A) have been compared with experimental results from the literature, as shown in Fig. 6, which also contains numerical results obtained by other researchers. Mean pressure coefficients normalized by reference velocity at the building height (U_H = 29.43 m/s) measured at the inlet boundary location for the center vertical lines at U/S and D/S faces of the parallelepiped (i.e. AB and CD) and center horizontal line at the roof (i.e. BC) of the parallelepipeds were used for the comparison. As shown in Fig. 6, the results from previous studies that utilized LES (Lim et al. 2009) or RNG k-ε (Wright and Easom 2003) is in better agreement with the boundary layer wind tunnel BLWT data compared to standard k-ε model (Wright and Easom 2003). The latter over predicted the pressure coefficients on the windward wall and the roof. In the present study RNG k-ε has been opted due to its relatively good agreement with BLWT compared to Standard k-ε and relatively lower computational resource demand compared to LES. As can be seen from

Fig. 6, the present simulation (Case 1A) is in good agreement with boundary layer wind tunnel (BLWT) data from the literature, represented by the grey region. In comparison to full-scale testing (Richards et al, 2007), similar to reports in literature (Bitsuamlak 2006), the numerical result gives less accurate pressure coefficient values for the roof (RMSE=0.222) compared to the windward wall (RMSE=0.131) and leeward wall (RMSE=0.146). However it is to be noted that these errors are in similar order of magnitude with that of the variations observed in pressure coefficients measured in wind tunnels. When examining the CFD results it is necessary to account for the variations within the experimental data, described by the grey region of Fig. 6. It is to be noted that this comparison is made only to give an indicator on the quality of CFD value compared to industry wide accepted wind tunnel measurements from literature no additional effort was made in the present study to verify the quality of the wind tunnel measurements.

Following the comparisons of the numerical simulations with results from the literature, the blockage assessments were pursued. The velocity contours for Case 1 are shown in Fig. 3.7. Figures 3.7(a) and (b) show the contours on a horizontal plane at mid-height of the cube. Similarly, Figs. 3.7(c) and (d) show the contours on a vertical plane passing through the center of the cube. Figure 3.8 shows the path-lines for the recirculation zones for Case 1. Qualitatively, there is generally good agreement in terms of size of recirculation length behind the parallelepipeds. Quantitatively, Fig. 3.9 shows mean pressure coefficient comparisons for Cases 1A (ABL) and 1B (WoW). As can be seen from the figure, there is a very good agreement between the two, confirming the viability of using a proper wind-jet flows generated by using the WoW system with proper turbulence and boundary layer generation schemes representing ABL conditions.

Figures 3.10 and 3.11 show similar results for Cases 2 and 3, respectively. Slight differences in mean pressure coefficients (Cp values) were observed for Cases 2 and Case 3 at the roof and leeward wall. These differences could be due to blockage or inadequacy of the basic type of turbulence model used in the present study. This remains to be verified through use of better numerical models such as Large Eddy Simulation (LES). The authors are currently working on an experimental investigation using the 1:8 scale WoW replica and the full-scale WoW. Once the sources of these differences are identified, proper corrections can be applied when testing larger models.

Finally, the wind simulator proximity assessments were pursued. Similar to the blockage assessments, mean Cp values extracted from the center vertical lines at U/S and D/S faces of the parallelepiped (i.e., AB and CD) and the center horizontal line of the roof (i.e., BC) were used for comparison purposes. The mean Cp values for Cases 4, 5, 6, 7 and 8 were compared with the wind tunnel data obtained from the literature as shown in Fig. 3.12. There is generally good agreement between the CFD and the wind tunnel data for Cases 5, 6, 7 and 8. For Case 4, however, the comparison revealed exaggerated Cp values in the windward wall. This means that the pressure coefficients at the windward wall were created by higher wind speed than the wind speed used to obtain the pressure coefficients. It is to be recalled that wind speed measured at H ft from ground (H= cube height) before placing the cube in the testing position has been used to obtain the pressure coefficients. This is believed to be due to the close proximity of the test cube to the wind simulator blocking the flow before it expands upwards and to the sides thus resulting in a higher velocity that created the pressure system compared to the wind speed used for obtaining the pressure coefficients. Compared to windward wall, the roof Cp values were

less sensitive to test building proximity to the wind simulator as can be seen in Fig. 3.11. The insensitivity of the roof pressures to the proximity of the wind simulator is believed to be due to localized flow effect such as flow separation at the roof level, which is less independent of the proximity parameter. For Cases 5, 6, 7 and 8, where the test cube was placed at >2H distance from the wind simulator, the exaggerated positive pressure disappeared. Thus, it may be concluded that to obtain a good quality aerodynamic data on walls, the models needs to be placed at a distance of more than 2H from the wind simulator. However, for roof or roof top equipment tests the aerodynamic data are less sensitive to the proximity of the test-specimen to the wind simulator.

3.4 Conclusions

The following guidelines and observations based on the present study are warranted:

(i) Pressure coefficients were reasonably well reproduced.

(ii) For large test models, i.e. for cases where the height of the test model is larger than one third of the wind field height, carrying out proper blockage assessments is necessary.

(iii) Test buildings shall be preferably located at least 3H from the wind source (fans). If the model is placed closer than 3H, the quality of the aerodynamic data particularly in the windward wall can be compromised and appropriate correction needs to be applied. The roof aerodynamic data appears less sensitive compared to the windward wall.

These guidelines may be followed when conducting similar studies. The present study is limited to mean characteristics. In the future detailed validation focusing on the

transient characteristics as well will be carried out by comparing the CFD results with 1:8 WoW replica and full scale WoW blockage and wind source proximity data.

Acknowledgments

The support from National Science Foundation (through NSF Career award to the first author) and Florida Department of Emergency Management is gratefully acknowledged. Dr Emil Simiu's comments during the preparation of the manuscript are also gratefully acknowledged.

References

Bitsuamlak, G.T. (2006), "Application of computational wind engineering: A practical perspective", Third National Conference in wind Engineering, January 5-7, Kolkata, India.

Bitsuamlak, G.T., Gan Chowdhury, A. and Sambare, D. (2009), "Application of a full-scale testing facility for assessing wind-driven rain intrusion", Building and Environment, 44, 2430-2441.

Bitsuamlak, G.T., Stathopoulos, T., and Bédard, C. (2006), "Effect of upstream hills on design wind load: a computational approach", Wind and Structures. 9 (1), 37-58.

Bitsuamlak, G.T., Stathopoulos, T., Bédard, C. (2004), "Numerical evaluation of turbulent flows over complex terrains: A review", Journal of Aerospace Engineering, 17(4), 135-145.

Blocken, B. and Carmeliet, J. (2008), "Pedestrian wind conditions at outdoor platforms in a high-rise apartment building: generic sub-configuration validation, wind comfort assessment and uncertainty issues", Wind and Structures. 11(1), 51-70.

Blocken, B., Carmeliet, J. (2004), "A Review of Wind-driven Rain Research in Building Science", Jnl. of Wind Eng. Ind. Aerod., 92(13), 1079-1130.

Camarri, S., Salvetti, M.V., Koobus B., and Dervieux, A. (2005), Hybrid RANS/LES simulations of a bluff-body flow", Wind and Structure, 8(6), 407–426.

Chang, C. (2006), "Computational fluid dynamics simulation of pedestrian wind in urban area with the effects of tree", Wind and Structures, 9(2), 147-158.

Choi ECC (2000), "Variation of Wind-driven Rain Intensity with Building Orientation", Journal of Architectural Engineering; 6, 122–130.

Cóstola, D., Blocken, B. and Hensen, J.L.M. (2009), "Overview of pressure coefficient data in building energy simulation and airflow network programs", Building and Environment. 44, 2027-2036.

El-Okda, Y.M, Ragab, S.A., and Hajj, M.R. (2008), "Large-eddy simulation of flow over a surface-mounted prism using a high-order finite-difference scheme", Jnl. of Wind Eng. Ind. Aerod., Vol. 96, Issues 6-7, pp 900-912, 2008.

Franke, J., Hellsten, A., Schlünzen, H., Carissimo, B. (2007). "Best practice guideline for the CFD simulation of flows in the urban environment". COST Office Brussels, ISBN 3-00-018312-4.

Gan Chowdhury, A., Bitsuamlak, G.T. and Simiu, E. (2009a) “Aerodynamic, hydro-aerodynamic, and destructive testing”, Institute of Civil Engineers Journal of Structures and Buildings, accepted for publication.

Gan Chowdhury, A., Simiu, E., Leatherman, S.P. (2009b). “Destructive Testing under Simulated Hurricane Effects to Promote Hazard Mitigation.” ASCE Natural Hazards Review Journal, 10 (1), p. 1-10.

Hangan, H. and Kim, J.D. (2008), “Swirl ratio effects on tornado vortices in relation to the Fujita scale”, Wind and Structures, 11(4), 291-302.

Holscher, N., Niemann, H.J. (1998), “Towards quality assurance for wind tunnel tests: A comparative testing program of the Windtechnologische Gesellschaft”, Jnl. of Wind Eng. Ind. Aerod., 74, 599-608.

Huang, H., Kato, S. and Ooka, R. (2006), “CFD analysis of ventilation efficiency around an elevated highway using visitation frequency and purging flow rate”, Wind and Structures, 9(4), 297-313.

Huang, P., Gan Chowdhury, A., Bitsuamlak, G.T, Liu, R., (2009), “Development of Devices and Methods for Simulation of Hurricane Winds in a Full-Scale Testing Facility”, Wind and Structures, 12(2), 151-177.

Huang, P., Liu, R., Gan Chowdhury, A., Bitsuamlak, G., Erwin, J., Ahmed, S.S. (2008), “Turbulence Simulation of Small-Scale Wall of Wind Flows,” Proceedings of the 4th International Conference on Advances in Wind and Structures, Jeju, Korea.

Jiang, D., Jiang, W., Liu, H. and Sun, J. (2008), “Systematic influence of different building spacing, height and layout on mean wind and turbulent characteristics within and over urban building arrays”, Wind and Structures, 11(4), 275-289.

Lam, K.M. and To, A.P. (2006), “Reliability of numerical computation of pedestrian-level wind environment around a row of tall buildings”, Wind and Structures, 9(6), 473-492.

Lin, W. E. and Savory, E. (2006), “Large-scale quasi-steady modelling of a downburst outflow using a slot jet”, Wind and Structures, 9(6), 419-440.

Lim, C.H., Thomas, T.G., Castro, I.P. (2009), “Flow around a cube in a turbulent boundary layer: LES and experiment”, Jnl. of Wind Eng. Ind. Aerod., 97, 96-109.

Merrick, R., and Bitsuamlak, G.T. (2008), "Control of flow around a circular cylinder by the use of surface roughness", 4th International Conference”, Advances on Wind and Structures (AWAS08), Jeju, Korea.

Moonen, P., Blocken, B., Carmeliet, J. (2006), "Numerical modeling of the flow conditions in a closed-circuit low-speed wind tunnel", Jnl. of Wind Eng. Ind. Aerod., 94, 966-23.

Moonen, P., Blocken, B., Carmeliet, J. (2007), "Indicator for the evaluation of wind tunnel test section flow quality and application to a numerical closed-circuit wind tunnel", Jnl. of Wind Eng. Ind. Aerod., 94,1289-1314.

Murakami, S., Mochida, A. (1988), "3-D numerical simulation of airflow around a cubic model by means of the k-e model", Jnl. of Wind Eng. Ind. Aerod., Vol 31, 283-303.

Okajima, A., Yi, D., Sakuda, A., Nakano, T. (1997), "Numerical study of blockage effects on aerodynamic characteristics of an oscillating rectangular cylinder", J. Wind Eng. Ind. Aerodyn. 67&68, 91-102.

Richards, P.J., Hoxey, R.P., Connell, B.D., Lander, D. P. (2007), "Wind-tunnel modelling of the Silsoe Cube", Jnl. of Wind Eng. Ind. Aerod., 95, 1384–1399.

Selvam, S.P. (1997), "Computation of pressures on Texas Tech university building using large eddy simulation", Jnl. of Wind Eng. Ind. Aerod., 67&68, 647-657.

Sengupta, A., and Sarkar (2008), "Experimental measurement and numerical simulation of an impinging jet with application to thunderstorm microburst winds", Jnl. of Wind Eng. Ind. Aerod., 96(3), 345-365.

Stathopoulos, T. (1997), "Computational wind engineering: Past achievements and future challenges", Jnl. of Wind Eng. Ind. Aerod., 67-68, 509-532.

Stathopoulos, T. Wu, H. (2004), "Using Computational Fluid Dynamics (CFD) for pedestrian winds", Proceedings of the 2004 Structures Congress, Nashville, TN.

Tamura, T., Nozawa, K., and Kondo, K. (2008), "AIJ guide for numerical prediction of wind loads on buildings. Jnl. of Wind Eng. Ind. Aerod., 96, 1974–1984.

Tamura, T. (2006), "Towards practical use of LES in wind engineering", The fourth international symposium in Computational Wind Engineering (CWE2006), Yokohama, Japan.

Tominaga, Y., Mochida, A., Murakami, S., and Sawaki, S. (2008a), "Comparison of various revised k–ε models and LES applied to flow around a high-rise building model with 1:1:2 shape placed within the surface boundary layer", Jnl. of Wind Eng. Ind. Aerod., 96(4), 389-411.

Tominaga, Y., Mochida, A., Yoshiec, R., Kataokad, H., Nozu,T., Masaru, Yoshikawa, M., Shirasawa, T. (2008b), "AIJ guidelines for practical applications of CFD to

pedestrian wind environment around buildings", Jnl. of Wind Eng. Ind. Aerod., 96, 1749–1761.

Tutar, M., and Celik, I. (2007), "Large eddy simulation of a square cylinder flow: Modelling of inflow turbulence", Wind and Structure, 10(6), 511-532.

Wright, N.G., Easom, G.J. (2003), "Non-linear k–ε turbulence model results for flow over a building at full-scale", Applied Mathematical Modelling, 27(12), 1013-1033.

Zhang, N., Jiang, W., and Miao, S. (2006), "A large eddy simulation on the effect of buildings on urban flows", Wind and Structures, 9(1), 23-35.

Two-fan Wall of Wind: (a) front isometric view and (b) rear isometric view

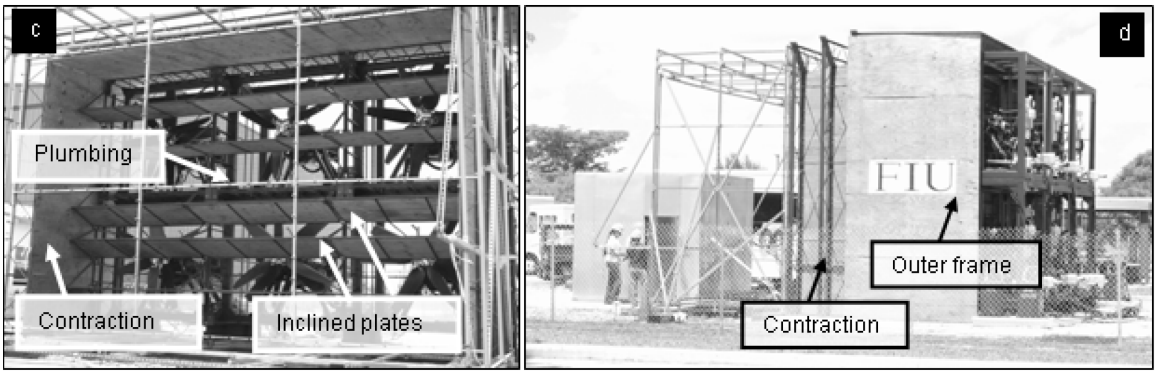

Six-fan Wall of Wind: (c) front view and (d) side view


(f) The new twelve-fan Wall of Wind

Figure 3.1 Evolution of the Wall of Wind full-scale testing facility at Florida International University.

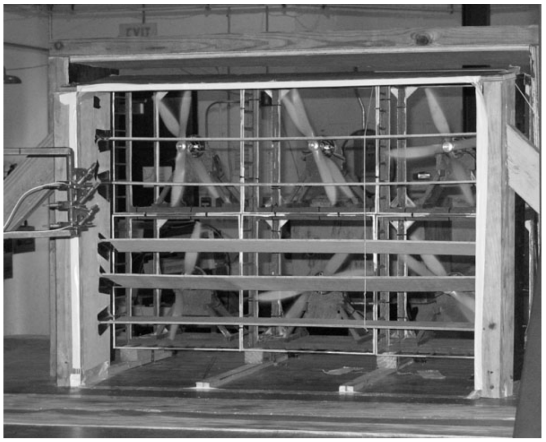

Figure 3.2 Six-fan WoW Small-scale (1:8) model.

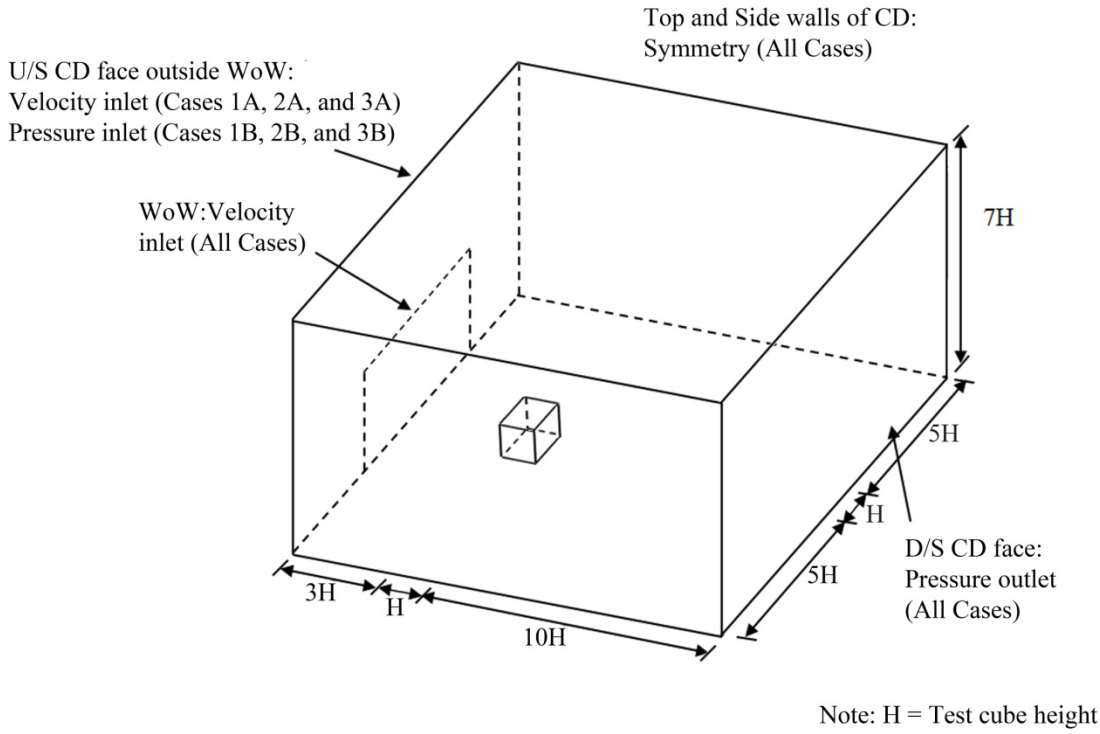

Figure 3.3 Computational Domain (CD) and Boundary Conditions as defined by FLUENT.

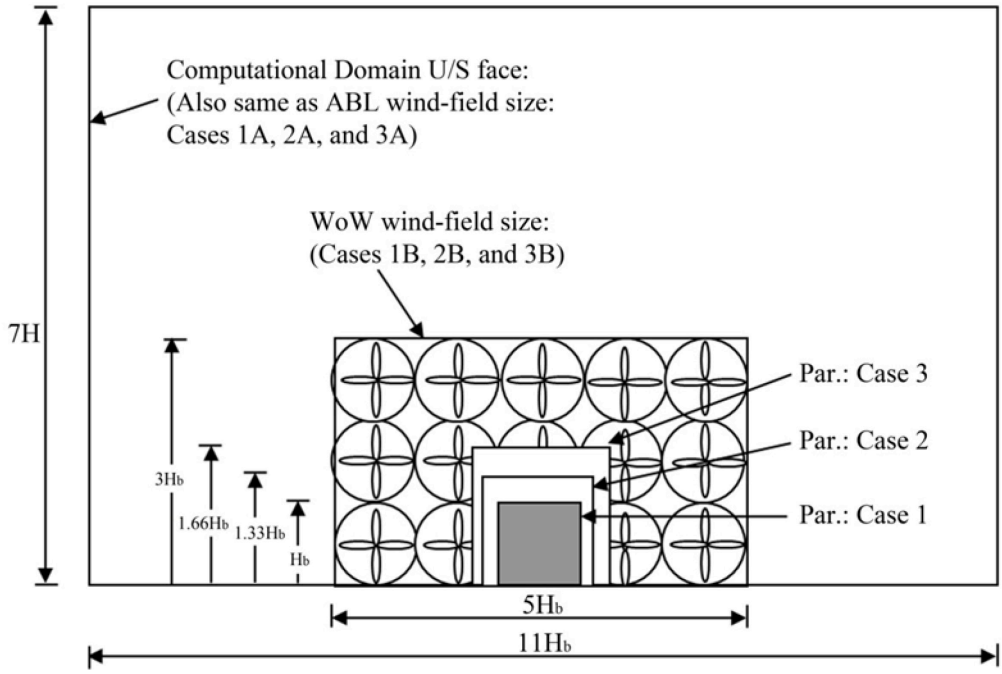

Figure 3.4 Sizes of test parallelepipeds and wind-fields at the inlet used for blockage assessment studies. Note that only the grey building has been used for wind simulation proximity assessment.

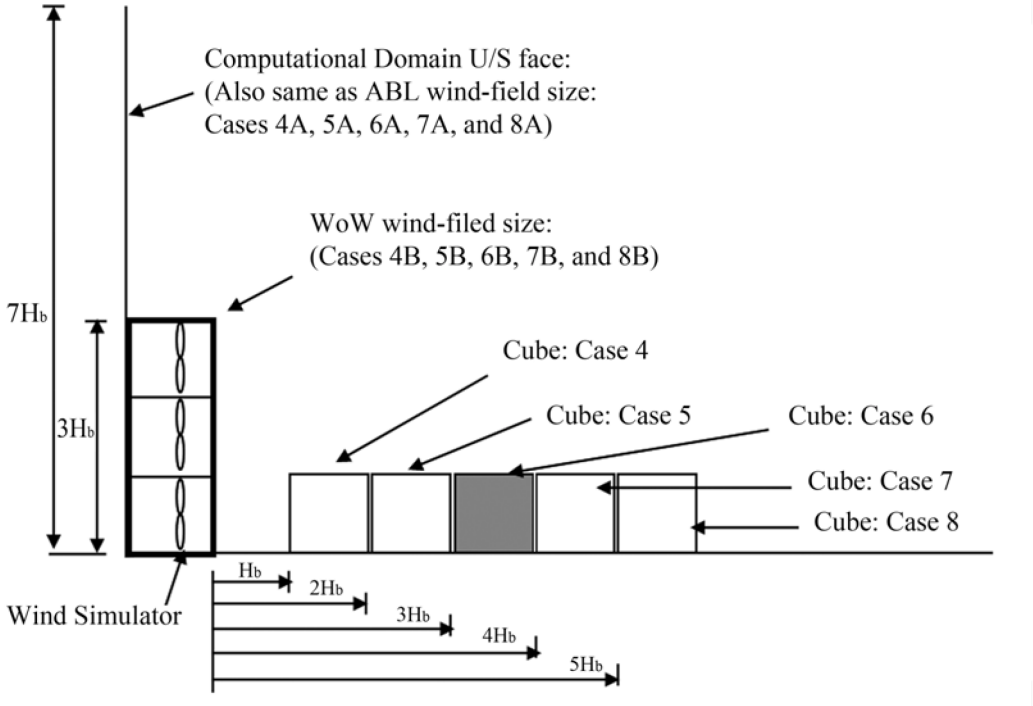

Figure 3.5 Test cube windward face distances from the wind simulator (fans) for different simulation cases (Hb, 2Hb, 3Hb, 4Hb, and 5Hb for Cases 4, 5, 6, 7 and 8 respectively).

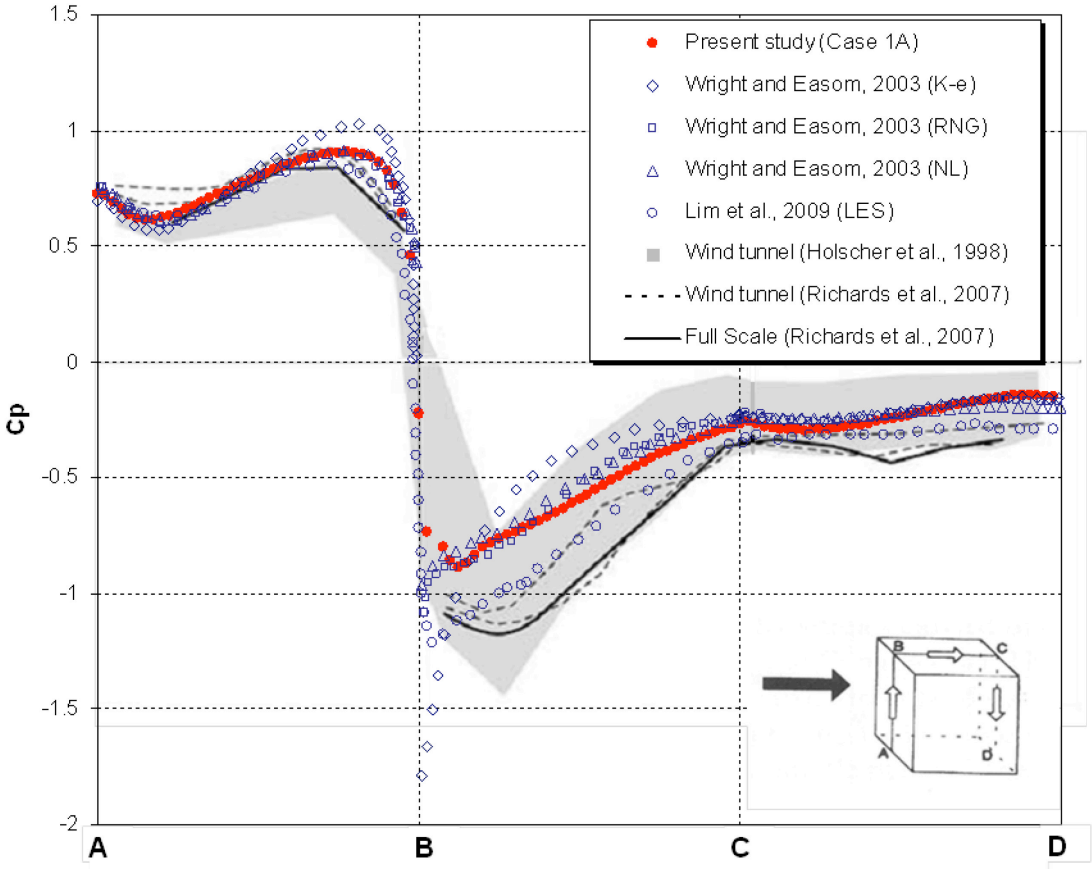

Figure 3.6 Comparison of mean wind pressure coefficients: Experimental measurements and numerical simulations by using several turbulence models. (after Bitsuamlak et al., 2002)

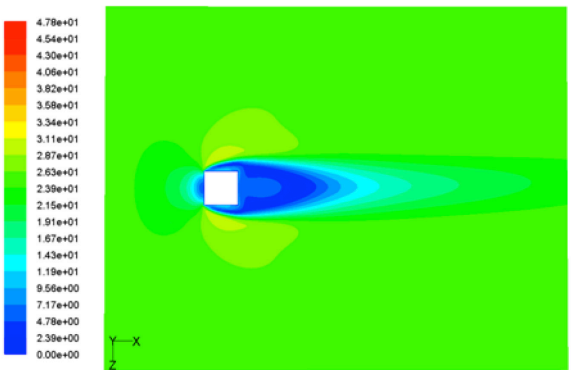

(a) Case 1A (ABL): Horizontal plane at mid-height of the parallelepiped.

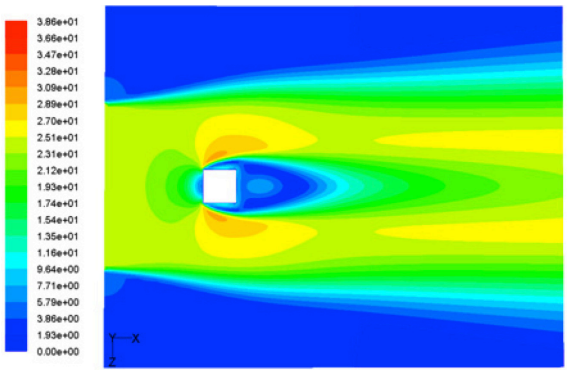

(b) Case 1B (WoW): Horizontal plane at mid-height of the parallelepiped.

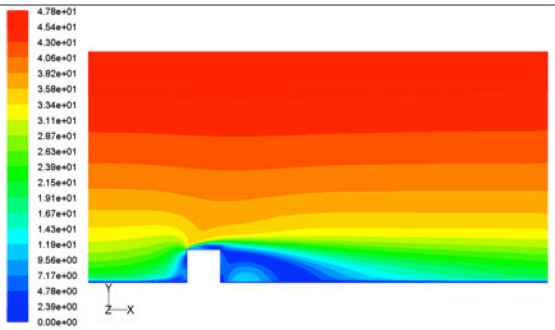

(c) Case 1A (ABL): Vertical plane at the center of the parallelepiped.

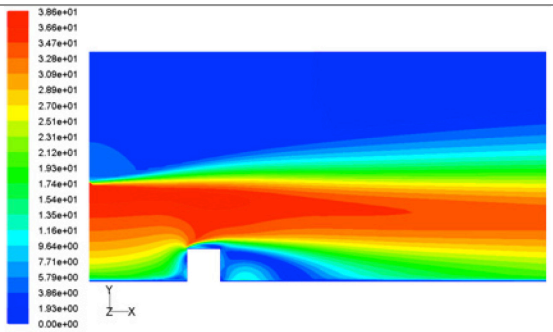

(d) Case 1B (WoW): Vertical plane at the center of the parallelepiped

Figure 3.7 Wind velocity contour plots for ABL and WoW simulation.

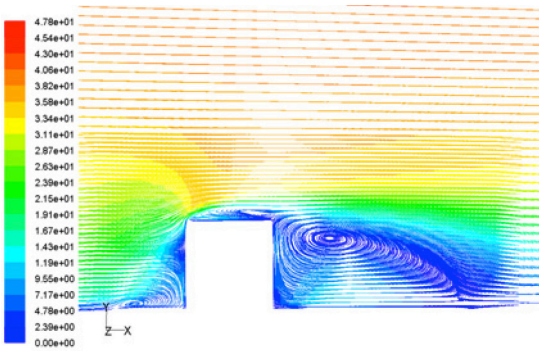

Case 1A (ABL)

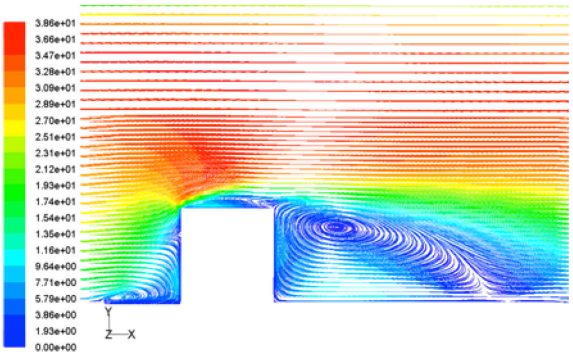

Case 1B (WoW)

Figure 3.8 Wind velocity path-lines and recirculation zones.

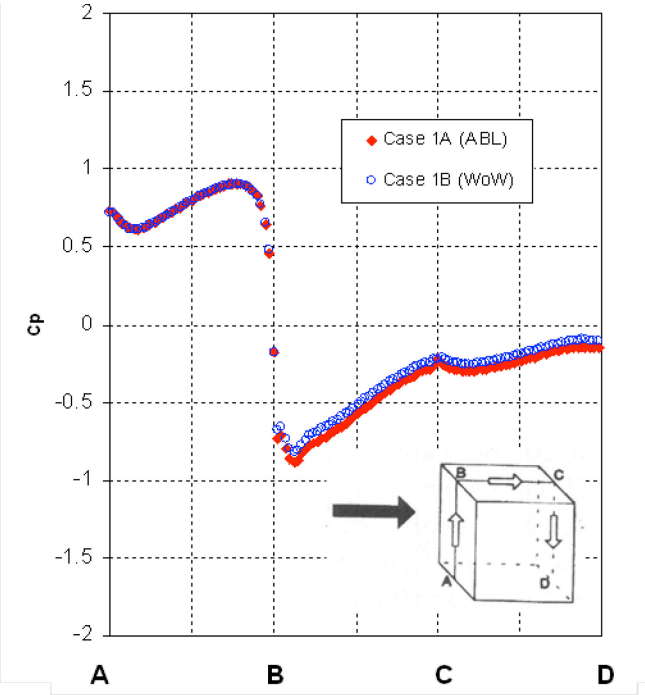

Figure 3.9 ABL and WoW mean pressure coefficient comparisons for Case 1 (3x3x3 m cube)

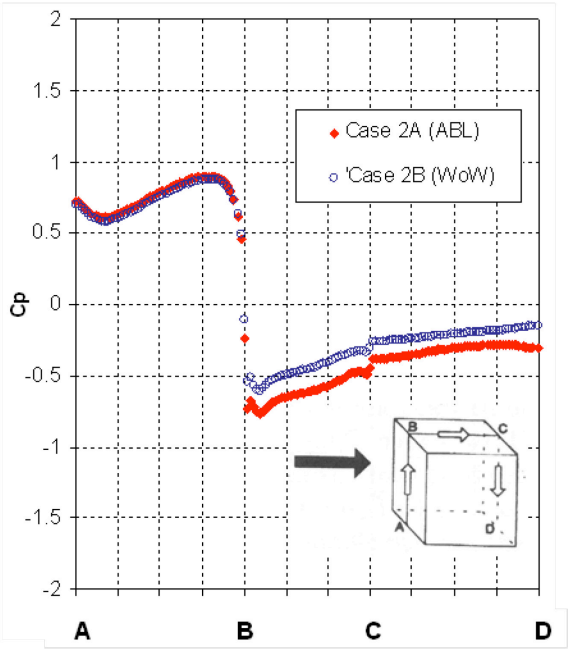

Figure 3.10 ABL and WoW mean Cp comparisons for Case 2 (4x4x3 m parallelepiped)

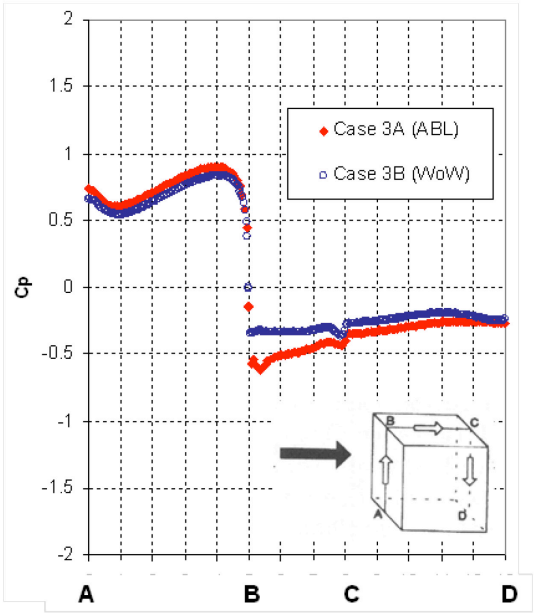

Figure 3.11 ABL and WoW mean Cp comparisons for Case 3 (5x5x3 m parallelepiped)

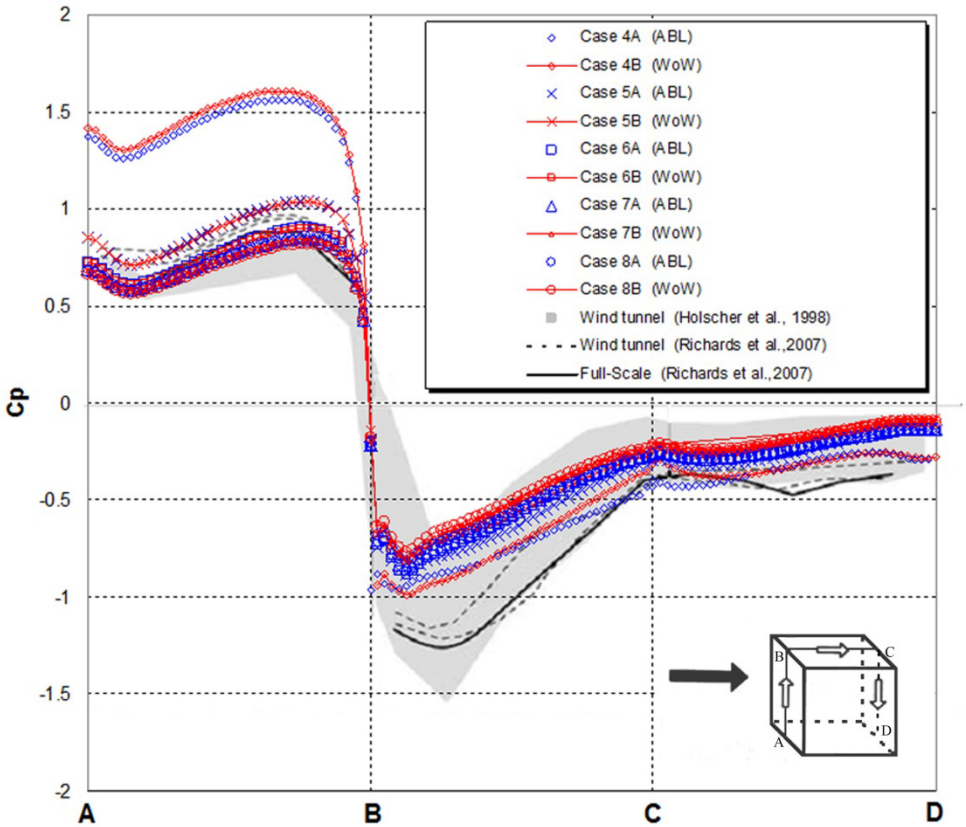

Figure 3.12 ABL and WoW mean Cp comparisons for Cases 4, 5, 6, 7 and 8 with wind tunnel data from literature.

4 NUMERICAL SIMULATION OF HURRICANE WIND LOADS ON LOW-RISE BUILDINGS WITH COMPLEX ROOFS

Agerneh K. Dagnew[a], Girma T. Bitsuamlak[*, b]

A Paper Prepared for the ASCE Journal of Structural Engineering and Presented in the 3rd AAWE 2012 Conference

Abstract

The present study attempts to evaluate wind loads on roofs using a numerical approach based on the Large Eddy Simulation (LES) method, by focussing on complex roofs that are not covered in building codes and standards. Two different types of complex roofs with and without neighbouring conditions under sub-urban terrain condition were considered. To assess the efficacy of the numerical models a comparison with boundary layer wind tunnel data was carried out for all four cases. The numerically generated mean and peak pressure coefficients agreed well with experimental data, although the agreement for mean values were better compared to peaks, windward better than leeward. It can be safely concluded that LES with proper grid density and inflow generation could be used as an additional resource at least for preliminary design wind load estimations.

Keywords: LES, wind tunnel, field measurement, inflow turbulence, pressure coefficient, complex roof, low-rise building, sub-urban

[a] Ph.D. Candidate, [*]Adjunct Prof., Laboratory for Wind Engineering Research (LWER), International Hurricane Research Center (IHRC) /Department of Civil and Environmental Engineering, Florida International University (FIU), Miami, FL 33174, USA

[b]Associate Prof., Department of Civil and Environmental Engineering, University of Western Ontario in London, ON, Canada.

4.1 Introduction

The recent experience with major hurricanes that have made landfall in North America is a grim reminder of the catastrophic effects of strong winds. Roof systems are exposed to higher loading than any other building element and are subjected to wind forces from many directions (Smith et. al, 1991). Suction pressures on the surface of the roof and roof corner vortices can lift both roof cladding and sheathing leading to water intrusion and cause further structural damage. The wind flow patterns over a roof are very complex because of the various possible shapes of a roof along with the turbulent ABL flow characteristics. Currently building codes and standard provisions, including ASCE 7 2005 and NBCC 1995, that were derived from Boundary Layer Wind Tunnel experiments provides design wind loads for common shapes such as mono slope, gable and hip (see Fig. 4.1).

While gable roofs comprise the majority of architectural form on engineered low-rise buildings, which are generally subject to deemed-to-comply provisions of building codes and standard, the overall housing stock exhibit a myriad of roof shapes. Post disaster studies have revealed that similar standards of residential low-rise construction of different geometric forms have suffered a disparity in wind-induced damage (Meecham, 1992, FEMA 2005). For complex shapes and surrounding conditions there is a gap in design wind load information. Building codes and standards such as ASCE 7-05/10 and NBCC 2005 refer to physical model testing for wind load evaluation of buildings with complex configurations such as a typical residential construction with complex roof shapes and architectural features. Although these tests are viable for high-rise buildings and other large complex projects, they may not be cost effective for residential houses.

The evolution of Computational Wind Engineering (CWE) based on the techniques of Computational Fluid Dynamics (CFD) is making numerical evaluation of wind loads an attractive proposition for the design community. This is particularly true in light of the positive trends in hardware and software technology development. The main purpose of this research project is to evaluate wind-induced loads on low-rise residential buildings with complex roof shapes computationally, and validate the results using experimentally obtained data. The present study targeted low-rise buildings with complex roof shapes with and without surrounding buildings that are not covered in the current building codes and standards. The outcome of the investigations in the long term is expected to support the case where building codes and standards in the future may begin to also consider CFD as one of the commonplace tools for wind load evaluation, especially for the design of low-rise residential houses.

4.2 The current state of computational wind engineering

Practical applications of CFD are widespread in areas such as pedestrian level wind evaluation, where mean wind velocities are required for evaluating comfort issues (Hanjalić and Kenjereš, 2008) and for building ventilation design applications (Jiru and Bitsuamlak, 2010). Some of the works in CFD applications for wind load evaluation includes non-linear Reynolds-averaged Navier-Stokes (RANS) modeling for full-scale low-rise buildings such as the Silsoe Cube (Wright and Easom, 2003), the computational prediction of flow-induced pressure fluctuations on the Texas Tech University (TTU) test building (Senthooran et al., 2004) and the computation of pressure on TTU (Selvam, 1996). Also, there has been CFD research on tall buildings such as the Aerodynamics of

Commonwealth Advisory Aeronautical Research Council (CAARC) model building – a benchmark tall building used to calibrate wind tunnels around the world -- (Dagnew et al., 2009, 2010; Braun and Awruch, 2009; and Huang et al., 2007); Large Eddy Simulation (LES) of flow and building wall pressure in the center of Tokyo (Nozu et al,. 2008); LES of wind effect on a full-scale supper-tall building (Huang et al., 2010); flow around high-rise buildings using various turbulence models by Tominaga et al (2008a); topographic studies over complex terrains (Tamura et al 2007, Stathopoulos, 1999, 2002; Ishihara et al., 1999, Bitsuamlak et al., 2004, 2005b, and 2007). More recently, exponential growth in computing technologies have helped analyze 3D complex wind flow fields using LES and Direct Numerical Simulation (DNS) with reasonable computational cost and enabled wind load estimation with high accuracy (Tamura et al., 2008).

Some countries have already established working groups to investigate the practical applicability of CWE and develop recommendations and guidelines for efficient implementation and use for wind resistant design of actual buildings and for assessing pedestrian level winds, within the framework of the Architectural Institute of Japan (AIJ) (Tamura et al. 2008, (Tominaga et al., 2008) and the European cooperation in the field of scientific and technical research (COST, 2007; Franke, 2006). AIJ provides methods for predicting wind loading on buildings by RANS and LES. While COST Action 732 (COST732, 2007) outline a best practice guideline for successful CFD simulation of wind flows in the urban environment using steady RANS equations.

Wind loads for residential buildings are affected in a complex way by many factors, such as incoming wind characteristics (wind speed, turbulence intensity, integral

length scales, etc.), topography and surface roughness, immediate surroundings, building/roof shape and orientation. Hence, before getting to the wind load evaluation phase any CWE simulation should put an effort to incorporate all of these factors in a manner that is as realistic as possible in order to produce a usable outcome.

4.3 Experimental test setup

4.3.1 Low-rise building with regular roof shape (gable and hip)

Wind tunnel tests were conducted on 1:15 scale models of one-story single-family residential buildings to study the distribution of roof pressure. For the current investigation, two different roof geometries were fabricated, a 3:12 slope gable roof model (Fig. 4.2(a)), and a 3:12 slope hip roof model (Fig. 4.2(b)). The scale model has dimensions of L=1.2m(4ft), W=0.6 m(2ft) and H=0.3m(1.1ft) where L and W denote the longer and shorter widths respectively and H denotes the roof ridge height. At this size, the maximum building model blockage ratio in the wind tunnel was approximately 9% (only marginally higher than the maximum blockage of 8% recommended in ASCE-7 (2010). The wind tunnel tests were carried out at RWDI's boundary layer wind tunnel facility in Florida USA. The wind tunnel has a cross-section of 2.13m x 2.44m (7ft x 8ft) and the test model was placed on a turntable located 13.3m (43.5ft) downstream of the tunnel entrance. An attempt was made to generate only the lower part of the atmospheric boundary layer at a relatively large scale. The test was conducted in an open terrain exposure. The Reynolds numbers in the present study was calculated to be $7.84E^{05}$. The mean wind speed profile fits well with a target profile obtained with a power law exponent of 0.15(~1/6.5). Moreover, the turbulence intensity profile also fits well to a target profile of $1/\ln(z/zo)$ recommended based on the large-scale depression system

measurements (Holmes, 2007). A full-scale value of 0.02m was taken for the roughness coefficient zo as per the recommendation of ASCE7 (2010) for exposure category C.

4.3.2 Low-rise buildings with complex roof shapes

BLWT tests on two house models with complex roof shapes were used for comparison with the CFD data. The two houses were similar to the ones use for field measurement as part of the Florida Costal Monitoring Program (FCMP) (Liu et al., 2009). The two buildings were represented as FL27 and FL30, respectively. These were two of the 42 home neighborhoods in FCMP. The wind tunnel tests were collected at Western Boundary Layer Wind Tunnel Laboratory (see acknowledgment) as part of as part of NSF Grant CMMI-0928563. FL-27 is a one-story single-family residence located in Gulf Breeze, Florida (Figure 4.3). The gable roof consists of multiple levels, with the main ridge at 6m elevation above grade.

The BLWT tests used a suburban exposure similar to the ASCE7-10 exposure B (suburban exposure). From the Google images provided in Figure 4.4, both FL27 and FL30 are surrounded with 1 or 2 story single-family dwellings on one side and wooded area on the other side, within a radius of 0.5 miles (800 m). The wind tunnel accounted the surrounding terrain within 1 mile radius of the target building. Figure 4.5(a) shows the 1: 50 scale model of LF27 which contains 496 taps systematically distributed on the roof. Figure 4.5(b) shows the FL30 model building with 474 taps on its roof. The boundary layer simulation of the model buildings with neighboring houses were done by placing the test house model at the center of the turn table (Fig. 4.6) surrounded by the scaled models of the houses located within a radius of 250 ft (full-scale). The radius of

the surrounding assumed for the BLWT study took into consideration of the model building size.

4.4 Numerical modeling

The numerical evaluation of wind effects on buildings involves various modeling steps. The pre-processing step consists the conceptual modeling to the CAD preparation and to the generation of high quality computational meshes. Due to the complexity of the wind/structure interaction, care should be taken during the model preparation phase. This includes the selection of appropriate turbulence model, such as RANS, LES, and hybrid RANS/LES models, which can realistically capture the important structures of the wind flow. To ensure the best use of the turbulence models in getting the accurate numerical prediction of wind-induced effects, the sizing of the computational domain and prescription of the boundary conditions should also be carefully defined. Parallel simulations were carried out using a solver of commercially available software, Fluent14 (Ansys Inc., 2012). All simulations were carried in the Multidisciplinary Analysis Inverse Design Robust Optimization and Control Laboratory (MAIDROC) lab, which has 272 processors parallel computing nodes, but using only 28 CPUs due to the limitations on the number of software licenses. The following sections describe in detail the procedures and the modeling principles used in the present study.

4.4.1 Geometrical model preparation of test buildings for CFD

The geometrical modeling for the CFD simulation adopted the same wind tunnel scale building models. For the two regular shape CFD models, gable and hip roof buildings, only an isolated building case was investigated using a 1:15 scale, since the wind tunnel data was carried out for an isolated building. Figure 4.7 shows the three-

dimensional perspective view of the regular roof model buildings. For buildings with complex roof shapes the dimensions and the surrounding context for the LES simulation were determined from a combination of the actual wind tunnel model at Western and information provided by the University of Florida research group. The adopted LES is the same as the scale of the BLWT testing, i.e. 1:50. Figure 4.8 provides the overall dimensions for FL27 and FL30 LES models. Figure 4.9 show the topology of FL27 and FL30 with the surrounding buildings inside the idealized turntable of the computational domain.

4.4.2 The LES model and inflow turbulence

LES is a multi-scale computational modeling approach that offers a more comprehensive way of capturing unsteady flows. The use of LES as a wind load evaluation tool has been significantly improved in recent years through the following numerical techniques (a) numerical generation of transient inflow turbulence (Kraichan, 1970; Lund et al., 1998; Nozawa et al., 2002, 2005; Smirnov et al., 2001; Batten et al., 2004), (b) development of efficient sub-grid scale turbulence modeling techniques suitable for unsteady three-dimensional boundary separated flows, and (c) numerical discretization with conservation of physical quantities for modeling complicated geometry (Tamura et al. 2008). Because of these advancements, LES holds promise to become the future computational wind engineering (CWE) modeling for which turbulent flow is of pivotal importance (Tamura, 2008; Tucker and Lardeau, 2009; Sagaut and Deck, 2009). In the present study, the Dynamic Smagornisky-Lilly subgrid-scale (SGS) model based on Germano et al. (1996) and Lily (1992) have been employed. In this

method the Smagornisky constant, C_s, is computed dynamically according to the resolved scales of motion inside the domain.

For the present study, in addition to the mean velocity and turbulence intensity profiles that were similar to the wind tunnel, transient velocity fluctuations were superimposed at the inlet boundary of the LES simulations. A method called the discretizing and synthesizing random flow generation (DSRFG) for the transient inflow turbulence, which has the flexibility to prescribing any arbitrary 3D spectrum for the amplitude of the fluctuation such as the von Karman spectra (Huang et al., 2010) were used. The synthesized velocity field is presented below for discussion purposes and the detailed formulation and derivation can be found in the original paper (Huang et al., 2010).

$$u(x,t)=\sum_{m=k_0}^{K_{ma}}\sum_{n=1}^{N}\left[p^{m,n}\cos\left(\tilde{k}^{m,n}\tilde{x}+\omega_{m,n}t\right)+q^{m,n}\sin\left(\tilde{k}^{m,n}\tilde{x}+\omega_{m,n}t\right)\right] \tag{4.1}$$

where $p^{m,n}$ and $q^{m,n}$ are the vector form of the fluctuation amplitude. For inhomogeneous and anisotropic turbulence the distribution of $k^{m,n}$ is done by remapping the surface of the sphere after the components of $P^{m,n}$ and $q^{m,n}$ are aligned with the energy spectrum. In addition to the flexibility of prescribing any arbitrary 3D spectrum, the DSRFG method uses the length scale ($L_s=\sqrt{L_u^2+L_v^2+L_w^2}$) as a scaling factor and this resulted in the generation of spatially correlated flow fields with the relevant length scales.

4.4.3 Computational domain and boundary conditions

The computational domain (CD) defines the region where the flow field is computed. The size of the CD should be large enough to accommodate all relevant flow features that will have potential effects on altering the characteristics of the flow field within the region of interest (Franke, 2006, COST 2007, AIJ 2008). In addition, the sizing also should take into account the computational overhead that will be incurred by using an excessively large domain. For the present study multiple steady state preliminary simulations were conducted to size the computational domains and the combination of sizes which resulted in a blockage ratio of less than 5% were used for the main simulations. The blockage ratio is defined as the ratio of the projected area of the surfaces of the model buildings in the flow direction to the area of the inlet boundary. Table 4.1 summarizes the dimensions of the models, the computational domain, and the resulted blockage ratio of the cases considered in the present study. For FL27 and FL30 with the neighboring houses, the CD was sized using the maximum building height within the vicinity of the target model and the resulting blockage ratio was 7 and 6%, respectively.

Boundary conditions (BC) represent the effect of the surroundings that have been cut off by the CD and idealize the influence of the actual flow environment under consideration. BCs could dictate the solution inside the CD and have significant effects on the accuracy of the solution. At the inlet boundary, the mean wind velocity and turbulence intensity profiles similar to the wind tunnel were prescribed. For example the wind speed and turbulent intensity profiles of the complex roof shape buildings (FL27 and FL30) measured at the UWO wind tunnel (Fig. 4.10) were applied for the CFD

simulation. The mean velocity profile was prescribed by the power law (with exponent $\alpha = 0.1658$), and the turbulence intensity profile was found by curve fitting (Fig. 4.10). For velocities, a no-slip boundary is used at the solid walls. A symmetry boundary condition was employed at the top and lateral surfaces of the CD. Since details of the flow variables were not known prior to the simulation, an outflow boundary was applied at the outlet plane. Figure 4.11 shows a typical CD and boundary conditions modeling for the benchmark simulations.

The computational domain and boundary conditions were setup for buildings with complex roof shape after careful CAD modeling and topology cleanup, as shown in Fig. 4.12. For the case with the neighboring buildings the CD size were increased to accommodate the surrounding buildings (Fig. 4.13).

4.4.4 Computational grid, spatial, and temporal discretization schemes

The computational grids were generated using Ansys Meshing CutCell Cartesian meshing algorithm. This mesh tool has a unique ability to generate a large fraction of hexahedral cells in complex configurations. The mesh operation involves a two-stage inflation process to resolve the inner boundary layer and generate sufficient quality for convergence. Successive adaptations have been done to refine the cells' sizes and resolve the near-wall region of the model buildings. In the inner sub-layer region, the boundary layer meshes were inflated from the ground surface and the first cells were placed at a distance $y_p = 0.0005\,m$ with a stretching ratio of 1.05. This ensured $y^+ \left(u_* y_p / \nu, wall\ unit \right)$ to be less than 5 units. In addition, the computational domain was subdivided into multi-body parts to have better control and distribution of the

computational grid points around the model building and wall boundary. The regions within the vicinity of the sharp edges were treated by clustering very fine grid cells with a stretching ratio of 1.05, to help negotiate the change of the topology (Fig. 4.14 and 4.15).

For discretization of convection terms central-differencing based schemes give the least numerical diffusion and the best accuracy compared to the upwind schemes, as demonstrated by Marinuzzi and Tropea (1993). However, for high *Re* flows in the wake region, such as the present cases, this scheme can become unstable, giving unphysical oscillations (wiggles). The bounded central differencing (BCD) scheme, essentially based on the normalized variable diagram (NVD) approach (Leonard, 1991) together with a convection 'boundedness' criterion can detect and remove these wiggles in the wake region. Because of this the BCD scheme has been used for all the simulations of the present study. For temporal discretization, second-order schemes are advised for most computational wind engineering applications and have been used in the present study. A second-order scheme for pressure discretization has been applied. For pressure-velocity coupling, the Pressure Implicit with Splitting of Operators (PISO) algorithm with skewness and neighboring correction is recommended for the transient simulation and has been used in all LES simulation. PISO is based on the higher degree of the approximate relation between the corrections for pressure and velocity (Ansys Inc., 2012). The simulations have been carried out at the supercomputer center at Florida International University. The parallel computations have been carried out using 28 CPUs. A computational time step of 0.001s with 5 sub-iterations, per time step, was used in all the simulations. First the simulation run for enough flow time and once the solution reached a stable condition, the fluctuating pressure data were recorded for 2s flow-time.

Also, for the residuals a strict convergence criterion of 10^{-5} has been applied to ensure full convergence of the simulations.

4.5 Results and discussion

4.5.1 Wind-pressure coefficients for regularly shape low-rise residential roofs

Wind induced forces can be obtained from the time-history of the pressure data. In the present work, pressure coefficients obtained from the CFD simulations and the wind tunnel tests were converted into non-dimensional mean pressure coefficients (C_p), normalized with the dynamic pressure head and defined using the following expression:

$$C_P = \frac{P - P_o}{\frac{1}{2}\rho_a V_H^2} \tag{4.2}$$

where P is the pressure measured on the building roof surface, P_0 is the reference pressure, ρ is the density of air, and V_H is the reference wind speed at mean roof height of the building.

Gable roof building: For the numerical investigation of wind pressure coefficients were evaluated for three wind directions were considered (Table 4.2)

Figure 4.16 shows the mean pressure coefficients measured at the pressure taps located at centerline of the roofs perpendicular to the ridgeline. For the straight wind (0^0 AoA) the LES predicted well except at the taps near the edge of the roof where flow separates. For the oblique wind directions (Case 1 and 2) the LES resulted in a good prediction comparable to the BLWT result. Figure 4.20 shows the comparisons of the mean pressure coefficients contour plot for the BLWT and LES. From the illustration it can be seen that for Case 1 the oncoming flow separated at the leading edge of the roof

and remain separated to the lee-ward region of the roof, as indicated by the negative pressure on the surface of the roof (Fig. 4.17(a) and (b)). This introduced very high suction pressure at the windward edge of the roof and the suction intensified at the ridge edge. For the oblique wind AoA (Case 2) the distribution of the pressure contours show the formation of corner vortices, responsible for uplift wind forces (Fig. 4.17(c) and (d)). Large structures (eddies) on the longer side of the roof and on the shorter side of the roof small structure with high fluctuation were formed. This type of fluctuating pressure could initiate the failure of roof coverings. For the 90^0 wind direction (Case 3) the oncoming flow reattached back to the roof at lee-ward and as a result part of the roof in the reattachment region experienced a low positive pressure (Fig. 4.17(e) and (f)). Overall there is a good agreement between the LES simulations of the gable roof models with and the experiments.

Hip roof: LES was used to assess the performance of hip roof building in comparison with the gable roof and its response for wind directionality effects three wind directions have been considered for the numerical and wind tunnel simulations. Table 4.3 summarizes the cases studied for the hip roof building.

Figure 4.18 shows the comparison of the mean pressure coefficients of the hip roof. The mean Cp is computed from the time-history of pressure recorded during the LES simulation and the BLWT testing. The LES simulations predicted the mean C_p very well, especially for the 0^0 wind AoA. There is slight over-prediction of the time-averaged C_p for the oblique wind. For Case 3 (90^0) the Cp measured at the centerline of

the hip roof showed very small pressure coefficients ($C_p \approx 0$). This is in line with the response of the gable roof building for the same wind direction (Fig. 4.18(c)).

Figure 4.19 shows the contour map of a typical hip roof under turbulent wind field. The LES reproduced most of the important flow features such as separation, re-attachment and corner vortices on the surface of the building. Qualitatively, there is a good agreement between the LES and the BLWT results. The use of a time-history approach and transient inflow turbulence contributed to the improved prediction of wind loads for oblique wind direction, which usually for such type of wind the numerical simulations fail to accurately estimate the wind effects. The assumption of constant integral length and turbulent intensities in the lateral and vertical directions, due to the size of the model scale it was not possible to measure these properties in the lower part of the study buildings during the wind tunnel testing, attributed to the slight discrepancies of the LES results.

4.5.2 Wind-pressure coefficients on complex roofs of low-rise houses

The numerical investigation of wind-induce pressure loads on buildings with regular and complex roof shapes were carried out using the technique of LES. Table 4.4 shows the cases considered for the complex roof buildings study. The time-history of pressure data was recorded at the pressure taps that are systematically distributed on the critical section of the roofs (Fig. 4.20). The mean pressure coefficients of the LES simulations and the BLWT data for the complex roof FL27 were plotted along the pressure tap lines and compared, as shown in Fig. 4.21. The prediction of the time-

averaged Cp by the LES follows the same pattern as the experimental data. Figure 4.22 shows the mean pressure coefficient profiles for FL30 measured at the highlighted taps.

The contour map of the mean pressure coefficients illustrates how the neighboring buildings could affect the wind load distribution of the target or study building, shown in Fig. 4.23. The interference and sheltering effects resulting from the surrounding houses modifies the contour map. In some cases it increases in the pressure loads and in another instance it increases the suction pressure load. These highlight the importance of consider these effects when evaluating the design wind loads for roofs of irregular shapes buildings. Overall the mean pressure coefficient profile of the LES simulations near the ridge showed some discrepancies from the experiment. The pressure load distribution on the roofs of these models displayed a variation that is completely different from the one by the regular shape models. However, considering the sharp edges of the building and the assumptions used in translating the wind tunnel data to the CFD modeling (such as the assumption of constant integral length in the lateral and span, turbulent intensity), the results are very encouraging.

4.5.3 Peak load estimation

Estimation of the largest wind-induce peak load is very crucial in determining the internal design forces of structures, structural and non-structural components, and assessing their reliability under sever wind storm. In the present study the time histories of fluctuating wind pressure recorded from HFPI-type LES simulation were used to estimate the non-Gaussian peaks of low-rise buildings with regular. Sadek and Simiu (2002) procedure of estimating the peak stochastic response of low-rise buildings to wind was used. One advantage of using such a method is that it provides statistically

representative peak as the estimation uses the information contained in a whole sample record that that at just one instant in time. This is particularly useful for CFD based simulation as the length of the sample is usually short, mainly dictated by physical constraint such as computational resource. The result showed that CFD can be used to estimate the peak pressure loads. However, it's computationally expensive to measure large data record.

4.5.4 Velocity flow field visualization

To illustrate the importance of studying wind directionality, velocity streamlines of two wind direction were studied. Figure 4.24 and 4.25 show the surface velocity streamlines of FL27 and FL30 with neighboring buildings, respectively. The neighboring structures clearly changed the flow dynamics of at the incidence plane of the study buildings. Because of these, channeling, sheltering, and wake effects were observed.

4.6 Conclusions

The numerical investigation of wind-induce pressure loads on buildings with regular and complex roof shapes were carried out using the technique of LES. The study of the roof pressure distribution revealed that the mean pressure coefficient predicted by the LES simulation is in a good agreement with the wind tunnel data. The study also showed that oblique angle wind could introduce uplift pressure loads. The models with complex roof shapes showed mixed pressure distribution on the roof (positive and negative pressure) as opposed the regularly shaped models where separation and reattachment location are clearly known. An attempt has been made to estimate peak value from the numerical data. However, considerably discrepancy has been occurred.

LES captured the common fact that mean pressures on the gable roof are generally higher than those on the hip roof which has been confirmed by a number of similar previous studies as well. On both roof models, high suction pressures were observed on areas close to the windward edge and near the middle ridge. This makes sense physically since these are the areas where flow separation is expected to occur. The highest magnitude roof suction pressures were observed in the corner areas close to the edges for both roof types. On the hip roof model, the highest suction pressure was observed when the wind came from the diagonal directions, while the highest suction pressures on the gable roof model was observed when the wind came perpendicular to the short dimension.

LES was found very useful for complex roof cases, where building standards and codes do not provide design wind loads. The mean pressure coefficients between LES and the wind tunnel data revealed that there is a general agreement between the two. The flow visualization from LES could be useful to rationally encourage design of low rise buildings for wind performance. It is fair to conclude that CFD simulations such as LES can be used as an alternative tool for wind pressure load evaluation of low-rise building at least for preliminary design

Acknowledgments

This research was supported by the *National Science Foundation CAREER* under Grant No. 0846811. Any opinions, findings, and conclusions or recommendations expressed in this material are those of the authors and do not necessarily reflect the views of the granting agency. The financial support from Florida Department of Emergency Management (FDEM) is gratefully acknowledged. We are grateful to Drs Gurley, Prevat,

Masters and Kopp for providing us the wind tunnel data used for the complex roof comparison (NSF Grant CMMI-0928563).

References

ASCE-7 (2010), ASCE/SEI 7-10 Minimum design loads for buildings and other structures. American Society of Civil Engineers, Reston, VA.

ASCE (2010), Minimum Design Loads for Buildings and Other Structures, Reston, VA, American Society of Civil Engineers.

Ansys Inc. (2012), "Ansys Fluent 14 User's Guide", Ansys Inc., Lebanon. 13.0.

Batten, P., Goldberg, U., Chakravarthy, S. (2004), "Interfacing statistical turbulence closures with large-eddy simulation", AIAA Journal 42(3), 485–492.

Blessing, C., Chowdhury, A. G., Lin, J., Huang, P. (2009), "Full-scale validation of vortex suppression techniques for mitigation of roof uplift", Engineering Structures, 31(12), pp. 2936–2946.

Bitsuamlak, G.T., Stathopoulos, T., Bédard, C., (2007). "Modeling the Effect of Topography on Wind Flow Using a Combined Numerical–Neural Network Approach", Journal of Computing in Civil Engineering, ASCE, Vol. 21, No. 6, pp 384-392

Bitsuamlak, G.T., Stathopoulos, T., Bédard, C., (2005), "Effect of upstream hills on design wind load: a computational approach", Wind and Structures. Vol. 9, No. 1, pp. 37-58.

Bitsuamlak, G.T., Stathopoulos, T., Bédard, C., (2004), "Numerical evaluation of turbulent flows over complex terrains: A review", Journal of Aerospace Engineering, Vol. 17, No 4, pp. 135-145.

Braun, A.L., Awruch, A.M. (2009), "Aerodynamic and aeroelastic analyses on the CAARC standard tall building model using numerical simulation", Computers and Structures 87, 567-581.

COST (2007), "Best practice guideline for the CFD simulation of flows in the urban environment", COST Action 732.

Dagnew, A.K., Bitsuamalk, G.T., Ryan, M. (2009), " Computational evaluation of wind pressures on tall buildings", 11th American conference on Wind Engineering. San Juan, Puerto Rico.

Federal Emergency Management Agency (FEMA) (1992). " Building performance in hurricane Andrew in Florida observations", Recommendations and Technical Guidance", Federal Insurance Administration, USA.

Franke. J. (2006), "Recommendations of the COST action C14 on the use of CFD in predicting pedestrian wind environment".

Germano, M. U. Piomelli, P. Moin, and W. H. Cabot. (1996), "Dynamic Subgrid-Scale Eddy Viscosity Model". In Summer Workshop. Center for Turbulence Research, Stanford, CA.

Hamid, S., (2005), "Exposure and vulnerability components of the Florida public hurricane loss projection model", Engineering team Final Report, Laboratory for insurance, finance, and economic research, International Hurricane Research Center, Florida International University.

Hanjalic´,K., Kenjereš, S., (2008), "Some developments in turbulence modeling for wind and environmental engineering", J. Wind Eng. and Ind.Aerodyn.96, 1537–1570.

Holmes, J., (2007), "Wing loading of structures," 2nd ed. Taylor & Francis.

Huang and Q.S. Li., (2010), "Large eddy simulation of wind effects on a super-tall building", Wind and Structures, Volume 13, Number 6.

Huang, S., Li, Q.S., Xu, S., (2007), "Numerical evaluation of wind effects on a tall steel building by CFD",. Journal of Constructional Steel Research 63, 612-627.

Irwin, P. A. (2008), "Bluff body aerodynamics in wind engineering", Journal of Wind Engineering and Industrial Aerodynamics, 96, pp. 701-712.

Ishihara, T., Hibi, K., Oikawa, S., (1999), "A wind tunnel study of turbulent flow over a three-dimensional steep hill", Journal of Wind Engineering and Industrial Aerodynamics 83, 95-107.

Jiru, T.E., Bitsuamlak, G.T., (2010), "Computational fluid dynamics applications in predicting natural ventilation performance of buildings: A review", International Journal of Natural Ventilation, Vol. 9, No. 2, 131-147.

Leatherman, S.P., Gan Chowdhury, A., Robertson, C. J., (2007), "Wall of Wind Full-Scale, Destructive Testing of Houses and Hurricane Damage Mitigation," Journal of Coastal Research.

Lilly, D.K., (1992), "A Proposed Modification of the Germano Subgrid-Scale Closure Model", Physics of Fluids. 4. 633–635.

Lund, T.S., Wu, X., Squires, K.D., (1998), "Generation of turbulent inflow data for spatially-developing boundary layer simulations" J. of Computational Physics140, 233-258.

Martinuzzi, R., Tropea, C., (1993). The flow around surface-mounted, prismatic obstacles ,placed in a fully developed channel flow. J. Fluids Eng 115, 85–92.

Meecham, D., (1992), "The improved performance of hip roofs in extreme winds - A case study", Journal of Wind Engineering and Industrial Aerodynamics, 73 (1-3), pp. 1717–1726.

NBCC (1995), "National Building Code of Canada", National Research Council of Canada (NRC), Ottawa,Canada

NBCC (2005), "National Building Code of Canada", National Research Council of Canada (NRC), Ottawa, Canada

Nozawa, K., Tamura, T. (2002), "Large eddy simulation of the flow around a low-rise building immersed in a rough-wall turbulent boundary layer", *J. Wind Eng. And Ind. Aerodyn.* 90, 1151–1162.

Nozu.T., Tamura.T, Okuda.Y, Sanada.S. (2008), LES of the flow and building wall pressures in the center of Tokyo. J. Wind Eng. Ind. Aerodyn. 96, 1762–1773.

Kraichnan R.H. (1970), "Diffusion by a random velocity field", *Physics of Fluids*, **13(**1), pp. 22–31.

Sagaut, P., Deck, S. & Terracol, M. (2006), "Multiscale and multiresolution approaches in turbulence", London, UK: Imperial College Press.

Senthooran,S., Lee,D.D., Parameswaran,S., (2004), A computational model to calculate the flow-induced pressure fluctuations on buildings. J.Wind Eng. and Ind.Aerodyn. 92, 1131–1145.

Selvam, R.P., (1997), Computation of pressures on Texas Tech University building using large eddy simulation. J. Wind Eng. Ind. Aerodyn. 67–68, 647–657.

Smirnov, R., Shi, S., Celik, I., (2001), "Random flow generation technique for large eddy simulations and particle-dynamics modeling", *J. of F. Eng.* 123, 359–371.

Smith, Lee, T., and McDonald, J. R., (1991), "Roof Wind Damage Mitigation: Lessons from Hugo" In *Hurricane Hugo One Year Later*, Benjamin A. Sill and Peter R. Sparks, Editors. New York: American Society of Civil Engineers.

Sparks, P.R., Baker, J., Belville, J., Perry, D.C., (1985), "Hurricane Elena, gulf coast, August 29–September 2", committee on natural disasters, Commission on Engineering and Technical Systems, Natural Research Council, USA.

Stathopoulos. T., Wu, H. (2004), Computational Fluid Dynamics (CFD) for pedestrian winds. Proceedings of the 2004 Structures Congress, Nashville, TN.

Tamura, T., (2008), Towards practical use of LES in wind engineering. J. Wind Eng. And Ind. Aerodyn. 96, 1451–1471.

Tamura, T., Nozawa, K., Kondo, K. (2008), AIJ guide for numerical prediction of wind loads on buildings. J.Wind Eng. and Ind.Aerodyn 96, 1974-1984.

Tamura, T, Okuno.A, Sugio.Y, (2007), LES analysis of turbulent boundary layer over 3D steep hill. J. Wind Eng. Ind. Aerodyn.95, 1463-1475.

Tominaga, Y., Mochida, A., Murakami, S., Sawaki, S. (2008), Comparison of various revised k– ε models and LES applied to flow around a high-rise building model with 1:1:2 shape placed within the surface boundary layer. Journal of Wind Engineering and Industrial Aerodynamics 96, 389-411.

Tucker, P. G, & Lardeau, S. (2009), "Applied large eddy simulation", *Phil. Trans. R. Soc. A July 28,* 367 (1899) 2809-2818.

Table 4.1 Dimension of the mode buildings and blockage ratio of the computational domains

Case	Building dimensions (L x W x H) (in)	Wind direction (degree)	Blockage ratio (%)
Gable	48 x 24 x 12.875	0	3
		45	4
		90	1.7
Hip	48 x 24 x 12.875	0	4.3
		45	4
		90	1.7
Fl27	16.48 x 15.30 x 4.48	120	4
FL30	13.2 x 11.52 x 4.08	120	4.4

Table 4.2 Cases considered for LES and BLWT studies: Gable roof

Case	Roof type	Terrain exposure	Azimuth (degree)
Case 1	Gable	Open	0^0
Case 2	Gable	Open	45^0
Case 3	Gable	Open	90^0

Table 4.3 Cases considered for LES and BLWT studies: Gable and hip roof buildings

Case	Roof type	Terrain exposure	Azimuth (degree)
Case 1	Hip	Open	0^0
Case 2	Hip	Open	45^0
Case 3	Hip	Open	90^0

Table 4.4 Cases considered for LES and BLWT studies: Complex roof shap buildings

Case	Roof type	Terrain exposure	Azimuth (degree)
FL27	Complex	Exposure B	120^0
FL27 with neighboring	Complex	Exposure B	120^0
FL30	Complex	Exposure B	120^0
FL30 with neighboring	Complex	Exposure B	120^0

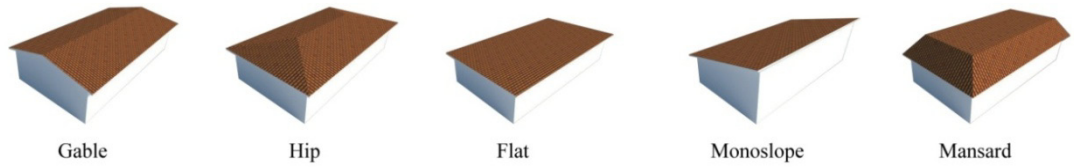

Figure 4.1 Typical types of roofs addressed in wind codes and standards.

(a) (b)

Figure 4.2 Wind tunnel testing set up for low-rise building with (a) Gable and (b) Hip roof.

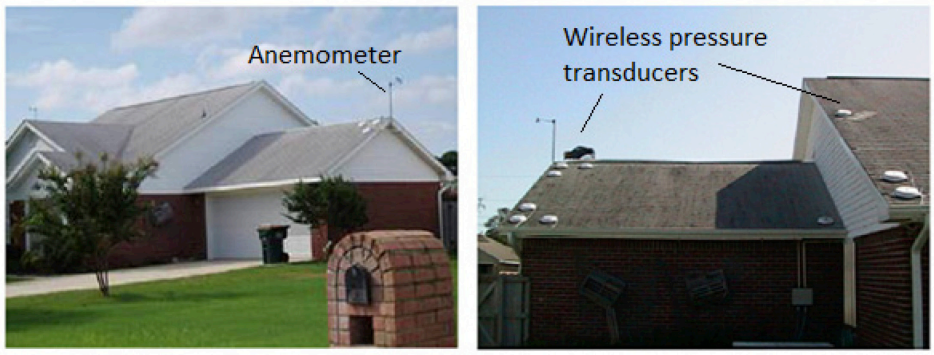

Figure 4.3 Photographs of the actual FL-27 house showing anemometer location and pressure sensor (after Liu et al., 2009).

Figure 4.4 Google image of surrounding exposures of study buildings FL27 (top) and FL30 (bottom) (after Kopp and Gavanski -- part of NSF Grant CMMI-0928563-- 2010; Liu et al., 2009).

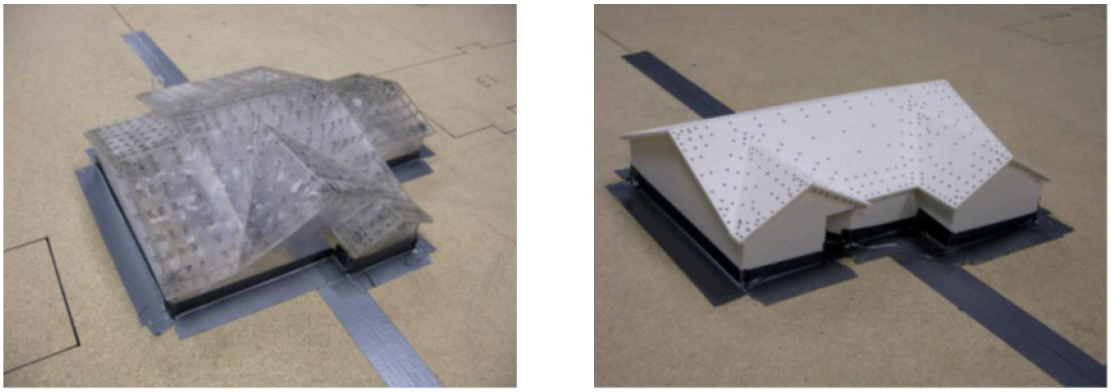

(a) (b)

Figure 4.5 Wind tunnel models of houses with complex roof shapes: (a) house model FL27 and (b) house model FL30 (after Kopp and Gavanski, 2010 -- part of NSF Grant CMMI-0928563).

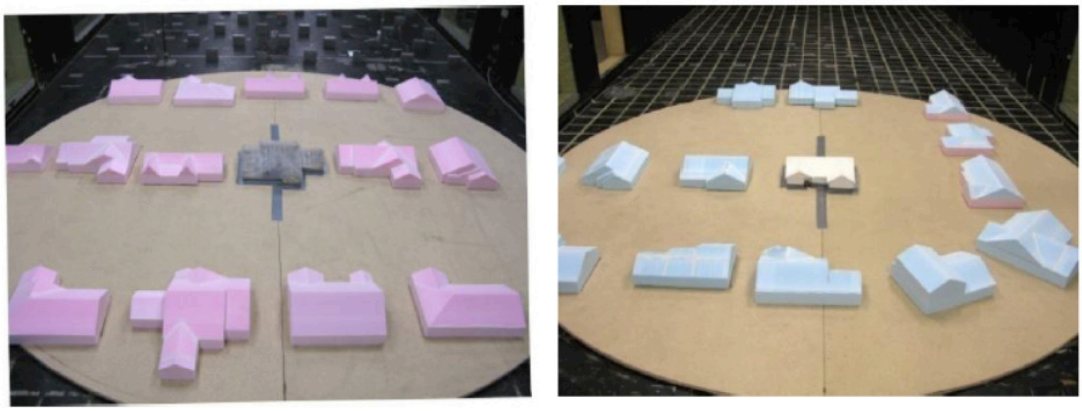

Figure 4.6 Wind tunnel setup of study houses with neighboring buildings: FL27 with neighboring house (left) and FL30 with neighboring houses (right) (after Kopp and Gavanski, 2010 -- part of NSF Grant CMMI-0928563).

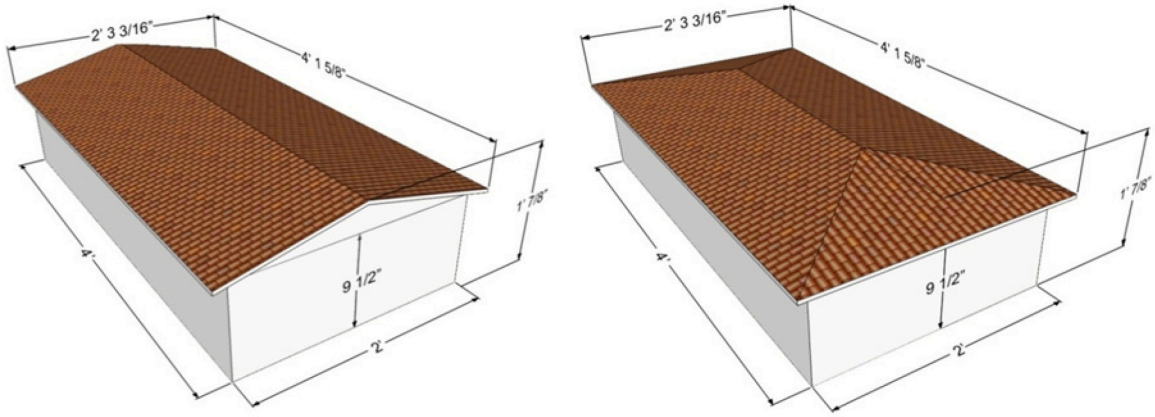

(a) (b)

Figure 4.7 Three-dimensional perspective drawings of residential buildings: (a) Gable and (b) Hip.

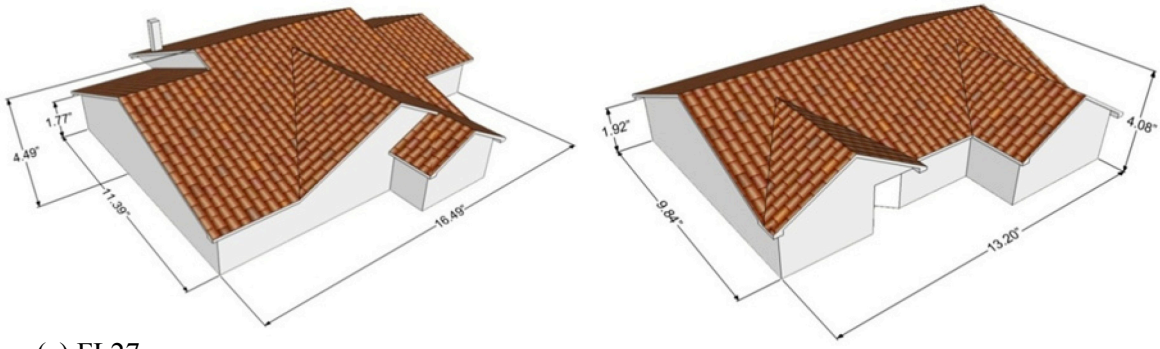

(a) FL27 (b) FL30

Figure 4.8 CAD models of single house models with complex roof shapes.

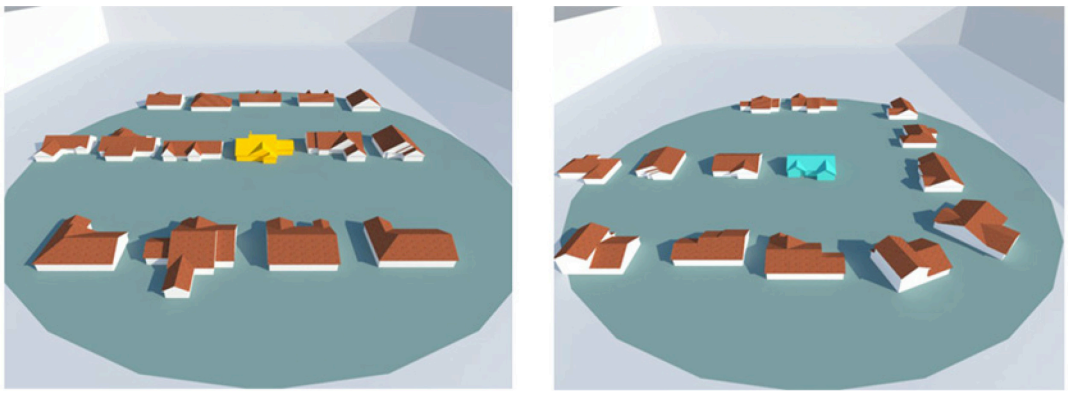

(a) FL27 (b) FL30

Figure 4.9 Geometrical models of the FCMP residential houses with neighboring buildings.

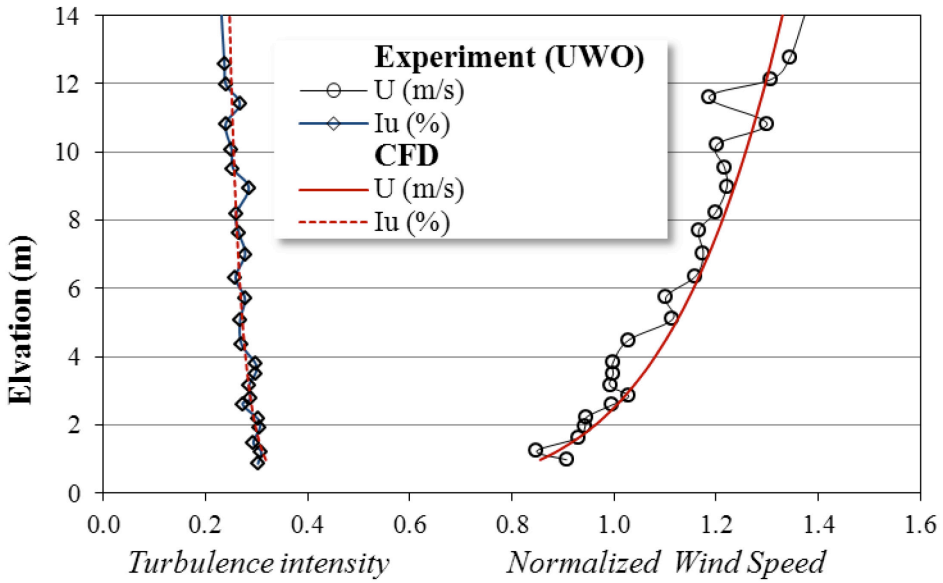

Figure 4.10 Mean wind speed referenced at mean roof height, h, and turbulence intensity profile in the suburban exposure (zo = 0.23 m) in full-scale dimensions (NSF Grant CMMI-0928563).

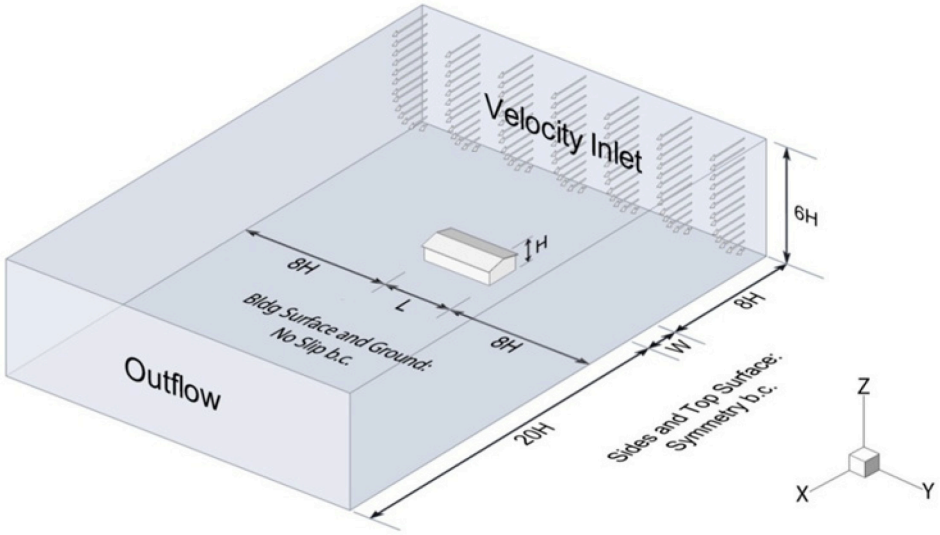

Figure 4.11 Computational domain and boundary conditions: Gable roof model.

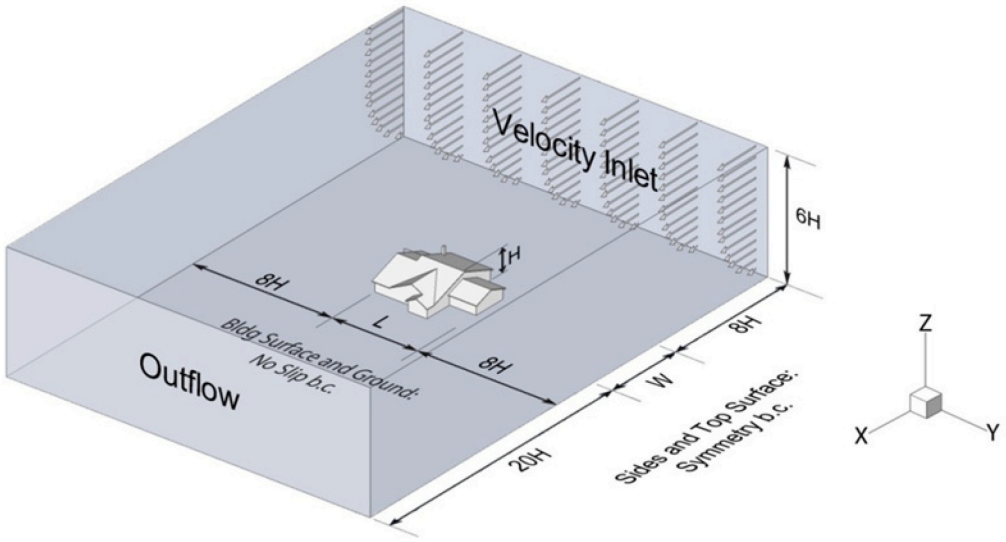

Figure 4.12 Computational domain and boundary conditions for FL27 model building.

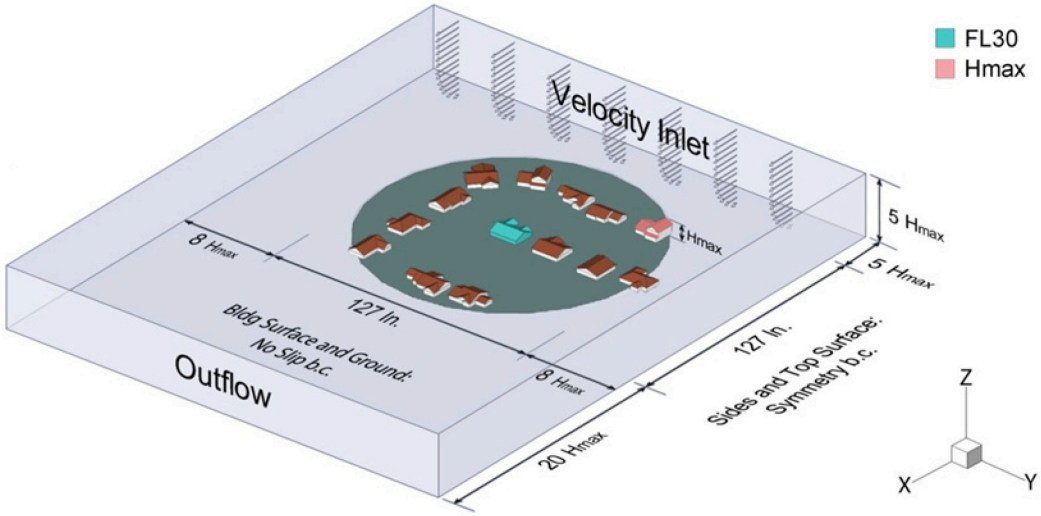

Figure 4.13 Computational domain and boundary conditions of FL27 and FL30 with neighboring houses.

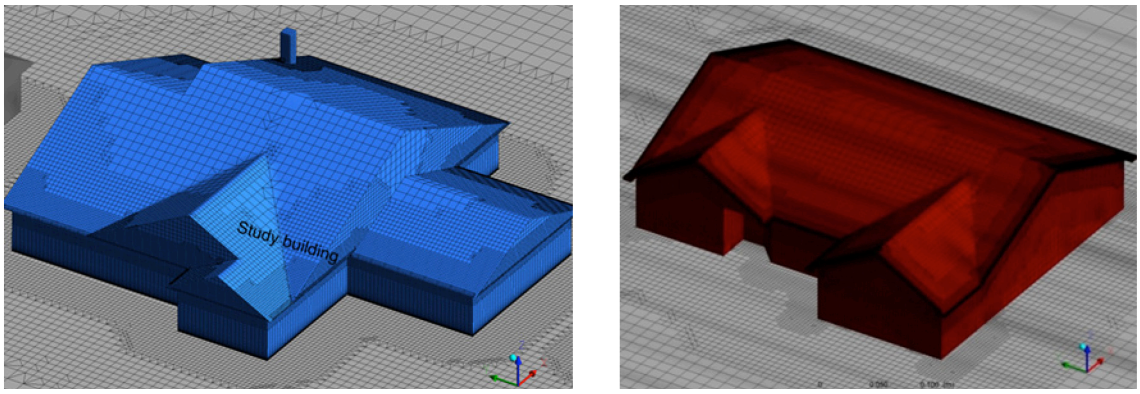

Figure 4.14 Computational mesh for FL27 and FL30 model buildings.

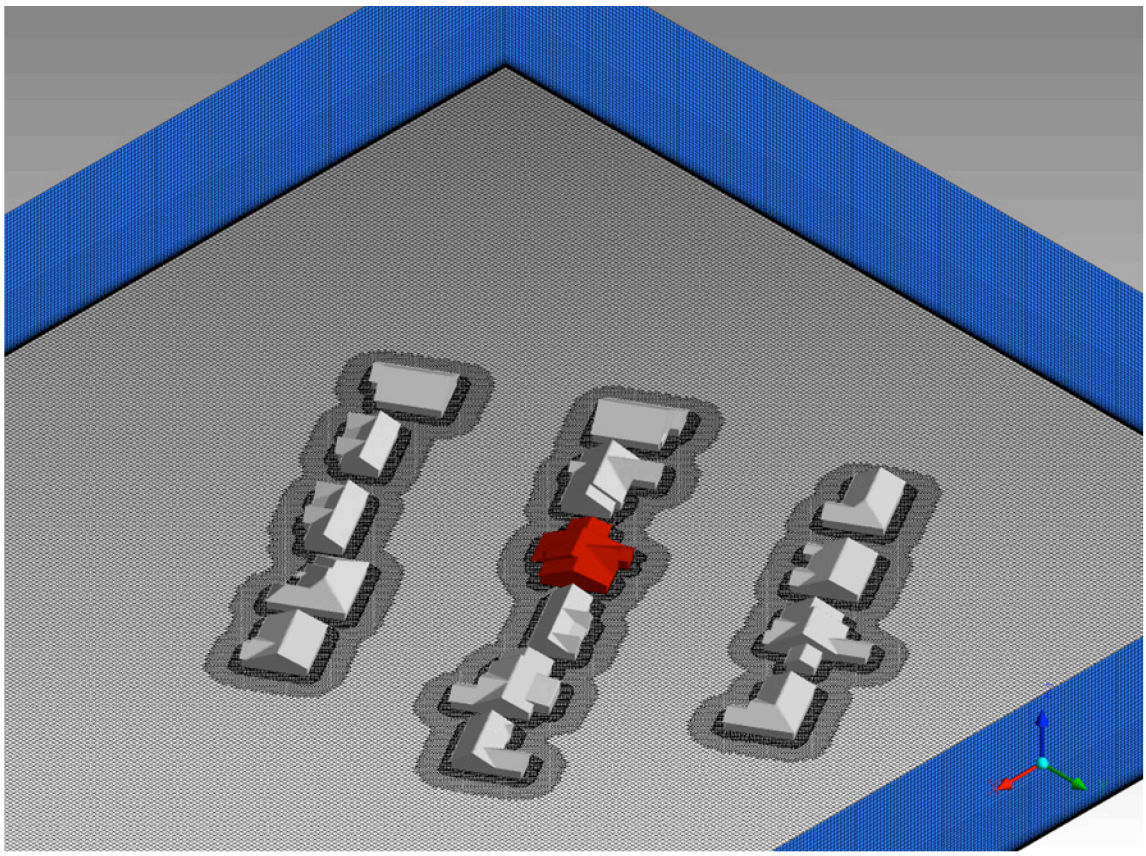
Figure 4.15 Computational mesh for FL27 with neighbouring buildings.

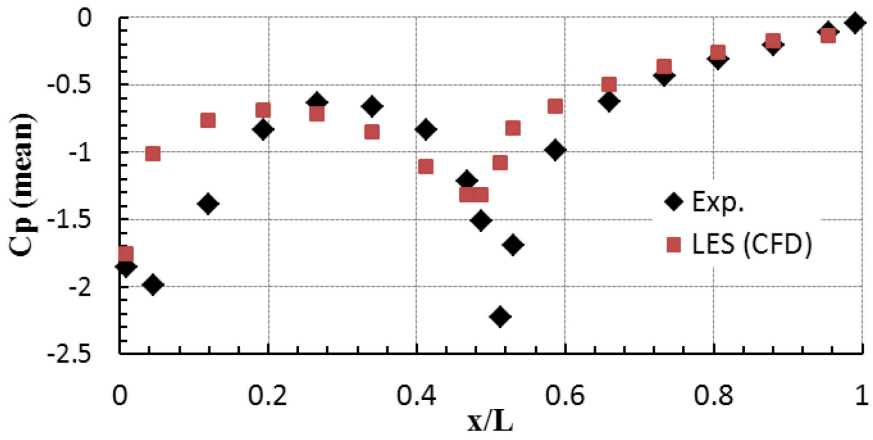

(a) Case 1

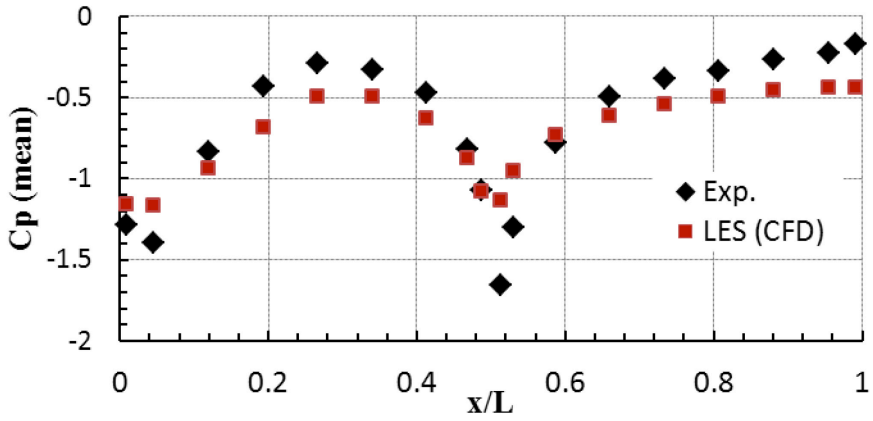

(b) Case 2

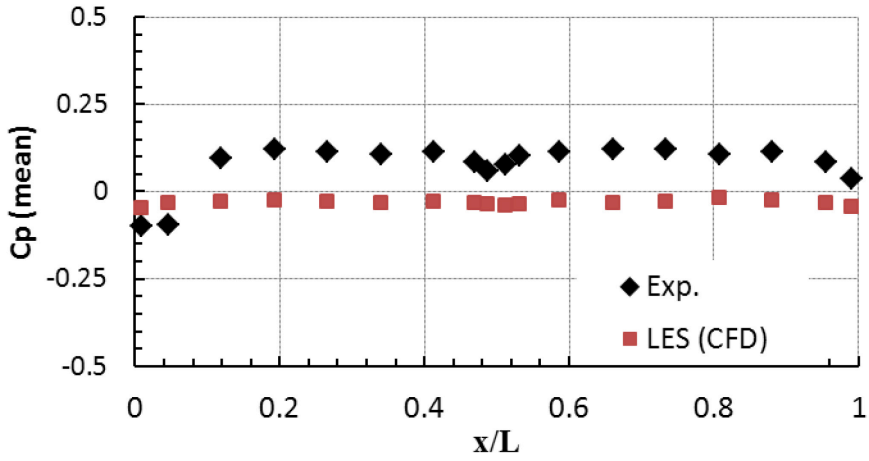

(c) Case 3

Figure 4.16 Comparison of mean pressure coefficient of LES and BLWT data: (a) 0^0, (b) 45^0, and (c) 90^0 wind AoA.

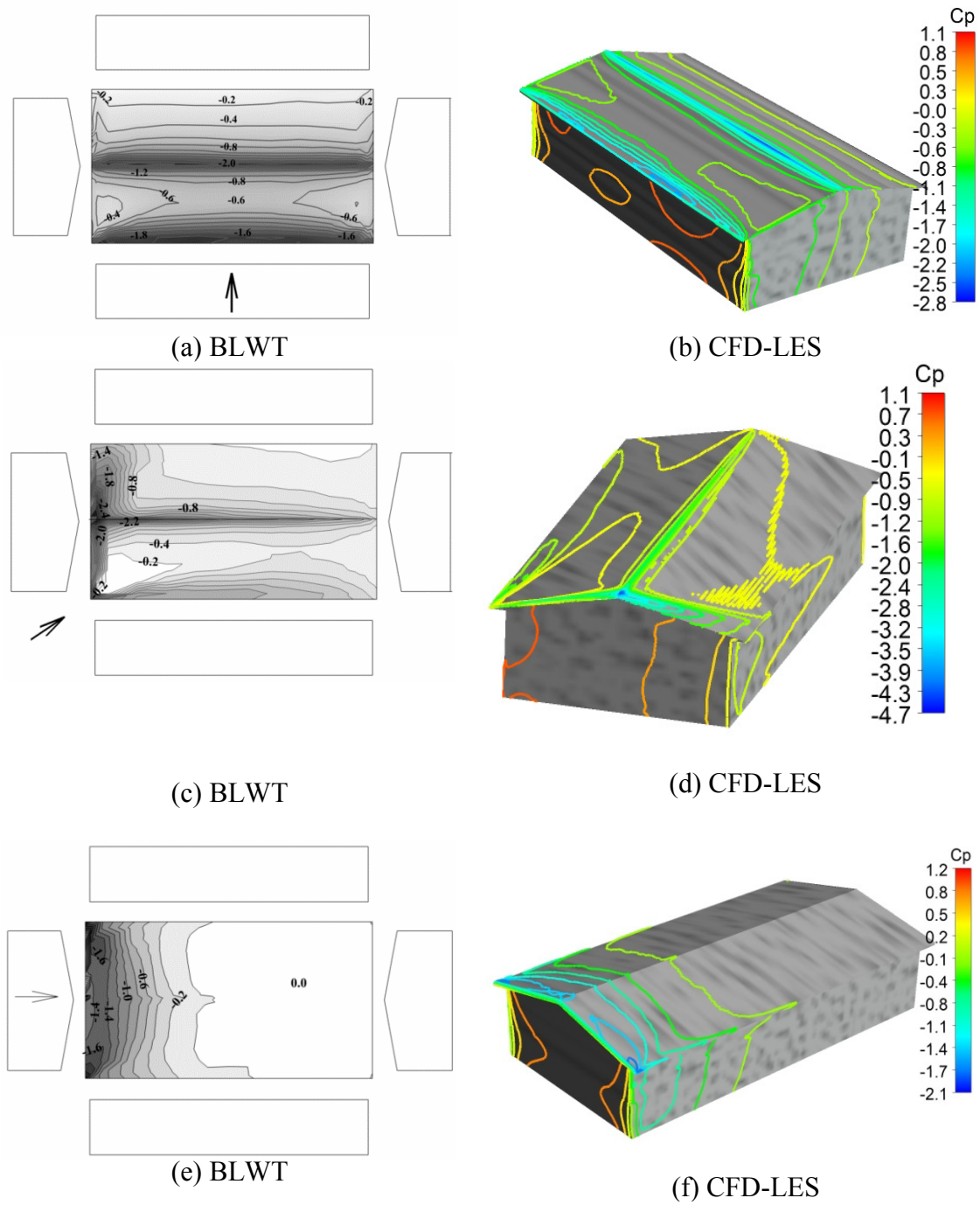

Figure 4.17 Wind tunnel and CFD contour map of mean pressure coefficients on the gable roof building: (a) 0^0, (b) 45^0, and (c) 90^0 wind angle of attack.

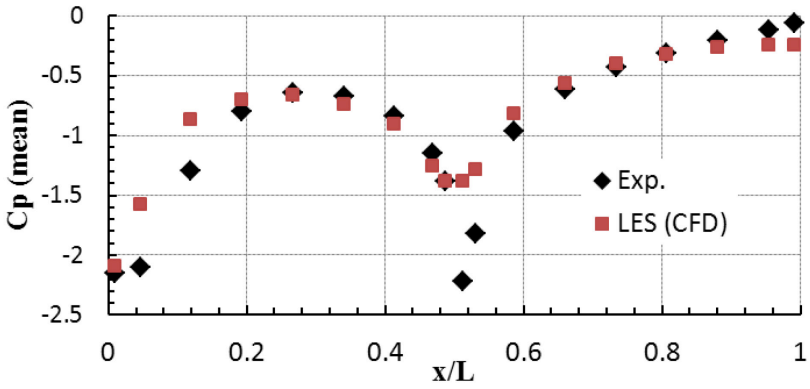

(a)

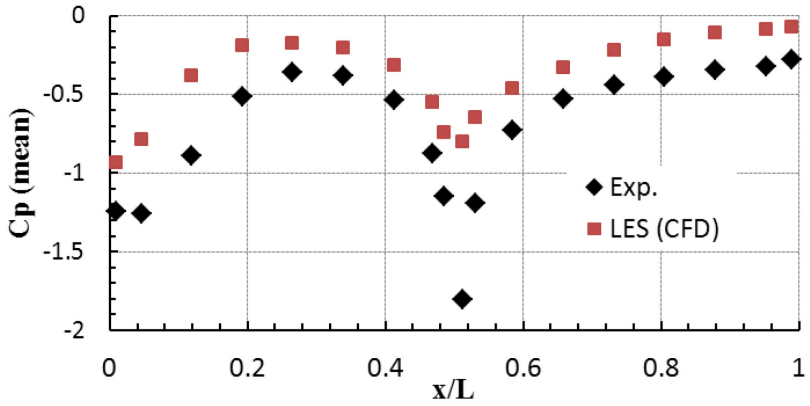

(b)

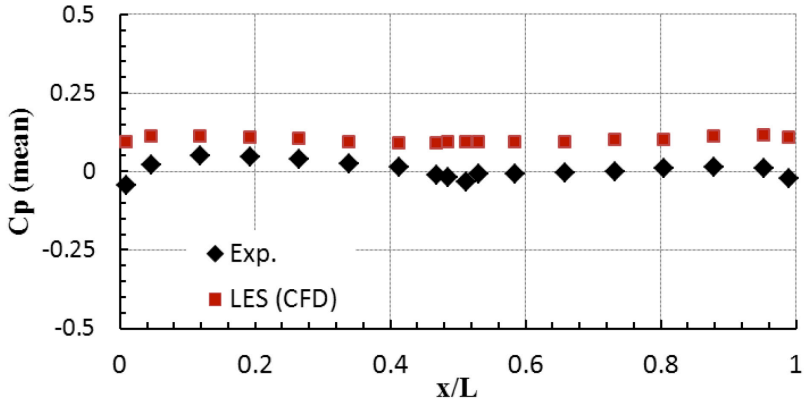

(c)

Figure 4.18 Comparison of mean pressure coefficient of LES and BLWT data: (a) 0^0, (b) 45^0, and (c) 90^0 wind AoA on the roof of a hip roof building.

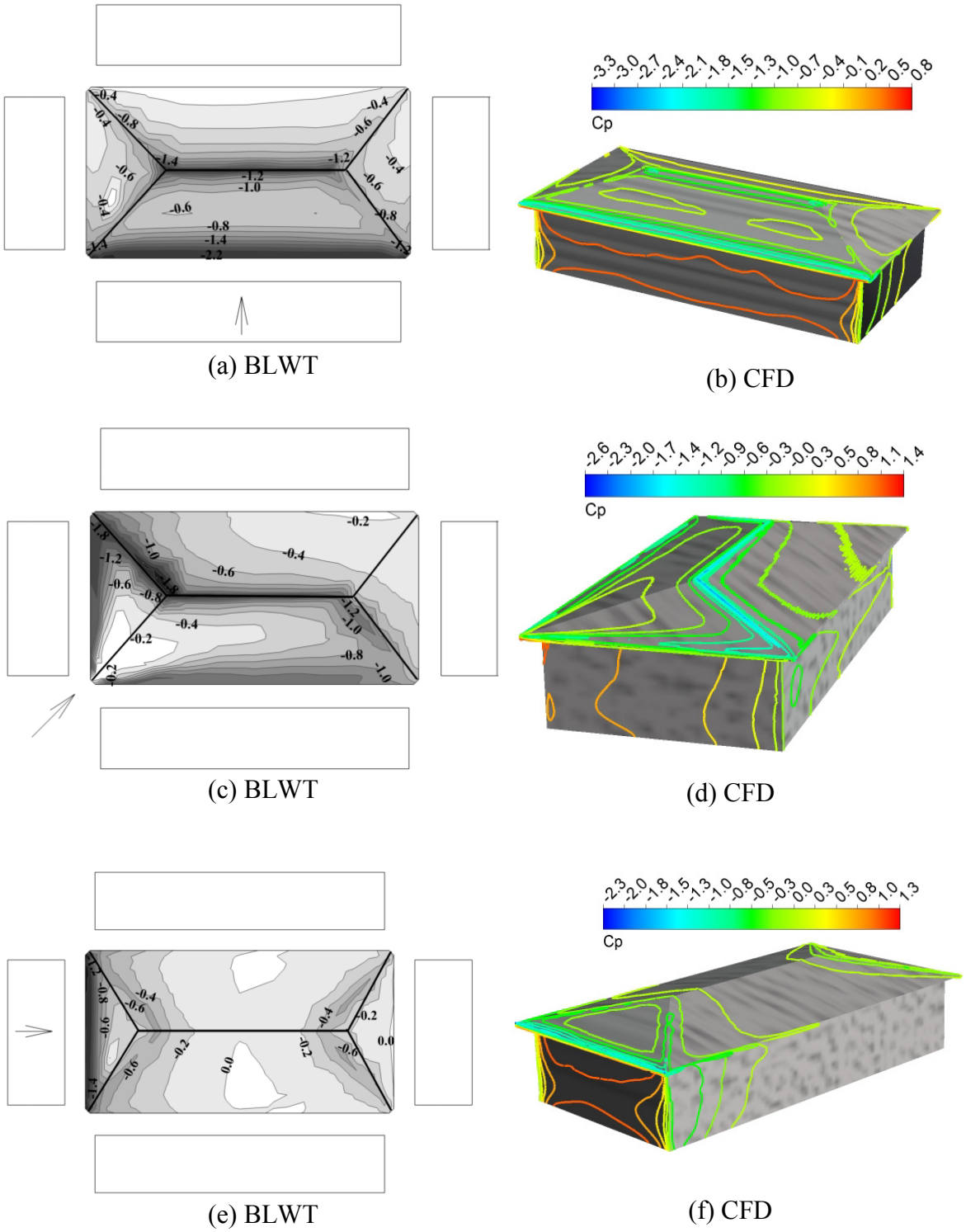

(a) BLWT (b) CFD

(c) BLWT (d) CFD

(e) BLWT (f) CFD

Figure 4.19 Wind tunnel and CFD contour map of mean pressure coefficients for hip roof building: (a) 0^0, (b) 45^0, and (c) 90^0 wind angle of attack.

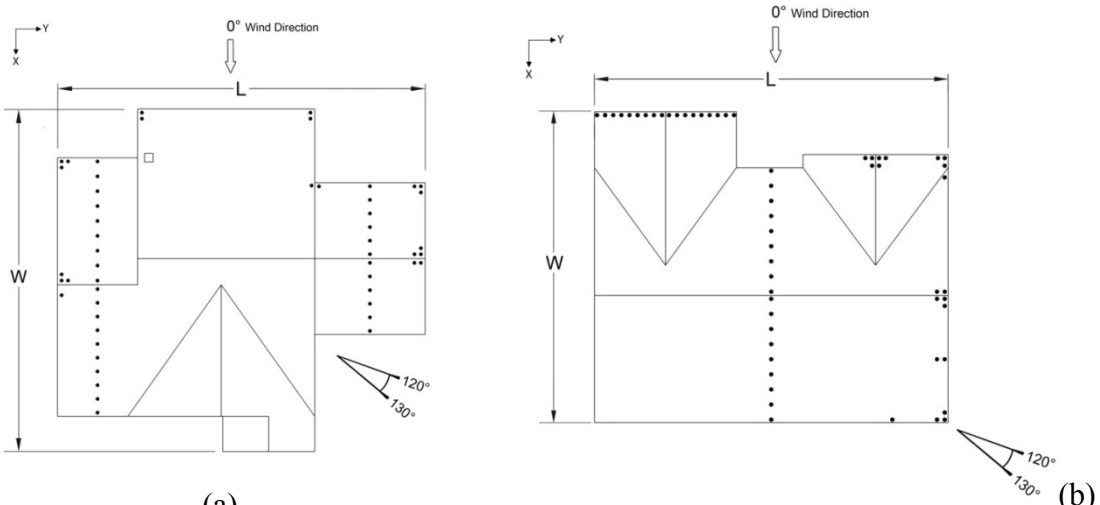

(a) (b)

Figure 4.20 Distribution of pressure taps for LES simulation: (a) FL27 and (b) FL30.

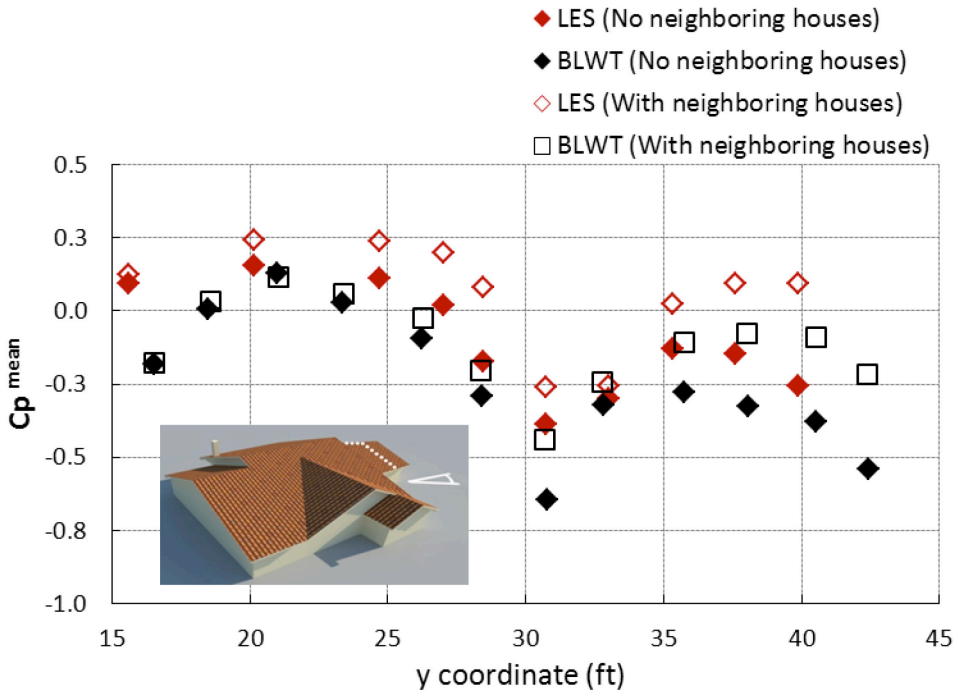

(a)

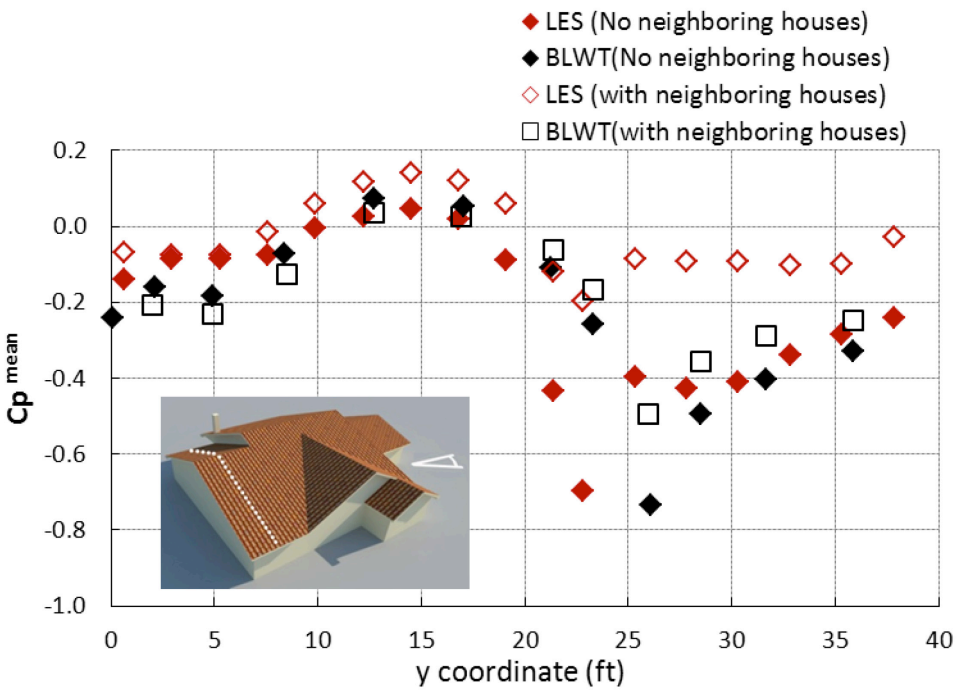

(b)

Figure 4.21 Mean pressure coefficient of FL27 from CFD and BLWT: (a) plot along the east of the roof and (b) plot along west side of the roof.

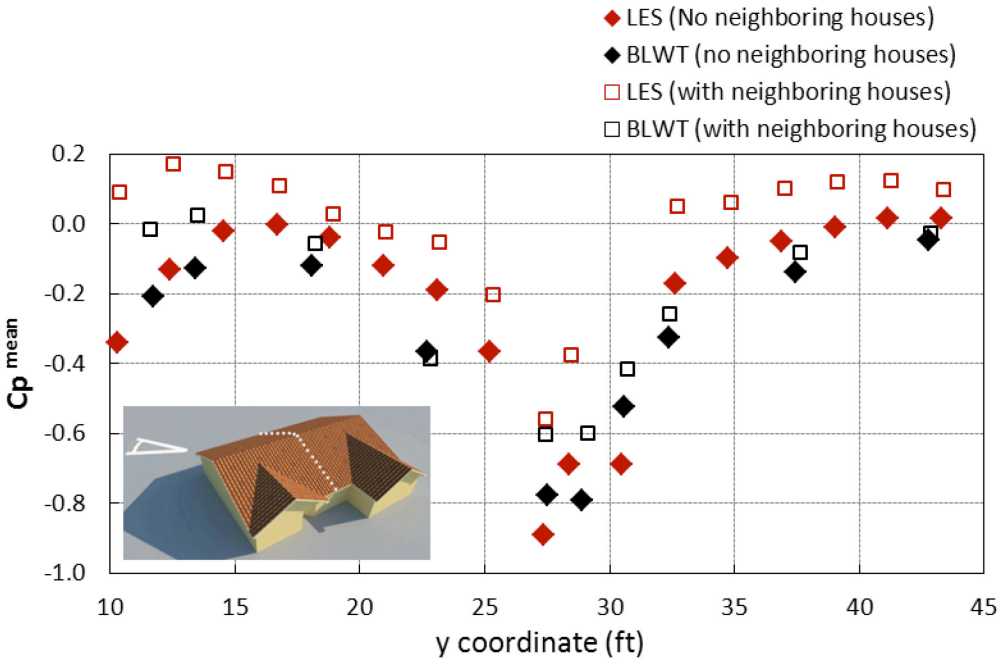

(a)

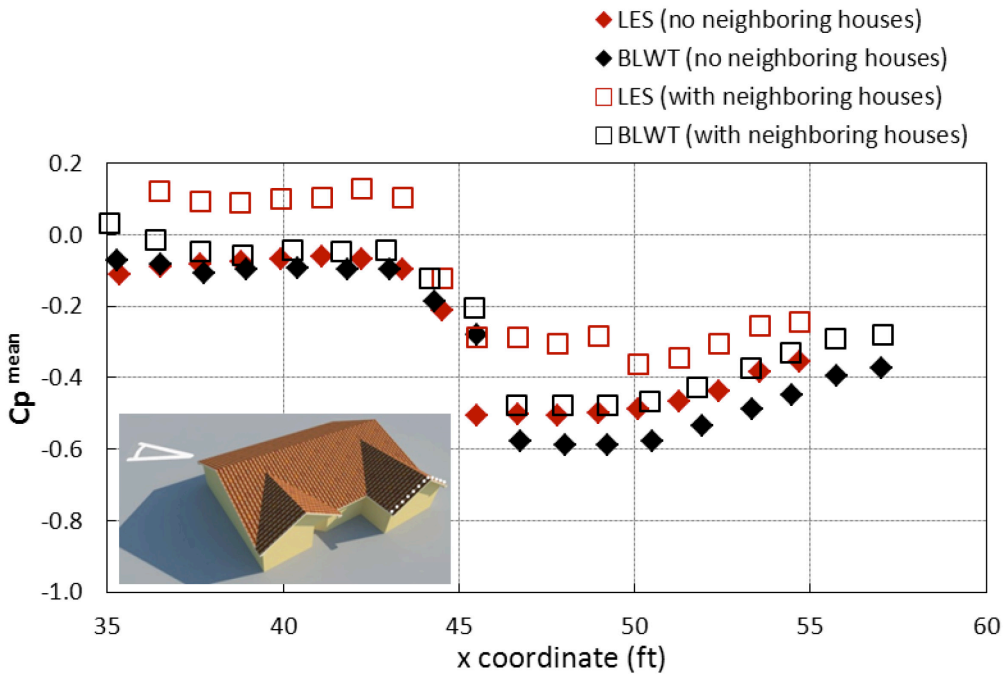

(b)

Figure 4.22 Mean pressure coefficients of FL30 from CFD and BLWT: (a) plot along the east of the roof and (b) plot along west side of the roof.

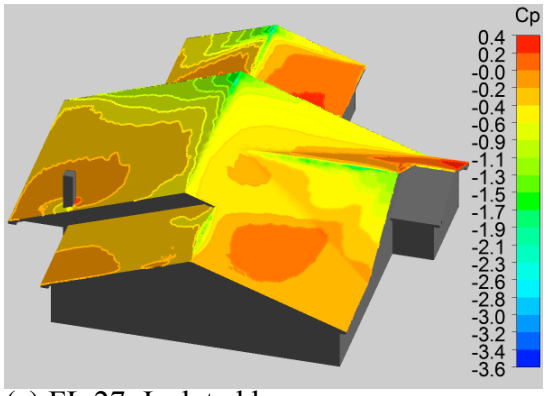

(a) FL 27: Isolated house

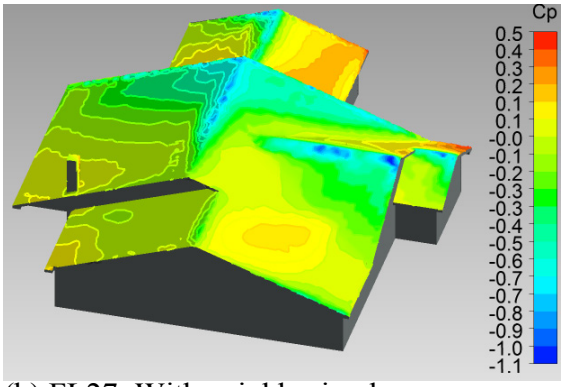

(b) FL27: With neighboring houses

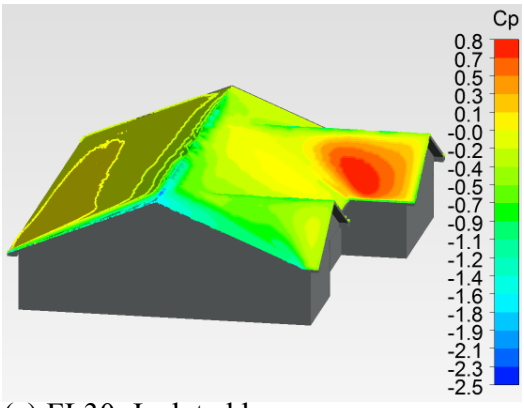

(c) FL30: Isolated house

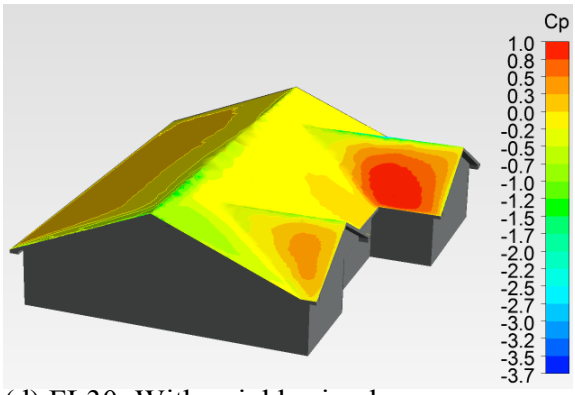

(d) FL30: With neighboring houses

Figure 4.23 CFD contour maps of mean pressure coefficients.

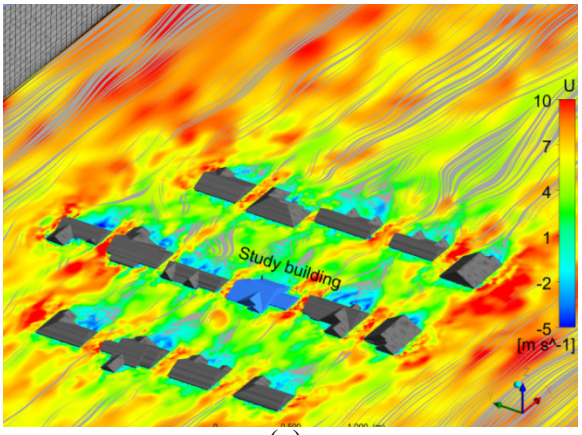

(a)

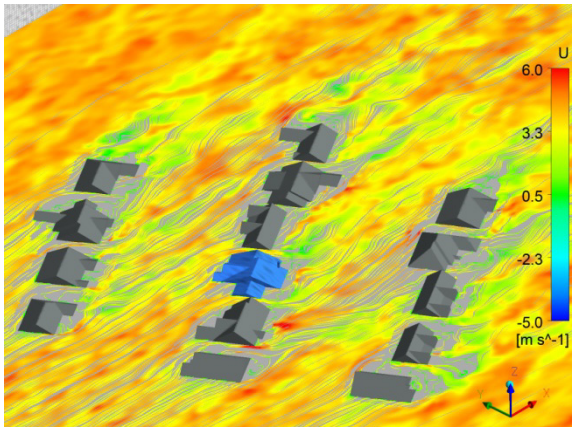

(b)

Figure 4.24 Surface velocity streamlines of FL27 with neighboring houses: (a) 0^0 and (b) 120^0.

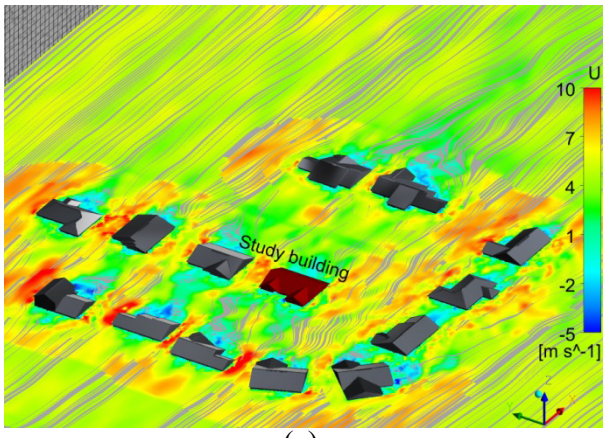

(a)

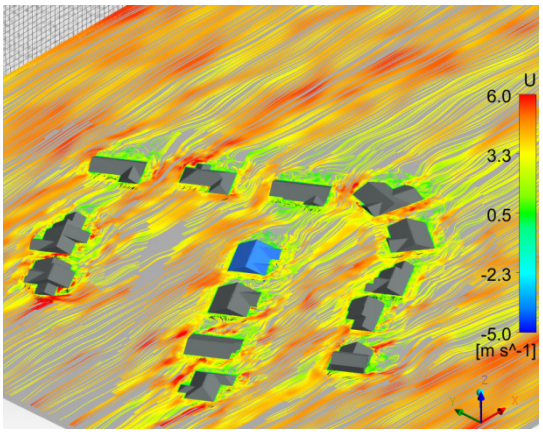

(b)

Figure 4.245 Surface velocity streamlines of FL30 with neighboring houses: (a) 0^0 and (b) 120^0.

5 COMPUTATIONAL EVALUATION OF WIND LOADS ON A STANDARD TALL BUILDING USING LARGE EDDY SIMULATION

Agerneh K. Dagnew[a], Girma T. Bitsuamlak[*, b]

A Paper Submitted to the Journal of Wind Engineering and Industrial Aerodynamics

(under review)

Presented in the CWE2010 and the 11th ACWE2009 Conferences

Abstract

In this paper wind induced aerodynamic loads have been evaluated through large eddy simulation (LES) for a standard tall building that is commonly used by several boundary layer wind tunnel (BLWT) laboratories for calibration purposes. Test configurations with and without the presence of an adjacent building have been considered. Statistical parameters extracted from an empty BLWT atmospheric boundary layer (ABL) flow over an open terrain have been used to prescribe the transient inlet boundary for LES simulations. High frequency pressure integration (HFPI) approach has been employed. A total of 280 pressure taps have been systematically distributed on the surfaces of the LES model building and the corresponding BLWT model building used for validation purposes. A detailed inflow boundary condition impact analysis on the

[a] Ph.D. Candidate, *Adjunct Prof., Laboratory for Wind Engineering Research (LWER), International Hurricane Research Center (IHRC) /Department of Civil and Environmental Engineering (CEE), Florida International University (FIU), Miami, FL 33174, USA

[b]Associate Prof., Department of Civil and Environmental Engineering, University of Western Ontario in London, ON, Canada.

accuracy of the LES wind load evaluation using three different methods has been carried out. The comparison of the LES results with the experimental data that showed better agreement for the inflow fluctuation generated by using the synthetic method than the random flow generated by Simirnov's and Lund's recycling methods. LES predicted wind loads comparable with the BLWT data both for an isolated building case and for cases where adjacent buildings were placed in the vicinity of the study building, which introduced more turbulence and sheltering effects.

Keywords: LES, BLWT, ABL, inflow turbulence, wind force coefficients, power spectrum, tall building.

5.1 Introduction

Several wind load evaluation studies for buildings in boundary layer wind tunnels have been reported by various researchers, and more recently through a numerical approach. Recent advances in hardware and software technology coupled with development of reliable sub-grid turbulence models and numerical generation of inflow turbulence, which replicates upstream conditions, is making a computational wind load evaluation an attractive proposition (Tamura et al., 2008). Previous numerical studies are focused both on short and tall buildings. Numerically studied full-scale low-rise buildings included the Silsoe Cube (Wright and Easom, 2003), Texas Tech Building (Senthooran et al., 2004) and the Wall of Wind Test Building (Bitsuamlak et al., 2010). High-rise buildings included (Nozawa and Tamura, 2002; Tominaga et al., 2008a), and others. Huang et al. (2007) and Braun and Awruch (2009) studied the external

aerodynamics of a standard tall building known as the Commonwealth Advisory Aeronautical Laboratories model (CAARC, after Melbourne, 1980) and investigated flow patterns, mean and root-mean-square (rms) pressure coefficients on the building perimeter.

With other buildings present in close proximity, the dynamics of the wind flow becomes much more complex and flow interference occurs (Khandure et al., 1998). The most commonly reported interference effects are (a) sheltering which leads to reduction of drag force on the downstream building and amplification of the fluctuating force due to turbulence buffeting (Thepmongkorn et al., 2002; Lam et al., 2008), (b) flow channeling due to close spacing of buildings (Princevac et al., 2010), (c) flow asymmetry which could possibly introduce wind–induced torsion, and (d) wake buffeting. Most of the pre-existing numerical studies for assessment and evaluation of interference effects has been limited to the use of Reynolds-averaged Navier-Stokes (RANS) equations (Zhang and Gu, 2008, Lam and To, 2006).

For a numerical model to be successful, similar efforts taken in their BLWT counterpart to produce proper inflow characteristic is necessary. In this study numerical simulation which systematically investigated the effects of various inflow turbulence generations for LES are presented. LES of the CAARC model has been carried out for with and without adjacent building test configurations. A detailed validation through comparison with wind tunnel data obtained from RWDI USA LLC, Miramar FL (Dagnew et al., 2009; Dagnew and Bitsuamlak, 2010).

5.2 Inflow turbulence generation

The application of LES for estimating time-history of dynamic wind load, which requires transient inlet boundary conditions, heavily depends on the generation of accurate inflow turbulence at the inlet boundary. Inlet boundary conditions of LES simulations, of high Reynolds number turbulent flow, should possess accurate representation of oncoming inflow turbulence, satisfying prescribed spatial and temporal correlations (Tamura, 2008). In bluff body aerodynamics the grid spacing is mostly too coarse to resolve any large component of the turbulent spectrum. This is especially so near the inlet boundary, where few grid cells are allocated in order to reduce computational cost while the majority of the cells are clustered in the near-wall region to resolve boundary layers, flow separation and reattachment, and wake and recirculating regions. However, the purpose of the inlet boundary condition is to supply scales relevant to the grid, i.e., ensuring the inlet turbulence have integral length and time scales related to the grid size (Δx, Δy, Δz), and the computational time step Δt.

There are several techniques to generate turbulence fluctuations. A comprehensive review by Tabor and Baba-Ahmadi (2009) and Huang et al. (2010) discussed various methods commonly used for generation of inflow turbulence at the inlet boundary of LES simulations. These include recycling methods, precursor databases, and synthetic turbulence methods. The present study investigated the suitability of these methods for LES-based wind load evaluation of tall buildings. To perform the suitability study an experimental ABL wind flow simulation has been conducted and flow statistics have been measured.

5.2.1 Experimental ABL wind flow simulation

A practical approach for obtaining the inlet boundary flow variables for CFD simulations is to generate a time history of wind velocities through empty BLWT measurements (Fig. 5.1(a)). Then mean flow variables obtained from statistics of the time-history data generated by the wind tunnel for the standard profiles such as open, suburban, and urban profiles can be used in the numerical method to accurately prescribe the inlet boundary of the LES simulation. Once the flow statistics are generated, they can be used repeatedly by the LES model as required without the need to go back to the wind tunnel. In the present study the wind tunnel ABL wind flow simulation have been conducted at the RWDI USA LLC testing facility that has a testing section of 2.6 m wide by 2.14 m tall. The floor has mechanical actuator to control the degree of surface roughness. Approximately 2.54 cm by 2.54 cm flat plate on 30.48 cm in by 30.48 cm in diamond pattern roughness cubes are used to replicate rural terrain type surface roughness. For the present case a data with record length of 180 sec data with sampling frequency of 515 Hz has been collected at RWDI BLWT. An open type exposure with "power low exponent of 0.16" was obtained from the ABL experimental simulation (Fig. 5.1(b)). Statistics of fluctuating turbulence such as length-scale and turbulence intensities are then obtained from the time history of the velocity data measured in the BLWT that were subsequently used by the various inflow turbulence generators.

The integral length scale is estimated from the wind velocity spectrum after applying frequency smoothing by dividing the raw data into K sub-blocks of M points using Welch's method in MATLAB software package. Table 5.1 summarizes the turbulence characteristics of the simulated ABL wind flow.

5.2.2 Numerical generation of inflow turbulence for LES simulation

5.2.2.1 Recycling method

The recycling method is based on Lund et al. (1998) proposal where the computational domain is subdivided into two domains. This method can be implemented in two different ways. Using an auxiliary simulation where an empty computational domain simulation is done and the turbulence data will be stored for subsequent simulation (Fig. 5.2(a)). Once the simulation is run enough number of flow-through times, i.e., the flow statistics are stable, a plane of data will be extracted and stored for later use by the main simulation. The other method is by a combined domain approach, where the domain upstream of the calculation domain, also called "driver domain", is used to generate spatially developing boundary layer flow by re-scaling instantaneous velocity at a plane, also called the recycling plane, and remapping the flow back to the inlet boundary (Fig. 5.2(b)). The "calculation domain" will use the plane of data generated on the fly by the "driver domain". Kataoka and Minoruu (2002) later simplified Lund's method by assuming that the growth of the inner boundary layer thickness is insignificant within the computational domain. Hence, instead of recycling the whole value of the instantaneous velocity components only the fluctuating components will be recycled. In this method the velocity components at the inlet boundary are defined as follow

$$\begin{aligned} u_{inlet}(y,z,t) &= \langle u\rangle_{inlet}(z) + \phi(\theta)\times\{u(y,z,t) - \langle u\rangle(y,z)\}_{recy} \\ v_{inlet}(y,z,t) &= \phi(\theta)\times\{v(y,z,t) - \langle v\rangle(y,z)\}_{recy} \\ w_{inlet}(y,z,t) &= \phi(\theta)\times\{w(y,z,t) - \langle w\rangle(y,z)\}_{recy} \end{aligned} \tag{5.1}$$

where subscripts $\langle . \rangle$ denotes the time-averaged value in the span-wise direction and $\langle u \rangle_{inlet}$ is the prescribed mean velocity profile. And the damping function $\phi(\theta)$ which prevents development of the turbulence in the free stream is given by

$$\phi(\theta) = \frac{1}{2}\left\{1 - \frac{tahn\left[8.0(1-\theta)/(-0.4(\theta-0.3)+0.7)\right]}{tanh(8.0)}\right\} \tag{5.2}$$

where $\theta = z/z_G$, and z, z_G are height and gradient height, respectively.

In this paper one study case was to investigate the modified Lund's recycling method (Kataoka and Minoruu, 2002). Inhomogeneous perturbations were by the Weighted Amplitude Wave Superposition (WAWS) technique and added to the inlet boundary (Swaddiwudhipong et al., 2007). The WAWS method is based on Shinozuka (1985), where a fluctuating velocity filed is generated from samples of a single random Gaussian process with zero mean and prescribed model energy spectral.

$$u'(t) = \sqrt{2}\sum_{k=1}^{N}\sqrt{S_u(f_k)}\Delta f \cos(2\pi f_k t + \varphi_k) \tag{5.3}$$

where $S_u(f_k)$ is the one-sided von Karma spectral model of $u'(t)$, f_k, $k = 1,...,N$ are central frequencies of the interval Δf and φ_k is the random phase angle uniformly distributed from 0 to 2π. For the present study the energy spectrum of fluctuating velocities were described by the von Karman model spectrum (Simiu and Scanlan, 1995).

5.2.2.2 Synthesized turbulence

A synthesized turbulence fluctuations generation technique is based on the method of Kraichnan (1970). In this method an arbitrary energy spectrum is used to

prescribe the amplitude of velocity fluctuation as a function of a wavenumber. Using this method two type of inflow turbulence were generated

a) Inhomogeneous random flow generation

Smirnov et al. (2001) modified Kraichan's method by incorporating turbulence length- and time-scales. These modifications ensured the generation of divergence-free isotropic fluctuations. A brief presentation of the random flow generation technique is given as follows

$$u_i(\tilde{x},t)=\sqrt{\frac{2}{N}}\sum_{n=1}^{N}[\,p_i^n\cos(\tilde{k}_j^n\tilde{x}_j+\omega_n\tilde{t})+q_i^n\sin(\tilde{k}_j^n\tilde{x}_j+\omega_n\tilde{t})] \tag{5.4}$$

where $\tilde{x}_j$, $\tilde{t}$ are scaling parameters for the length- and time-scale of turbulence, k_i^n and ω_n are sample of wave number vectors and frequencies of the modeled turbulence spectrum, respectively. The Gaussian model spectrum employed in this method is expressed as

$$E(k)=16(2/\pi)^{1/2}k^4\exp(-2k^2) \tag{5.5}$$

The spectrum model is mainly designed to represent the large energy carrying structures and thus unable to capture eddies within the inertial subranges. However, turbulent ABL flows have demonstrated a cascade of energy between turbulent eddies. In such flow the inertial sub-range plays a vital role in transferring energy from large-energy containing range to small-scale eddies of dissipation range. The small-scale eddies in the dissipation range are in the same order of Kolomogrov scale (η) and the energy will eventually be converted to internal energy and dissipate. Considering the modeling principles of LES, i.e. resolving the flow up to the filtering (grid size) and modeling

small-scales, the length-scale of inertial sub-range lies between the integral length scale and Kolomogrov scale and their contribution is very significant. For example the ANSYS Fluent 13 package has implemented this technique as a Spectral Synthesizer for generation of inflow turbulence at the inlet boundary of unsteady simulations. Hence, for computational wind engineering applications such as the wind effect on structures submerged in the ABL region, the inflow fluctuations should be representative of a realistic turbulence spectrum such as the von Karman spectrum model (Lumley and Panofsky, 1964; Li et al., 2007). In the work of Huang et al. (2010) further modification of Kraichnan's method is done to generate a flow field that can satisfy any given arbitrary spectrum. The technique (also called DSRFG) uses discretization of arbitrary 3D spectrum and synthesized fluctuation and to generate spatially correlated turbulent flow field. For illustration purpose we have used the Spectral Synthesizer technique and investigate its effects on wind load evaluation.

b) Homogenous random flow generation

Davidson (2007) and Senthooran et al. (2004) employed a synthesized turbulent inlet boundary for hybrid LES-RANS and RANS simulation, respectively. In the present studying addition to the Spectral synthesizer and recycling method, the three-dimensional fluctuating velocity components were also generated using the synthesized isotropic turbulent fluctuations method. The random velocity field, which is defined as a finite sum of discrete Fourier modes, is given here for illustration purpose

$$u_i^{'}(x_j) = 2\sum_{n}^{N} \hat{u}^n \cos(k_j^n x_j + \psi^n)\sigma_i^n \tag{5.6}$$

where $\hat{u}^n, \psi^n$, and σ_i^n are the amplitude, phase and direction of the Fourier mode n, respectively. The notation used here follows that in (Billson et al., 2004; Davidson, 2007) and more information can be found in these papers. The wavenumber vector k_j^n is chosen randomly on a sphere of radius k_n. For an incompressible turbulent flow $k_n.\sigma_n = 0$ where $n = 1,..., N$ .This ensures isotropy of the generated velocity filed. The wavenumber k_n and the spatial direction are thus perpendicular. The wavenumber k_n is characterized by its spherical coordinates (k_n, θ, ϕ). The random variables $\psi_n, \varphi_n, \alpha_n$ and θ_n were chosen randomly from their probability density functions. The amplitude $\hat{u}^n$ of each mode is computed from the three-dimensional model spectrum $E(k_n)$ in such a way that the isotropic fluctuations simulate the shape of the modified von Karman-Pao spectrum.

$$E(k_n) = \alpha \frac{2K}{3k_e} \frac{(k/k_e)^4}{[1+(k/k_e)^2]^{17/6}} \exp^{[-2(k/k_e)^2]} \tag{5.7}$$

The spectrum $E(k_n)$ is subdivided into N modes (typically 150-600), equally large.

$$\hat{u}^n = \sqrt{E(k_n)\Delta k}_n \tag{5.8}$$

where K is the turbulent kinetic energy and $k_\eta = \varepsilon^{1/3}\nu^{-3/4}$ is the Kolmogorov wavenumber, ν is the molecular viscosity, and ε is the dissipation rate. Whereas α is a numerical constant which determines the kinetic energy of the spectrum and the wavenumber k_e corresponds to the most energy containing eddies where $E(k_n)$ reaches maximum.

The fluctuating velocity fields generated by Eq. (5.6) are statistically independent of each other and thus have zero autocorrelation. Time correlation is created by using an asymmetric infinite time filter and a new fluctuation velocity field is computed at every time step.

$$(v')^m = a(v')^{m-1} + b(v')^m \tag{5.9}$$

where $a = \exp(-\Delta t / \tau)$, $b = (1 - a^2)^{0.5}$ and $m, \Delta t, \tau$ denotes the time step number, computational time step, and turbulence time scale and it defines the time separation for which the autocorrelation function is reduced to $\exp(-1)$ respectively. The method offers a convenient way to prescribe turbulent length- and time- scales independently (Billson et al., 2004). For the present study the length- and time- scales measured from BLWT were used.

5.3 Outline of BLWT experiment and LES simulation for wind load evaluation

5.3.1 High frequency pressure integration (HFPI) technique

The HFPI method is based on the simultaneous measurement of pressures at several locations on a building surface. The pressure taps were installed at a fine enough resolution over the building surfaces. The study (CAARC) building had a rectangular prismatic shape with dimensions 30.48 m (x) by 45.72 m (z) by 182.88 m (y) height. The BLWT HFPI model was instrumented with 280 pressure taps. Time histories of pressures were measured and stored for post-test analysis. The design wind loads were calculated by integrating the instantaneous pressure over the corresponding contributory area. The geometrical modeling and pressure tap distribution adopted for the LES simulation mimics the BLWT-HFPI model. All the experiments have been carried out at

1:400 scale. The individual pressure time histories were used to form time series of the base loads, from which wind load statistics and spectra were obtained. Figure 5.3(a) and (b) show the pressure tap layout for the BLWT HFPI model and the corresponding CFD setup, respectively along with the overall equivalent full-scale dimensions, direction notations, and wind flow angle. The wind flow is described in a Cartesian coordinate system (x, y, z), in which the x-axis is aligned with the stream wise flow direction, the z-axis is in the lateral direction and the y-axis is in the vertical direction.

5.3.2 Study cases for the LES simulation

In the present study, three building configurations have been investigated (Fig. 5.4). Where Case 1 presents the isolated CAARC building model under various inflow turbulences, Case 2 and Case 3 simulate a scenario where half and full-height adjacent building is situated upwind of the CAARC model, respectively. Table 5.2 summarizes LES cases considered, along with the wind angle of attack, and mesh resolution

5.3.3 Computational domain and boundary conditions

The computational domain (CD) defines the region where the flow field is computed. It should be large enough to accommodate all relevant flow features that will have potential effects in altering the characteristics of the wind flow field (Franke, 2006, COST 2007, AIJ 2008). The CD for Case 1 extended $8D_z$ (D_z is width of the CAARC building model) upwind of the model building and $25D_z$ downstream of the target building. Laterally it spanned $8D_z$ away from the side surfaces of the building model and the top boundary has been placed at $2.5H$ (H is the model building height). Figure 5.5 illustrates the computational domain and boundary conditions used for Case 1. The

blockage ratio calculated based on the ratio of the wind-ward face of the CAARC model to the inlet plane was about 2%, which is less than 5% ratio as recommended by COST (2007). Boundary conditions define the surroundings that have been cut off by the CD and idealize the influence of the actual flow environment under consideration. It significantly affects the accuracy of the CFD prediction. At the inlet boundary, the mean wind velocity profile measured in the wind tunnel testing has been prescribed using the law-of-the-wall. For the ground and building surfaces no-slip wall boundary conditions have been assumed. A symmetry boundary condition is employed at the top and lateral surfaces. Since details of the flow variables were not known for the present cases, an outflow boundary has been applied at the outlet plane. For Case 2 and Case 3, the upwind CD is increased by $2D_z$ to accommodate but the boundary conditions remained the same.

5.3.4 Computational grid

5.3.4.1 Grid sensitivity analysis

Grid sensitivity analyses on an empty computational domain using RANS simulation were done and the velocity and turbulence profile were examined, as shown in Fig. 5.6. The RANS simulations over predicted the velocity gradient at the lower part of the boundary layer but the high resolution mesh showed a slight improvement. We further tested the mesh using LES simulation and measured velocity and turbulence profiles at various locations on the upstream part of the domain. As shown in Fig. 5.7 the velocity profile from the LES simulation matched the wind tunnel measurement. The LES under predicted the turbulence intensity measured at the incident plane.

5.3.4.2 Main simulation

For the main simulation we have used very fine grid cell in the near-wall regions and ensured the non-dimensional wall distances ($1 < y^+ < 5$) well within the inner sub-layer. The cut-off wave number of energy spectrum between resolved and subgrid scale is related to the grid size and use of excessive grid stretching could cause numerical divergence. Therefore, a stretching ratio of 1.05 between successive grid points was applied for the present simulation. We believe that we took all necessary practical steps before the main simulation carried out.

The Reynolds number based on building height H and the measured roof top velocity U_H, measured at 1.22 m upwind of the test building, was $3x10^5$. Hence, the boundary layer regions required a high-resolution mesh clustered near the building surfaces. O-grid hexahedral meshes were generated by using the technique of blocking in Ansys ICEM CFD mesher (Ansys ICEM CFD user manual, 2011). In the inner sub-layer region, the boundary layer meshes were inflated from the wall surface and the first cell were placed at a distance $y_p = 0.0001m$ with a stretching ratio of 1.05. This ensured y^+ to be less than 5 units and minimized the cut-off error of the wavenumber in the LES modeling (Murakami, 1998). In addition, the computational domain was subdivided into multi-body parts to have better control and distribution of the computational grid points around the model building and wall boundary (See Fig. 5.8). For the target building, the O-grid meshing which covers a region of $5D_z x 5D_z$ was generated using 80 grid cells using the Geometrical edge meshing law and the grids were clustered near the building with a stretching ratio of 1.05 and 52 grid points uniformly distributed in the lateral

direction. In the lateral direction outside of the $5D_z x 5D_z$ region, 26 grid points with initial spacing of 0.057 and a stretching ratio of 1.075 were used. In the x-direction (stream-wise), 40 grid points where the first grid point were placed at 0.01mwith a stretching ratio of 1.041 from the building bounding box to the inlet plane, which spans $8D_z$. For the downstream domain starting from the end of the o-grid bounding box ($5D_z x 5D_z$) to the outflow boundary, 60 grid points at a spacing of 0.01(with stretching ratio of 1.041) were used. Vertically 158 grids points with $y_p = 0.0001$ were distributed while the grid points are clustered near the ground surface and the top surface of the building model (with stretching ratio of 1.05). For Case 1 a total of 4,782,784 3D computational grid cells were used. For Case 2 and 3, the same mesh generation technique was adopted. A total of 6,913,565 and 6,913,562 hexahedral cells were used for Case 2 3, respectively.

5.3.5 Turbulence modeling and numerical schemes

5.3.5.1 The LES model

LES is a multi-scale computational modeling approach that offers a more comprehensive way of capturing unsteady flows. The use of LES as a wind load evaluation tool has been significantly improved in recent years through the following numerical techniques (a) numerical generation of transient inflow turbulence (Kraichan, 1970; Lund et al., 1998; Nozawa et al., 2002, 2005; Smirnov et al., 2001; Batten et al., 2004), (b) development of efficient sub-grid scale turbulence modeling techniques suitable for unsteady three-dimensional boundary separated flows, and (c) numerical discretization with conservation of physical quantities for modeling complicated

geometry (Tamura et al. 2008). Because of these advancements, LES holds promise to become the future computational wind engineering (CWE) modeling for which turbulent flow is of pivotal importance (Tamura, 2008; Tucker and Lardeau, 2009; Sagaut and Deck, 2009). In the present study, the Dynamic Smagornisky-Lilly subgrid-scale (SGS) model based on Germano et al. (1996) and Lily (1992) have been employed. In this method the Smagornisky constant, C_s, is computed dynamically according to the resolved scales of motion.

5.3.5.2 Adopted numerical schemes for LES

For discretization of convection terms central-differencing based schemes give the least numerical diffusion and the best accuracy compared to the upwind schemes, as demonstrated by Marinuzzi and Tropea (1993). However, for high *Re* flows in the wake region, such as the present cases, this scheme can become unstable, giving unphysical oscillations (wiggles). The bounded central differencing (BCD) scheme, essentially based on the normalized variable diagram (NVD) approach (Leonard 1991) together with a convection boundedness criterion can detect and remove these wiggles in the wake region. Because of this the BCD scheme has been used for all the simulations of the present study. For temporal discretization, second-order schemes are advised for most computational wind engineering applications and have been used in the present study. A second-order scheme for pressure discrtization has been applied. For pressure-velocity coupling, the Pressure Implicit with Splitting of Operators (PISO) algorithm with skewness and neighboring correction is recommended for the transient simulation and has been used in all LES simulation. PISO is based on the higher degree of the approximate relation between the corrections for pressure and velocity (Ansys Inc. 2011).

The simulations have been carried out at the supercomputer center at Florida International University. The parallel computations have been carried out using 28 CPUs. A computational time step $\Delta t = 5 \times 10^{-4}\ s$ with 5 sub-iterations, per time step, were used in all the simulations. Once the simulation run for enough flow time and the solution statistics reached at stable conditions, the time histories of the pressure and fluctuating velocities data were recorded for $2\ s$ flow-time. Also, a strict residual convergence criterion of 10^{-5} has been applied to the residual to ensure full convergence of the simulation.

5.4 Results and discussion

5.4.1 Assessment of numerically generated inflow turbulence

An auxiliary simulation is a common way of conducting ABL wind flow simulations, numerically. Comparative studies of inflow turbulence generation methods have been carried out using auxiliary domain flow simulations. Three different inflow turbulence generation techniques have been investigated to assess their suitability for LES based wind load evaluations. Table 5.3 summarizes all the three cases considered in the parametric study.

Where Inflow-1 defines the inlet boundary based on Smirnov's random flow generation algorithm, which is implemented in the commercial software Ansys Fluent 13 solver as Spectral Synthesizer method (Ansys Inc., 2007). It computes fluctuating velocity components by synthesizing a divergence-free velocity-vector field from the summation of Fourier harmonics. At the inlet in addition to the mean velocity profile which was defined using equation (11), for the turbulence generator of Inflow- 1 the of

kinetic energy and dissipation rate are prescribed using $K = 3/2(IU_{avg})^2$ and $\varepsilon = 3/2(C_\mu k^{1.5})/l$, respectively. For Inflow-2 Lund's recycling method and randomly generated fluctuations using the weighted amplitude wave superposition (WAWS) method were superimposed to the instantaneous velocity at the recycling plane of the auxiliary domain. Inflow-3 is based on homogeneous synthetic inflow turbulence generation techniques, as described in Sec. 2.2. In-house C code was developed based on this method and turbulence data was generated and stored for subsequent simulation. Then the stored instantaneous velocity components were mapped to the inlet boundary of the main simulation, for every time step. For all the cases considered the statistical flow parameters (for example integral length, turbulence intensity (TI), and mean wind velocity) have been obtained from BLWT data (see Sec. 2.1). For all cases considered in the inflow turbulence investigation, the inlet boundary condition has been prescribed as

$$\begin{aligned} \bar{u}_i(y,z,t) &= U_{inlet}(y) + u'_{in}(y,z,t) \\ \bar{v}_i(y,z,t) &= V_{inlet}(y) + v'_{in}(y,z,t) \\ \bar{w}_i(y,z,t) &= W_{inlet}(y) + w'_i(y,z,t) \end{aligned} \tag{5.10}$$

where $U_{inlet}(y)$ is the mean wind velocity profile measured from the wind tunnel experiment. The mean velocities in the lateral and vertical directions have been set as $W_{inlet}(y) = V_{inlet}(y) = 0$ and the stream-wise velocity plotted in Fig. 5.9, $U_{inlet}(y)$ measured from wind tunnel has been defined as follow

$$\begin{aligned} \langle u \rangle / u* &= y^+ && y^+ < 5 \\ \langle u \rangle / u* &= 2.5\ln(y^+) + 5.5 && 30 < y^+ < 500 \\ \langle u \rangle / u_H &= (z/H)^{0.16} && y^+ > 500 \end{aligned} \tag{5.11}$$

5.4.1.1 Application of the transient inflow turbulence to LES

Time histories of velocity components were monitored at various points at the centerline of the incident plane during the LES of the axillary domain. Figure 5.10 shows the samples of generated fluctuation in the stream-wise direction. The fluctuations were monitored in the upstream domain at the level of the model building height. As shown in the figure the fluctuation generated by Inflow-1 and -2 showed poor spatial correlation compared to Inflow-3. The magnitude of the perturbation generated by Inflow-2 is very small. In cases where large upwind computational domain is used, the fluctuation could dissipate before it reaches to the incident plane and subsequently will affect the resulting wind load.

To further examine the performance of the numerically generated velocity fluctuation for the LES, the spectra of sample fluctuations monitored at the model building height (H) were compared with the von Karman model spectrum (Fig. 5.11). As pointed out in Section 3.3, the spectrum resulted from Inflow-1 decays rapidly and follow the Gaussian spectrum model i.e., it only reproduces the large eddies and undermine eddies in the inertial sub-range. Compared to Inflow-1, Inflow-2 showed slight improvement in terms of reproducing eddies in the inertial sub-range but still not sufficient enough to represent a realistic wind field. When generating inflow turbulence for the LES simulation the velocity fluctuation should be well reproduced at lease up to $fH/U = 10$, since the velocity fluctuation in the inertial sub-range greatly affects the transfer of energy between eddies and the development and behavior of separated shear layers. The wind flow field generated by using Inlfow-3 satisfied this requirement.

Figure 5.12 shows the two-point correlation of the vertical velocity simulated by the three turbulence generators. The normalized two-point spatial correlation is computed using $B_{ww}^{norm}(x,\hat{x}) = \overline{v'(x)v'(x+\hat{x})} \Big/ v_{rms}(x)v_{rms}(x+\hat{x})$. Although the same number of computational grid and identical resolution were used, the spatial correlation resulted from Inflow-1 and Inflow-2 decay rapidly with separation distance $\hat{x}$. For Inflow-3, the two-point correlation shows gradual decrease as it approaches the wall, which is an indication of a strong spatial correlation (Davidson 2009). Figure 5.13 illustrates the spatial representation of velocity fluctuations at the inlet boundary of the LES simulation from Inflow-1 and inflow-3. As demonstrated by the figure, uncorrelated eddies are formed by Inflow-1 while realistic turbulence eddies with proper spatial correlation were generated by Inflow-3.

5.4.2 Mean wind pressure coefficient for isolated CAARC model

To gauge the prediction accuracy of LES for design wind loads evaluation and assess the effects of oncoming inflow turbulence, an explanatory detailed study on the isolated CAARC building model (Case 1) has been carried out with various inlet boundaries. Figure 5.14 depicts the comparison between numerically obtained mean-pressure coefficients with the BLWT data on the perimeter of the building measured at $2/3\,H$. Where the time-averaged non-dimensional pressure coefficients C_p were defined by

$$C_p = \frac{P - P_0}{\frac{1}{2}\rho U_H{}^2} \tag{5.12}$$

where U_H is the reference velocity at the building height H, $P - P_0$ is the dynamic pressure head, and ρ is the density of air. On the wind-ward face, there is a very good agreement between the BLWT C_p values with those obtained from the present LES and those collected from literature (Huang et al., 2007; Braun and Awruch, 2009). On the sidewalls where flow separation occurred due to the sharp corner, the numerical results from Inflow-1 deviated from the BLWT measurements, especially at the trailing edge. LES with Inflow-1 also over-predicated the mean C_p on the lee-ward face. Inflow- 2 and -3 showed very close agreement with the BLWT data on the side and lee-ward faces. The numerical data from literature under-predicted the pressure on the sidewall and lee-ward faces but these noticeable discrepancies could be due to the difference in the boundary conditions used compared to the current setup. This comparison demonstrated how the oncoming flow affected the predication accuracy, thus attesting to the necessity of prescribing appropriate oncoming turbulence for unsteady simulations, such as LES.

Figure 5.15 presents representative mean-pressure contour plots for wind-ward and lee-ward faces of Case 1. On the wind-ward face, the LES mean C_p contours estimated by the three inlet boundaries showed good agreement with the BLWT data. The mean C_p LES predictions for the lee-ward face showed marginal discrepancy with BLWT compared to the better agreement observed for wind-ward C_p values. Among, the three inflow conditions, Inflow-3 was marginally performing better than Inflows-1 and -2 predictions. Figure 5.16 shows the root-mean-square (rms) of surface pressure coefficients. The rms produced by Inflow-3 on the wind-ward face, a place where the inflow fluctuation effect could be seen more apparently (compared to other faces which

potentially experience more fluctuation due to flow separation) was in better agreement with BLWT's *rms*. On the lee-ward face, the numerical result slightly deviated from the BLWT data.

5.4.3 Steady and fluctuating wind force coefficients for single building

Following Obasaju (1992), the drag and lift coefficient, C_D and C_L, respectively are computed from the time history data of the LES simulation by considering the wind shear profile as follows

$$C_D = \frac{F_D}{(1/2\rho D_z \int_0^H U^2 dy)} \tag{5.13}$$

$$C_L = \frac{F_L}{(1/2\rho D_z \int_0^H U^2 dy)} \tag{5.14}$$

where F_D and F_L are the steady part of the along- and across-wind forces and become the same as F_X and F_Y when the angle of attack $\alpha = 0^0$, respectively. Using the stream-wise velocity profile measured in the BLWT, it can be shown that

$$\int_0^H U^2 dy \approx 0.781 U_H^2 H \tag{5.15}$$

Whereas the root-mean-square values of the fluctuating parts of F_X, F_Y, and torsional moment M are computed from the fluctuating components of the force time history as $C_{\sigma F_X} = \sigma_{F_X} / (1/2\rho U_H{}^2 D_Z H_{Level})$, $C_{\sigma F_Y} = \sigma_{F_Y} / (1/2\rho U_H{}^2 D_Z H_{Level})$, and $C_M = \sigma_{M_Y} / (1/2\rho U_H{}^2 D_Z{}^2 H_{Level})$, respectively. Here U_H is the mean wind velocity at the model building height H and D_Z is the width in the wind-ward face.

Time-history of wind pressure coefficients on the 280 pressure taps strategically distributed on the surface of the model building (Fig. 5.3(b)) were recorded at each computational time step. At each level 28 pressure taps, and 7 taps per face, were placed. The drag and lift coefficients of study Case 1 (for the three different inlet conditions) have been computed from the vector sum of tap forces (i.e. pressure measured at each tap multiplied by its tributary area) in the along- and across-wind directions, respectively. Fig. 5.17 presents the vertical distribution of the steady force coefficients calculated at each pressure tap level. There was a good agreement between the LES and BLWT predictions of the steady force coefficients, especially LES with Inflow-3. Fig. 5.18 compares fluctuating *rms* force coefficients at each pressure tap level. The LES simulation demonstrated strong fluctuation on the along-wind direction when Inflow-3 was used.

Table 5.4 lists the comparison of the total LES and experimental steady (C_D, C_L, and C_M) and the *rms* force and torsional moment coefficients ($C_{\sigma F_X}$, $C_{\sigma F_Y}$, and $C_{\sigma M}$, respectively). In all the three turbulence generation techniques considered, there was almost 10% over-prediction of LES C_D compared to the experimental data. While the simulation from Inflow-1 and -2 under-predicated the lift force coefficient C_L, perturbation generated by Inflow-3 resulted in an improved C_L prediction compared to Inflow-1 and -2. For the *rms* coefficients, Inflow-3 showed much better performance, 15% over-predication of $C_{\sigma F_X}$, less than 5% over-predication of $C_{\sigma F_Y}$ and matching well for torsion moment compared to BLWT data (although the wind angle of attack considered for LES is not the critical one for torsion). The assumption of homogenous

flow field, one of the limitations of the present study, as applied in Inflow-3 could also attributed to the over-prediction of the load coefficients. Figure 5.19 illustrates the time histories of C_L and C_D, where the time-history of C_D showed small periodicity compared to C_L and strong fluctuation on the along-wind direction when Inflow-3 was used as the inlet boundary. Obasaju (1992) pointed out the need for longer averaging time in estimating C_D for high Reynolds number flow, as it changes irregularly. However, it was not computationally feasible to get statistics from CFD simulations for such long averaging times with most computational facilities such as those used in the present study. Hence, the over-estimation of the load coefficients by the CFD could be attributed to the short statistical averaging time (2 s) compared to the 180 s taken for the wind tunnel data. Overall the results from LES, especially from Infow-3, were very encouraging.

5.4.4 Power spectra of the along- and across-wind loads for single building

The along- and across-wind force spectra obtained from the present LES simulation and the BLWT experiment are shown in Fig. 5.20 and 5.21, respectively. Where the spectra are presented in the form of $nS(n)/\sigma^2$ versus nD_z/U_H, where n is the frequency, $S(n)$ is the spectral density, and σ^2 is the variance. The forces at every pressure tap level were obtained by integrating the loads across the two opposite faces while the torsional moment were calculated by multiplying each tributary load with the corresponding lever arm from the geometric center of the model building. The total along-wind force spectrum predicted by Inflow-1 and Inflow-2 started decaying quickly within the frequency range of the inertial sub-range, which plays a vital role in

transferring energy between large and small eddies for turbulent flow (Fig 5.20(a)). Higher frequency fluctuation was predicted by Inflow-3, which agreed well with the experimental data. This is an indication that the synthesized turbulence method generated eddies within the inertial sub-range. Figure 5.20(b) shows the along-wind spectrum of the top tap level which is in the region of flow separation. It gave some insight on how each method handled the separated turbulent flow. The total across-wind force spectra from the experiment results showed a sharp peak near the Strouhal number ($S=nD_z/U_H$), defined by using the roof-top velocity U_H, corresponding to the reduced frequency of $nD_z/U_H=0.1$. This clearly suggested that strong and periodic organized Karman vortexes were shed throughout the building height. The spectrum predicted by Inflow-1 and Inflow-2 showed a peak at a lower reduced frequency of ≈ 0.065 and spread to other frequencies. Whereas for Inflow-3 there was an improved prediction and the spectra peaked at the same reduced frequency of ≈ 0.1 as the wind tunnel prediction (Fig. 21(a)).

To further validate the prediction accuracy of the numerical models, the wind force spectrum at the top pressure tap level , where strong flow separation occurred, are presented in Fig. 21(b). The power spectrum followed the same trend as the total wind force spectrum although it showed a broad peak and gradual decaying of eddies. The comparison of the total torsional moment spectra showed a typical peak around a Strouhal number of $nD_z/U_H=0.1$, which is corresponding to the peak frequency range of the across-wind spectra (Fig. 5.22).

5.4.5 Flow field visualization

The time-averaged and instantaneous velocity flow field of, taken at one instant of time, CAARC building model using various transient inlet boundaries are presented in Fig. 5.23 and 5.24, respectively. All the basic flow features of bluff body were captured by the LES simulations (Shah and Ferziger, 1997). The oncoming flow separates at the leading sharp corners (at the three corners of the wind-facing wall) and initiates a recirculation zone on the sidewalls and at the roof of the building, which are foot prints of the arch vortex in the downstream face, as illustrated in Fig. 5.23(a) to (f). The location of the arch vortex and the recirculation contraction zone in the wake region predicated by Inflow-1 and Inflow-2 are further downstream in the wake region than the one predicted by Inflow-3. This might have contributed to the over-prediction of C_D as well. The flow formed a recirculation zone above the roof and remained separated, as illustrated in vertical sections plots of Fig. 5.23(b), (d), and (e). Figure 5.24 illustrates the formation and shedding of asymmetric vortex at the trailing edge of the side faces and the wake zone. The streamlines of the instantaneous velocity revealed the complex and irregular nature of the wind-structure interaction flow field where the symmetric vortices are broken and formed by alternating asymmetric vortices. The flow field from Inflow-3 demonstrated a flow separation zone in the upstream face (Fig. 5.24 (b), (d), and (f)). Strong unsteadily moving vortices are formed by the synthetic inflow turbulence (Inflow-3) and they are responsible for better prediction of the lift-force coefficients, C_L and $C_{\sigma F_Y}$.

5.4.6 CAARC with adjacent building

In experimental and computational wind loads on tall buildings, the more realistic scenario could be a configuration with adjacent buildings in vicinity of the study building. The presence of a neighboring building alters the aerodynamic characteristics of tall buildings and adds complexity to the flow for LES. As a part of the ongoing research, the present study has attempted to assess these interference effects numerically. The configurations with an immediate adjacent building considered in the present study were listed in Table 5.2 and Fig. 5.4. Cases 2 and 3 represented the CAARC model with an upstream neighboring building with space separation (S), based on the wind-ward width (B) of the building, of $S/B = 0.67$. The general settings of CAARC with adjacent building such as boundary conditions, discretization schemes for both time and convection terms were kept similar to Case 1. Table 5.5 lists the comparison between the LES and experimental force and torsional moment coefficients of the CAARC model building with an adjacent building situated on the upwind direction.

As expected, the adjacent building introduced sheltering effect on CAARC that attributed to the reduction in the total along- and across-wind forces. For Case 2, the half-height adjacent building blocked the direct wind action up to H/2 and interfered with the flow around the rest of the building height. It is worth noting how the flow separated at the adjacent building and reattaches back to the study building (Fig. 5.25(a) and (c)). These combined phenomena and the narrow wake consequently reduced the drag- and lift-coefficients of the study building. Case 3 also displayed very interesting phenomena, where the flow remained separated from the side walls and sheds alternating Karman vortices (Fig. 5.25(b) and (d)). As a result a wider wake was created and the lift-

coefficient of the study building has increased significantly (Table 5.5). However, the flow reattaches at the roof of the study building and formed reversed flow on the wind-ward face (Fig. 5.26 (b) and (d)). This phenomenon had introduced strong suction on the wind-ward face of the study building, which resulted in negative drag coefficient (Table 5.5)

Whereas for Case 2 the velocity speed-up from separation of flow at the roof of the adjacent building injected flow towards the wind-ward face of the study building and along- wind force in the flow direction remained strong (Fig. 5.26(a) and (c)). The LES also performed well in predicting the torsional moment. Because of the symmetrical nature of the flow for the considered wind angle of attack, the torsional moment has been very small in all cases. The LES, averaged over two sec flow time, over-predicted the steady and fluctuating forces and moment. It also revealed very interesting flow details on how the flow field behaves when there is neighboring building.

5.4.6.1 Spectral density

The total along-wind spectra of CAARC with an adjacent building are shown in Fig. 5.27. The LES spectrum of drag fluctuation of Case 2 agreed well with the experimental spectrum. However the spectrum for Case 3 was slightly off. For the across-wind fluctuation spectra (Fig. 5.28), Case 2 shows a similar trend as the single building case spectra (Fig. 5.21(a)) except that there was slightly lower peak at the Strouhal number $nD_z/U_H = 0.1$ (Fig. 28(a)), this could be attributed to the sheltering effect of the neighboring. Case 3 demonstrated flat across-wind spectrum without typical peak at the vortex shedding frequency. Overall the numerical simulations reproduced the fluctuating force and capture eddies within the inertial sub-rang.

5.5 Conclusions

- Computational assessment of aerodynamic characteristics of a standard tall building (CAARC) with and without a neighboring building were performed and results were compared with BLWT data. The effects of inflow turbulence have been examined from the turbulence modeling principle of LES and computational wind load evaluation perspective.
- Three different inflow transient boundary conditions were investigated that utilized basic flow statistics (such as TI, wind speed, integral length scale) from the BLWT ABL data both using representative data for LES and for consistency reasons during the comparison. Inflow-3 that adopted fluctuation generated by using a synthetic method showed a better agreement with the BLWT data than the random flow generated by Simirnov's (also called spectral synthesizer) and Lund's recycling methods. The result further attested the need for proper inflow transient boundary conditions in agreement with suggestions by other CFD researchers. This in fact is analogous to the extreme care and effort that is taken during ABL flow simulation in the BLWT thorough use of upwind roughness elements, spires, or other types of active and passive flow controls. Similar care is expected from a numerical modeler.
- Generally, it can be concluded that LES with proper boundary conditions and enhanced computational resources could prove useful for wind load applications. In the author's opinion, the computational resource still is the bottle neck for full-fledged use of LES making it still expensive and more time consuming than standard BLWT wind load studies. One such limitation in the present study was perhaps the limited period of LES pressure time-history data generated than what might have

been necessary to accurately predict the design wind force coefficients very similar to experimental method.

- The sheltering effects introduced by the neighboring building fairly captured by the numerical simulation when adjacent buildings are placed upwind of the study building. Mean pressure coefficient increased for Case 2 when compared with the isolated CAARC model (Case 1).
- Sheltering effects and other complex interference mechanisms could be effectively explained owing to the continuous simulation capability of numerical simulations in space and time, thus leading to better understanding of wind/structure interactions and development of mitigation solutions that will lead to enhanced wind performance of buildings.
- Wind tunnel experimental data are indispensable for correct boundary prescription and validation of LES.
- The present study was limited to one wind direction, as part of the ongoing project the authors are in the process of investigating wind directionality effects under an urban setting using a numerical approach. This will be done using inhomogeneous inflow turbulence.

References

Ansys Inc., 2011. ANSYS FLUENT14 User's Guide. Ansys Inc., Southpoint 275 Technology Drive Canonsburg, PA.

Ansys Inc., 2011. ANSYS ICEM CFD User Manual. Ansys Inc., Southpoint 275 Technology Drive Canonsburg, PA.

Batten, P., Goldberg, U., Chakravarthy, S., 2004. Interfacing statistical turbulence closures with large-eddy simulation. *AIAA Journal 42(3), 485–492.*

Bitsuamlak, G.T., Dagnew, A.K., and Chowdhury, A.G., 2010. Computational assessment of blockage and wind simulator proximity effects for a new full-scale testing facility . Wind and Structures. 13(1), 21-36.

Billson, M., Eriksson, L.E. and Davidson L., 2004. Modeling of synthetic anisotropic turbulence and its sound emission. The 10th AIAA/CEAS Aeroacoustics Conference, AIAA 2004- 2857, Manchester, United Kingdom.

Braun, A.L., Awruch, A.M., 2009. Aerodynamic and aeroelastic analyses on the CAARC standard tall building model using numerical simulation. Computers and Structures 87, 567-581.

COST., 2007. Best practice guideline for the CFD simulation of flows in the urban environment COST Action 732.

Dagnew, A.K., Bitsuamalk, G.T., Ryan, M., 2009. Computational evaluation of wind pressures on tall buildings. The11th American conference on Wind Engineering, San Juan, Puerto Rico, June 20-26.

Dagnew, A.K., Bitsuamalk, G.T., Ryan, M., 2009. Computational evaluation of wind pressures on tall buildings. 11th American conference on Wind Engineering. San Juan, Puerto Rico.

Davidson, L., 2007. Using Isotropic Synthetic Fluctuations as Inlet Boundary Conditions for Unsteady Simulations. Advances and Applications in Fluid Mechanics, 1(1), 1-35.

Davidson, L., 2009. Hybrid LES-RANS: back scatter from a scale-similarity model used as forcing. Phil Trans R. S. A 367, 2905-2915.

Franke. J., 2006. Recommendations of the COST action C14 on the use of CFD in predicting pedestrian wind environment.

Germano, M. U. Piomelli, P. Moin, and W. H. Cabot. 1996. Dynamic Subgrid-Scale Eddy Viscosity Model". In Summer Workshop. Center for Turbulence Research, Stanford, CA.

Huang, S., Li, Q.S., Xu, S., 2007. Numerical evaluation of wind effects on a tall steel building by CFD. Journal of Constructional Steel Research 63, 612-627.

Huang, S.H., Li, Q.S., Wu, J.R., 2010. A general inflow turbulence generator for large eddy simulation. Journal of Wind Engineering and Industrial Aerodynamics 98, 600-617.

Huang, S.H., Li, Q.S., 2010. Large eddy simulation of wind effects on a super-tall building. Wind and Structures, An Int'l Journal 13(6).

Kataoka, H., Mizuno, M., 2002. Numerical flow computation around aeroelastic 3D square cylinder using inflow turbulence. Wind and Structure, An Int'l Journal 5 (2–4), 379–392.

Khanduro, A.C., Stathopoulos, T., Bedard, C. (1998). "Wind-induced interference effects on buildings-a review of the state-of-art." *Engineering Structures Vol.20, 617-630.*

Kondo, K., Murakami, S., Mochida, A., 1997. Generation of velocity fluctuations for inflow boundary condition of LES. Journal of Wind Engineering and Industrial Aerodynamics 67-68, 51-64.

Kraichnan R.H., 1970. Diffusion by a random velocity field. *Physics of Fluids*, 13(1), 22–31.

Lam, K. M. and To, A. P., 2006. Reliability of numerical computation of pedestrian-level wind environment around a row of tall buildings. Wind and Structures, 9(6), 473-492

Lam, K.M., H. Leung, M.Y., Zhao, J.G. ,2008. Interference effects on wind loading of a row of closely spaced tall buildings. Journal of Wind Engineering and Industrial Aerodynamics 96, 562-583.

Leonard, B.P., 1991. The ultimate conservative difference scheme applied to unsteady one-dimensional advection, Comput. Method. Appl. M., 88, 17-74.

Lim, H.C., Thomas, T.G., Castro, I.P., 2009. Flow around a cube in a turbulent boundary layer: LES and experiment. Journal of Wind Engineering and Industrial Aerodynamics 97, 96-109.

Lilly, D.K., 1992. A Proposed Modification of the Germano Subgrid-Scale Closure Model. Physics of Fluids. 4. 633–635.

Lumley, J.L., Panofsky, H.A., 1964. The Structure of Atmospheric Turbulence. Wiley-Interscience, New York, pp. 239.

Lund, T.S., Wu, X., Squires, K.D., 1998. Generation of turbulent inflow data for spatially-developing boundary layer simulations. J. of Computational Physics140, 233-258.

Martinuzzi, R., Tropea, C., 1993. The flow around surface-mounted, prismatic obstacles placed in a fully developed channel flow. J. Fluids Eng 115, 85–92.

Melbourne, W.H., 1980. Comparison of measurements on the CAARC standard tall building model in simulated model wind flows. Journal of Wind Engineering and Industrial Aerodynamics 6, 73-88.

Murakami, S., 1998. Overview of turbulence models applied in CWE–1997. Journal of Wind Engineering and Industrial Aerodynamics 74-76, 1-24.

Nozawa, K., Tamura, T., 2002. Large eddy simulation of the flow around a low-rise building immersed in a rough-wall turbulent boundary layer. Journal of Wind Engineering and Industrial Aerodynamics 90, 1151-1162.

Nozawa, K., Tamura, T., 2003. Numerical prediction of pressure on a high-rise building immersed in a turbulent boundary layer using LES. *I*n: Proceeding of annual meeting of JACWE 95, 169–170.

Obasaju, E.D., 1992. Measurment of forces and base overturning moments on the CAARC tall building model in a simulated atmospheric boundary layer. Journal of Wind Engineering and Industrial Aerodynamics 40, 103-26.

Princevac, M., Baik, J., Li, X., Pan, H., Park, S., 2010. Lateral channeling within rectangular arrays of cubical obstacles. Journal of Wind Engineering and Industrial Aerodynamics 98, 377-385.

Shah, K.B., Ferziger, J.H., 1997. A fluied mechanics view of wind engineering: large eddy simulation of flow over a cubical obstacle. In R.N. Meroney, B. Bienkiewicz (eds.), Computational Wind Engineering, 2, 211-226, Elsevier, Amsterdam.

Sagaut, P., Deck, S., 2009. Large eddy simulation for aerodynamics: Status and perspectives. Phil Trans R. S. A 367, 2849-2860.

Senthooran, S., Lee, D., Parameswaran, S., 2004. A computational model to calculate the flow-induced pressure fluctuations on buildings. Journal of Wind Engineering and Industrial Aerodynamics 92, 1131-1145.

Shinozuka M., 1985. Lecture at CISM course on stochastic methods in structural engineering. International Centre for Mechanical Science, Udine.

Simiu, E., 1976. Equivalent static wind loads for tall building design", J. of Struct. Div., ASCE, 102(4) 719-737.

Smirnov, R., Shi, S., Celik, I., 2001. Random flow generation technique for large eddy simulations and particle-dynamics modeling. *J. of F. Eng.* 123, 359–371.

Swaddiwudhipong, S., Anh, T.T.T, Liu, Z.S., Hua. J., 2007. Modeling of wind load on single and staggered dual buildings. Engineering with Computers 23(3), 215-22.

Tabor, G.D, Baba-Ahmadi. M.H., 2009. Inlet condition for large eddy simulation: A review. J. of Computers and Fluids 39 (4), 553-567.

Tamura, T., Nozawa, K., Kondo, K., 2008. AIJ guide for numerical prediction of wind loads on buildings. Journal of Wind Engineering and Industrial Aerodynamics 96, 1974-1984.

Tamura, T.,2008. Towards practical use of LES in wind engineering. Journal of Wind Engineering and Industrial Aerodynamics 96, 1451–1471.

Tamura, T., Nozawa, K., Kondo, K., 2008. AIJ guide for numerical prediction of wind loads on buildings. Journal of Wind Engineering and Industrial Aerodynamics 96, 1974–1984.

Thepmongkorn, S., Wood, G.S., Kwok, K.C.S., 2002. Interference effects on wind-induced coupled motion of a tall building. Journal of Wind Engineering and Industrial Aerodynamics 90, 1807-1815.

Tominaga, Y., Mochida, A., Murakami, S., Sawaki, S., 2008a. Comparison of various revised k–ε models and LES applied to flow around a high-rise building model with 1:1:2 shape placed within the surface boundary layer. Journal of Wind Engineering and Industrial Aerodynamics 96, 389-411.

Tucker, P. G, & Lardeau, S., 2009. Applied large eddy simulation. Phil. Trans. R. Soc. A July 28*,* 367 (1899) 2809-2818.

Wright, N.G., Easom, G.J., 2003. Non-linear k–e turbulence model results for flow over a building at full-scale. Applied Mathematical Modeling 27(12), 1013-1033.

Yoshie, R., Mochida, A., Tominaga, Y., Kataoka, H., Harimoto, K., Nozu, T., Shirasawa, T., 2007. Cooperative project for CFD prediction of pedestrian wind environment in the Architectural Institute of Japan. Journal of Wind Engineering and Industrial Aerodynamics 95, 1551-1578.

Zhang, A., Gu, M., 2008. Wind tunnel tests and numerical simulations of wind pressures on buildings in staggered arrangement. Journal of Wind Engineering and Industrial Aerodynamics 96, 2067-2079.

Table 5.1 Measured inflow wind characteristics of rural terrain.

Level	**Elevation(m)**	$U(m/s)$	**Turbulent intensity (%)**			**Integral length (m)**		
			I_x	I_y	I_z	${}^{x}L$	${}^{y}L$	${}^{z}L$
1	0.1524	10.381	24.00	7.30	16.30	0.480	0.090	0.160
2	0.3048	11.458	22.50	8.90	14.80	0.540	0.145	0.175
3	0.4572	12.061	21.00	10.30	14.50	0.550	0.160	0.192
4	0.6096	12.810	19.60	11.00	13.90	0.600	0.175	0.200
5	0.9144	13.647	16.90	10.20	12.40	0.630	0.185	0.205
6	1.2192	14.438	15.60	9.30	11.30	0.640	0.190	0.210
7	1.5240	14.995	12.80	6.90	9.30	0.650	0.125	0.191

Table 5.2 LES cases.

Case	**Configuration**	**Wind AoA**	y+
Case 1	Isolated	00	1 < y+ < 5
Case 2	Half height adj. bldg. upwind of CAARC	00	1 < y+ < 5
Case 3	Full height adj. bldg. upwind of CAARC	00	1 < y+ < 5

Table 5.3 Comparative study of inflow turbulences.

Inlet boundary	**Turbulence generation method**
Inflow-1	Spectral synthesizer method (Smirnov et al., 2001)
Inflow-2	Recycling method (Lund et al., 1998)
Inflow-3	Synthesized turbulence (using the method in Sec. 2.2)

Table 5.4 Comparison of total steady and *rms* force coefficients.

Inflow turbulence generation method	C_D	$C_{\sigma F_X}$	C_L	$C_{\sigma F_Y}$	C_M	$C_{\sigma M}$
Inflow-1	1.6957	0.6027	0.0042	0.9245	0.0019	0.1703
Inflow-2	1.6264	0.5453	0.0043	1.3209	0.0014	0.2456
Inflow-3	1.6091	1.2484	0.0100	1.2260	0.0013	0.2424
BLWT exp.	1.533	1.0737	0.0356	1.1818	0.0007	0.2150

Table 5.5 Force coefficients: CAARC with adjacent building.

Case	C_D		$C_{\sigma F_X}$		C_L	
	LES	**Exp.**	**LES**	**Exp.**	**LES**	**Exp.**
Case 1	1.6091	1.533	1.2484	1.0737	0.0100	0.0354
Case 2	1.0250	0.8302	0.8420	0.5573	0.0120	0.0017
Case 3	-0.4760	-0.1709	0.6369	0.7687	0.0087	0.1006

Table 5.5 (continued)

$C_{\sigma F_Y}$		C_M		$C_{\sigma M}$	
LES	**Exp.**	**LES**	**Exp.**	**LES**	**Exp.**
1.2259	1.1818	0.0013	0.0007	0.2424	0.2149
0.5794	0.5434	0.0002	0.0009	0.3402	0.1811
0.6300	0.8644	0.0009	0.0035	0.2524	0.2458

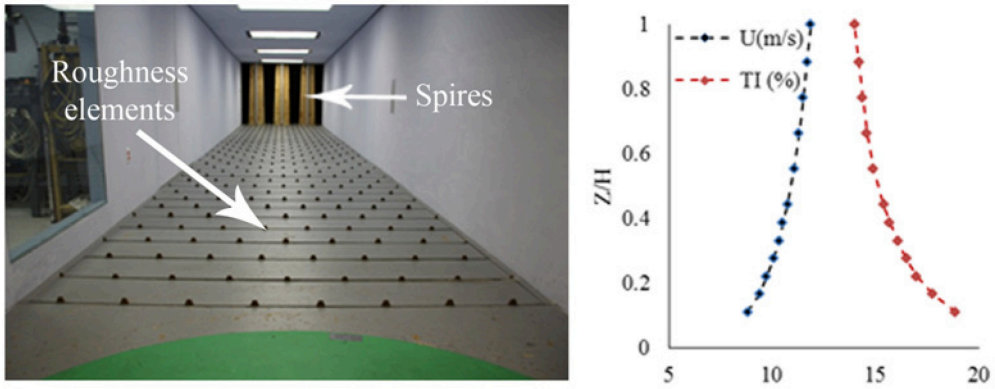

Figure 5.1 (a) An empty wind tunnel set up for ABL testing at RWDI Miramar, FL; and (b) Measured mean wind velocity and turbulence intensity (TI).

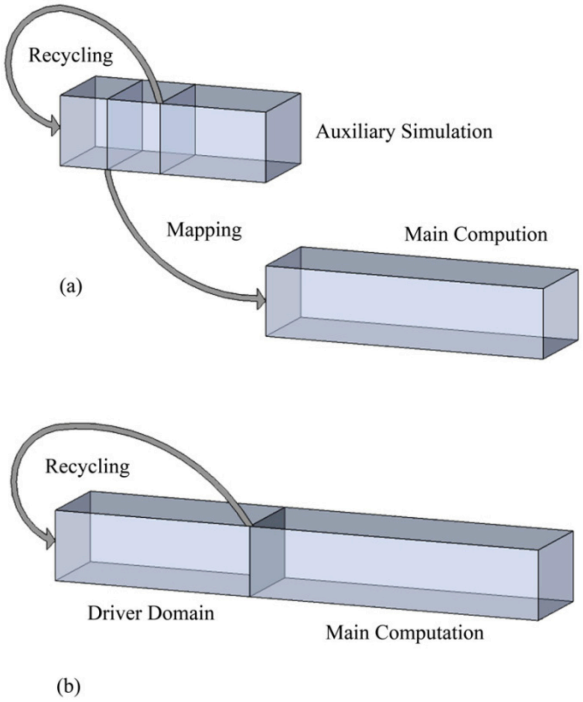

Figure 5.2 Implementation of Lund's recycling method: Where (a) auxiliary pre-computation is mined to produce velocity inlet data and (b) computational domain is subdivided into driver and main computation domain.

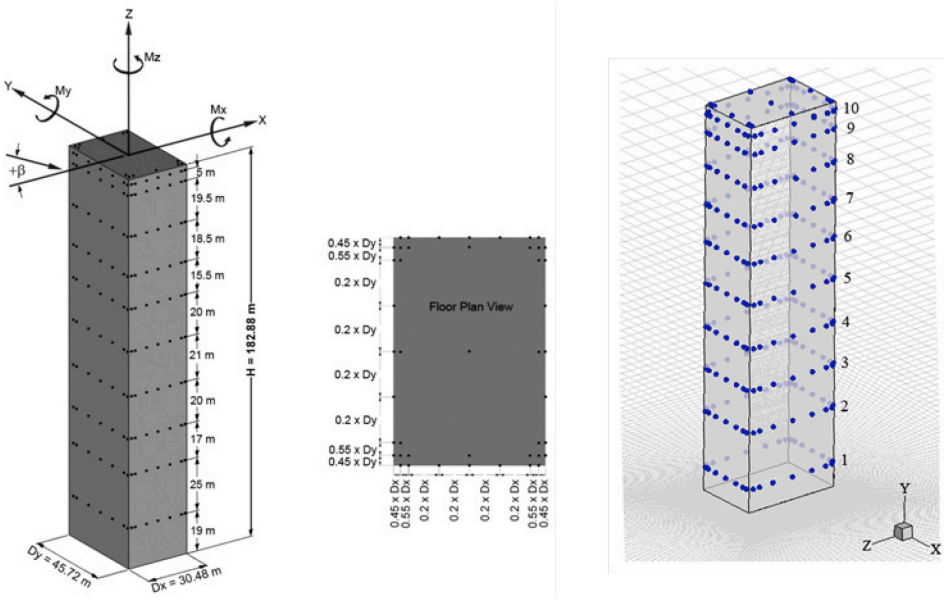

Figure 5.3 CAARC building model: Dimension and pressure tap locations (a) and (b) BLWT, (c) CFD.

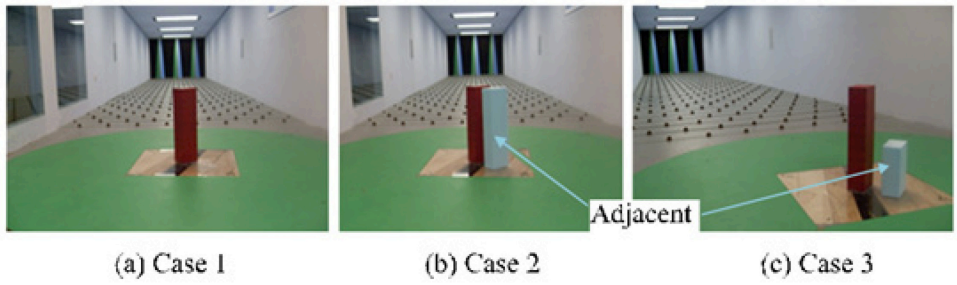

Figure 5.4 Experimental load evaluation test configurations: Isolated CAARC model (a) and with adjacent (b) full-height, and (c) half-height building.

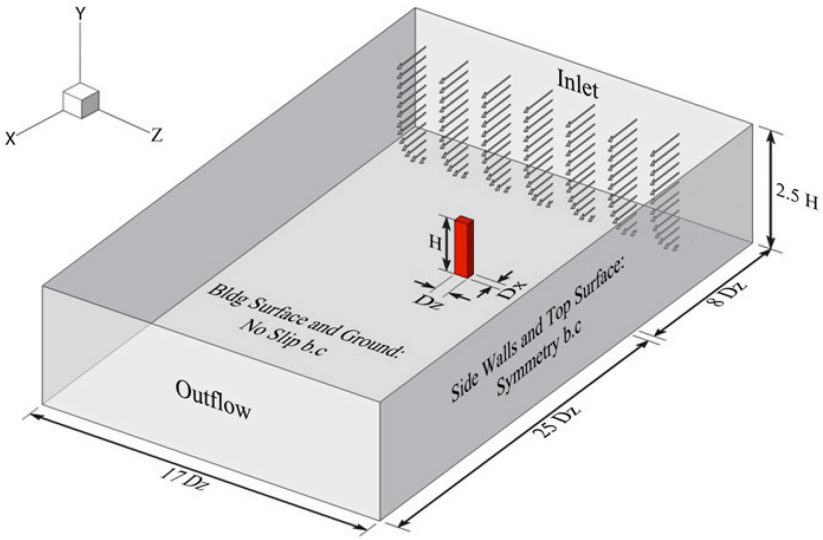

Figure 5.5 Computational domain and boundary conditions for Case 1.

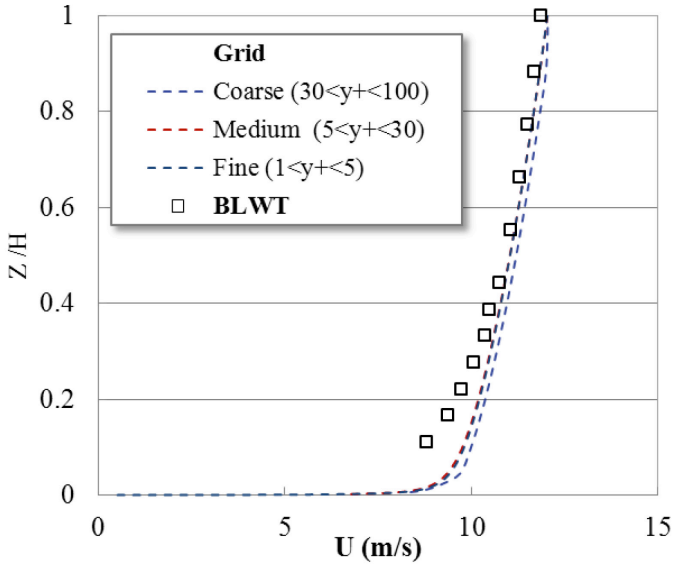

Figure 5.6 Grid sensitivity analysis on an empty channel flow using RANS turbulence modeling.

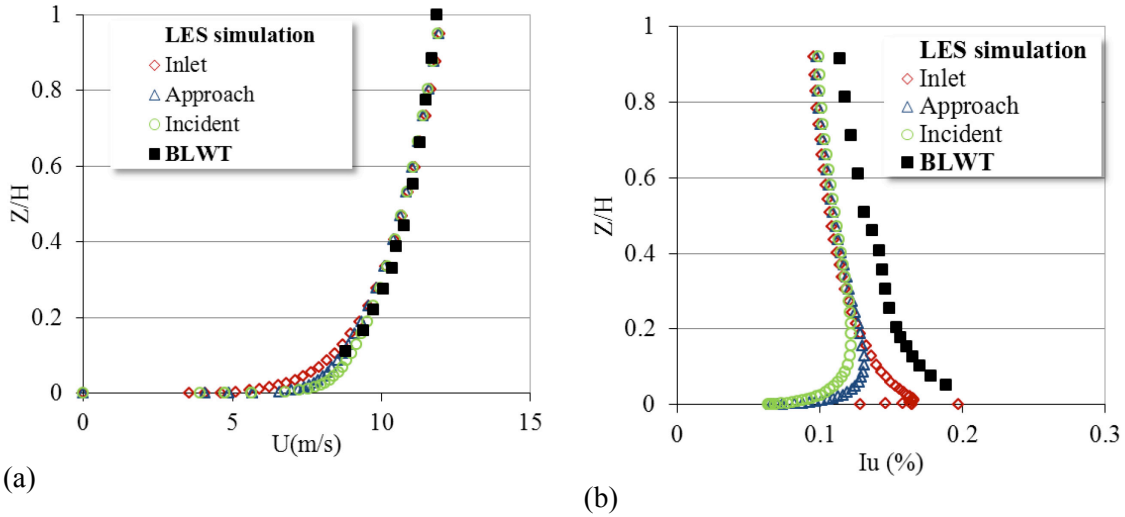

Figure 5.7 Velocity and turbulence profiles measured from the LES simulation of an empty domain with high resolution mesh. Inlet plane; Approach flow is measure at $4D_Z$ and the incident flow is measured at $8D_Z$.

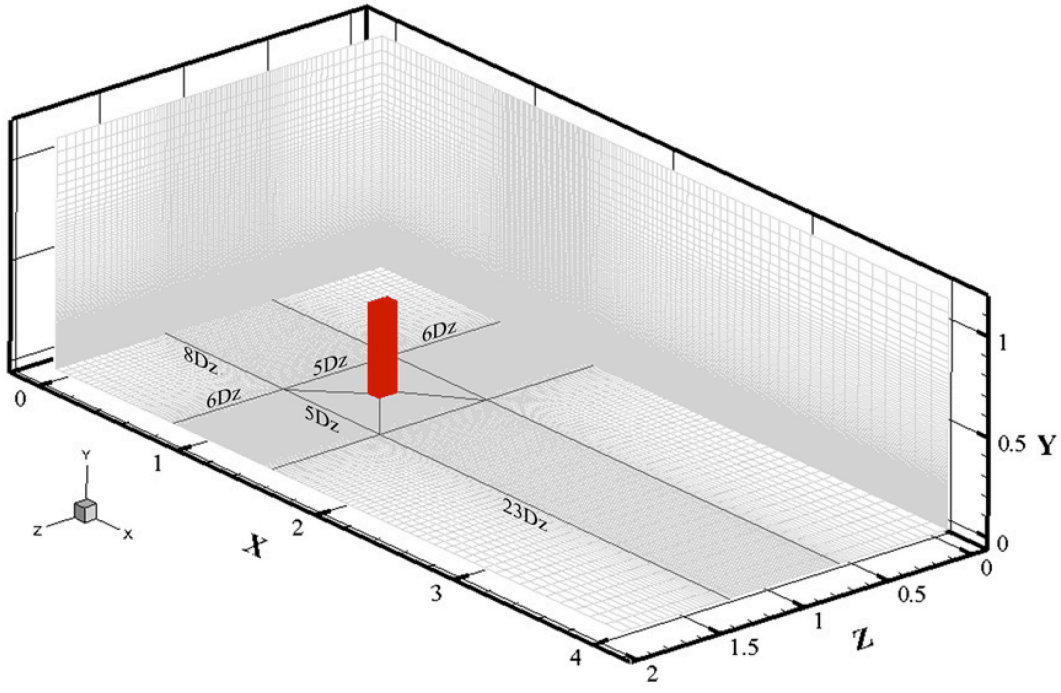

Figure 5.8 Arrangement of computational grids.

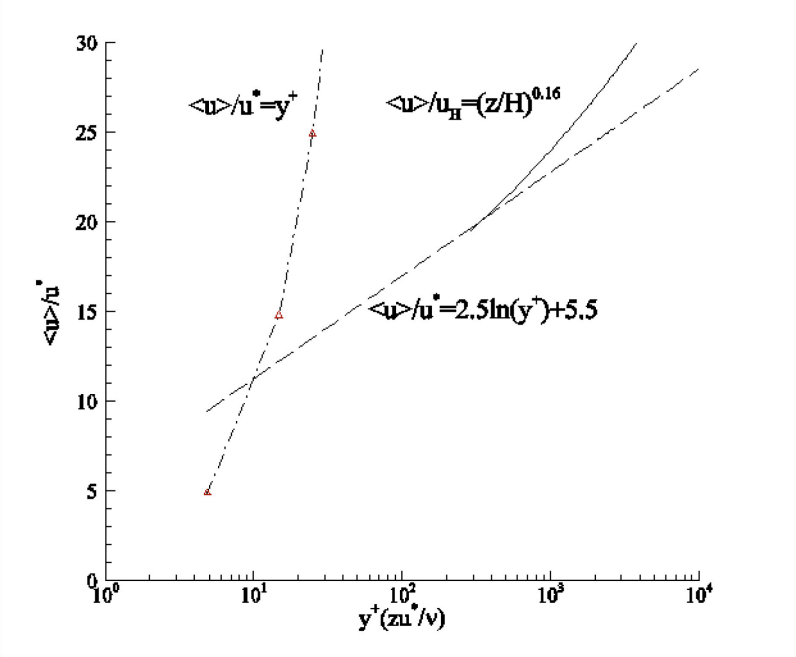

Figure 5.9 Measured inlet velocity profile in semi-log scale.

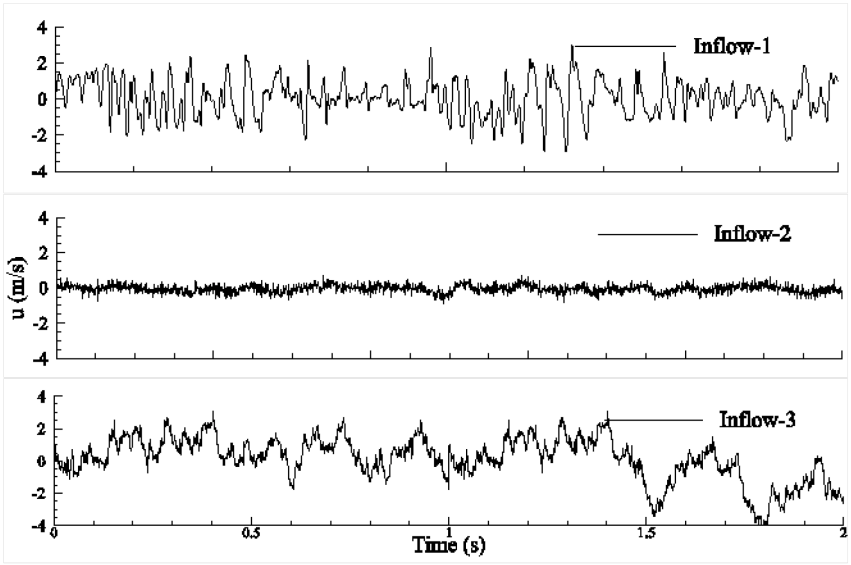

Figure 5.10 Comparison of numerically generated stream-wise wind velocity fluctuation samples at the target building height.

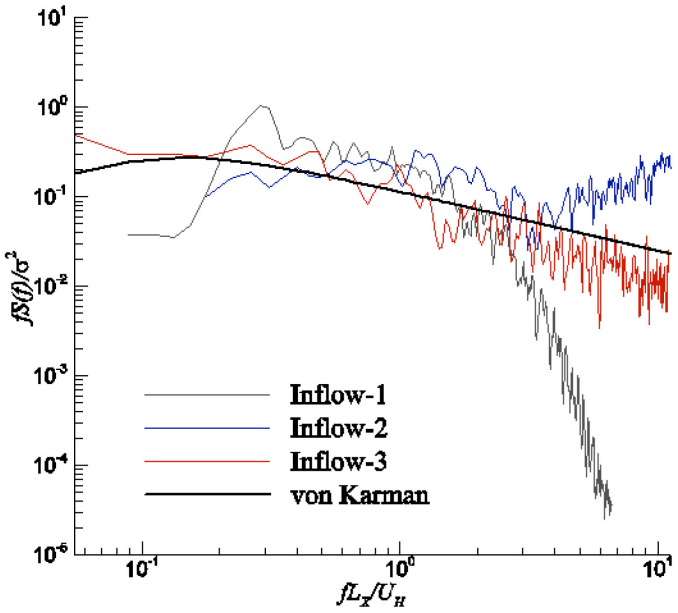

Figure 5.11 Comparison of numerically simulated spectra with von Karman spectrum model at the model building height (L_U=0.55m, and U_H=12.12 m/s).

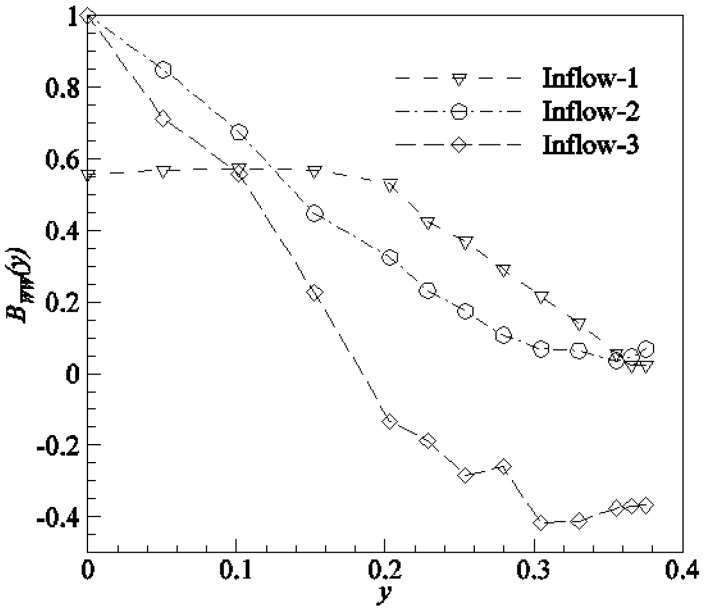

Figure 5.12 Normalized two-point correlation of vertical velocity fluctuation.

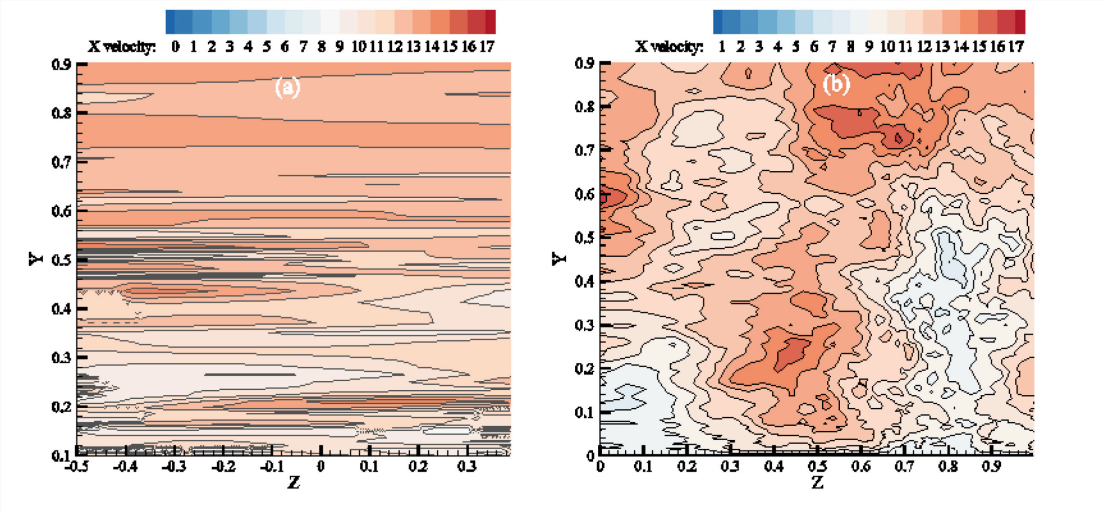

Figure 5.13 Spatial representation of the stream-wise instantaneous velocity fluctuation at the inlet boundary: (a) Random flow generation method (Inflow-1) and (b) Synthetic inlet boundary (Inflow-3).

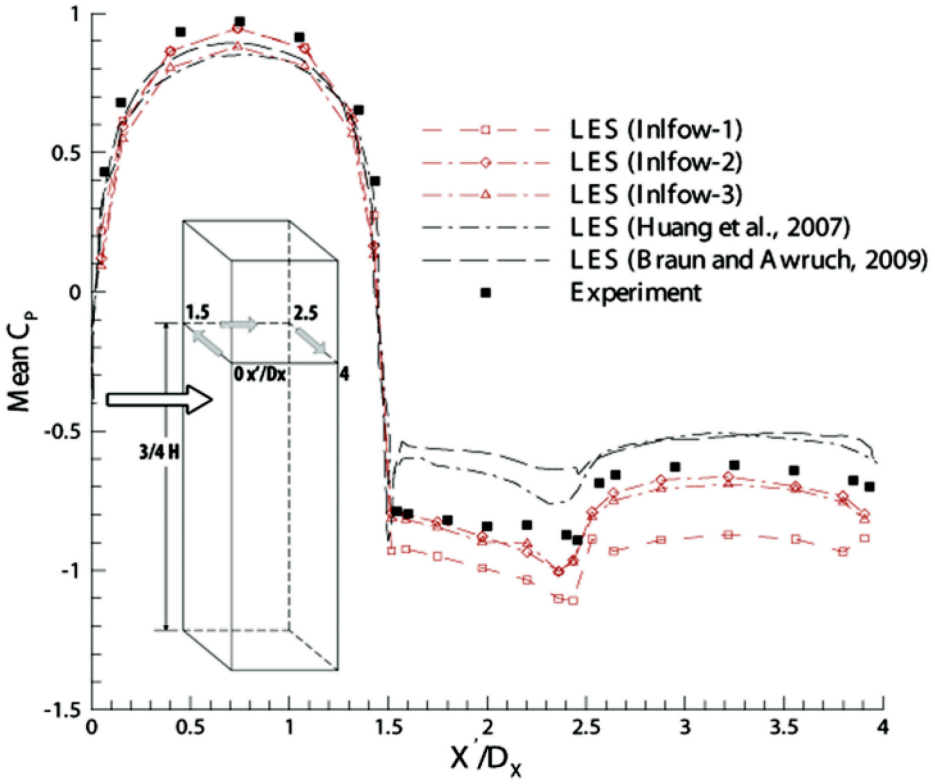

Figure 5.14 Comparison of mean pressure coefficient at 2/3 H of CAARC model building.

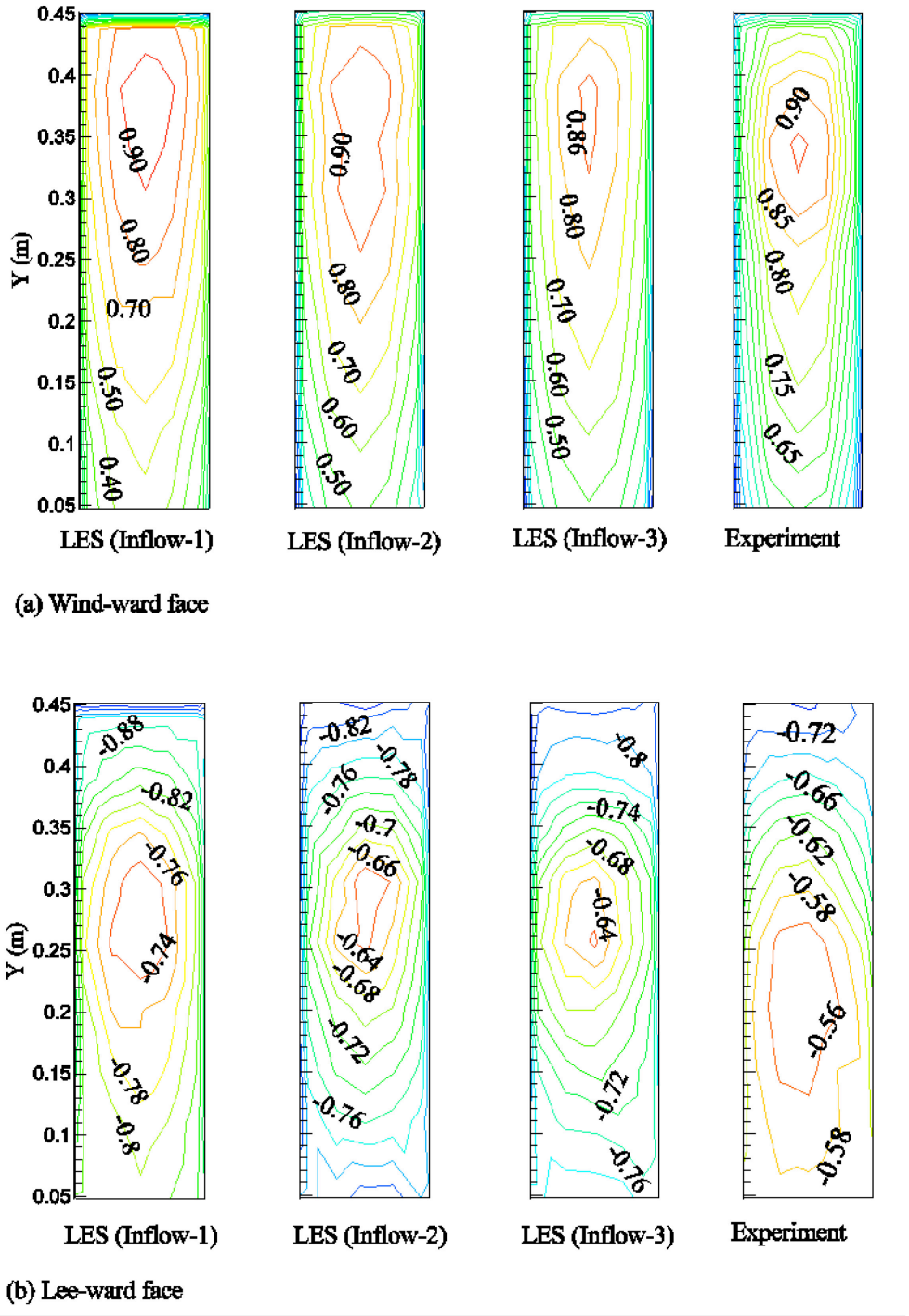

Figure 5.15 Pressure coefficient distribution over frontal and back faces of CAARC in a simulated ABL flow: Comparison between LES with various oncoming turbulence models and BLWT experiment.

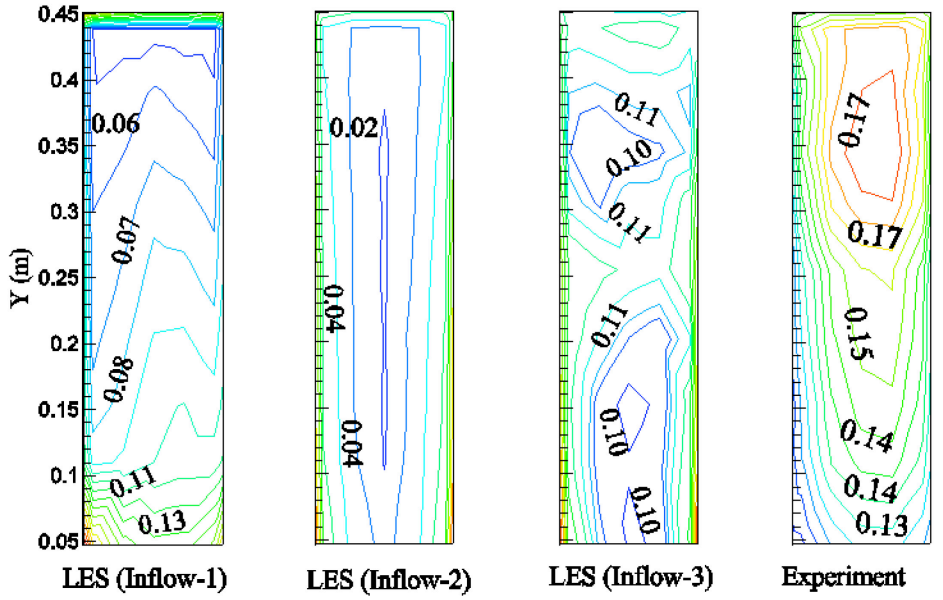

(a) Wind-ward face

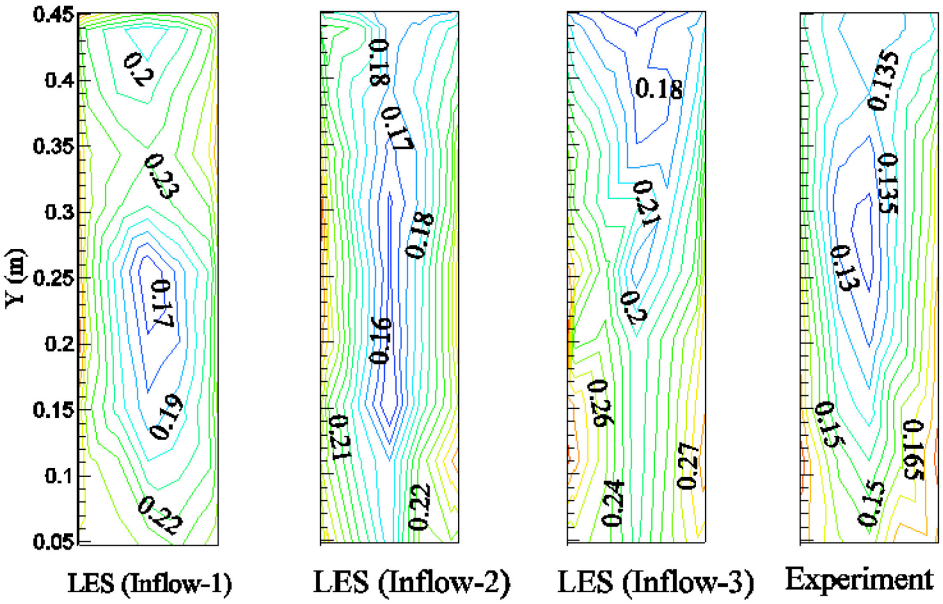

(b) Lee-ward face

Figure 5.16 Distribution of fluctuating pressure coefficient over the frontal and lee-ward faces of CAARC in a simulated ABL flow filed: Comparison between LES with various oncoming turbulence models and BLWT experiment.

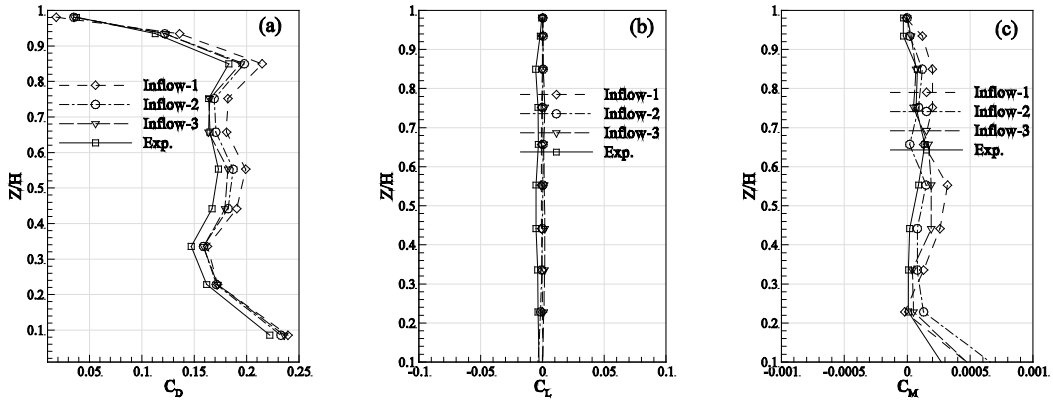

Figure 5.17 Vertical distribution of mean (a) drag, (b) lift, and (c) torsional moment coefficients.

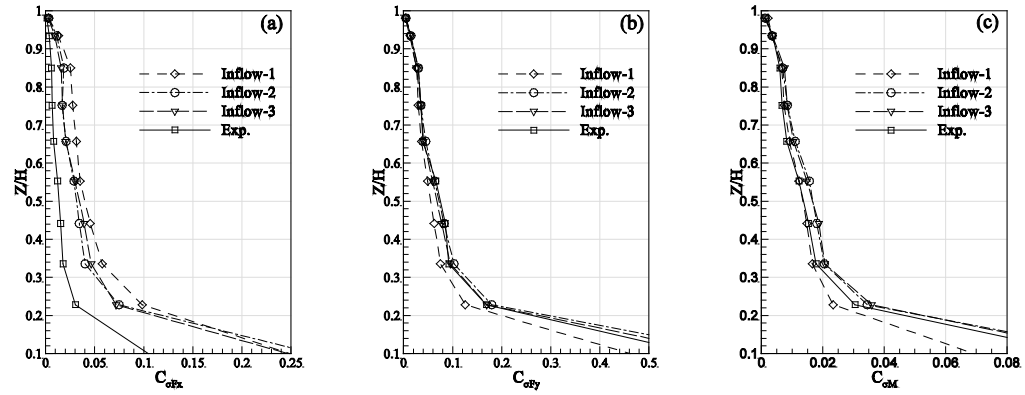

Figure 5.18 Vertical distribution of fluctuating (a) drag, (b) lift, and (c) torsional moment coefficients.

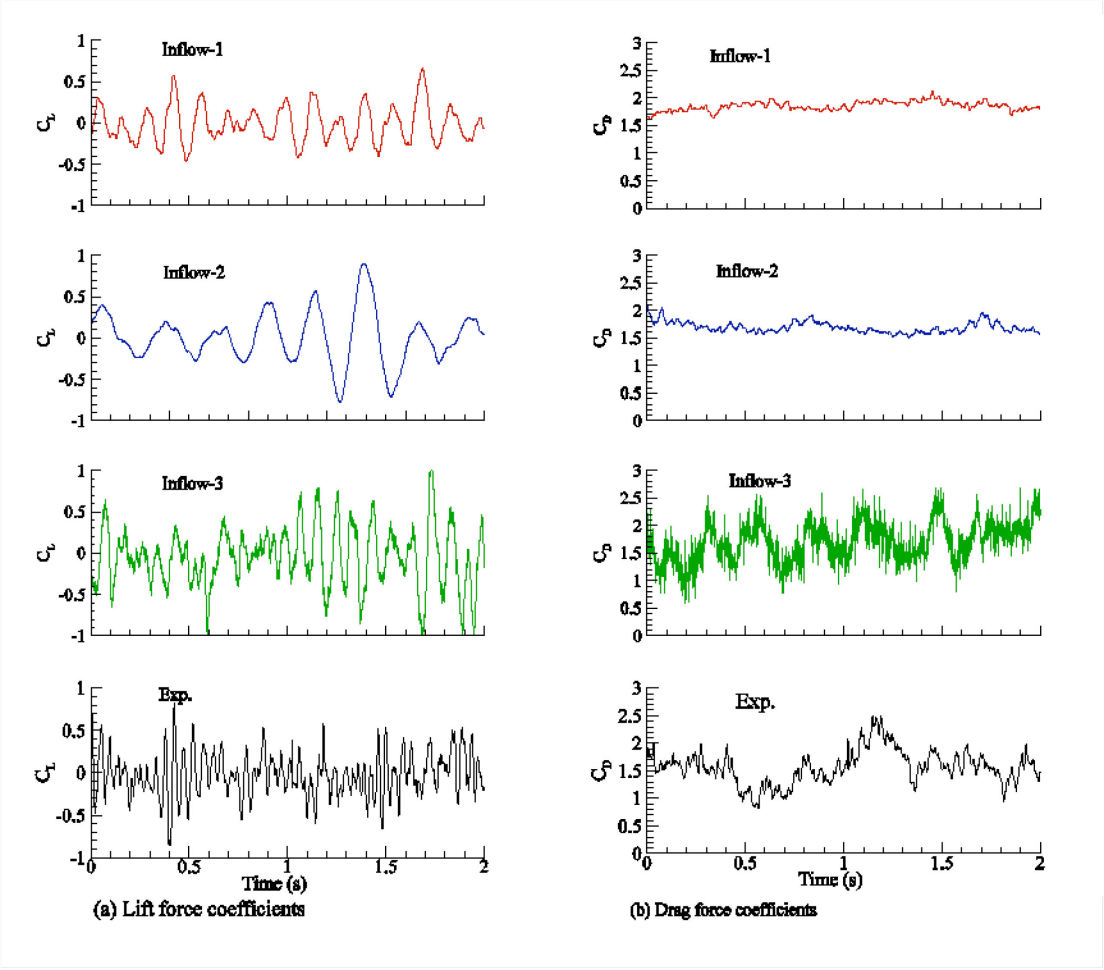

Figure 5.19 LES and BLWT time histories of C_L and C_D

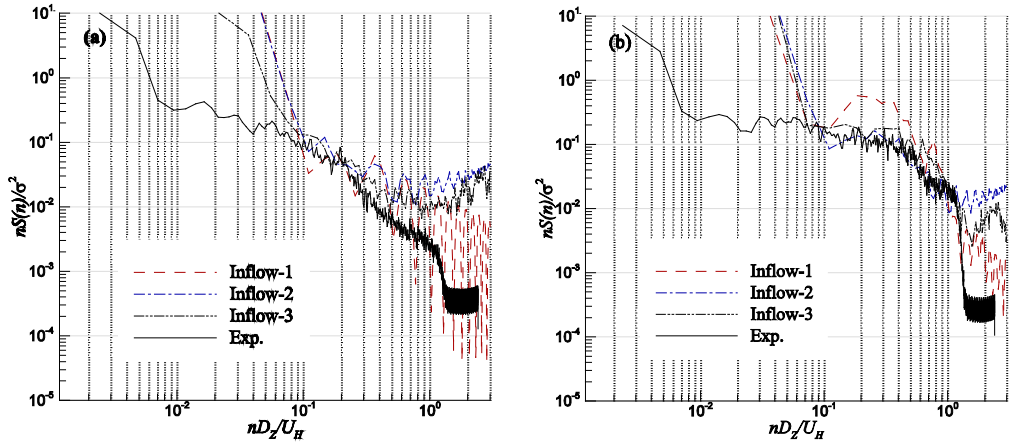

Figure 5.20 Comparison of along-wind force spectrum spectra predicted by LES and BLWT: (a) total force and (b) at the building model height (H=0.46).

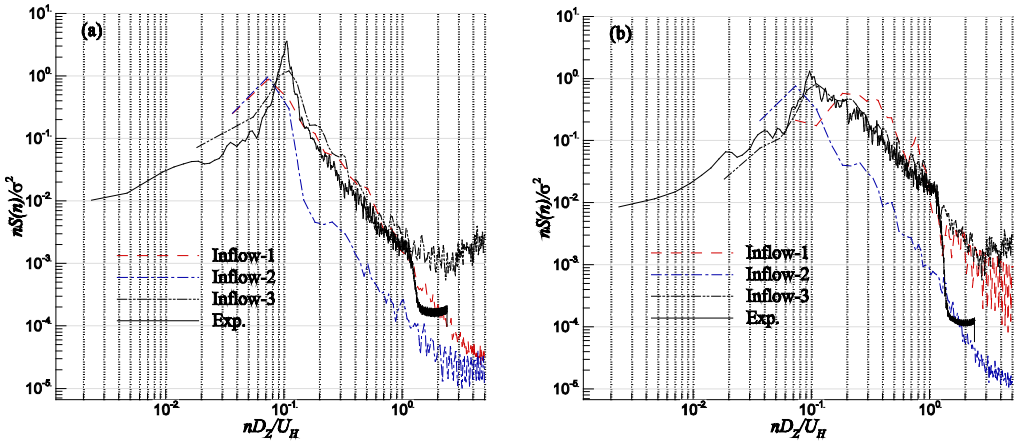

Figure 5.21 Comparison of across-wind force spectrum spectra predicted by LES and BLWT: (a) total force and (b) at the model building height (H=0.46).

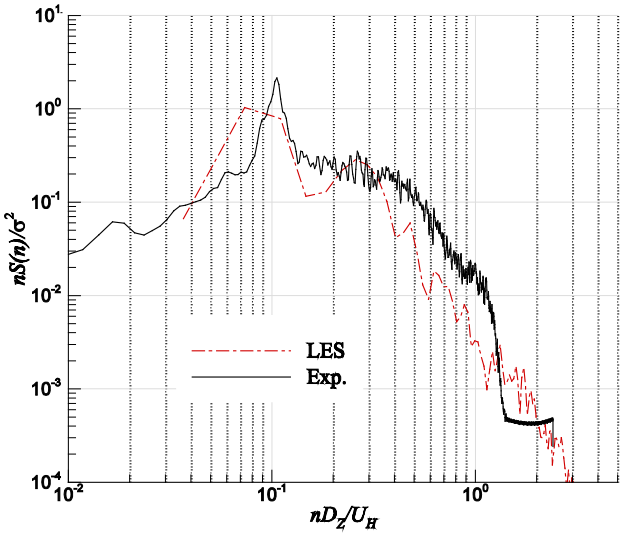

Figure 5.22 Torsional moment spectrum (Synthetic turbulence).

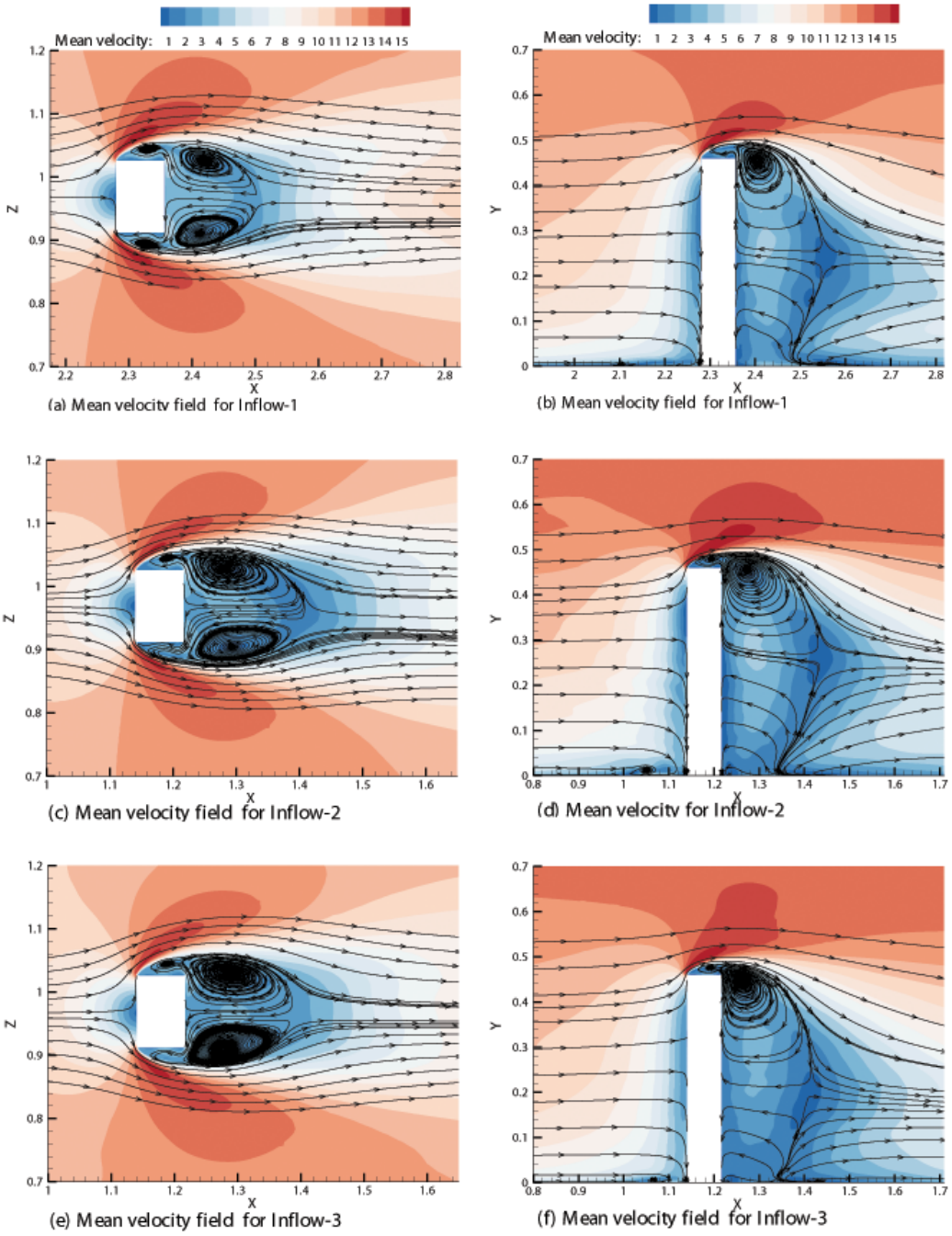

Figure 5.23 Mean wind velocity contour and velocity streamlines: horizontal plane (Left) and a vertical section at centerline (Right).

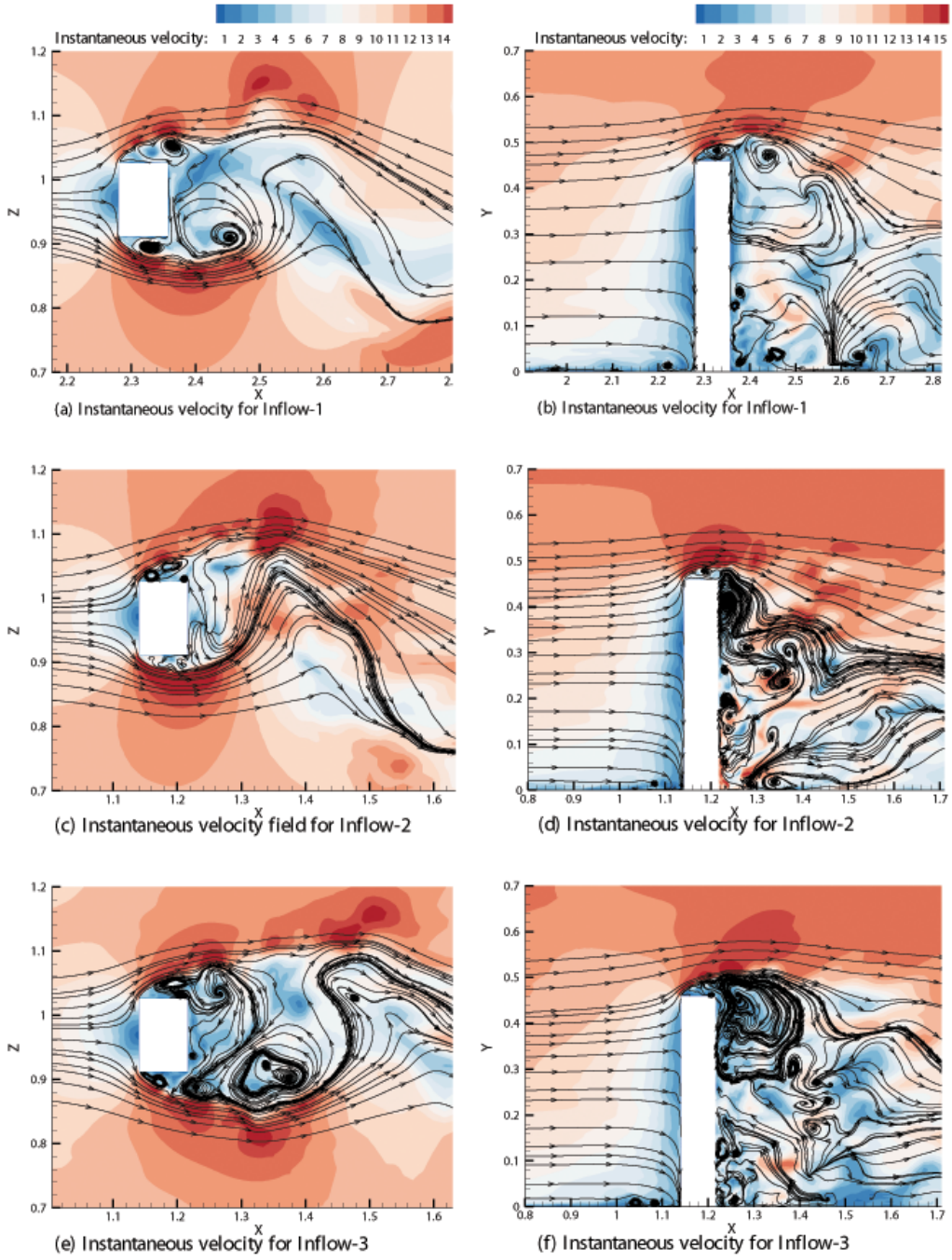

Figure 5.24 Instantaneous wind velocity contour and velocity streamlines: horizontal plane (Left) and a vertical section on centerline (Right).

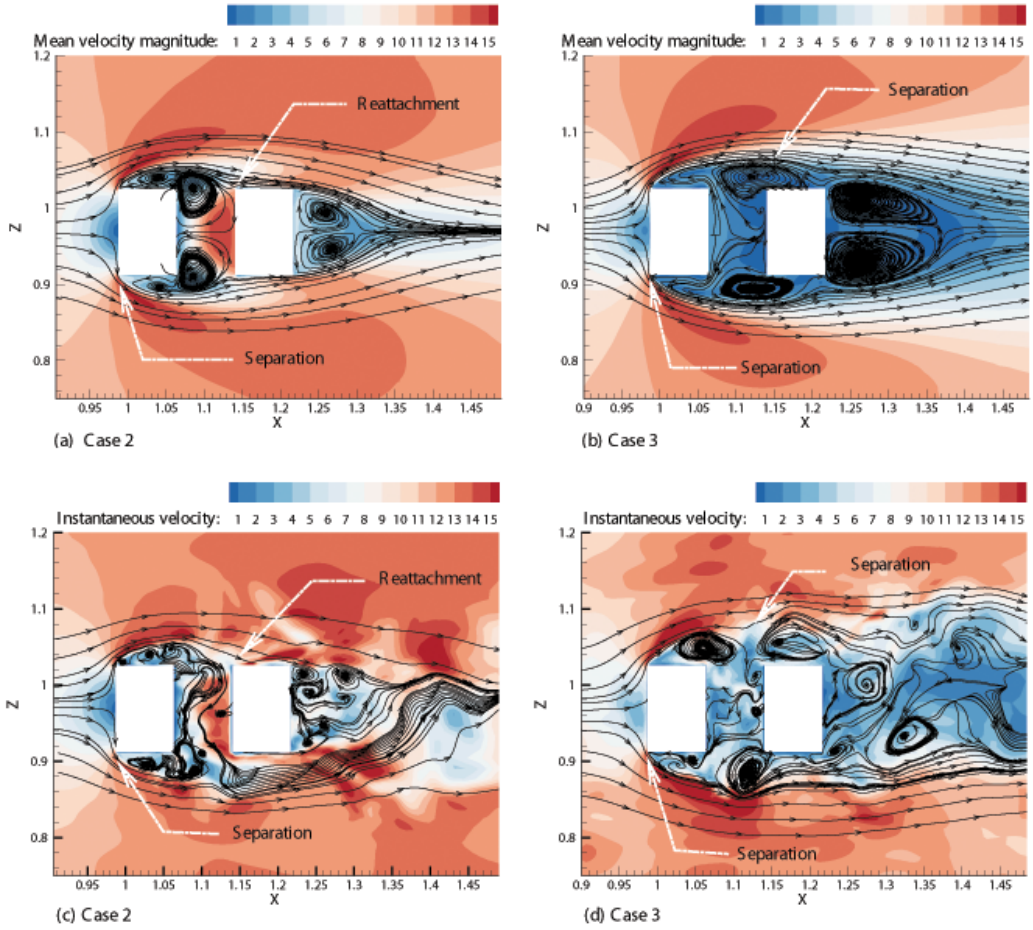

Figure 5.25 Flow field of CAARC with an adjacent building: Mean velocity magnitude (top) and (bottom) instantaneous velocity on a horizontal plane at H/3.

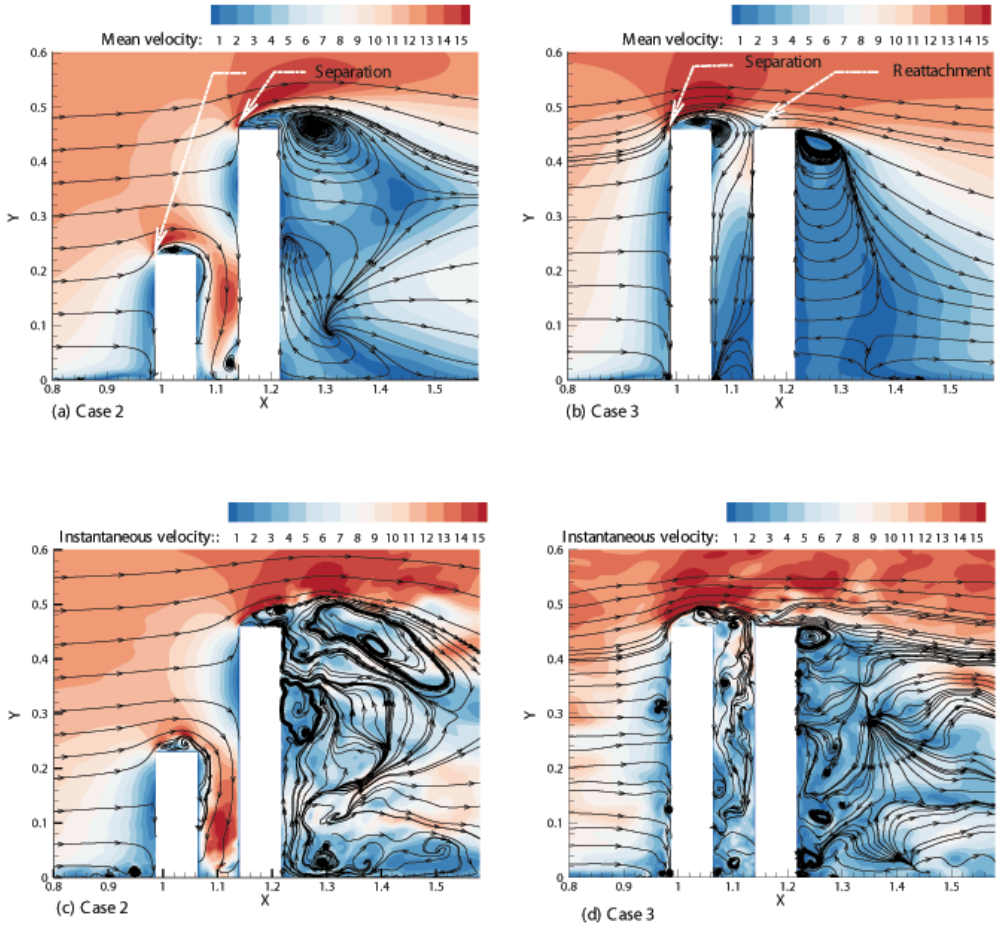

Figure 5.26 Flow field of CAARC with an adjacent building: Mean velocity (top) and instantaneous velocity (bottom) at the vertical center plane.

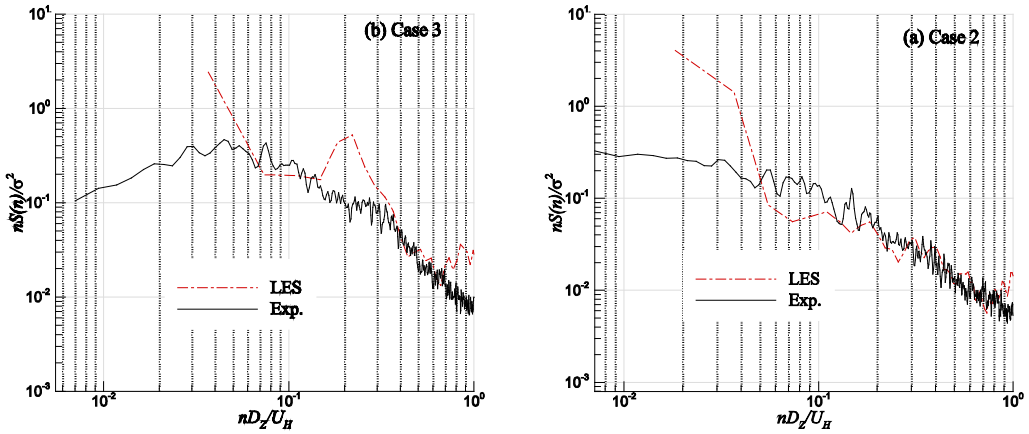

Figure 5.27 Along-wind force spectra for: (a) Case 2 and (b) Case 3

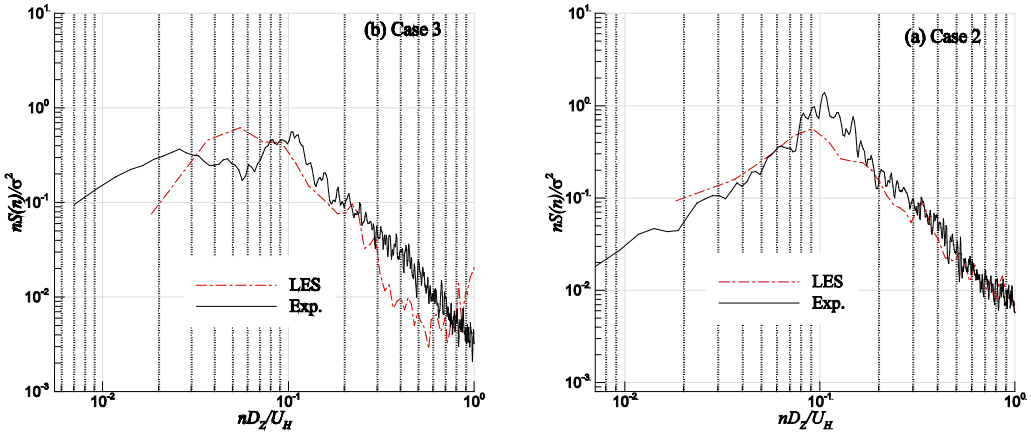

Figure 5.28 Across-wind force spectra for: (a) Case 2 and (b) Case 3

6 LARGE EDDY SIMULATION FOR WIND-INDUCED RESPONSES OF TALL BUILDINGS LOCATED IN A CITY CENTER

Agerneh K. Dagnew[a], Girma T. Bitsuamlak[*, b]

A Paper Prepared for the Journal of Wind Engineering and Industrial Aerodynamics and Presented in the 2012 EMI/PMC Conference

Abstract

Wind-induced external aerodynamic loads were computationally evaluated for a standard tall building, known as the Commonwealth Advisory Aeronautical Research Council (CAARC) model building, located in an urban city center. Geographic information system (GIS) data was used to model the complex building forms and surfaces. At the inlet boundary the transient inflow turbulence was generated using the method called discretization and synthesizing of random flow generation (DSRFG), which reproduced non-isotropy and non-stationarity of the actual turbulent atmospheric boundary layer (ABL) flow. The study employed high frequency pressure integration (HFPI) type large eddy simulation (LES) to evaluate wind pressure loads on the façade of the CAARC model. Over 280 pressure taps strategically distributed on the façade of the study building to monitor the time history of pressure fluctuations. Three different

[a] Ph.D. Candidate, *Adjunct Prof., Laboratory for Wind Engineering Research (LWER), International Hurricane Research Center (IHRC) /Department of Civil and Environmental Engineering (CEE), Florida International University (FIU), Miami, FL 33174, USA

[b]Associate Prof., Department of Civil and Environmental Engineering, University of Western Ontario in London, ON, Canada.

configurations have been studied to analyze the interference effects of the surrounding buildings and explore the potential of LES in predicating the dynamic wind loads of high-rise building in a complex urban-like setting. The numerical results have been compared with the boundary layer wind tunnel (BLWT) data carried out at RWDI USA LLC. The result showed good agreement for overturning moments.

Keywords: Inhomogeneous turbulence, LES, wind-induced responses, tall buildings, city center.

6.1 Introduction

Several experimental, boundary layer wind tunnels, wind load evaluation studies for buildings have been reported by various researchers, and recently there is a growing number of numerical works using computational fluid dynamics (CFD). The majority of the numerical studies have mainly focused on a single low-rise building model and very few works have been done on tall buildings. Some of the numerical studies that focuses on wind load evaluation of a high-rise buildings, an isolated cases, include (Nozawa and Tamura, 2002; Huang and Li, 2010), external aerodynamics of a standard tall building known as the Commonwealth Advisory Aeronautical Laboratories model (CAARC, after Melbourne, 1980) by (Huang et al., 2007; Braun and Awruch, 2009), and LES of CAARC with and without an adjacent building followed by validation through wind tunnel data obtained from RWDI USA LLC, Miramar FL (Dagnew and Bitsuamlak, 2010).

Evaluation of wind effects on high-rise buildings located in a metropolitan city center, where group of tall buildings are constructed in close proximity, have been very

challenging due to the complexity of the flow and the computational cost required to model the surrounding buildings. Moreover, the dynamics of the wind flow become very turbulent and flow interference occurs (Khanduro et al., 1998). Because of this, the majority of the numerical prediction of wind-induced effects for a built environment are limited to the study of pedestrian level wind comfort using the improved forms of Reynolds-Averaged-Navier−Stokes (RANS) turbulence modeling (Hanjalić and Kenjereš, 2008) and in some cases LES (Tamura, 2008; Nozu et al., 2008; Nozu and Tamura, '*in press*'). Recent advances in hardware and software technology coupled with new developments in turbulence modeling make it possible to numerically simulate wind flow in an urban-like complex setting for evaluating design wind loads. This is particularly so with the use of high resolution geographic information system (GIS) data available to realistically reproduce the actual building shape. The present study attempted to evaluate the wind-induce response of the CAARC model building located in downtown Miami, FL using LES simulations. Three different scenarios have been considered.

6.2 Outline of wind tunnel tests

6.2.1 Experimental ABL simulation

An experimental test has been done to simulate an ABL flow profile for rural (Open/Sub) upwind terrain condition. The experiment was conducted at the RWDI USA LLC testing facility that has a testing section of 2.6 m wide by 2.14 m tall. The floor has mechanical actuator to control the degree of surface roughness. Approximately 2.54 cm by 2.54 cm flat plate on 30.48 cm in by 30.48 cm in diamond pattern roughness cubes are used to replicate rural terrain type surface roughness. Time history of velocity data with

record length of 180 sec with sampling frequency of 515 Hz has been measured in the BLWT. Statistics of fluctuating turbulence such as length-scale and turbulence intensities were then calculated and the data was subsequently used by the numerical inflow turbulence generators. Table 6.1 summarizes the turbulence characteristics of the simulated ABL wind flow.

6.3 Experimental wind load testing for validation of LES data

For validation and comparison of the LES wind load data, wind tunnel studies were done for three configurations using the high frequency pressure integration (HFPI) method (Fig. 6.1). Where the first configuration (Case 1) simulates the isolated CAARC building model, the second configuration (Case 2) represents a scenario where the CAARC model building placed in a large city center, and the third case (Case 3) is same as Case 2 but with a similar sized tower immediately adjacent to the target building. The study (CAARC) building had a rectangular prismatic shape with dimensions 30.48 m (x) by 45.72 m (y) by 182.88 m (z) height. The HFPI technique is based on the simultaneous measurement of pressures at several locations on a building surface. The pressure taps were installed at a fine enough resolution over the building surfaces. The BLWT HFPI model was instrumented with 280 pressure taps. Time histories of pressures were measured and stored for post-test analysis. The geometrical modeling and pressure tap distribution adopted for the LES simulation mimics the BLWT-HFPI model (Fig.6.2). All the experiments have been carried out at 1:400 scale. A rural upwind terrain condition (corresponding approximately to a power law with $\alpha = 0.17$) was simulated for all wind directions by means of floor roughness and upwind spires at RWDI wind tunnel test

facility (Dragoiescu et al., 2006). The individual pressure time histories were used to form time series of the fluctuating design wind loads.

6.4 Transient inflow turbulence generation for LES

At the inlet boundary of the LES simulation inhomogeneous and anisotropic fluctuating turbulence was generated by using the discretization and synthesizing of random flow generator (DSRFG) method (Huang et al., 2010). This technique proved to have an advantage over other synthetic inflow turbulence generation methods (such as Smirnov et al., 2001) in terms of generating a realistic wind flow field satisfying ABL flow conditions such as generating eddies in the inertial sub-range and improving spatial correlation of the generated flow fields. The DSRFG method for the generation of a synthesized velocity field of homogenous and inhomogeneous anisotropic turbulence is presented as follows

$$u(x,t)=\sum_{m=k_0}^{K_{ma}}\sum_{n=1}^{N}\left[p^{m,n}\cos\left(\tilde{k}^{m,n}\tilde{x}+\omega_{m,n}t\right)+q^{m,n}\sin\left(\tilde{k}^{m,n}\tilde{x}+\omega_{m,n}t\right)\right] \tag{6.1}$$

where

$$p^{m,n}=\frac{\varsigma\times k^{m,n}}{\left|\varsigma\times k^{m,n}\right|}\sqrt{a\frac{4E(k_m)}{N}}, \tag{6.2}$$

$$q^{m,n}=\frac{\varsigma\times k^{m,n}}{\left|\varsigma\times k^{m,n}\right|}\sqrt{(1-a)\frac{4E(k_m)}{N}}, \tag{6.3}$$

$$\tilde{x}=\frac{x}{L_s},\ \tilde{k}^{m,n}=\frac{k^{m,n}}{k_0},\ \left|k^{m,n}\right|=k_m\ , \tag{6.4}$$

$$\omega_{m,n}\in N(0,2\pi f_m),\ f_m=k_m U_{avg} \tag{6.5}$$

where ς and ξ are vector forms of the corresponding ς_i^n and ξ_i^n. The frequency and the mean velocity are represented by f and U_{avg}, respectively. For inhomogeneous and anisotropic turbulence, the distribution of the wavenumber $k^{m,n}$ is obtained by remapping on the surface of the sphere after the components of $P^{m,n}$ and $q^{m,n}$ are aligned with the energy spectrum. The aligning and remapping is done according to the following equations

$$p_i^{m,n} = sign\left(r_i^{m,n}\right)\sqrt{\frac{4}{N}E_i\left(k_m\right)\frac{\left(r_i^{m,n}\right)^2}{1+\left(r_i^{m,n}\right)^2}} \tag{6.6}$$

$$q_i^{m,n} = sign\left(r_i^{m,n}\right)\sqrt{\frac{4}{N}E_i\left(k_m\right)\frac{1}{1+\left(r_i^{m,n}\right)^2}} \tag{6.7}$$

$$k^{m,n}.p^{m,n} = 0 \tag{6.8}$$

$$k^{m,n}.q^{m,n} = 0 \tag{6.9}$$

$$\left|k^{m,n}\right| = k_m \tag{6.10}$$

where $r_i^{m,n}$ is a random number, independently picked from a three dimensional normal distribution with $\mu_r = 0$ and $\sigma_r = 1$. In the present study, the spectra of the velocity components were described using the von Karman spectra model (Simiu and Scanlan, 1996) as follow

$$S_u\left(f\right) = \frac{4\left(I_u U_{avg}\right)^2\left(L_U / U_{avg}\right)}{\left[1+70.8\left(fL_u / U_{avg}\right)^2\right]^{5/6}} \tag{6.11}$$

$$S_v(f)=\frac{4\left(I_u U_{avg}\right)^2\left(L_v/U_{avg}\right)\left(1+188.4\left(2f\left(L_v/U_{avg}\right)\right)^2\right)}{\left[1+70.8\left(2fL_v/U_{avg}\right)^2\right]^{11/6}} \tag{6.12}$$

$$S_w(f)=\frac{4\left(I_w U_{avg}\right)^2\left(L_w/U_{avg}\right)\left(1+188.4\left(2f\left(L_w/U_{avg}\right)\right)^2\right)}{\left[1+70.8\left(2fL_w/U_{avg}\right)^2\right]^{11/6}} \tag{6.13}$$

Figure 6.3 illustrates the comparison between the spectra of the simulated, the wind tunnel, and the von Karman model turbulence fluctuations at the building model height and inflow velocity fluctuation. The inhomogeneous velocity filed generated by the DSRFG method using the scaling and orthogonal technique well reproduced the spectrum that realistically represent an actual wind fluctuation and captured eddies well within the inertial sub-range.

6.4.1 Spatial and temporal correlation

One of the improvements incorporated in the DSRFG method compared to its predecessor was the use of the integral length scale of turbulence, L_s, as a scaling factor for spatial correlation. Thus, L_s will adjust the spatial correlation between two points and ensure the generation of a spatially correlated field. Recently, Castro et al. (2011) examined the temporal and spatial correlation of the DSRFG method and pointed out some modifications. The formulations of the spatial and temporal correlation of the DSRFG method are given below

$$\overline{u_i(x,t))u_i\left(x',t\right)}=\sum_{m=1}^{M}\sum_{n=1}^{N}\frac{2}{N}E_i(k_m)cos\left[\tilde{k}_j^{m,n}\left(\frac{x_j'-x_j}{L_s}\right)\right] \tag{6.14}$$

$$\overline{u_i(x,t)u_i(x,t+\tau)}=\sum_{m=1}^{M}\sum_{n=1}^{N}\frac{2}{N}E_i(k_m)cos\left(\tau\omega_{m,n}\right) \tag{6.15}$$

For the spatial correlation coefficients between two points i and j, the correlation matrix of the target matrix is computed from the spectra and coherence function (Eq. 6.16). Comparisons have been made between the normalized spatial correlation coefficient of the velocity fluctuations generated by the DSRGF method and the target function. The simulated fluctuation computed using the length scale L_s shows a similar trend with the target function (Fig. 6.4). As Huang et al. (2010) highlighted in his study, the choice of different L_s will affect the spatial correlation of the flow field. Figure 6.5 shows the temporal correlation, the velocity components generated by the DSRFG method showed good time correlation in comparison with the target function (Eq. 6.17).

$$S_{ci,j} = \sum_{m=1}^{M} \sqrt{S_{u,i}(f_m) S_{u,j}(f_m)}\, exp\left(\frac{-C_u^y \left| y_i - y_j \right| f_m}{U_{avg}} \right) \tag{6.16}$$

$$R(m\delta\tau) = \frac{1}{M-m} \sum_{j=0}^{M-m} u_i(j\delta\tau)\, u_i[(j+m)\delta\tau] \tag{6.17}$$

6.5 Setup of the LES simulation for wind load evaluation

The geometrical model of the CAARC test site and surrounding context for the LES simulation was determined from a combination of the RWDI wind tunnel model images and information provided from Google Earth and Google Maps. The CAARC building was placed on the southeast end of the Infinity tower at the Brickell building lot with approximately a 1km radius of surrounding context. Test area images were then compiled from Google Earth and used as a reference underlay to create a full scale plan sketch using Google SketchUp Pro. The overall dimensions of the plan sketch were then

further refined in AutoCAD and scaled down to 1:400. The majority of the height information of the tall buildings in the surrounding context was obtained from the Wikipedia page titled "List of tallest buildings in Miami, FL". Figure 6.6 show the three configurations considered in the LES simulation of the present study. The computational domain (CD) for Case 1 extended $8\mathrm{D_y}$ ($\mathrm{D_y}$ is width of the CAARC building model upwind of the model building and $25\mathrm{D_y}$ downstream of the target building. Laterally it spanned $8\mathrm{D_y}$ away from the side surfaces of the building model and the top boundary has been placed at $2.5\mathrm{H}$ (H is the model building height). Figure 6.7(a) shows the CD for Case 2 and 3, where the domain was sized according to COST (2007) and AIJ guidelines (Tamura et al., 2008). The blockage ratio calculated based on the inlet boundary plane and obstruction area of buildings was less that 5% ($\approx 4.65\%$). For all cases of the LES simulations, the measured mean wind velocity profile ($\alpha = 0.17$) and the inflow turbulence (generated according to Sec. 3) were imposed at the inlet boundary. For the side and the top surfaces of the computational domain a symmetry boundary condition was assumed. At the ground and building wall surfaces a no-slip boundary condition was applied. The outlet, placed at far enough distance downstream of the study building to allow development of wake flow, was prescribed as an outflow boundary condition.

The computational grids were generated using Ansys Meshing CutCell Cartesian meshing algorithm, which is very powerful mesh generation tool. This meshing tool has a unique ability of generating a large fraction of hexahedral cells in complex configuration. The meshing operation involves a two-stage inflation process to generate sufficient quality for convergence using the orthogonal quality measure (Fig. 6.7(b)). Moreover, the

CutCell method reduces manual geometry cleanup thereby reducing the turnaround time required for meshing complex geometry such as a city center.

In the present study, the governing equations for the LES simulation was formulated based on the incompressible Navier−Stokes filtered forms. For the sub-grid-scale (SGS) modeling, the Dynamic Smagornisky-Lilly sub-grid-scale model was employed. In this method the Smagornisky constant (C_s) is computed dynamically according to the resolved scales of motion. For discretization of the convection terms the bounded central differencing (BCD) scheme has been used. For pressure and temporal discretization, second-order schemes are advised for most computational wind engineering applications and have been applied. The Pressure Implicit with Splitting of Operators (PISO) algorithm with skewness and neighboring correction has been used for the pressure-velocity coupling in all the LES simulations, which is based on higher a degree of the approximate relation between the corrections for pressure and velocity and highly recommended for transient simulations such as the present cases.

6.6 Results and discussion

The wind-induce response of CAARC building model under the simulated LES and wind tunnel experiment is shown in Table 6.2, where the mean base overturning moments (M_x, M_y) have been normalized by $1/2\rho U_H^2 H^2 D_z$, following Melbourne (1979). For Case 1 where high resolution grids were used, the LES prediction of the overturning moment coefficient agrees well with the wind tunnel data. While for Case 2 and 3, the LES under predicted the over turning moment coefficients. This could be attributed to the use of coarse computational meshes, due to resource limitation, and wall function in the setup of the LES simulations. In general the results are very encouraging and better

numerical predictions can be found using high resolution grids, especially at the upwind domain and in the near-wall regions.

The instantaneous velocity flow field of CAARC building model under various configurations is illustrated in Fig. 6.8. The streamline of the velocity is taken at one instance of time of the LES simulation. The oncoming flow separates at the leading sharp corners (at the three corners of the wind-facing wall) and initiates a recirculation zone on the sidewalls and at the roof of the building. The LES also captured the alternating Karman vortices downstream of the target building. Figure 6.9 presents the instantaneous velocity field of configuration of Case 2 and 3 at a horizontal plane. The complex flow field demonstrated that the neighboring structures changed the dynamic of the wind as it approaches the target building. The presence of the complex surrounding structures resulted flow interference, channeling, and wake effects on the CAARC model building. These were responsible for the increased lift force coefficients of Case 2 and 3 compared to the single building model (Case 1).

6.7 Conclusions

Computational assessment of aerodynamic characteristics of a standard tall building (CAARC) under urban surrounding were performed and results were compared with BLWT data. The inhomogeneous inflow turbulence implemented at the inlet boundary has been examined from the turbulence modeling principle of LES and computational wind load evaluation perspective. Sheltering, channeling, wake effects and other complex interference mechanisms could be effectively explained owing to the continuous simulation capability of numerical simulations in space and time, thus leading to a better understanding of wind/structure interactions and development of mitigation

solutions that will lead to enhanced wind performance of buildings. The present study was limited to one wind direction, as part of the ongoing project the authors are in the process of investigating wind directionality effects under an urban setting using high resolution LES.

Acknowledgments

This material is based in part upon work supported by the National Science Foundation CAREER project under Grant Number 0846811. Any opinions, findings, and conclusions or recommendations expressed in this material are those of the author(s) and do not necessarily reflect the views of the National Science Foundation. This research was supported in part by the National Science Foundation through TeraGrid resources provided by National Center for Super-computing Applications (NCSA). We are grateful to RWDI Miramar Inc. for providing us with the wind tunnel data used for comparison purposes.

References

Braun, A.L., Awruch, A.M. (2009). "Aerodynamic and aeroelastic analyses on the CAARC standard tall building model using numerical simulation." Journal of Computers and Structures 87, 567-581.

Castro, G.H., Paz, R.R., Sonzogni, V.E. (2011). "Generation of turbulent inlet velocity conditions for large eddy simulations." Mecánica Computacional Vol XXX, págs., 2275-2288.

COST. (2007). "Best practice guideline for the CFD simulation of flows in the urban environment COST Action 732."

Dagnew, A.K., Bitsuamalk, G.T. (2010). "LES evaluation of wind pressures on a standard tall building with and without a neighboring building." The Fifth International Symposium on Computational Wind Engineering (CWE2010), Chapel Hill, North Carolina, USA May 23-27.

Dragoiescu, C., Garber, J., Kumar, S.S. (2006). "A comparrison of force balance and pressureintegration techniques for prediciting wind-induced response of tall buildings." Structures Congress 2006: Structural Engineering and Public Safety Proceedings of the 2006 Structures Congress.

Hanjalić, K., Kenjereš, S. (2008). "Some developments in turbulence modeling for wind and environmental engineering." Journal of Wind Engineering and Industrial Aerodynamics 96, 1537-1570.

Huang, S.H., Li, Q.S., Wu, J.R. (2010). "A general inflow turbulence generator for large eddy simulation." Journal of Wind Engineering and Industrial Aerodynamics 98, 600-617.

Huang, S.H., Li, Q.S. (2010). "Large eddy simulation of wind effects on a super-tall building." Wind and Structures, An Int'l Journal 13 (6),557-580.

Huang, S., Li, Q.S., Xu, S. (2007). "Numerical evaluation of wind effects on a tall steel building by CFD." Journal of Constructional Steel Research 63, 612-627.

Khanduri, A.C., Stathopoulos, T., Bédard, C. (1998). "Wind-induced interference effects on buildings — a review of the state-of-the-art." Engineering Structures 20, 617-630.

Melbourne, W.H. (1980). "Comparison of measurements on the CAARC standard tall building model in simulated model wind flows." Journal of Wind Engineering and Industrial Aerodynamics 6, 73-88.

Nozawa, K., Tamura, T. (2002). "Large eddy simulation of the flow around a low-rise building immersed in a rough-wall turbulent boundary layer." Journal of Wind Engineering and Industrial Aerodynamics 90, 1151-1162.

Nozu, T., Tamura, T. (2012). "LES of turbulent wind and gas dispersion in a city." Journal of Wind Engineering and Industrial Aerodynamics, doi:10.1016/j.jweia.2012.02.024

Nozu, T., Tamura, T., Okuda, Y., Sanada, S. (2008). "LES of the flow and building wall pressures in the center of Tokyo." Journal of Wind Engineering and Industrial Aerodynamics 96, 1762-1773.

Smirnov, R., Shi, S., Celik, I. (2001). "Random flow generation technique for large eddy simulations and particle-dynamics modeling." Journal of Fluid Engineering 123, 359–371.

Simiu, E., Scanlan, R.H. (1996). "Wind Effectson Structures-Fundamentals and Applications to Design." John Wiley & Sons, Inc., New York.

Tamura, T. (2008). "Towards practical use of LES in wind engineering." Journal of Wind Engineering and Industrial Aerodynamics 96, 1451-1471.

Tamura, T., Nozawa, K., Kondo, K. (2008). "AIJ guide for numerical prediction of wind loads on buildings." Journal of Wind Engineering and Industrial Aerodynamics 96, 1974-1984.

Tominaga, Y., Mochida, A., Murakami, S., Sawaki, S. (2008). "Comparison of various revised k–ε models and LES applied to flow around a high-rise building model with 1:1:2 shape placed within the surface boundary layer." Journal of Wind Engineering and Industrial Aerodynamics 96, 389-411.

Table 6.1 Measured inflow wind characteristics of open terrain.

Level	**Elevation (m)**	**Mean velocity**	**Turbulent intensity (%)**			**Integral length (m)**		
		$U(m/s)$	I_x	I_y	I_z	${}^{x}L$	${}^{y}L$	${}^{z}L$
1	0.1524	10.381	24.00	7.30	16.30	0.480	0.090	0.160
2	0.3048	11.458	22.50	8.90	14.80	0.540	0.145	0.175
3	0.4572	12.061	21.00	10.30	14.50	0.550	0.160	0.192
4	0.6096	12.810	19.60	11.00	13.90	0.600	0.175	0.200
5	0.9144	13.647	16.90	10.20	12.40	0.630	0.185	0.205
6	1.2192	14.438	15.60	9.30	11.30	0.640	0.190	0.210
7	1.5240	14.995	12.80	6.90	9.30	0.650	0.125	0.191

Table 6.2 Wind-induced responses of CAARC by LES and BLWT.

Configuration	C_{M_x}		C_{M_y}	
	LES	**BLWT**	**LES**	**BLWT**
Case 1	-0.0010	-0.0043	0.5834	0.6309
Case 2	-0.0047	-0.0068	0.3467	0.4590
Case 3	-0.0197	-0.0088	0.4391	0.4900

Figure 6.1 Wind tunnel test configurations.

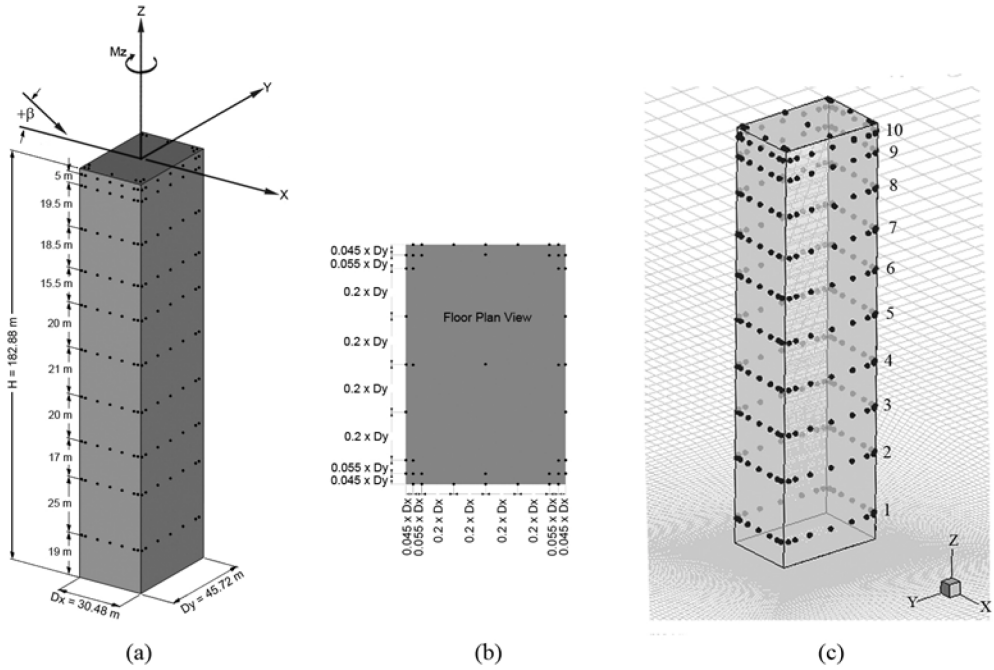

(a) (b) (c)

Figure 6.2 CAARC standard tall building model with full-scale dimensions and pressure tap locations for: BLWT (a &b) and LES (c).

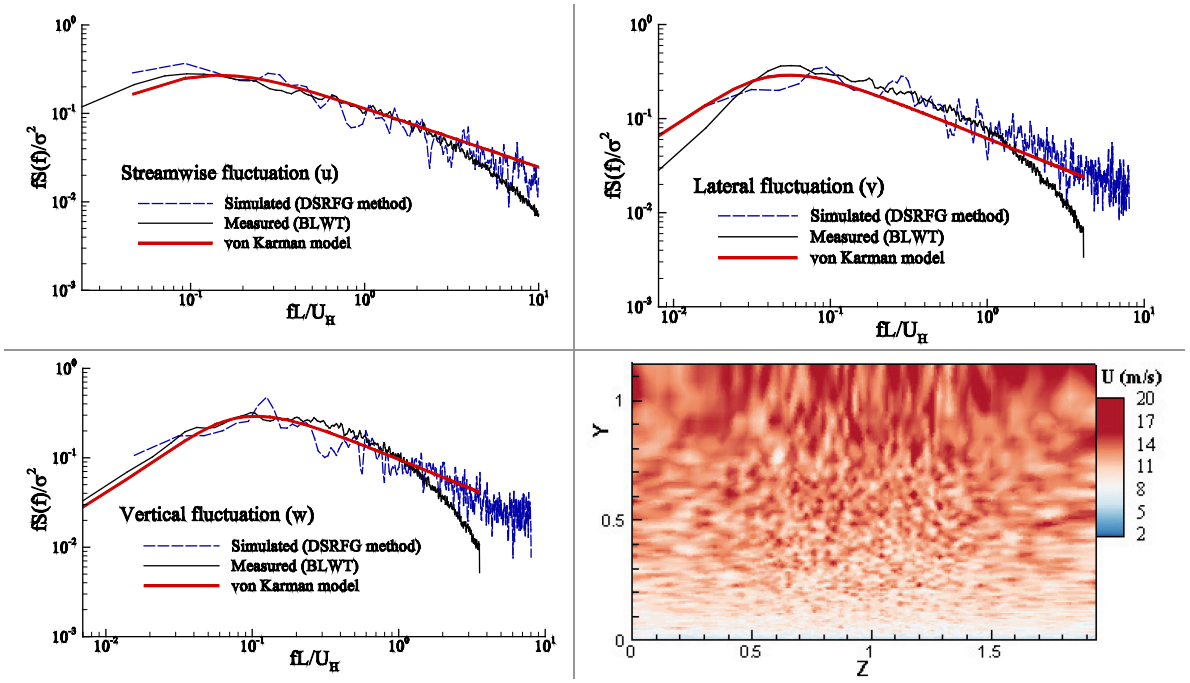

Figure 6.3 Comparison of simulated spectrum with the BLWT data; inflow boundary turbulence.

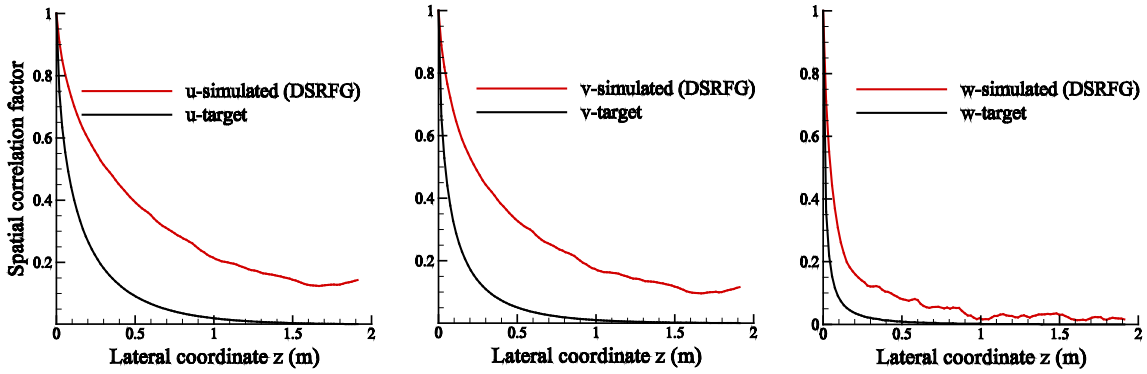

Figure 6.4 Normalized spatial correlation of fluctuating velocity components u, v, and w.

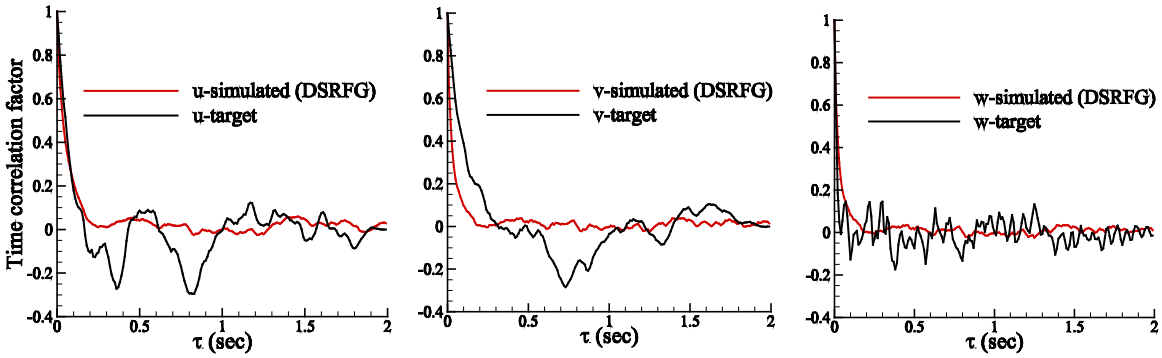

Figure 6.5 Normalized time correlation of fluctuating velocity components u, v, and w.

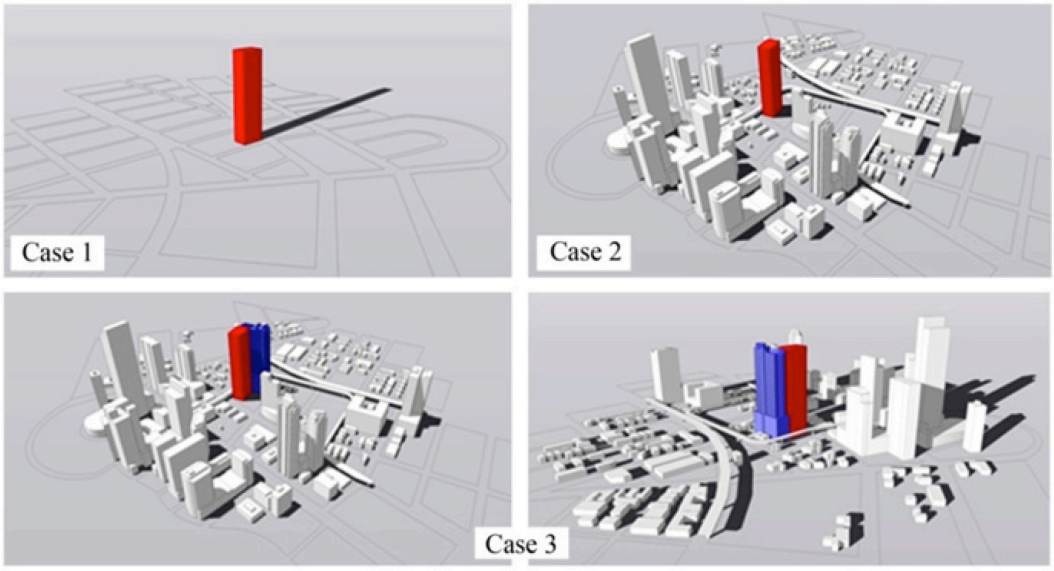

Figure 6.6 Geometrical models of CAARC building with and without surrounding buildings.

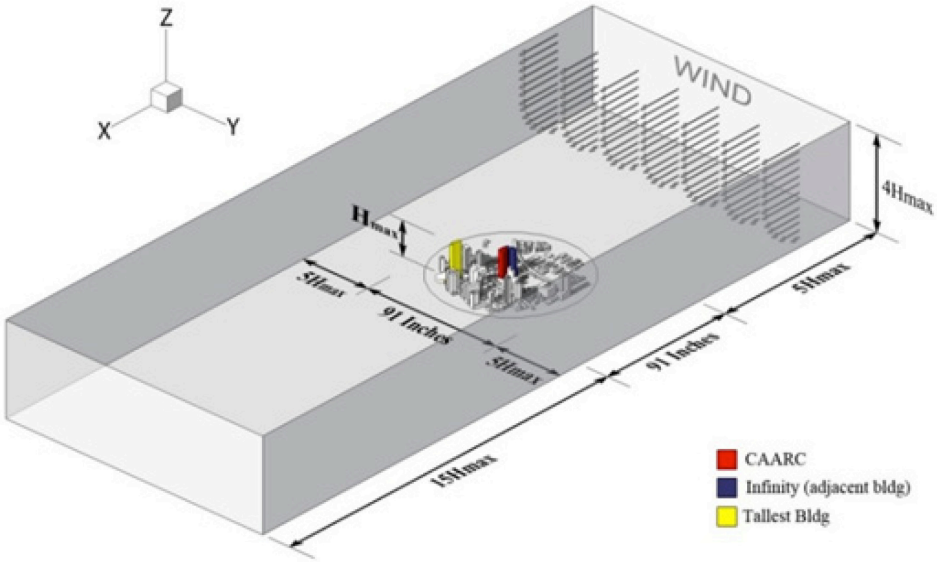

(a)

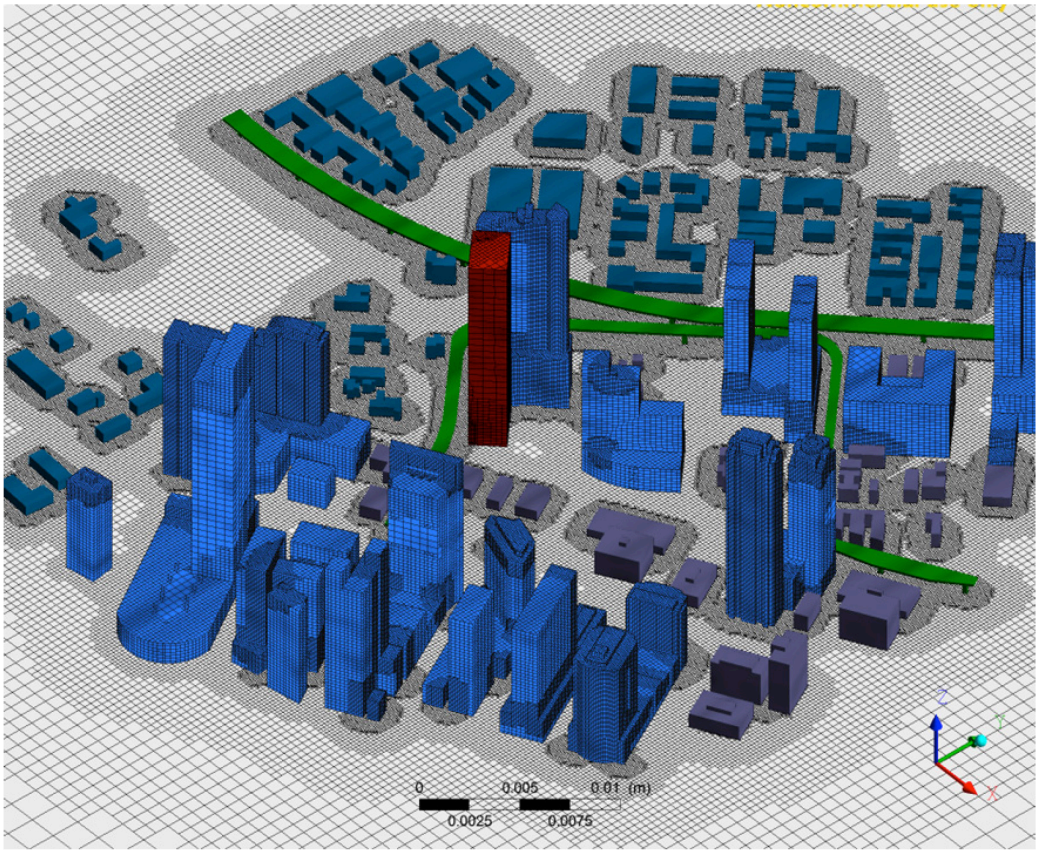

(b)

Figure 6.7 CAARC with surrounding context: (a) computational domain and (b) mesh of CAARC with complex surroundings.

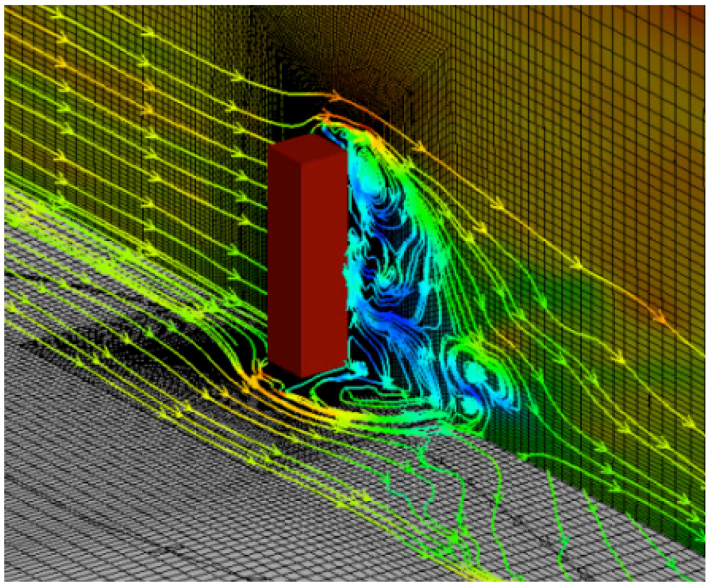

(a) Case 1

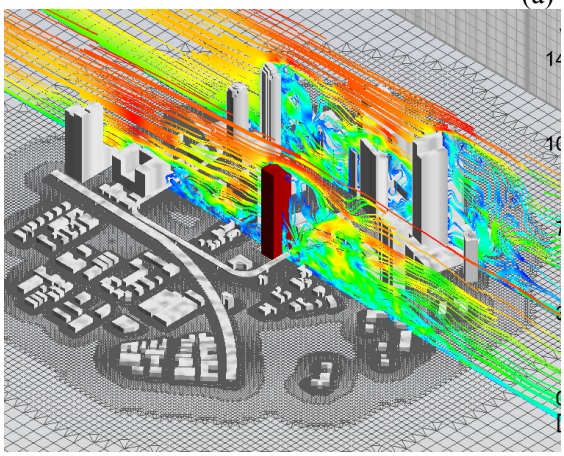

(b) Case 2

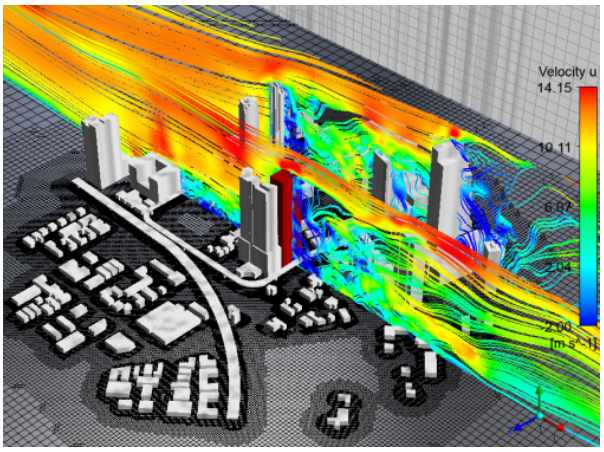

(c) Case 3

Figure 6.8 Streamwise velocity fluctuation at a vertical plane.

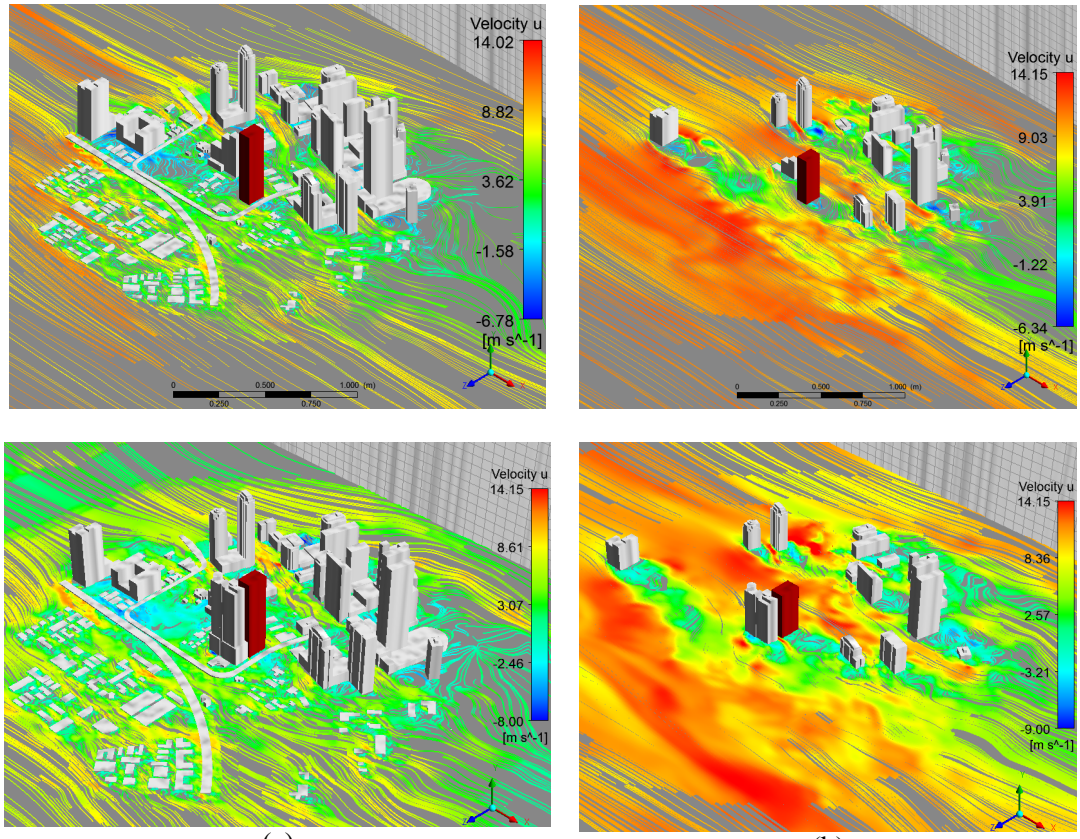

(a) (b)

Figure 6.9 Instantaneous 3D velocity streamlines of Case 2 (top) and Case 3 (bottom): (a) at z=0.1H and (b) at z=0.5H.

7 CONCLUSIONS, RECOMMENDATIONS AND GUIDELINES FOR FUTURE RESEARCH

The evolution of computational wind engineering is making numerical evaluation of wind loads a potentially attractive proposition. In the present study a computational model was developed following a Large Eddy Simulation approach, opted for its accuracy for building aerodynamics "bluff bodies" which are characterized with high turbulence and flow separations at building corners. Compared to the experimental wind load evaluation which relies on discrete point measurements, the LES model produced useful continuous aerodynamic data on the entire surface of the building. It also provided detail flow visualizations for the wind field around a study building that provided useful information on flow separation and reattachment, recirculation zone, and vortex generation.

This was instrumental in understanding the complex wind/building interactions better, accounting both immediate surroundings and upwind exposure effects. In addition, at the present early stage of numerical modeling for building aerodynamics, it is imperative that the accuracy of the simulation is expected to be validated rigorously to identify its strengths and weaknesses. Hence, all numerically generated aerodynamic data in the present study was validated in comparison with experimental data obtained from boundary layer wind tunnel experiments. It is believed that the computational approach will allow circumventing the limitations of wind tunnels as a design tool and encourage aerodynamic considerations in the building design process, which is a rarity in current practice.

Moreover, the more specific conclusions as a result of the present computational evaluation of wind loads on buildings have been provided in the following sections. These sections are ordered according to the research topic to preserve continuity.

7.1 Comprehensive and critical review of the current state of CFD

The state-of-the-art of computational wind engineering has been discussed by critically reviewing the work of several researchers. Based on the key findings in turbulence modeling, boundary conditions, and high Re numbers turbulent flow, and computational cost, the following guideline for CFD application to wind load evaluation are summarized as follows:

- The recent significant progress made in turbulence modeling, efficiency in computing machines and developments in novel parallel algorithms enabling industrial applications of CFD techniques. These include wind effect studies on actual buildings, both on low-rise and high-rise with in urban setting.
- Unsteady simulation such as LES has pivotal importance for wind engineering applications.
- Generation of the ABL wind flow field is the critical step in applying CFD for the wind load evaluation process.
- Model- and full-scale data are very valuable for validation of CFD results at the present early stage in their application.
- An accurate time-dependent analysis, such as for example LES and hybrid RANS/LES, is essential to produce the time-history of pressure fluctuation,

similar to what is being done in wind tunnel experiments. This enables the prediction of peak-type quantities for the preliminary design of buildings.

- In general computationally obtained mean values showed a good agreement with full-scale and wind tunnel experiments, especially on the windward face but were problematic in leeward faces.
- Very limited, almost none, work has been done in estimating peak wind loads using CFD.
- For large-scale simulations the computational cost still remains a concern but the hybridization of turbulence models (for example hybrid RANS/LES), a robust parallelization, and new programing routine which can exploit the graphical processing unit of CPUs, and the emergence of cloud computing by private vendors are some of the encouraging efforts to make CFD affordable in the foreseeable future.

7.2 Comparative numerical modeling application for the design and fabrication of novel wind engineering facilities

A comparative numerical simulation for various size specimen located at various distance from the wind source has been found to be very useful in the design and construction of new open jet facilities such as the Wall of Wind.

- The RANS and LES based CFD simulation helped in identifying the placement fans into a well-defined single jet flow whose characteristics mimic the mean and turbulent hurricane winds.
- It also helped to develop a guideline on the maximum size of the test specimens the hurricane simulator can test and the proximity distance where specimens

should be placed with respect to the wind sources (fans) to obtain sound aerodynamic data with minimal blockage and proximity effects. These guidelines are routinely followed at the Wall of Wind at the moment. The guideline is expected to be useful for configuring new design concepts and modifications in similar facilities in the future.

7.3 Numerical evaluation of wind loads on low-rise building roofs

LES simulations on low-rise buildings with regular and complex roof shapes have been carried out. The study focused on the wind-induced pressure loads of the roof systems. Inherent to the responses of low-rise buildings to turbulent wind, the following observations are summarized with respect to the estimation accuracy of LES.

- A meticulous effort was required in the geometrical modeling, especially in the ridge, corner and roof-wall connection regions. It helped in distribution and generation of high quality grid cells around those regions. Perhaps, this constitutes one of the most time-consuming aspects of the numerical modeling process in future practical applications.
- The high-resolution spatial discretization applied at the inner boundary layer, around the vicinity of the sharp corners and ridges of the model enabled the reproduction of the basic flow features and distribution of mean pressure coefficients on the regular and complex shape buildings.
- The numerical models with complex roof shapes showed mixed pressure distribution on the roof (positive and negative pressure) as opposed to the regularly shaped models where the separation and reattachment locations were clearly identified.

- Despite assuming constant integral length and turbulence intensity (lateral and vertical directions), the study of the roof pressure distribution revealed that the mean pressure coefficient predicted by the LES simulation is in a good agreement with the wind tunnel data.
- For the gable and hip roof models, high suction pressures were observed on areas close to the windward edge and near the middle ridge consistent to the experimental results. The flow separations in these regions that resulted in these peaks were properly captured though the CFD visualizations.
- LES was found very useful for complex roof cases, where building standards and codes do not provide design wind loads.
- The numerical study also showed that oblique angle wind could introduce uplift pressure loads due to the formation of corner vortices, which is consistent with the experimental observations.
- Time histories of pressure data obtained from the LES simulations were very useful for the estimation of the time averaged mean, standard deviation (*rms*), and the peak minimum and maximum pressure coefficients. The short record duration resulted in an over-estimation of peak values by the LES simulations. This could be improved by taking a longer record sample in the future.
- The flow visualization from the LES is useful to rationally encourage the design of low-rise buildings for improved wind performance.

7.4 Aerodynamics of tall buildings

The external aerodynamics of a standard tall building, also commonly known as the CAARC model, under various surrounding configurations has been examined with

the help of high-resolution CFD simulations. To understand the full extent of the wind-structure interaction and the capability of the LES in handling turbulent flow, successive numerical studies were carried out. First the single building case for multiple wind directions followed by an immediate adjacent building and complex surrounding (city center) simulation cases. The city center case simulations were carried out for down town Miami, FL. The geometrical model of the complex city center was created using a combination of information obtained from the wind tunnel model and a Google aerial map. After rigorous cleanup of the topology, the CAD model was exported for meshing. After careful consideration, it was necessary to conduct an experimental testing on an empty wind tunnel to obtain basic flow characteristics of open and sub-open terrain conditions. The flow statistics such as mean velocity and turbulence intensity profiles and integral length scales were calculated from the velocity fluctuation measured at 10 points along the height of the wind tunnel. Then this data was used to generate a spatially correlated time-dependent random flow that satisfies the ABL flow criterion. The inflow turbulences were used to prescribe the inlet boundaries of the LES simulations. For the HFPI-type LES simulations, over 280 pressure taps were created inside the computation domain and systematically distributed on the surfaces of the model. Then time histories of the fluctuating pressures were measured and the design wind load quantities were calculated and compared with the wind tunnel data. The wind-induced loads on the CAARC model building were obtained numerically. The experimental wind pressure data used for the validation of the CFD results were done for an open and sub-open terrain exposure.

Pertaining to the responses of high-rise buildings to wind and the numerical modeling principles of high *Re* numbers flow, the following remarks were drawn:

- The grid sensitivity analysis showed how the mean flow quantities are affected by the size of the computational cells. Computational grids that resolve the inner boundary layer adequately estimated wind flow parameters (such as wind speed and TI) at the incident plane.
- LES with inflow turbulence performed better and captured flow structures with relevant length scale.
- Numerically generated random inflow turbulences considerably affected the accuracy of the LES based simulations. Those random flow generators, particularly the synthetic turbulence family, which incorporated the turbulence integral and temporal-scale, produced a realistic divergent-free wind flow field that accurately represented the ABL flow.
- The spatial and temporal correlation showed that inflow turbulence generated using the von Karman spectrum model better matched with the wind tunnel simulated spectrum and reproduced the high frequency range of flow structures within the inertial subranges, which is in line with the modeling principle of LES simulation.
- The result further attested the need for proper inflow transient boundary conditions in agreement with suggestions by other CFD researchers. This in fact is analogous to the extreme care and effort that is taken during ABL flow simulations in the BLWT, with thorough use of upwind roughness elements, spires, or other types of active and passive flow controls.

- For the isolated tall building case, the LES with a transient inlet boundary using the discretizing and synthesizing random flow generation (DSRFG) method showed superior performance in predicting aerodynamics forces such as drag- and lift-force, and bending and torsional moment coefficients.
- The along-wind and cross-wind loads predicted by the LES simulation showed close comparison with the experimental data. It is to be recalled that the cross-wind loads are not provided in building codes and standards.
- Based on the results of the isolated building model, the city-center simulation was necessary to fully explore the potential of LES simulations.
- The complex geometry of the city center simulation required a greater deal of time to economically distribute the computational meshes. Large volume of grid cells was allocated in the near wall regions of the model building. However, the presence of small structures such as the twin bridges and the residential buildings in the vicinity of the CAARC model restricted the control over the size of the minimum grid point.
- The effect of the neighboring buildings within the 1km radius of the study building formed channeling, sheltering, and wake interference effects on the model building. The LES simulation allowed to thoroughly understanding these phenomena.
- The channeling, sheltering and wake effects introduced by the immediate adjacent building and the surrounding structures were very noticeable and changed the wind load distribution on the envelope of the model building.

- The large-scale simulation mechanisms effectively explained the complex wind-structure interaction. Owing to the continuous simulation capability of numerical simulations in space and time, thus leading to a better understanding of wind/structure interactions and development of mitigation solutions that will lead to enhanced wind performance of buildings.
- Wind tunnel experimental data are indispensable for the correct boundary prescription and validation of LES.

7.4.1 Extended application of the complex surrounding case simulation

- The results from the complex surrounding case simulation can be extended for studying pedestrian wind level comfort,
- Tracing of flying objects/debris from upwind structures in the event of wind hazards
- Gas dispersion in the event of a chemical attack, and
- Wind driven rain studies
- Will help in developing evacuation guidelines during catastrophic wind events such as hurricanes.

In general, it is fair to conclude that CFD simulations such as LES can be used as an alternative tool for wind pressure load evaluation of low-rise building at least for preliminary design. Generally, it can be concluded that LES with proper boundary conditions and enhanced computational resources could prove useful for wind load applications. In the author's opinion, computational resource are still the bottle neck for full-fledged use of LES making it still expensive and more time consuming than standard BLWT wind load studies. One such limitation in the present study was perhaps the

limited period of LES pressure time-history data generated than what might have been necessary to accurately predict the design wind force coefficients (peak) very similar to the experimental method.

7.5 Recommendations for future research

- Incorporating roughness effects in the upstream domain of the computational domain will help in achieving the ABL flow.
- Wind load evaluation study by accounting the roughness of the wall surfaces instead of using no-slip wall boundary.
- Performing RANS/LES simulation and compare the computational efficiency and accuracy with LES.
- Finding optima record length of pressure time-history of computational results that takes into account the computational cost and accuracy. As length of sampling greatly affects the wind design quantities, particularly peak values.
- Integrating CFD with catastrophe modeling software such as HAZUS-MH and estimate wind loads on buildings.
- Investigating the applicability of CFD for performance based design and vulnerability analysis of low-rise buildings.
- Considering the effect of buoyancy in the numerical modeling of ABL simulation.

7.6 Guidelines for numerical wind load evaluation using CWE

Below are some helpful guidelines for wind load evaluation of bluff-body using the technique of CWE

- The LES results are greatly dependent on the input mean wind flow parameters such as the mean velocity and turbulence intensity profile in all directions (x, y, z). Hence, care should be taken when prescribing the inlet boundary. As this not only affects the convergence of the simulation and computational time but also will compromise the quality of the aerodynamic data.
- For low-rise buildings, pertaining to scaling issues, measuring relevant length scales using a model-scale test is very difficult particularly in the lower ABL region. Therefore, full-scale data is more appropriate for defining these parameters at the inlet boundary of the numerical simulation. When the length- and time -scale data are scarce, proto type numerical simulations should be done.
- For a city center simulation, getting accurate building and other neighboring structures is very crucial. Hence using tools like ArcGIS and Lidar data will be valuable in getting the elevation information.

VITA

AGERNEH KENUBIH DAGENEW

1999-2004	B.Sc. Civil Engineering Jimma University, Technology Faculty Jimma, Ethiopia
2004-2005	Assistant Lecturer Jimma University, Technology Faculty, Department of Civil Engineering, Jimma, Ethiopia
2005-2007	M.Tech. Structural Engineering Indian Institute of Technology Roorkee, Roorkee, India
July 2007-Dec 2007	Lecturer, Consultant Engineer Jimma University, Technology Faculty, Department of Civil Engineering, Jimma, Ethiopia
2008-2012	PhD Candidate, Civil Engineering Florida International University Miami, Florida, USA
2008-2009	Instructor and Research Assistant Civil and Environmental Engineering Florida International University Miami, Florida, USA
2009-2012	Research Assistant Civil and Environmental Engineering Florida International University Miami, Florida, USA

Publications
Refereed journal papers

1. **Dagnew, A.K**., Bitsuamlak, G.T., 2012. "Computational evaluation of wind load: A review," ***Accepted for publication*** *in Wind & Structures, An Int'l Journal*.

2. Bitsuamlak, G.T., **Dagnew, A.K**., Chowdhury, A.G., 2010. "Computational assessment of blockage and wind simulator proximity effects for a new full-scale testing facility," *Wind & Structures, An Int'l Journal* Vol. 13 No. 1, 21-36.

3. **Dagnew, A.K**., Bitsuamlak, G.T., 2012. "Large eddy simulation of wind load on a standard

tall building with and without adjacent building," *Journal of Wind Engineering and Industrial Aerodynamics, the Journal of the International Association for Wind Engineering. "**Under review"***

4. **Dagnew, A.K**., Bitsuamlak, G.T. 2012. "Large eddy simulation for wind-induced response of tall buildings located in a city center," *Journal of Wind Engineering and Industrial Aerodynamics, the Journal of the International Association for Wind Engineering.* "***in preparation"***

Conference proceedings

1. **Dagnew, A.K**., Bitsuamlak, G.T., 2012. "Numerical investigation of wind-induced pressure loads on low-rise residential buildings with complex roof shapes," *The 3rd American Association for Wind Engineering Workshop (AAWE), Hyannis, Massachusetts, August 12-14.*

2. **Dagnew, A.K**., Bitsuamlak, G.T., 2012. "Large eddy simulation for wind-induced response of tall buildings located in a city center," *Engineering Mechanics Institute & 11th ASCE Joint Specialty Conference on Probabilistic Mechanics and Structural Reliability (EMI/PMC 2012), Notre Dame, IN, June 17-20*.

3. **Dagnew, A.K.,** Bitsuamlak, G.T., 2010. "LES evaluation of wind pressures on a standard tall building with and without a neighboring building," *The Fifth International Symposium on Computational Wind Engineering (CWE2010), Chapel Hill, NC, May 23-27.*

4. Bitsuamlak, G.T., **Dagnew, A.K**, James Erwin, J., 2010. "Evaluation of wind loads on solar panel modules using CFD," *The Fifth International Symposium on Computational Wind Engineering (CWE2010), Chapel Hill, NC, May 23-27.*

5. **Dagnew, A.K**., Bitsuamlak, G.T., Ryan, M., 2009. "Computational evaluation of wind pressures on tall buildings," *The 11th American Conference on Wind Engineering, San Juan, Puerto Rico.*

6. Bitsuamlak, G.T., Gan Chowdhury, A., **Dagnew, A.K**., 2008. "Computational blockage and wind simulator proximity effects assessment for a new full-scale testing facility", *The 4th International Conference, Advances on Wind and Structures (AWAS08), Jeju, Korea.*